University of Stavanger

Faculty of Science and Technology

MASTER'S THESIS

Study program/ Specialization: Petroleum Technology / Drilling	Spring semester, 2017 Open / ~~Restricted access~~
Writer: Sima Alise Nepal	…… (Writer's signature)
Faculty supervisor: Dan Sui External supervisor(s): Amare Leulseged, IRIS	
Thesis title: Controller design for back pressure Managed Pressure Drilling when using oil based mud in long wells.	
Credits (ECTS): 30 ECTS	
Key words: OBM, WBM, kick tolerance, Kick detection, influx control, conventional well control procedure, automated controller design, PI-controller, Wemod, IRIS drill for Matlab,	Pages- 179 Stavanger, 14 June 2017 Date/year

Front page for master thesis
Faculty of Science and Technology

Abstract

In all drilling operations, downhole pressure requires to be closely monitored and measured at all times. Mainly, drilling fluid is used to balance the formation pressure downhole, a pressure that is created so that formation fluids are contained. In case, where the drilling fluid is excessively high or low, fracture or collapse may take place. In order to design the Mud Weight (MW) of the drilling fluid properly, the knowledge of annular pressure is extremely necessary. It must be inside a certain limit in order to avoid severe damage or harm to personnel, the environment and to the rig itself.

One of the methods, to precisely control the downhole pressure, is with Managed Pressure Drilling (MPD). In this operation, the mud system is closed by using a choke along with back-pressure pump to properly manage circulation process, an important technique when influx is seen in the well.

The main objective of this paper is to improve the ability to control pressure precisely in back-pressure MPD operation. The simulation takes its basis on long wells with Water Based Mud (WBM) and Oil Based Mud (OBM). A moderate gas kick is also initiated and circulated out with OBM and WBM for manual and automated operation. Automated operation is based on one of the most common control systems, namely Proportional, Integrate (PI) controller.

Methodology used in this research is based on IRIS flow model, along with a configuration tool provided by *IRIS drill for Matlab* called *Wemod.* Configuration uses details about the well, the fluid and specification of geo-pressure and temperature properties. *Matlab* is further used to reproduction of pressure relations.

By comparisons of mud systems OBM is more preferable in High Pressure and High Temperature (HPHT) wells, mainly due to the poor performance of water in WBM. However, in case of normal pressure and temperature conditions, OBM is associated with more environmental concerns and greater cost and therefore, WBM is preferred.

In simulation of moderate kick, in manual operation, the total time of influx was almost double that of automated operation. Thus, proving that automated operation has ability to handle a greater influx size, and be able to perform circulation by only using half of the time of manual operation. While comparing kick size with different fluid types, OBM with greater Oil Water Ratio (OWR), different stresses and different gel strength, underestimates a large part of the influx size. Circulation still takes equal amount of time for both fluid types, even when the influx is much greater for WBM.

Table of Contents

Acknowledgement

First of all, I would like to thank IRIS for setting the objective of this thesis, a very interesting and challenging work that, in my belief, will aid the industry in the future. IRIS has also provided essential software configuration, *Wemod*, that was extremely useful and has shown a vital importance in my simulation work. I would like to thank, "IRIS drill for Matlab" for providing all the important files and the simulation software, without which my work would be incomplete.

Both of my supervisors, faculty supervisor being Dan Sui and my external supervisor Amare Leulseged, have been extremely cooperative and helpful from the very beginning of my thesis. I am extremely thankful, for their advice, encouragement, suggestions, patience and their time devoted to this work. I am truly, very lucky to be supervised and guided by them. Amare Leulseged from IRIS has especially been a big part of my simulation work, and for that I acknowledge him from the bottom of my heart. At last I would like to thank my husband, for encouraging me and being by my side till the very end of my work.

Acronyms

APP- Annular Pressure Profile

BHP- Bottom Hole Pressure

BPM- Bingham Plastic Model

ECD- Equivalent Circulating Density

GWR- Gas Water Ratio

HPHT- High Pressure High Temperature

IRIS- International Research Institute in Stavanger

MASP- Maximum Allowable Surface Pressure

MD- Measured Depth

MPD – Managed Pressure Drilling

MW- Mud Weight

NPT- Non- Productive Time

NS- North Sea

OBD- Overbalanced Drilling

OBM – Oil Based Mud

OWR- Oil Water Ratio

PLM- Power Law Model

PV- Plastic Viscosity

PVT- Pressure Volume Temperature

RCD- Rotating Control Device

ROP- Rate of Penetration

RSM- Robertsen and Stiff Model

SPP- Stand Pipe Pressure

TVD – True Vertical Depth

WBM- Water Based Mud

WDP- Wired Drill Pipe

YP- Yield Point

List of Figures

List of Table

Chapter 1: Introduction

In our society today, the demand for energy is increasing, compelling the oil industry to make use of creative and innovate technology, methods and solutions to fulfil their needs. In many circumstances, drilling must take place in tough conditions, for instance in deep sea, where the temperature and pressure are above normal conditions.

Well control has therefore, been a priority in the industry, without which the industry places their workers, the environment and the well itself in danger. The topic of well control, covers the technique used to maintain the fluid column hydrostatic pressure and the estimation of formation pressure, in order to prevent influx from entering the well. Formation fluids that are under pressure, if not balanced, may enter the well and escape to the surface. If influx is not controlled, the result may ultimately lead to a blowout. Blowout brings a great threat to environment, people and the surroundings. Collapse from the formation surrounding the well, may also be avoided by using pressure control. By considering aforementioned arguments, understanding pressure relations in well control is extremely crucial prior to drilling any well.

Normally drilling fluids are used to balance the formation pressure downhole, a pressure that is created so that formation fluids are contained. MPD is one of the methods to control the bottom hole pressure (BHP). To obtain a constant BHP, annulus is closed and drilling fluid flows out through a choke system, which allows for precise control of annular pressure. The back-pressure pump is automatically adjusted and is used as an additional aid to control the annular pressure profile.

The main objective of this thesis is to improve the ability to control pressure precisely in back pressure MPD in long wells using OBM, compared to shorter wells with WBM. One other objective also to initiate a moderate kick and circulate it out, for manual and automated operation and thus, to determine advantage or disadvantage of these operations.

Before the case study is conducted, a theoretical part is included. At first, background is given for simplicity and explanation of MPD, the purpose of back-pressure in such operations and a short introduction about drilling fluids and pressure profiles.

Furthermore, the thesis develops to Chapter 2, covering fluids sections. A theoretical work needed to be defined and understood in order to study the pressure dynamics of long wells

for the different fluid types. A further progression to Chapter 3 is made, where the definition of kick tolerance is given and the method to detect influx is defined and to be able to estimate its size. This will aid to determine its possibility of circulation.

The dynamic and the friction pressure loss model given from IRIS is described in Chapter 4. Further on, the explanation of how to control the influx is described in chapter 5, a method applied to manual and automated operation. The controller used in automated operation, for this work is the PI controller. An introductory chapter of the PID controller is presented in Chapter 6.

Finally, a series of case studies are conducted for WBM and OBM in order to compare their performances. For both fluids, the pressure variations are studied for different rheological models, changes in density, gel strength and change in stresses. Subsequently, the case study progresses to introduction of a small moderate kick by using configuration tool program called *Wemod,* developed by IRIS (International research Institute of Stavanger).

This configuration tool uses a transient well flow model and zonal flowrate estimation. It is based on IRIS' well flow model to control drilling parameters and to generate simulated measurements to test and develop the control design. The framework is especially appropriate for solution of numerical problems derived from multiphase well flow modelling. The dynamic model uses partial differential equations describing, mass, momentum and energy balances using Navier – Strokes equations (presented on Chapter 4).

Further on, the research initiates a certain amount of kick size, that is circulation out and thus, the determination of kick tolerance is found for manual operation. Automated operation is then run with the same wellbore properties and the same influx size is created as for manual operation. Later, their performance and kick tolerance are measured and compared.

Since, the use of *Wemod* has been a crucial part of the case study, an introduction to the configuration program is given in appendix 1.

Background

1.1 Manage Pressure Drilling

MPD describes the process to control the annular pressure profile throughout the wellbore, where the focus and objectives are related to establishing a downhole pressure profile and to identify its environmental limits and accordingly, manage the hydraulic pressure profile.

The operation is simply to stretch or eliminate casing points and hence drill beyond the depth or pressure change for conventional method. In conventional method, the main concern is to contain formation fluid inflow during drilling. In overbalanced drilling (OBD) drilling fluids are exposed to atmospheric pressure to generate Equivalent Circulating Density (ECD), that leads to BHP in between the pore and the fracture pressure. MPD shown in yellow is beneficial to overcome drilling problems by the managing surface pressure to stabilize the BHP, by keeping ECD as close to pore pressure as possible.

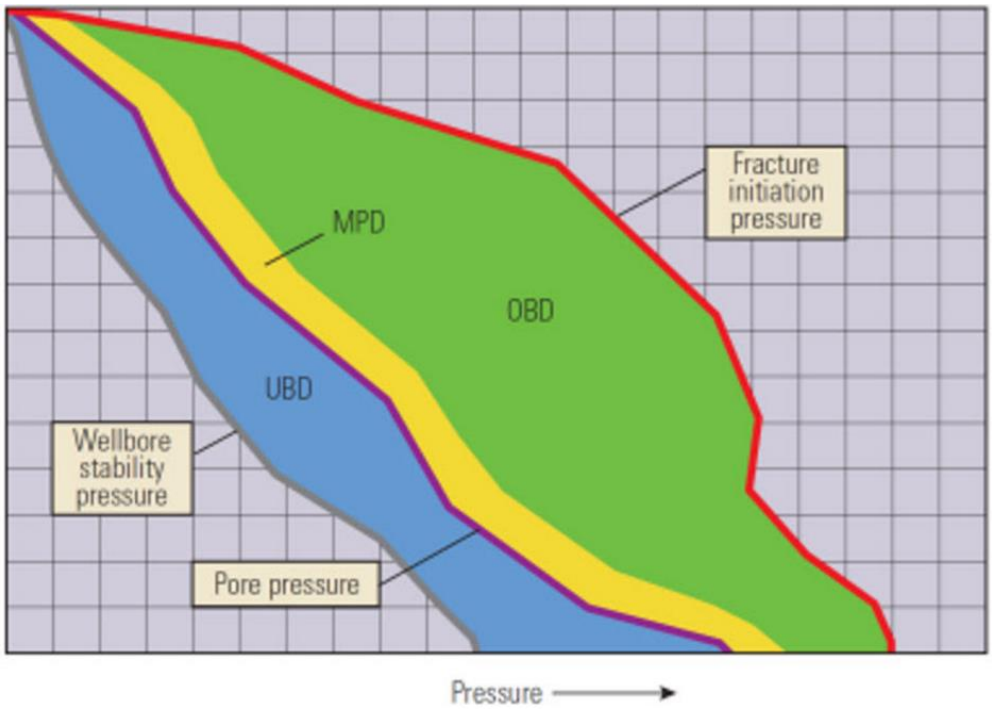

Figure 1.1.1 Shows the depth versus pressure for the different operations (underbalanced operation, MPD and overbalanced operation). Red line represents fracture pressure, purple shows the pore pressure and grey line shows the collapse pressure. (Glossary, 2017)

MPD allows thus to drill in narrow pore and fracture windows and has little margin for errors. If the BHP slightly falls beyond the pore pressure kick is generated, which may

result in (underground) blowout if it contains a large amount of gas. Kick detection at an early stage is therefore crucial design in a MPD operation. (Mahdianfar, 2016)

MPD also consists of the control of back-pressure by using a closed and pressurized mud return system such as a back-pressure pump. The intension is to avoid continuous influx of formation to surface. Some of the benefits of using MPD operations is summarized in the Table 1.1.1 (Toralde, 2011)

Removal of casing string
Kick detection method and control
Better hole cleaning
Improved formation stability / less formation damage
Less probability of lost returns
Immediate change in BHP during well control
Reservoir characterization

Table 2.1.1 Benefits of MPD operations

Benefits from MPD operation therefore reduces Non-Productive Time (NPT) and saves cost. (Dave Elliot, 2011)

1.2 Back-pressure in MPD

MPD process includes the control of back-pressure using a closed and pressurized mud return system. The main intention as aforementioned is to avoid continuous influx of formation to surface. Back-pressure is adjusted at the surface and controls annular pressure profile. It is also applied to compensate the annular friction losses during MPD operations.

MPD equipment and choke manifold can be used to continue circulation by increasing the back-pressure until the flow in and out are balanced. Then, influx may thus be circulated out.

1.3 Drilling Fluids

Drilling fluids have many intentions, with the main being transportation of drilling cuttings to the surface, maintain pressure balance and to cool and lubricate the drill string. There are many different types of drilling fluids in various phases, they can exist as a liquid, a mixture between liquid and gas or as gas. The two common drilling fluids are WBM and OBM. Their main composition is described in Figure 1.3.1 and 1.3.2. A more detail of different types of WBM and OBM is shown in Figure 1.3.3. (Helge Hodne, 2014)

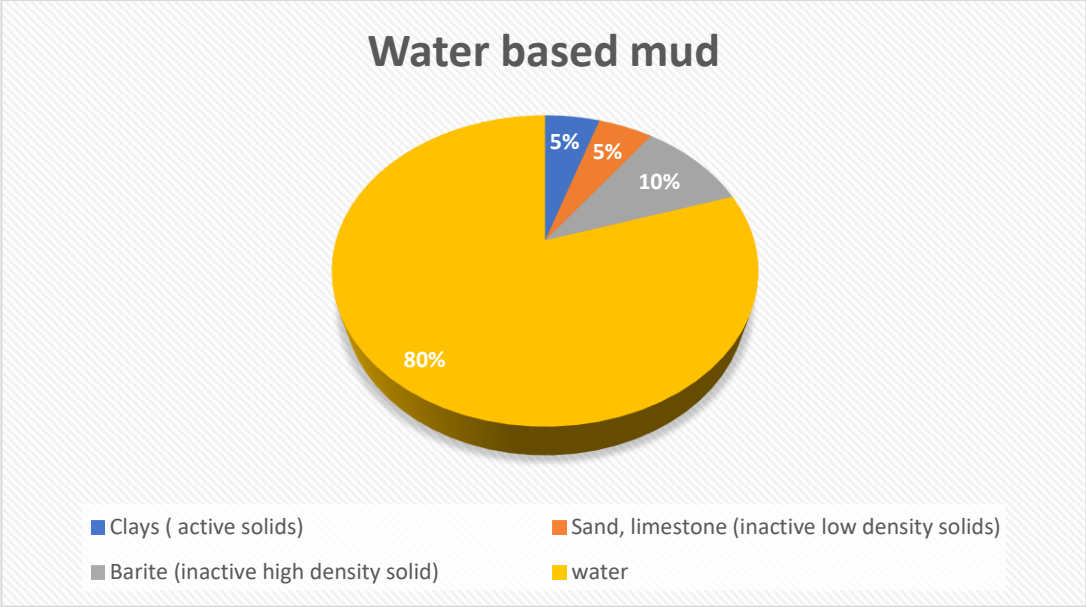

Figure 1.3.1 Example composition of WBM, showing the common additives used.

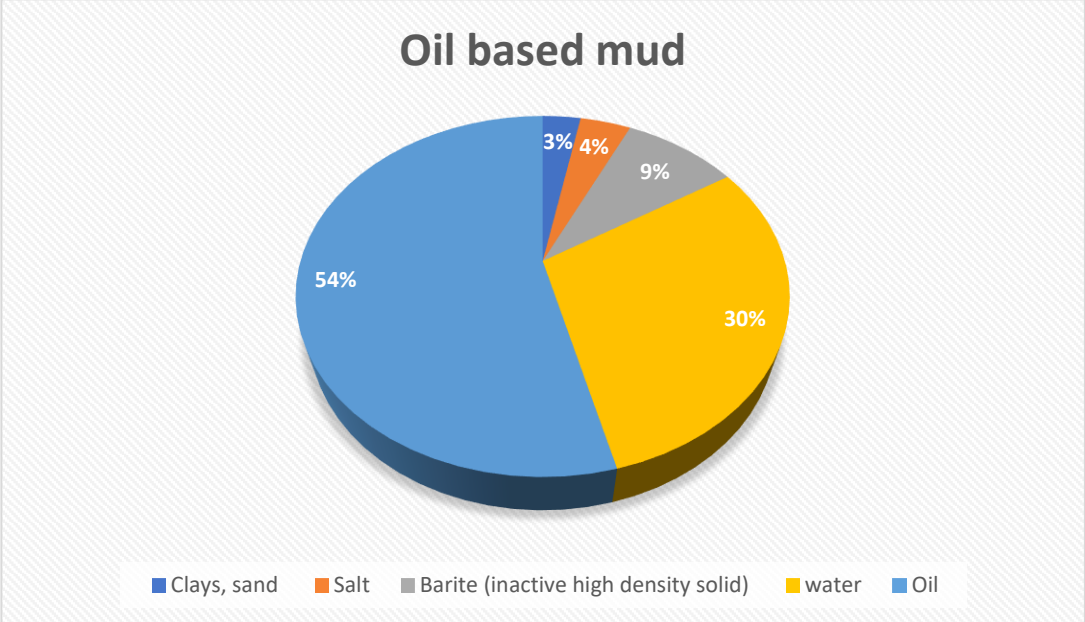

Figure 1.3.2 Example composition of OBM, showing the common additives used.

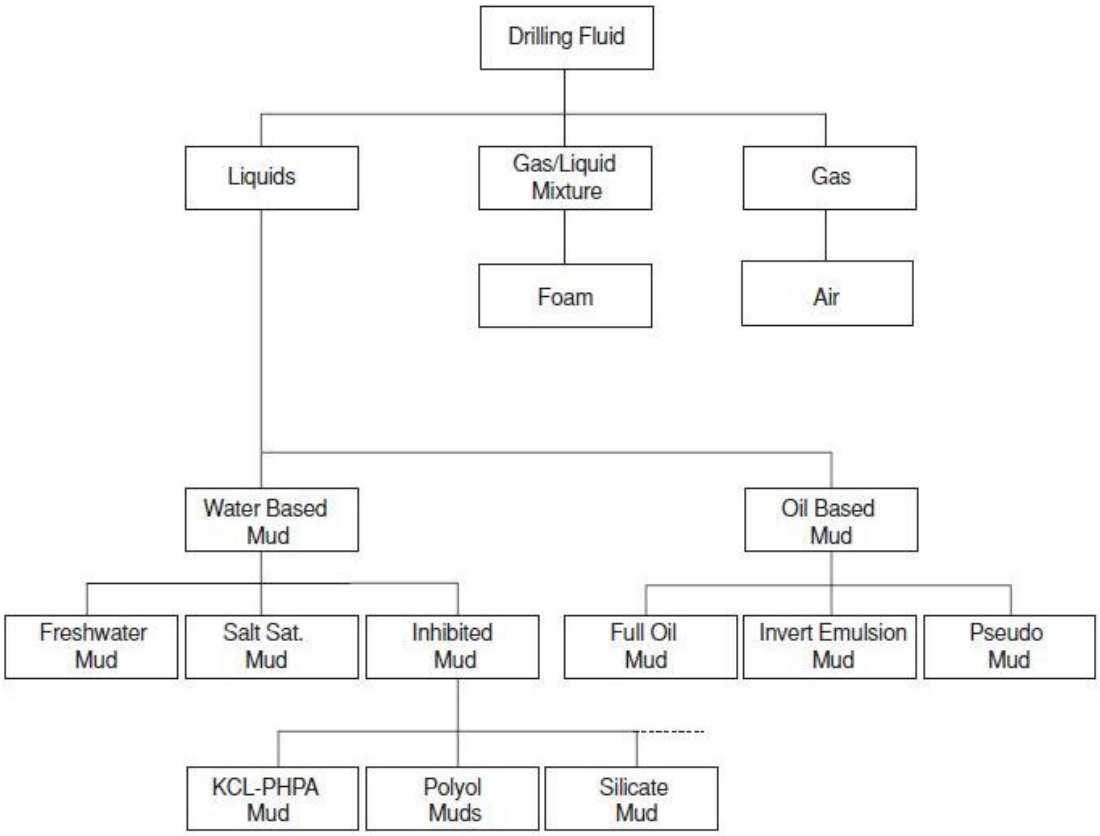

Figure 1.3.3 Represents different types of drilling fluid. (Effendi, 2015)

In drilling fluids, bentonite is usually added to control the viscosity and barite to give weight to the mud. There are other important parameters of drilling fluid such as gel strength, filter cake formation, sand content and pH.

Viscosity is defined as resistance to flow. One of the main reasons to include a viscous fluid in the borehole, is to transport cuttings to the surface. (Lulu, 2016)

Gel strength is the measurement of the suspension properties of a drilling fluid. Its main task is to keep the solids in the fluid in suspension, until they are transported out to the surface. For this to occur, solids must be mixed into a slurry with fluid and by that, are able to avoid settling. (Swensen, 2014)

The filter cake maintains the integrity of the borehole by stabilising the fluid and avoid loss of mud to the formation. A greater amount of sand in the fluid creates a thicker filter cake, which causes sand settling, wear on pump and create interference with casing setting and pipe movement. pH of the drilling fluid is also important as it is a confirmation of the water quality, and its change can indicate presence of certain minerals. (Robin, 2017)

Variables mentioned above are adjusted and tested in different conditions for different wells with different properties. This research paper will consider OBM and WBM with different densities and viscosities.

1.4 Pressure profiles

While drilling it is important to maintain the ECD in open hole section within the pressure limits so that the wellbore does not collapse or fracture at any point. The pressure profile also determines, how many casings that are required during drilling and at what depth casing shoe shall be placed. The pressure limits are fracture pressure and the pore pressure. BHP should stay within this working window, as shown in Figure 1.4.1. The density within the pressure limit enables wellbore stability.

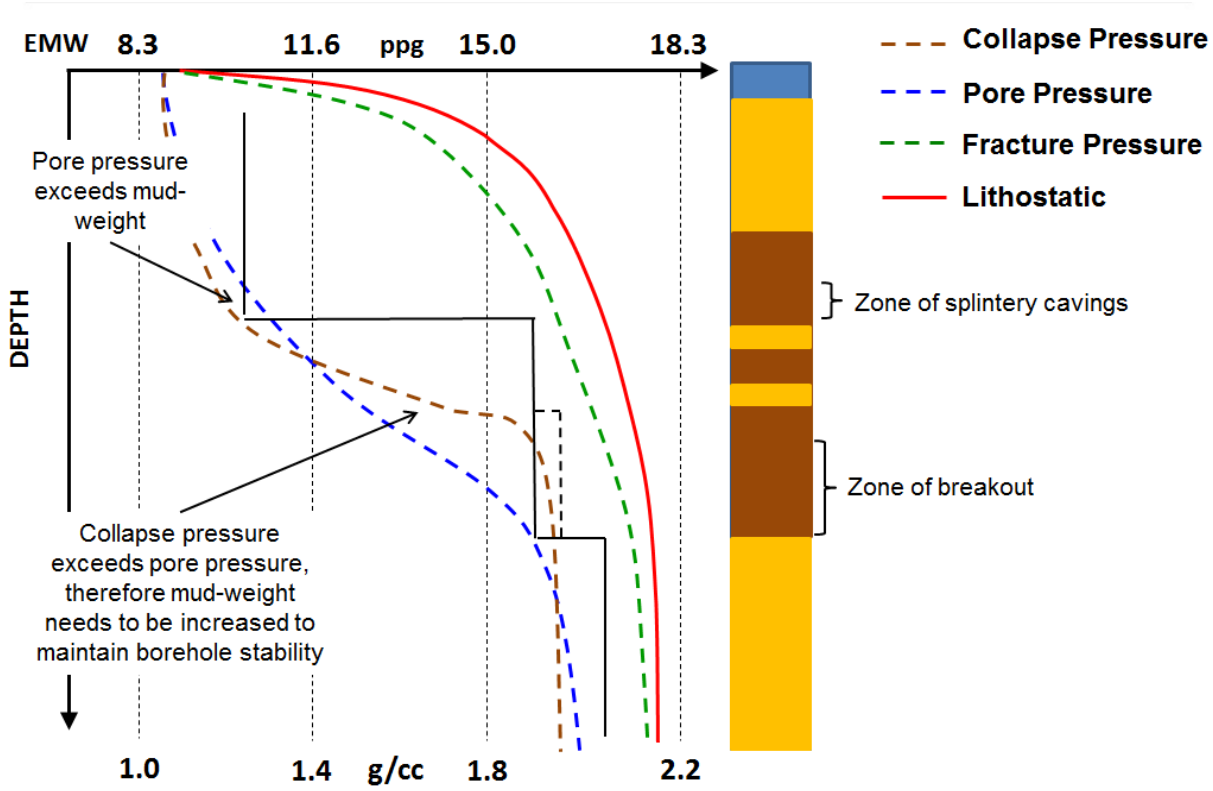

Figure 1.4.1 Shows example of ECD from Kvitebjørn 34/11-a-13. (Bashforth, 2016)

Lack of wellbore stability causes NPT in drilling wells. NPT may be caused by issues such as stuck pipe, increased torque and drag, collapse, pack off etc. Wellbore stability requires a geo-mechanical model, where stresses are calculated from the offset wells. These models are used to generate collapse pressure and fracture gradient.

Chapter 2: Fluids

2.1 Rheological models

2.11 Bingham Plastic

Bingham plastic rheological model is widely used in the oil industry and describes the flow characteristics of several mud types. It is used to describe a visco-plastic material that behaves like a rigid body at low stresses but flows as a viscous fluid at high stresses. Mathematically it is given by the following equation.

$$\tau = \tau_0 + PV(\gamma) \qquad Eq.2.11$$

Where,

τ	$shear\ stress$
τ_0	$Yield\ point\ (y - intercept)$
PV	$Plastic\ viscosity$
γ	$Shear\ rate$

Fluids in Bingham Plastic Model (BPM) show a linear relation between shear stress and shear rate after an initial shear stress has been reached, called the yield point, YP.

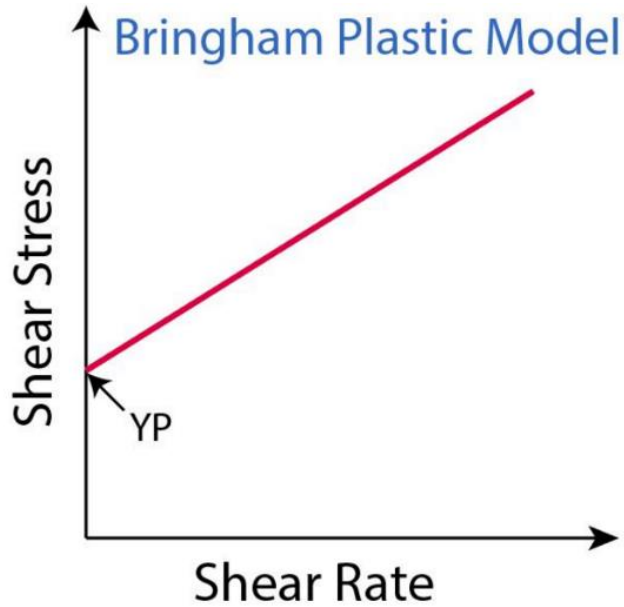

Figure 2.11.1 Shows the relationship between shear stress and shear rate for BPM. (Rachain J, 2010)

The slope of the curve is Plastic Viscosity (PV) and the y-intersection is the YP which is also known as the threshold stress. PV should ideally be as low as possible to enable fast drilling. High PV indicates a viscous base fluid by excess solids. Dilution can be conducted in order to lower PV. (Galindo-Rosales, 2017)

Furthermore, YP must be adequate to circulate cuttings out of borehole but also be under a certain point to avoid creating unnecessary pump pressure. YP is therefore adjusted, to match the model. BPM will be further used in case study in Chapter 7.1 and 7.2 to compare the pressure responses of OBM and WBM.

2.12 Power law

The power law model (PLM) can express many different fluids, which is mathematically given by

$$\tau = K(\gamma)^n \qquad Eq.2.12$$

K	$consistency\ index$
n	$flow\ behaviour\ index$

The division of fluids are distinguished by the flow index "n".

When,

- $n = 1$ Newtonian fluid (viscous forces proportional to strain rate)
- $n > 1$ shear thickening (viscosity increases with the rate of shear strain) (less common)
- $n < 1$ Pseudo plastic (more common)

The model can describe both shear thinning and shear thickening fluids. A fluid whose viscosity decreases as shear rate increases is known as a pseudo plastic fluid or shear thinning fluids. Shear thickening fluid is described as, shear viscosity that increases with increasing shear stress, also known as dilatant fluid. All these three fluid behaviours can be summarized in the Figure 2.12.1.

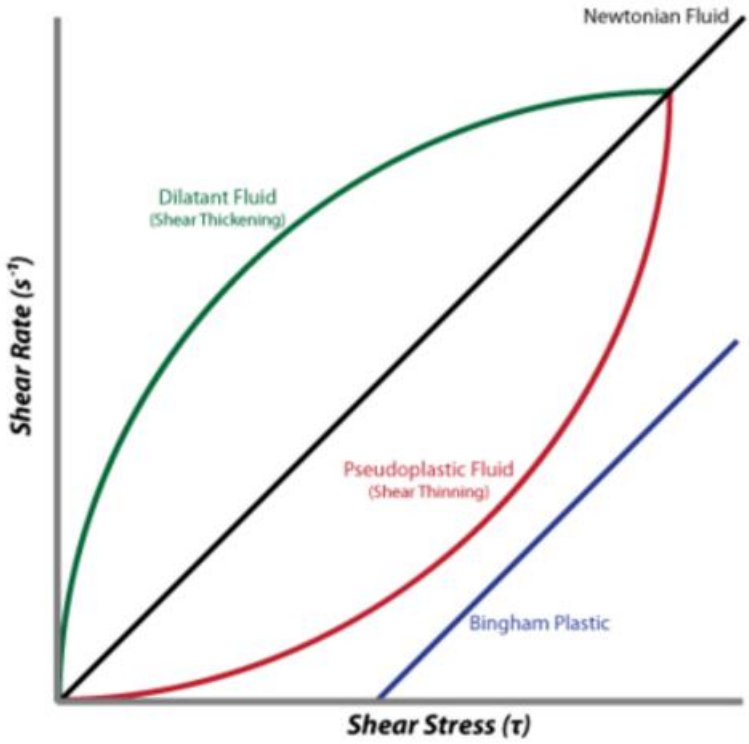

Figure 2.12.1 Shows the relationship between shear rate and shear stress for different fluids, that is, Bingham plastic, Newtonian fluid, shear thickening and shear thinning fluid. (Ryazanov, 2017)

PLM has been found to be able to describe the shear thinning behaviour of a variety of cementitious suspensions, however it does not predict any YP as done in BPM model. (Færgestad, 2016) The main drawback of this model is when shear rate is equal to zero, the shear stress is also zero, which does not describe drilling fluids. In drilling fluids, there exists a residual shear strength at zero shear rate. Water based polymer mud fluids are described well using this model. PLM as the BPM will be used in case study in Chapter 7.1 and 7.2, to compare the pressure responses of WBM and OBM respectively. (Ochoa, 2006), (Rao, 2014).

2.13 Robertsen Stiff model

The previous models suggested are not able to derive an explicit relation between shear rate and the volumetric flow rate in a pipe or an annulus. Therefore, a new model is suggested, Robertsen Stiff model (RSM), that will describe yield-pseudo plastics such as in drilling fluids and cement slurries. This model uses the PLM for calculations, which includes also a correction factor C:

Mathematically the model can be expressed as,

$$\tau = A(\gamma + C)^B \qquad Eq.2.13$$

Where,

A	$Equivalent\ to\ Power\ law\ parameter\ K$
B	$Equivalent\ to\ Power\ law\ parameter\ n$
C	$Correction\ factor\ of\ shear\ rate$

The three-parameter model has been proven to describe the behaviour of drilling fluids with bentonite. The model has also successfully been used for cement slurries.

When, $B = 1$ and $C \neq 0$ the fluid is described by BPM. The representation of the yield stress, that is, when the shear rate is equal to zero, can be shown mathematically as,

$$\tau_0 = A * C^B \qquad Eq.2.14$$

The model expresses another simple equation that describe explicit relationships between the wall shear rate and the volumetric flow rate in pipe or annulus, which is essentially derived from the Equation 2.14.

$$\tau = A\,\gamma \qquad Eq.2.15$$

Equation 2.15 can be derived when $B = 1$ and $C = 0$, which is the condition for Newtonian fluids. When $B \neq 1$ and $C = 0$ the fluid is represented by the PLM. Therefore, A and B parameters are similar to the parameters described in PLM. The correction factor C is represented differently, then done in yield stress of the BPM.

RSM describes the parameter C to be a correction to shear rate rather than shear stress. The effective shear rate is given by, $(\gamma + C)$ or shear rate required for power law fluid to produce similar shear stress. Further relationships derived, has been proven to be the difference between PLM and the suggested RSM.

The correction factor, C, can be further expressed by,

$$C = \frac{\gamma_{min} * \gamma_{max} - \overline{\gamma^2}}{2\overline{\gamma^2} - \gamma_{min} - \gamma_{max}} \qquad Eq.2.16$$

Where,

γ_{min}	$minimum\ shear\ rate\ value$
γ_{max}	$maximum\ shear\ rate\ value$
$\bar{\gamma}$	$shear\ rate\ giving\ \bar{r}, (average\ shear\ rate)$

One of the methods to determine A and B represented in the Equation 2.13, is to take the logarithm on both side and plot $\tau\ versus\ (\gamma + C)$.

$$\log \tau = \log A + B \log\ (\gamma + C) \qquad Eq.2.17$$

A will then represent the y-intercept when $(\gamma + C) = 1$, and B will be the gradient of the straight line.

Experiments were conducted, by comparing to the Fann-data, between two different fluid types to inspect which of the three-rheological model best represent the fluid. Their details are given in the table, with their comparison of the graphical result in Figure 2.14.

TABLE 1 — RESULTS FOR FLUID A

Shear Rate (sec^{-1})	Measured Shear Stress (lb/100 sq ft)	Proposed Model Shear Stress (lb/100 sq ft)	Power Law Shear Stress (lb/100 sq ft)	Bingham Shear Stress (lb/100 sq ft)	Proposed Model Percent Error	Power Law Percent Error	Bingham Percent Error
1,022.	17.0	16.4	15.1	18.0	-3.59	-10.95	5.92
511.	12.0	12.3	12.2	11.2	2.32	1.39	-6.97
340.7	10.0	10.4	10.7	8.9	3.96	7.07	-11.17
170.3	8.0	7.9	8.6	6.6	-1.52	7.56	-17.49
10.22	3.5	3.4	3.5	4.5	-3.37	1.28	27.34
5.11	3.0	3.1	2.8	4.4	2.48	-5.03	46.28
			Average error, percent:		±2.87	±5.55	±19.20
			Standard deviation:		0.92	3.78	15.45

TABLE 2 — RESULTS FOR FLUID B

Shear Rate (sec^{-1})	Measured Shear Stress (lb/100 sq ft)	Proposed Model Shear Stress (lb/100 sq ft)	Power Law Shear Stress (lb/100 sq ft)	Bingham Shear Stress (lb/100 sq ft)	Proposed Model Percent Error	Power Law Percent Error	Bingham Percent Error
1,022.	68.0	68.5	53.6	69.3	0.71	-21.14	1.98
511.	42.0	43.5	43.3	41.5	3.50	2.99	-1.23
340.7	34.0	34.1	38.1	32.2	0.28	12.20	-5.31
170.3	26.0	23.8	30.8	22.9	-8.55	18.35	-11.91
10.22	12.0	12.5	12.9	14.2	3.99	7.21	18.13
5.11	12.0	12.1	10.4	13.9	0.59	-13.52	15.81
			Average error, percent:		±2.94	±12.57	±9.06
			Standard deviation:		3.18	6.76	7.23

Figure 2.13.1 Shows the properties of the two different fluid types, including error for different rheological model. (R.E Robertsen, 1976)

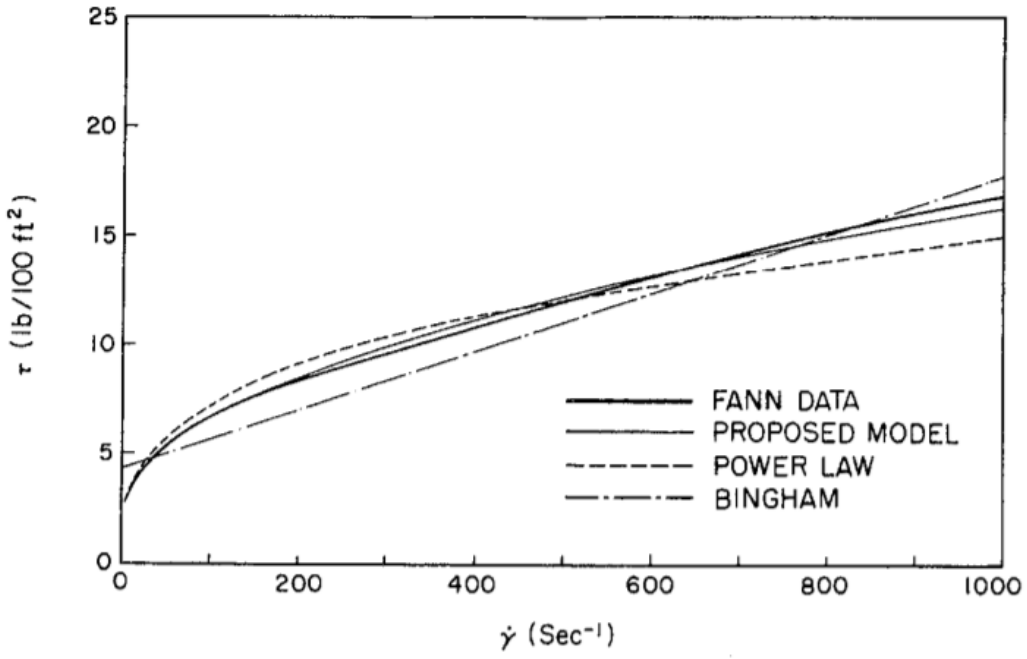

Figure 2.13.2 Represents the comparison of rheological model for fluid type A, represented in figure 2.13.1. (R.E Robertsen, 1976)

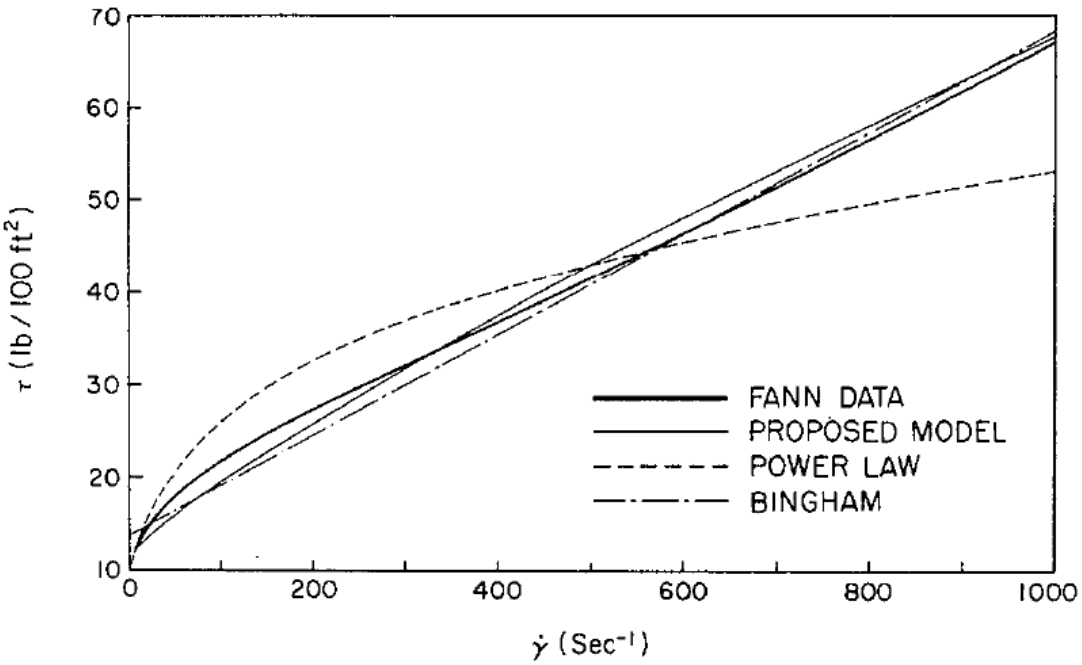

Figure 2.13.3 Represents the comparison of rheological model for fluid type B, shown in figure 2.13.1. (R.E Robertsen, 1976)

The conclusion from these graphs shows that the average error of the RSM was much less than that of BSM and PLM. Therefore, the RSM gives a decent estimate of the shear stresses and the effective viscosities for these fluids. Drilling fluid and cement slurries are pseudo-plastic fluids, which are well characterized by the model. RSM was also able to derive explicit relation between shear rate and volumetric flow rate for pipe or annulus. As seen from Figure 2.13.2 and 2.13.3, the RS model gives a better estimation of drilling fluids and will therefore be used in case study, to form a basis to compare other rheological models. It will hence also be used in Chapter 7, in kick scenario for both manual and automated operation.

2.2 HPHT models

The properties of rheological model for drilling fluids are normally approximated to be independent of pressure and temperature, which is good approximation in several cases. However, in wells where the temperature and pressure are above normal (temperature > 150 °C, pressure > 685 bar), this approximation no longer qualifies. The basic model is qualified for shallow wells, where the temperature changes are minimum, and wells where the difference between the pore pressure and fracture pressure is large.

There are also wells with small margins between pore and fracture pressure, that requires to be analysed regarding the temperature and pressure changes, to evaluate wellbore hydraulics and kick probability. Many wells in the North Sea (NS) have such well control problems.

The rheological properties of drilling mud at HPHT conditions may be measured before drilling the section, during pre-planning. These pressure and temperature dependencies of HPHT mud have been studied and are used when real-time data are not available.

The relation between HPHT effects and rheology can be studied through correlation models. One of the theoretical mathematical models presented for BPM and Casson's model is shown as,

$$f(p,T) = \exp\left(\frac{A + (BT + C)p}{T}\right) \qquad Eq.\,2.21$$

Where,

A	$Constant \ \ (°K)$
B	$Constant\ (1/Pa)$
C	$Constant\ (°K/Pa)$
T	$Temperature\ (°C)$
p	$Pressure\ (Pa)$
f	$A\ multiplicative\ factor\ of\ rheological\ model\ of\ one\ of\ the\ parameters\ (\mu, PV, \tau)$

A, B and C represent constants that does not depend on pressure or temperature but rather on the composition of the drilling fluid. These constants show different values for different rheological parameters due to substantial changes in pressure and temperature dependencies of shear rates. Equation 2.21 matches the two rheological models, BPM and Casson's model as mentioned above. However, it does not represent a well fitted solution for more precise rheological model, such as the RSM. One of the reasons is the correlations of the three-parameter model that makes it impossible to extract the accurate pressure and temperature dependencies due to measurement uncertainties. (Gravdal, 2011)

A new model was proposed where the shear stress has been multiplied by a factor that is a function of pressure, temperature and shear rate, for RS model.

$$\tau_0 * f(p,T,\gamma) = A(\gamma + C)^B \qquad Eq.2.22$$

The coefficient factors are adjusted to relevant shear rate and shear stress without the extraction of rheological parameters. The function allows for different pressure and temperature scenarios at both high and low shear rates. The main advantage with the function f is that correlation of rheological parameters are optimized. (Mahmood Amani, 2012)

The correlation based models are based on HPHT mud used in NS. These models are presented for WBM and OBM, and have been used in a fully discretized dynamical model in order to determine pressure at any depth in the well. As mentioned before, rheology must be measured beforehand for mud at HPHT conditions. If these data are not available, theoretical or empirical predictive models of temperature and pressure can be utilized.

The correlation model is shown for RS model, for high and low shear rates:

$$f(p,T,\gamma) = e^{g_1(p,T)}\gamma + e^{g_2(p,T)} \qquad Eq.2.23$$

$g_1(p,T)$	*Sum of linear, bilinear, quadratic terms in pressure and temperature and a constant term. Coefficient are found from best fit equation by the means of measured data.*
$g_2(p,T)$	
$f(p,T,\gamma)$	*A factor that multiplies shear stress at standard conditions at true shear rate.*

ECD must be determined correctly in HPHT conditions by the means of correct pressure and temperature dependent rheology and density. This rheology can be found from laboratory measurements at HPHT conditions or from development of a model for similar mud conditions. Prediction of ECD requires information about the temperature profile in the annulus, since rheology and density are both a function of temperature. The result will

be a density and viscosity profile, where the total ECD can be found. ECD given at a certain depth can be calculated using the following equation,

$$ECD = \frac{1}{TVD}\left(\int_0^{MD} \rho(z)dz + \frac{1}{g}\int_0^{MD}\left(\frac{dP}{dz}\right)_f dz\right) \qquad Eq.2.24$$

Where,

MD	$Measured\ depth, (\ m)$
TVD	$True\ vertical\ depth, (\ m)$
f	$Pressure\ and\ temperature\ dependent\ factor$
g	$Gravitational\ constant, \left(\frac{m}{s^2}\right)$
z	$Position\ along\ the\ well\ trajectory, (m)$
ρ	$Density\ of\ drilling\ fluid\ (p,T\ ), (\ s.g)$
P	$Pressure, (Pa)$

During the transient model, the temperature and pressure will change as time and position changes. The temperature profile is dependent of several parameters such as mud thermos physical properties, flow rate, well geometry and production history. These parameters are measured during drilling, and fed into a simulator which creates HPHT models. Importance of these time dependent effects are shown on the graphs below, from NS wells. Figure 2.2.1 shows the temperature profile for OBM and WBM. The temperature changes after circulation for a few hours due to the effect of heat transfer, heat due to friction, and the heat capacity for the different fluid types.

The Figure 2.2.2 shows the BHP changes during circulation as a function of time. It describes long time pressure variations. More detail information about HTHP model can be found in (R.Rommetveit, 1997).

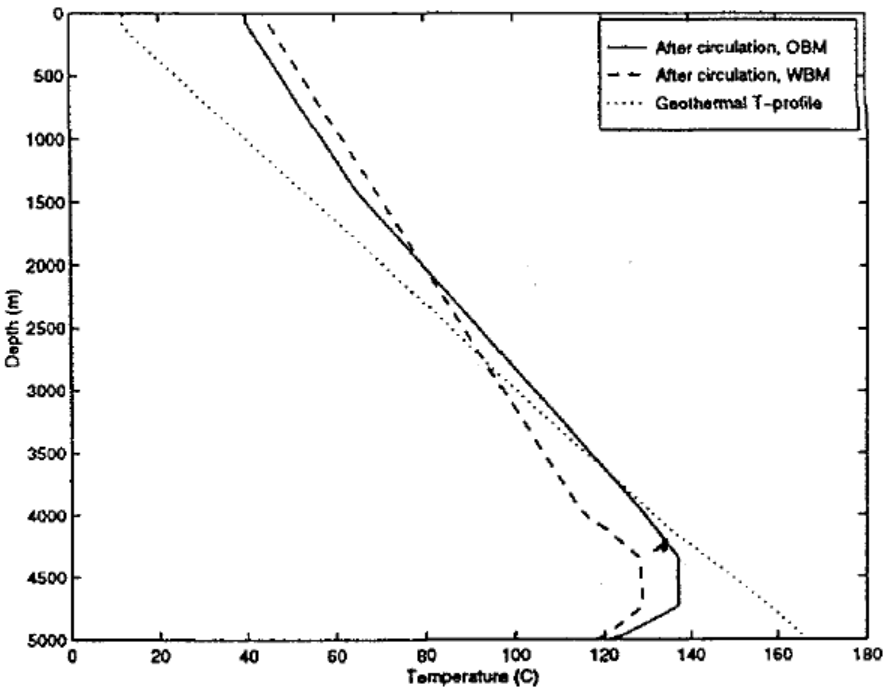

Figure 2.2.1 Shows the temperature profiles used for ECD calculations. Circulation temperature profile is calculated by the means of the simulator PRESMOD (R.Rommetveit, 1997).

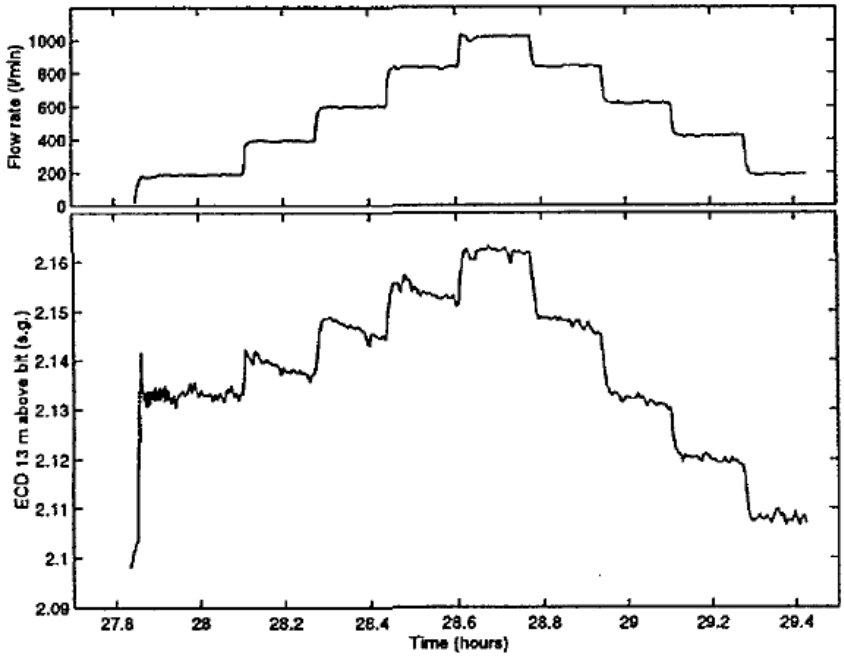

Figure 2.2.2 Measurement of BHP during a circulation sweep with bit at 5000 m in HPHT well in the North Sea. (R.Rommetveit, 1997)

A precise prediction of ECD model requires the knowledge of temperature and pressure profile, and the dependency of density, viscosity and gel strength of the mud. A proper understanding of pressure and temperature changes with respect to time will aid to

understand the changes of BHP in HPHT wells. Accuracy of ECD is very important in such cases to avoid collapse or fracture and to stay within the safe operational window between pore and fracture pressure. The RS-HPHT model will be further used in case study in Chapter 7.1 to 7.4, pre-set into the configuration tool Wemod.

2.3 Water density model

For proper optimization of production, the knowledge of reservoir fluid properties is essential. Properties such as viscosity, gas solubility, formation volume factor of formation water are examples of some of the parameters. Since, the study involved in this work, involves an influx (which is assumed for worst case to be of pure gas), may be pure gas or gas condensate.

Dodson and Standing explain the gas in water solutions and mixtures.

"*A small amount of dissolved gas increases the compressibility of water with Gas to water ratio in water containing dissolved gases*." (Cooper, 2010)

Compressibility of water

Compressibility of water can be estimated if the pressure, temperature and the GWR are known. In a case of under saturated water, Dodson and Standing explain a method to determine the compressibility of water. The first step involves determination of compressibility with the help of Figure 2.3.1.

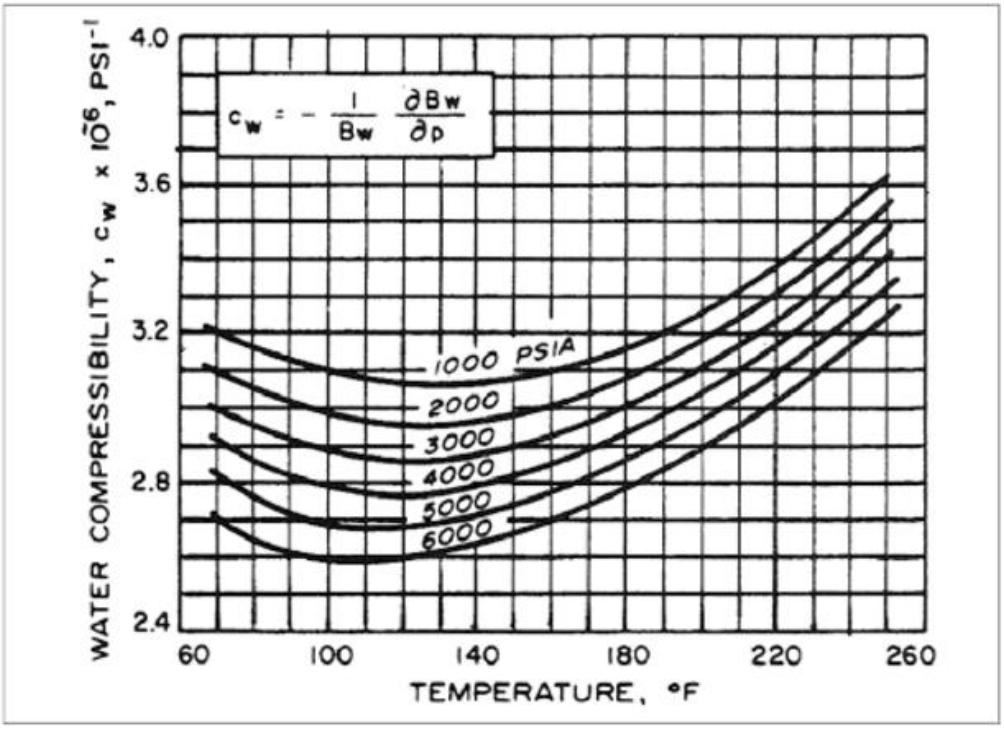

Figure 2.3.1 Shows water compressibility versus temperature presented by Dodson and Standing. This plot can be used only if reservoir pressure and temperature are known. (Abdus Satter, 2007)

The compressibility from this curve is calculated using the following equation,

$$c_w = \frac{1}{\overline{B_w}} \frac{\partial B_w}{\partial P} \qquad Eq.2.31$$

Where,

$\overline{B_w}$	$Average\ water\ formation\ volume\ factor$
∂B_w	$Net\ difference\ in\ water\ formation\ volume\ factor$
∂P	$Net\ difference\ in\ pressure$

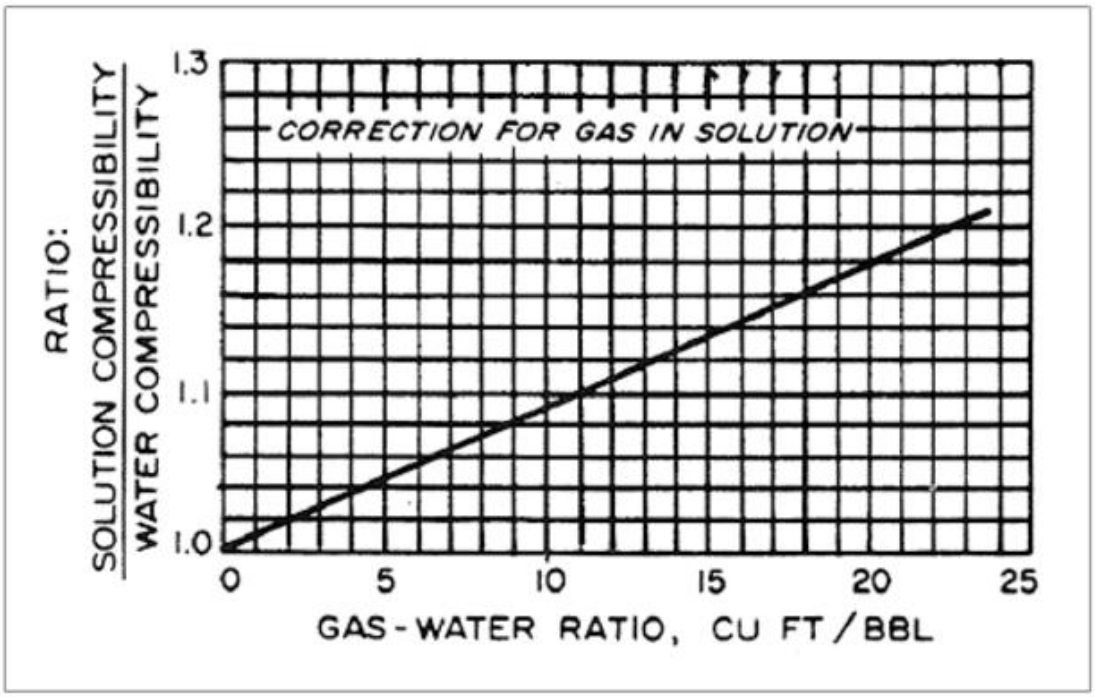

Figure 2.3.2 Represents correction factor for dissolved gas in water presented by Dodsen and Standing (Abdus Satter, 2007).

The second step is to find a correction factor for the compressibility of water. Figure 2.3.2 can be used to determine this value, in case of dissolved gas in water. To determine the correction-factor the Gas Water Ratio (GWR) must be known, as well as the ratio of solution compressibility divided by the water compressibility. Such corrections are more likely to be required in HPHT wells. (Y.A. Hazov, 1993)

Compressibility of formation water

Natural gas shows limited solubility in formation water. At first the computation starts with the solution of GWR for pure water, followed by salinity correction factor. Dodson and Standings correlations is able to estimate the compressibility of formation water if the temperature, pressure and salinity are known downhole. (Jr, 1989)

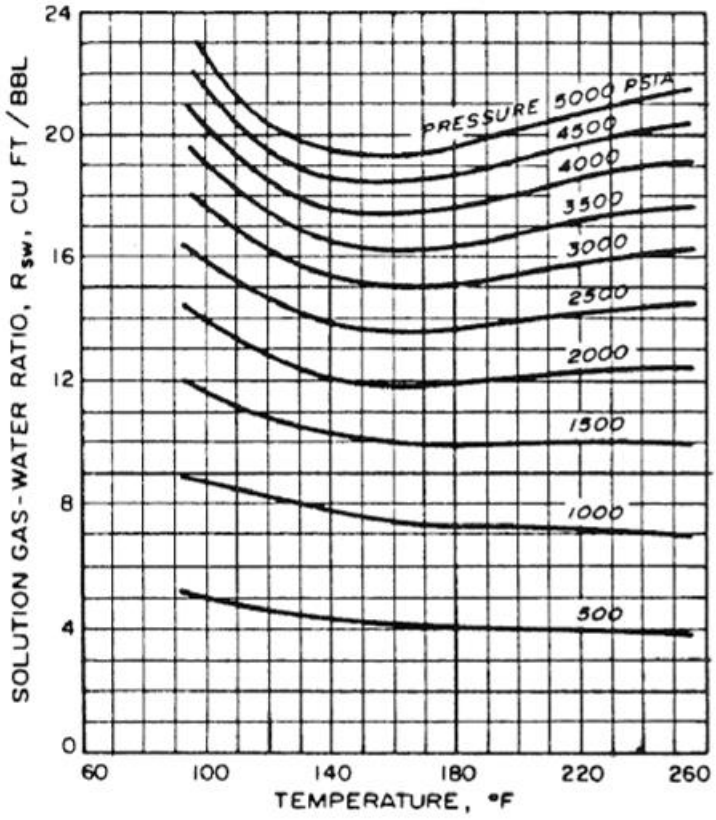

Figure 2.3.3 Solubility of natural gas in water versus temperature and pressure. (Abdus Satter, 2007)

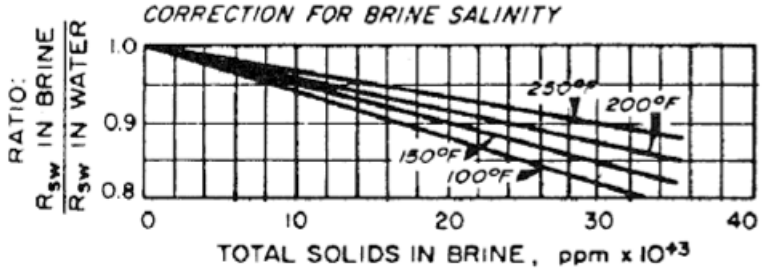

Figure 2.3.4 correction of gas solubility for solids content. (Abdus Satter, 2007)

In conclusion, the compressibility of water and formation water are important to estimate the non-linear pressure profile created due to these forces. They have special importance in HPHT conditions as this research will investigate such condition in Chapter 7.4. The pressure increase is influenced by free gas, for non-linear pressure profile. Whereas, for linear profiles the free gas is compressed. As for dissolved gas, the specific compressibility of water based fluid changes by a small amount.

Subsequently, the compressibility of water depends on many factors such as the reservoir pressure, dissolved gas water ratio and temperature. Dodson and Standing method is useful

in a case of under saturated water, where the compressibility can be estimated as the downhole pressure and temperature conditions are known.

2.4 Gel strength

Gel strength is a parameter measured with a viscometer by varying periods of static condition (normally 10sec, 10 minutes and 30 minutes). The readings explain the capability of drilling fluid to suspend particles at rest, also called YP in lbs per 100 ft^2. It is of special importance when drilling in long horizontal wells, due to the difficulty to transport cuttings. Figure 2.4.1 shows the behaviour of the gel strength versus MW for initial gel at 10 seconds and the gel formed after 10 minutes.

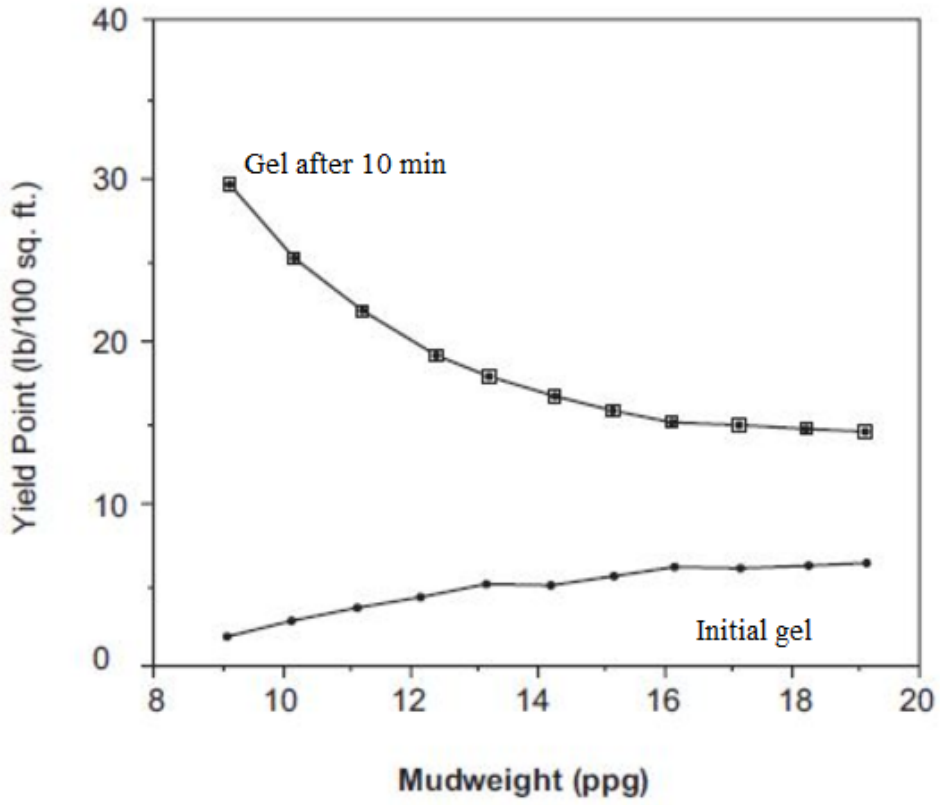

Figure 1.4.1 Shows the range of the YP for a certain MW after 10 seconds and 10 minutes. (Affendi, 2015)

Most of the drilling fluids used today are considered to be thixotropic, meaning, when the drilling fluid is static condition, it starts to gel. Gelling has many advantages such as suspension of cuttings during connections or when operation is suspended. Drilling fluid must properly suspend but not gel completely under static conditions. A proper suspension of particles leads to effective hole cleaning and proper cuttings removal and thus maintain a proper ROP.

Subsequently, gel strength has a significant importance to drill effectively and efficiently. However, it requires a compromise, it ought to be controlled because it is related to pressure to break its gels during reestablishment of circulation. In cases where the gel strength is too high, surface retention occurs, which creates problematic solids control or result in pressure losses, fractures and fluid losses. If, however, the gel strength is too low, the cuttings will not be suspended sufficiently and result is settling of particles that ultimately blocks circulation and result in stuck pipe incident. A further chain of problematic scenario occurs as a result of stuck pipe incident.

Since, the main focus of this research will be on horizontal long well drilling, it is important to address the proper gel strength regulation. In such long wells, pumps are often shut down during connections, and during pumping the flowrate is not constant in the whole borehole. When the fluid flows and grabs a hold of cuttings, the gel strength should suspend particles for minor flow. So, that all the cuttings are able to be transported out of the borehole.

The optimum gel strength is required to form at a high rate and remain persistence. Consequential gel structures will also be easily broken, when the drill string starts to rotate and when the pump initiates. On the other hand, in vertical sections lower gel strength are sufficient to suspend the particles mainly due to high annular velocity and lower active solid content.

The effect of gel strength is investigated in Chapter 7.1 and 7.2 for WBM and OBM.

2.5 OWR

OWR is a proportion that explains the fraction of oil based fluid compared to the water in the mud. Specifically, the ratio of oil versus water are both presented in liquid phase. It is calculated by using the following equation,

$$\%\ oil\ in\ liquid\ phase = \frac{volume\ oil\ in\ \% \times 100}{volume\ oil\ in\ \% + volume\ water\ in\ \%} \qquad Eq.\ 2.51$$

$$\%\ water\ in\ liquid\ phase = \frac{volume\ water\ in\ \% \times 100}{volume\ oil\ in\ \% + volume\ water\ in\ \%} \qquad Eq.\ 2.52$$

$$OWR = \frac{\%\ oil\ in\ liquid\ phase}{\%\ water\ in\ liquid\ phase} \qquad Eq.\ 2.53$$

Water and solid phases are both present in the case of OBM, increasing the OWR will require more oil to maintain the same rheology. The effect is seen when the mud density is increased. For WBM the typical value of OWR is equal to zero due to the lack of oil.

In case study the effect of OWR will be studied as the mud type WBM and OBM will be used to investigate the pressure responses. The OBM will have a OWR of around 4.5 whereas, the WBM it will be set to zero.

Chapter 3: Kick tolerance

Chapter 3.1 Definition of kick tolerance

There are many different definitions and calculations in the industry of kick tolerance to withstand well control incidents. Some methods say that kick tolerance is the maximum equivalent MW increase permitted by using formation integrity test at the shoe, while others say maximum kick volume that can be circulated out safely.

The definition given in this research is given particularly for MPD operation and states that, kick tolerance is,

"*The maximum influx volume that can be safely circulated out of the well"*. (R.E Robertsen, 1976)

The multiphase flow model given by IRIS in Chapter 4, takes into account transient state of the well and is able to provide a more accurate determination of kick tolerance.

MPD method have an improved method for kick detection and response time by the means of Rotating Circulating Device (RCD), which permits the use of back-pressure and Coriolis-meter, placed in return-line, to measure flow out. These methods affect the kick tolerance calculations. Correct placement of this devices enables quicker kick detection, by monitoring the flowrate in and out of the well. MPD technique also increases control of the BHP, in case of an influx. This is achieved by closing the choke valve on the return line and starting the back-pressure pump allowing BHP to be increased. (Helio Santos, 2012)

The maximum allowable surface pressure (MASP) can be determined using RCD pressure rating. Further analysis using MASP is done in section 5.2.

Equation 3.11 is based on steady-state model and can be used to find the maximum drilling depths, and resulting casing points if parameters such as pore pressure, fracture pressure, hole size and the mud density are known. The maximum kick volume and drilling depth can be shown with calculation by the means of MPD methods:

$$V_{max} = \left[\frac{S(F-\rho_m) - DT - \frac{P_{WH}}{0.052}}{(\rho_m - \rho_i)}\right] C_a \qquad Eq.3.11$$

$$D_{max} = \frac{S(F - \rho_m) - \frac{V_{max}}{C_a(\rho_m - \rho_i)} - \frac{P_{WH}}{0.052}}{I} \qquad Eq.3.12$$

Where,

V_{max}	$Maximum\ acceptable\ volume\ (ft^3)$
H_K	$Kick\ height\ in\ TVD\ (ft)$
C_a	$Annular\ capacity\ of\ wellbore\ (bbl/ft)$
S	$Shoe\ depth\ in\ TVD\ (ft)$
F	$Fracture\ gradient\ at\ shoe\ depth\ (ppg)$
I	$Kick\ intensity\ (ppg)$
D	$Total\ hole\ section\ depth\ when\ influx\ is\ taken.\ in\ TVD\ (ft)$
ρ_m	$Density\ of\ mud\ (ppg)$
ρ_i	$Influx\ density\ (ppg)$
P_{WH}	$wellhead\ pressure, psi$
D_{max}	$The\ drilled\ depth\ where\ kick\ tolerance\ criteria\ is\ satisfied\ (ft)$

Thus, the main advantage of using MPD techniques is to safely reduce kick tolerance criteria and to be able to drill longer, even when the margin between the pore pressure and fracture pressure gradient is small. A proper design method is essential to be able to drill longer using MPD due to casing loads.

Chapter 3.2 Kick detection method

Formation gas or fluid is known to enter the wellbore in a case where the wellbore pressure at a certain depth is less than the formation pressure. This is commonly denoted as a kick occurrence. Kick will end in a blowout, if it is not properly controlled and brings enormous harm to the environment, employers and damages the reservoir.

Kick can occur in many cases, such as when drilling through a gas bearing zone with a large formation pressure, swabbing effect, insufficient MW, lost circulation and improper hole fill ups.

Normally, several accurate flow measurement equipment's are used to get an early kick indication, as explained in section 3.1. However, the flow meters such as Coriolis meter cannot be used on high pressure inlet side of the well and flow detection is complicated due to gas solubility. A precise control of downhole pressure is essential in case of gas influx. Equipment such as wired drill pipe (WDP) can be used for this manner.

An approach for early kick detection method is presented from a research paper by SPE (society of petroleum engineers) . The approach shown in the paper is done with the aid of Coriolis flow meter, where the flowrate in and out were closely monitored. The main and easiest approach to monitor a kick occurrence is to look at the flow-out of the well, if it is greater than flow-in, then formation fluids enter the wellbore. However, in such case wellbore pressure must not be decreasing, which may occur when the mud pumps decrease. In those cases, the mud return may rise due to the effect of closing fractures. In true kick scenarios, the fluid gain at the surface occurs at a higher rate while the flow out and flow in show a significant difference.

As mentioned earlier the downhole pressure profile is necessary to provide an additional indication of kick by using the WDP. Variations in such profiles is given with the use of sensors that provide gas detection and enable us to find the location of influx. The sensors work best under vertical sections of the well due to gravitational dominant flow. Greater variations in pressure profiles are seen in cases where the influx length in higher at narrow annulus. At horizontal sections of the well however, the pressure sensors do not work as accurately because of the minor pressure variations.

If OBM is used in the well gas may dissolve in the mud, and make kick detection even more challenging due to even smaller pressure variations. In cases of small influxes, it is more beneficial to determine the depth where influx is located. Pit gain and the pump pressure can also be monitored to verify influx.

The suggested algorithm for early kick detection includes three main emergency levels,

1. $Level\ 1 - \ flow\ out > \ flow\ in$
2. $Level\ 2 - \ Annular\ pressure\ profile\ (when\ available)$
3. $Level\ 3 - \ pit\ gain\ variations$

The suggested algorithm can also be used for conventional operations as well as MPD operations.

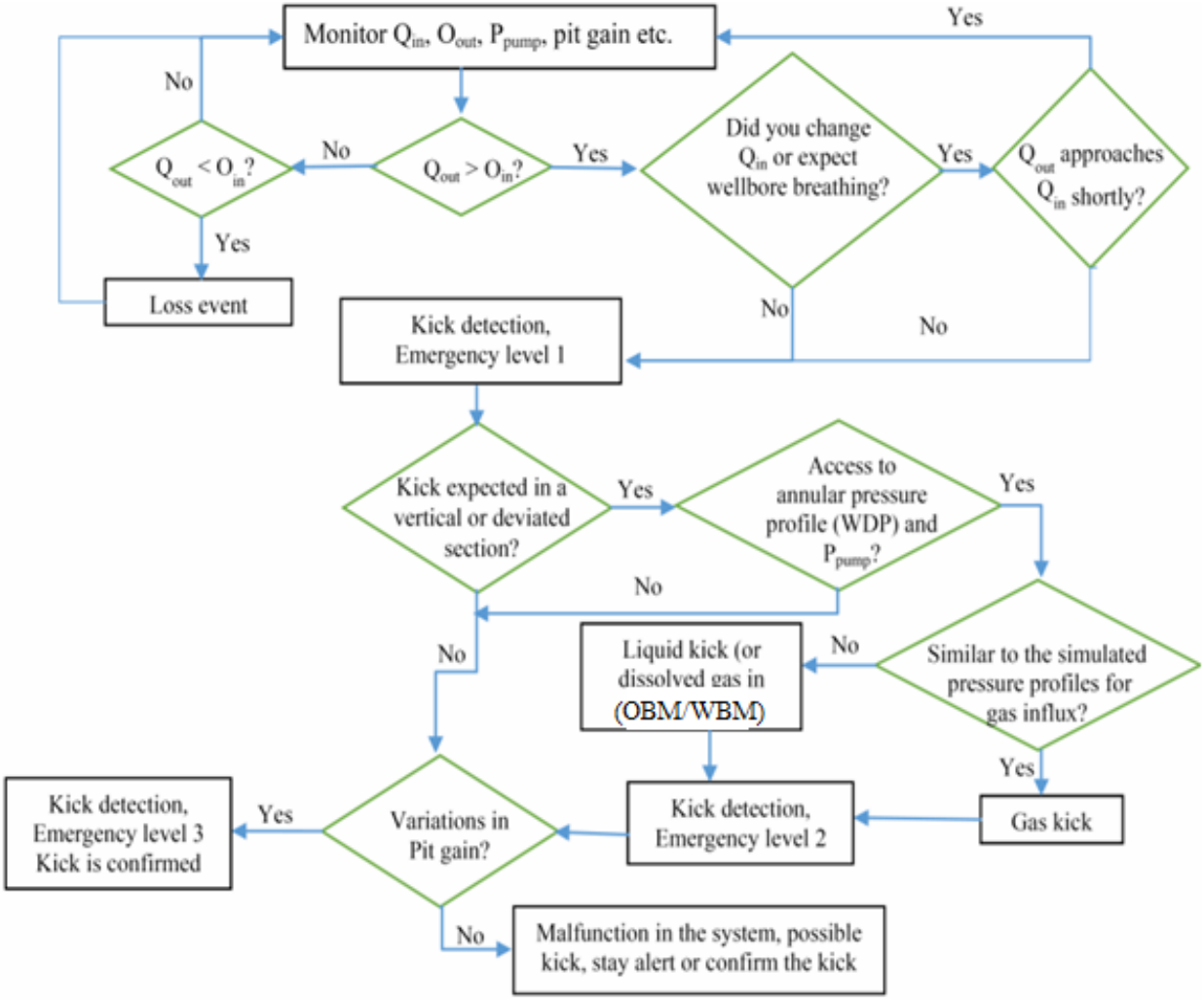

Figure 3.2.1 Shows the procedure to detect influx at an early stage (Ali Karimi Vajargah, 2014).

Where,

Q_{in}	*Flow rate in*
Q_{out}	*Flow rate out*
P_{pump}	*Pump pressure*
WDP	*Annular pressure profile*

Chapter 3.3 Determine kick size

There are several ways to respond in case of a kick scenario and selecting of the best possible decision is dependent on several factors such as the wellbore geometry, choice of drilling fluid, flow rate, size of influx, TVD and formation balance. All of these parameters vary from well to well, and therefore, a constant value or threshold cannot be stated.

A study of this matter was conducted by Karimi Vajagrah et al. (Z.Ma A. V., 2016), where the response was made by using simulation results by the means of graphs and tables.

The first step to consider when an influx is confirmed is to determine how large it is. This can be done by making a graph or generating a table as suggested by Karimi Vajagrah. One of the methods, is to generate a graph of casing peak pressure versus influx size, which again is limited by MASP and the lowest fracture pressure. These simulated values can be predicted before drilling and MASP, can be predicted for each influx size individually. Thus, the method can provide additional aid to determine the best response after the initiation of kick.

If the surface pressure is larger than MASP at any depth or the downhole pressure exceeds minimum fracture pressure at any depth, the influx will be expected to be great. In such circumstances, a conventional approach for shutting in will be preferred. Contrary, if the anticipated surface pressure is less than MASP other approaches may be required. Increment of pump pressure or back pressure pump are some of suggested approaches.

Correct influx size can also be predicted by observing the difference between flow-out and flow-in over a period of time. The determination of formation overbalance pressure, which is equal to hydrostatic pressure minus the formation pressure, should be conducted for each influx.

The MASP is defined to be

"*The highest pressure predicted to be encountered at the surface of the well*" (Z.Ma A. V., 2016)

This is known to be a predicted pressure and can be calculated by using the formation pressure – wellbore filled with formation fluid. A dry gas scenario, that is the worst case scenario is considered for the formation fluid.

In this paper, the MASP will be determined based on the rating of surface equipment by the means of casing burst pressure. MASP can be determined by a certain percentage multiplied by the casing burst pressure, and generally 80% dereating is used.

$$MASP = 0.80 * casing\ burst\ pressure \qquad Eq.3.31$$

The casing burst pressure depends on the outside diameter of the last casing used, nominal weight and the grade of the casing. Predicted pressure determined using the drilling data handbook considering grade Q-125 and the nominal weight of 86 (lbf/ft) is equal to 704 bar. Predicted MASP will be used further in chapter 7.4.

$$MASP = 0.80 * 704\ bar = 563\ bar \qquad Eq.3.32$$

Figure 3.31 shows that MASP can be used to estimate the influx size.

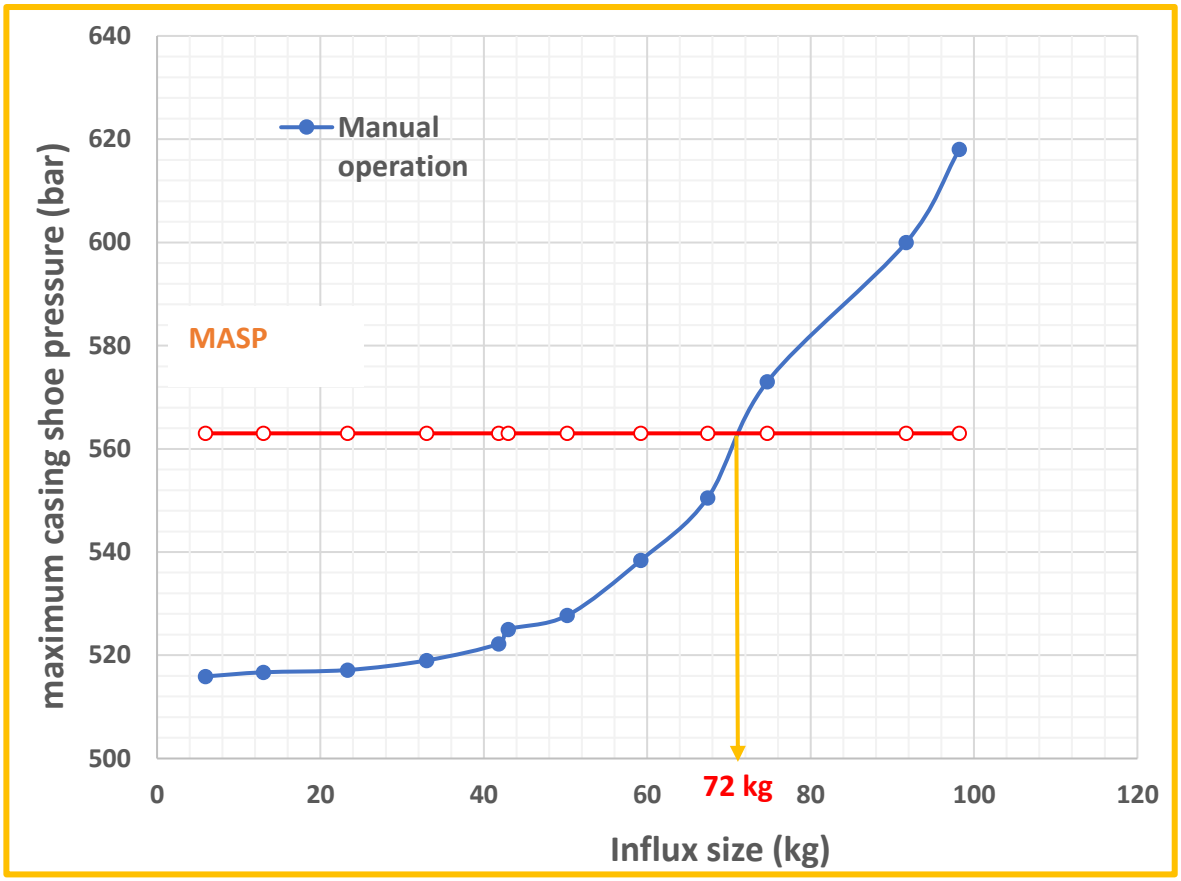

Figure 3.3.1 Shows the result of one of the case studies presented in Chapter 7.4. MASP is calculated to 563 bar and is used to estimate the maximum influx size of 72 kg.

MASP provides an estimate of the maximum influx size that can be circulated out of the well. For MPD operation, RCD pressure rating and the annular pressure should not exceed

the fracture pressure of the weakest formation. This is often located right at the casing shoe, therefore a curve of pressure at last casing shoe versus time is beneficial to support the determination of influx size. A construction of maximum surface back pressure versus influx size will also determine the influx size by the means of MASP.

ECD versus pit gain can also be constructed, where the minimum fracture pressure will be the threshold, where, graph of the maximum pit gain can be seen before fracturing the weakest point (casing shoe).

A more detailed study of the Figure 3.31 can be found in Chapter 7.4.

Chapter 4: IRIS flow model

Chapter 4.1 Dynamic model

The dynamic model that is presented in IRIS flow model takes its basis on one dimensional two-phase flow. Energy, momentum and mass, non-linear partial differential equations, are presented through this model for each phase individually. Conservation of mass considered for mass of phase k, states that

$$\frac{\partial}{\partial t}(\alpha_k A \rho_k) + \frac{\partial}{\partial s}(\alpha_k A \rho_k v_k) = \sum_l \Gamma_{kl} \qquad Eq.4.11$$

Where,

l	$The\ total\ number\ of\ phases$
kl	$Interaction\ between\ phase\ k\ and\ phase\ l$
Γ_{kl}	$Mass\ transferring\ rate\ from\ phase\ k\ to\ phase\ l,\ when\ l \neq k$
Γ_{kk}	$Mass\ rate\ of\ phase\ k\ through\ pipe\ wall$
ρ_k	$Density\ of\ phase\ k$
A	$Cross-sectional\ pipe\ area$
α_k	$Volume\ fraction\ of\ phase\ k$
v_k	$Velocity\ of\ phase\ k$

The momentum conservation equation is given as following for phase k,

$$\frac{\partial}{\partial t}(\alpha_k A \rho_k v_k) + \frac{\partial}{\partial s}(\alpha_k A \rho_k {v_k}^2) + \alpha_k A \frac{\partial}{\partial s} p_k + \sum_l K_{kl}\, v_{kl} + \alpha_k A \rho_k \frac{\partial}{\partial s}\varphi = \sum_l \Gamma_{kl}\, {v_{kl}}^* \qquad Eq.4.12$$

Where,

p_k	$Stress\ tensor\ of\ phase\ k$
K	$A\ positive\ function\ of\ relevant\ material\ parameters\ and\ geometry$

φ	$Body\ forces\ potential$
v_{kl}	$Velocity\ associated\ with\ transferring\ mass\ from\ phase\ k\ to\ l$
K_{kl}	$Interface\ friction\ factor$
${v_{kl}}^*$	$Velocity\ associated\ to\ wall\ flux\ mass\ transfer$

For this equation $v_{kl} = v_k - v_l$ and the interface friction factor is a positive number.

Conservation of energy considers, the conservation of enthalpy for the phase k, by taking the basis from one dimensional spatial averaging equation. (Liles, 1978)

$$\frac{\partial}{\partial t}(\alpha_k A \rho_k h_k) + \frac{\partial}{\partial s}(\alpha_k A \rho_k v_k h_k) + \frac{\partial}{\partial s}\left(\alpha_k A J_Q^k\right) - p_k \frac{\partial}{\partial t}(\alpha_k A) - \alpha_k A \frac{D_k}{Dt} p_k - \sum_l K_{kl} {v_{kl}}^2 = \sum_l \Gamma_{kl} h_{kl} + \sum_l J_Q^k \qquad Eq.4.13$$

Where,

h_k	$Specific\ enthalpy\ of\ phase\ k$
J_Q^k	$Axial\ heat\ flux\ for\ phase\ k\ per\ cross-sectional\ area$
$\frac{D_k}{Dt}$	$Shows\ the\ one\ directional\ substantial\ derivative\ for\ phase\ k$ $\frac{D}{Dt} = \frac{\partial}{\partial t} + v\frac{\partial}{\partial s}$
t	$Time$
$\Gamma_{kl}\ h_{kl}$	$Enthalpy\ carried\ out\ from\ phase\ k\ to\ phase\ l$

A summation of the phases given in the equation above yields

$$\sum phases = Enthalpy\ from\ pipe\ walls + net\ absorbed\ heat\ transfer\ from\ phase\ k\ to\ phase\ l + net\ heat\ conduction\ through\ pipe\ walls + dissipative\ work\ due\ to\ friction\ factor \qquad Eq.4.14$$

The two-phase model considers one-dimensional flow and puts its basis on the drift flux formulation. This particular model uses the flow set of equations for conservation mass, energy and momentum.

In these sets of equations, the mass fractions are denoted with "i" and sum of these mass fraction are taken for phase k.

$$\frac{\partial}{\partial t}\left(A\sum_{k}\alpha_k\rho_k\,x_k^i\right)+\frac{\partial}{\partial s}\left(A\sum_{k}\alpha_k\rho_k\,x_k^i v_k\right)=q^i \qquad Eq.4.15$$

Where,

i	$Mass\ fraction, where\ i=\ 1\ldots.,I$
x_k	$Mass\ fraction\ of\ phase\ k$
q^i	$Inflow\ through\ pipe\ walls\ of\ component\ i$

A pressure p is then applied to each phase and influx arrives with a momentum of qv. Conservation of moment is then represented when the sum of the phases is considered,

$$\frac{\partial}{\partial t}\left(A\sum_{k}\alpha_k\rho_k\,v_k\right)+\frac{\partial}{\partial s}\left(A\sum_{k}\alpha_k\rho_k\,{v_k}^2\right)+A\frac{\partial}{\partial s}p$$
$$=\tau_w\,S_w-\left(A\sum_{k}\alpha_k\rho_k\right)gsin\theta+qv_{\,influx} \qquad Eq.4.16$$

Where,

τ_w	$Wall\ shear\ stress,$ $\tau_w(p,T,c,geometry,mixture\ velocity)$
S_w	$Wetted\ wall\ pipe\ perimeter$
θ	$Pipe\ slope$
$qv_{\,influx}$	$Momentum\ of\ influx\ entering\ the\ pipe$

In case where liquid and gas phase are considered, the equation reduces to,

$$\frac{\partial}{\partial t}A(\alpha_l\rho_l v_l) + \frac{\partial}{\partial s}A\left(\alpha_l\rho_l {v_l}^2 + \alpha_g\rho_g {v_g}^2\right) + A\frac{\partial}{\partial s}p$$
$$= \tau_w\, S_w - A(K - \rho_{mix}\, gsin\theta) + qv_{\ influx} \qquad Eq.4.17$$

Where,

$\alpha_l + \alpha_g = 1\ and\ \ \rho_{mix} = \alpha_l\rho_l + \alpha_g\rho_g$ and K is the friction pressure loss term.

The conservation of energy takes the base in Equation 4.13 and 4.14 with the addition of phase pressure and neglecting the axial conduction,

$$\frac{\partial}{\partial t}\left(A\sum_k \alpha_k\rho_k\, h_k - Ap\right) + \frac{\partial}{\partial s}\left(A\sum_k \alpha_k\rho_k\, h_k v_k\right) - \left(A\sum_k \alpha_k v_k\frac{\partial}{\partial s}\, p\right)$$
$$= H_{wall} + Q_{absorbed} + Q_{wall} + Q_{dissipation} \qquad Eq.4.18$$

Where,

H_{wall}	$Enthalpy\ from\ pipe\ walls$
$Q_{absorbed}$	$net\ absorbed\ heat\ transfer\ from\ phase\ k\ to\ phase\ l$
Q_{wall}	$net\ heat\ conduction\ through\ pipe\ walls$
$Q_{dissipation}$	$dissipative\ work\ due\ to\ friction\ factor$

The slip relations presented in this model is given for phase k to be,

$$v_k = K_k(p, T, c, geometry)v_{mix} + S_K(p, T, c, geometry) \qquad Eq.4.19$$

The PVT model used is given as,

$$\Gamma: (p, T, c) \rightarrow (\rho, x, \alpha) \qquad Eq.4.20$$

A realistic and true flow behaviour is used to compute derived measures such as pressure, temperature, volume fractions, by using a numerical flow solver that consists of basic flow properties and specific geometrical flow designs. These measures are calculated by splitting wellbore into segments through space and time. Flow parameters are averages of space and time for each element.

The equations represented earlier (4.15-4.18) can be solved by explicit solution method or semi-implicit solution methods. In case of explicit solutions standard techniques for

hyperbolic conservation laws are used. A more descriptive solution is shown in (Johnny Frøyen, 2000). In cases where the time step lengths are restricted, the solution can be found from semi-implicit solutions.

The non-linear partial differential equations for energy, momentum and mass balance take the basis on Navier-Strokes equations. Dynamics of well flow are determine with these equations. In addition to mass, energy and momentum wall friction and gravity also play a role of well flow pressure behaviour.

The suggested differential equations alone are not adequate to describe physical processes and therefore correlations are provided. These correlations are provided by empirical closure relations, which gives information about phase velocities and pressure losses. Time dependent equations are provided in these relations and include many assumptions and inaccuracies. Assumptions are made for parameters such as flow regime, geometry of the wellbore, unknown fluid properties and unidentified pipe properties. These parameters are system dependent.

IRIS flow model takes its basis on measurement values to create a stable flow model that in the future is can be predicted. Study conducted for numerical model presented can be found more in detail in, (Trapp, 1986), (Doster, 1999), (Bendiksen, 1991).

The thermodynamic relations are provided by the assumption of thermodynamic equilibrium in PVT models. IRIS flow model uses simple ideal gas law and more complex mud PVT properties.

The numerical method is made by the means of experiments. The gas densities are defined by.

$$\rho_w = \rho_0 \exp\big(\, c\,(p - p_{atm})\big) \qquad Eq.4.21$$

Where,

ρ_w	$Calculated\ density\ of\ water$
ρ_o	$Density\ of\ pure\ water = \ 1000\ kg/m^3$
c	$compressibility$
p_{atm}	$Atmospheric\ pressure = 1.01325 * 10^5\ Pa$
p	$Measured\ pressure$ inside the pipe

Initially the model considers pipe of 1000 m with a diameter equal to 0.1 m, completely filled with water.

Where, c is the compressibility equal to

$$c = \frac{1}{\rho}\frac{d\rho}{dp} \qquad Eq.4.22$$

The compressibility used in this equation is similar to what was seen in the Equation 2.31. For the WBM, the model takes into account the compressibility of water and the formation water including their respective correction factors.

$$\rho_g = \frac{P}{rT} \qquad Eq.4.23$$

Where, the viscosities are constant of water and gas.

ρ_g	$Gas\ density$
P	$Pressure$
r	$Universal\ gas\ constant$
T	$Temperature\ in\ Kelvin$

This specific slip relation considered for the numerical model for IRIS flow model is given by,

$$v_g = 1.2(\alpha\, v_g + (1-\alpha)v_w + 0.534\, m/s \qquad Eq.4.24$$

The velocity is assumed to start from rest. Developing this numerical model, the boundary conditions used is mass influx at inlet and atmospheric pressure on outlet.

The focus here is made in two-phase horizontal flow where gas and water have been injected with a certain mass rate. By comparison of implicit and composite scheme the most reliable and true method is chosen by experimentation. A more detailed numerical method can be found in (Jhonny Frøyen, 2000).

The numerical method used ahead puts its basis on semi-implicit formulation of the drift-flux model, where the pressure update is implicit and the mass transport is explicit. A conclusion derived from the experiments says that the semi-implicit method is appropriate for both acoustic pulses, and mass transport. A larger time step may be used for the semi-

implicit scheme and a smoother front for the void wave is generated. A more simple transient flow model is presented by Kjell Kåre (Kjell kåre fjelde, 2014).

Chapter 4.2 Friction pressure loss model

For the drift flux model considered in chapter 4.1 a frictional pressure loss term must be defined for Equation 4.17.

The term for frictional pressure K is defined as,

$$K = c\frac{2f}{D_{hy}}\,\rho_{mix}\,v_{mix}^2 \qquad Eq.4.25$$

Where,

D_{hy}	$Hydraulic\ diameter$
ρ_{mix}	$Mixture\ density$
v_{mix}	$Mixture\ velocity$
f	$Fanning\ friction\ factor$
c	$Calibration\ factor$

For two-phase flow the following equation will be used,

$$\rho_{mix} = \alpha_l\rho_l + \alpha_g\rho_g \qquad Eq.4.26$$

$$v_{mix} = \alpha_l v_l + \alpha_g v_g \qquad Eq.4.27$$

Where,

α_l	$Fraction\ of\ liquid$
α_g	$Fraction\ of\ gas$
ρ_l	$Density\ of\ liquid$
ρ_g	$Density\ of\ gas$

The fanning friction factor is dependent on rheological model and the nature of the flow (laminar or turbulent). One phase flow is described by Reed & Pilehvari, (Reed, 1993), where effective diameter was defined. Shear rate of non-Newtonian fluid is formulated with wall shear rate for Newtonian pipe flow, by using the "n" factor, the fluid flow index.

For the drill string, the effective diameter is defined in the generalised form,

$$D_{eff} = \frac{4n}{3n+1} D \qquad Eq.4.28$$

For annulus it is given as,

$$D_{eff} = \frac{\frac{2}{3}(D_o - D_i)3n}{2n+1}$$

Where,

D_o	$Outer\ diameter$
D_i	$Inner\ diameter$
D	$D_{hy} = D\ for\ drill\ string$

Apparent viscosity was also defined by Reed & Pilehvari.

For PLM it is defined as,

$$\mu_{w,app} = \frac{K_{pl}\left(\frac{8v}{D}\right) n_{pl}}{\gamma_w} \qquad Eq.4.29$$

Considering that n_{pl} was constant, presentation of an equation for generalized Reynolds number was stated,

$$Re_g = \frac{\rho \ D_{eff} \ v}{K_{pl} \frac{\left(\frac{8v}{D}\right)^n}{\gamma_w}} \qquad Eq.4.30$$

Since the parameter n_{pl} was constant for Equation 4.29, it is only applicable for PLM. (H.H.Fan, 2014) The Reynolds number and fanning friction factor are related for laminar flow.

$$f = \frac{16}{Re_g} \qquad Eq.4.31$$

Where, the Re_g in the generalised form,

$$Re_g = \frac{D_{eff} v \rho}{\mu_{app}} \qquad Eq. 4.32$$

D_{eff}	$Effective\ diameter$
μ_{app}	$Apparent\ viscosity$
n	$Generalized\ flow\ index$
n_{pl}	$Flow\ index\ specified\ for\ Power-law\ model$
K_{pl}	$Pre\ factor\ of\ power\ law$

Effective diameter descrbied in Equation 4.28 attributes for geometry of the wellbore and non-Newtonian fluid effects. It is regarded as a connection link between Newtonian and non-Newtonian pipe flow through concentric annuli and the apparent viscosity.

The fanning friction factor for transition and turbulent flow includes the effect of roughness and is also presented by (Reed, 1993).

$$\frac{1}{\sqrt{f}} = -4log_{10}\left\{\frac{0.27\,\varepsilon}{D_{eff}} + \frac{1.26^{\left(n_{pl}\right)^{-1.2}}}{\left[Re_g f^{(1-0.5n_{pl})}\right]^{n_{pl}^{-0.75}}}\right\} \qquad Eq. 4.33$$

By determination of all the parameters above the frictional pressure term K can be estimated from equation 4.25.

The model used for drilling fluid will be based on Equation 4.30 – 4.33.

Chapter 5: Automated MPD for well control

Chapter 5.1 Conventional well control procedure in conventional drilling

NORSOK D-10 defines well control to be, "*collective expression for all measures that can be applied to prevent uncontrol release of wellbore waste to external environment or uncontrol underground flow*".

For conventional drilling operations, well is balanced by the formation pressure and the hydrostatic pressure of the drilling fluid. If in case the drilling fluid is not sufficient to balance the formation pressure, the fluid may enter the wellbore. In this situation, a kick will be taken. Secondary well control can detect the influx, contain it and remove it from the well in a safe way, such that the primary well control can be re-established.

The well control procedure for conventional drilling includes several operations,

1. Testing and verifying well barriers
2. Preventing kick occurrence
3. Detecting the kick when primary barrier fails
4. Controlling the influx
5. Removing the influx from the well bore and re-establishing the primary barrier

A kick in the well can be taken in several ways, the method considered in this research, will be insufficient drilling fluid (as the pore pressure gradient is greater than MW). The formation pressure will be greater than mud hydrostatic pressure acting on the borehole. In certain cases, more obvious solution would be to increase the MW. However, the increase in MW is a suitable approach when the MW does not exceed the fracture gradient. Loss of circulation fluid will be the result in such a case. There are also disadvantages to use a higher MW such as differential sticking.

There are several circulation methods used in our industry, one of the common being the Driller's method. This method takes its basis on keeping the BHP constant, or a little above the formation pressure, where two separate circulations takes place. In the first circulation, the influx is circulated out using the original MW. BHP is maintained by keeping circulating drill pipe pressure, constant. In case where the MW is not sufficient, kill mud is required to be circulated (a heavier mud) downhole, in the second circulation process. (K, 2015)

Thus, the second circulation process also requires constant BHP. This can be achieved by two methods, first one being constant casing pressure, while pumping kill mud, until it returns to the surface. Alternatively, calculation of drill pipe pressure can be conducted and monitored while pumping kill mud down the drill string. Subsequently, the pressure of drill pipe is kept constant. After the well is killed properly, and all the influx is circulated out successfully, the casing shoe pressure and the drill pipe pressure will become zero.

The Driller's method is more ideal in conditions where hole problems are more prone, in long static periods, where circulation does not take place. Other advantages of this method includes; simplicity as calculations is not required instantly, saves time as pump can start as soon as the drill pipe pressure builds up and effective control of the well (Rana S Roy, 2009). A summary of the Driller's method is given in the flowchart shown in Figure 5.1.1. (Cult, 2016)

Figure 5.1.1 Summary of the operational procedures for Driller's Method.

The focus in this thesis, will be in determining the influx size, controlling the influx and removing by circulation is a safe manner. This approach was discussed earlier in Chapter 3 and the case study is conducted in Chapter 7.4 and 7.5. Further on this chapter the method to control the influx for manual operation is proposed in section 5.2.

Chapter 5.2 Influx control for manual operation

A general procedure to control influx differs from well to well, as wellbore parameters such as geometry of the wellbore, fluid type, well depth, size of influx, are different. Therefore, it is difficult to generalise a proper response when influx enters the wellbore. For instance, a small kick size of 5 kg is considered small for conventional well, but could be considered large for slim hole design.

A method was proposed by Karimi Vajargah, which was found by simulation results and tables, by means of a 3-step algorithm (Ali Karimi Vajargah, 2014). This study puts its emphasis on early detection and initial action of influx for MPD and conventional operations. Validity is considered when kick is initiated early, while drilling or during circulation periods. As mentioned earlier, the focus is to keep the BHP constant, while circulating the influx out of the well by using Driller's circulation method. By keeping the BHP constant, further influx will be restricted and the annular pressure will stay within limits of formation weak zones and surface equipment.

Figure 5.2.1 shows an algorithm to follow when gas influx occurs when drilling with constant BHP for MPD and conventional operations. The initial step is to determine size of influx (Chapter 3.3), and to determine if the size is small, medium or large. The size can be predicted by using MASP presented in Chapter 3.3 and the lowest fracture pressure. If the surface pressure is larger than MASP or annular pressure is larger than fracture pressure at any depth, the influx will become large and conventional shut-in procedures may be followed. In case where the MASP is smaller than the fracture pressure, other techniques can be considered.

Before considering any technique, formation overbalance pressure should be assessed for every influx size. The size of influx may also be estimated from the difference between the flowrate-out and flowrate-in.

The most common and simple method to control the influx is to increase the mud pump flowrate. This leads to an increase in annular friction pressure drop and ECD. This method will only work when the increase in annular friction pressure drop is adequate to control the influx. Nevertheless, it is also essential to consider the limitation of pump pressure and maximum flow rate.

Selecting of the ramping up speed of the mud pump flowrate, should be carefully planned. Some differences can be seen between flow-out and flow-in, as a result of gas compressibility (see case study in Chapter 7.4 for examples).

It is also possible to increase the back- pressure pump, to control the influx and restrict the flow by the means of either manual or automated operated choke. It imposes additional frictional pressure loss. The back-pressure pump and the mud pump must equal the flow-out. In real-time scenario, the formation pore pressure is required to be inspected to define a proper limit to the back-pressure pump. (Jing Zhou, 2016)

While managing the influx by restricting the flow using choke, operations often take some time to take effect and more influx will be allowed to enter the well. The total accumulated influx may often be larger than predicted. Therefore, surface and annular pressure must stay within limits before the circulation can take place. After this step, the gas may be circulated to the surface and out of the well. After gas reaches the surface, it is separated from the drilling fluid. If any problems are encountered during the influx control or circulation process, conventional shut-in procedures are suggested. (J.E. Gravdal, 2010)

Summarizing the influx can be controlled by either of the methods, or a combination of these methods.

1. Control the choke opening
2. Increase the mud pump
3. Increase the back- pressure pump
4. Shut the well if the previous suggestions do not work, or when influx is too large.

Figure 5.2.1 takes basis in the knowledge that the influx size is determined and without the proper determination of kick size, any response is extremely challenging.

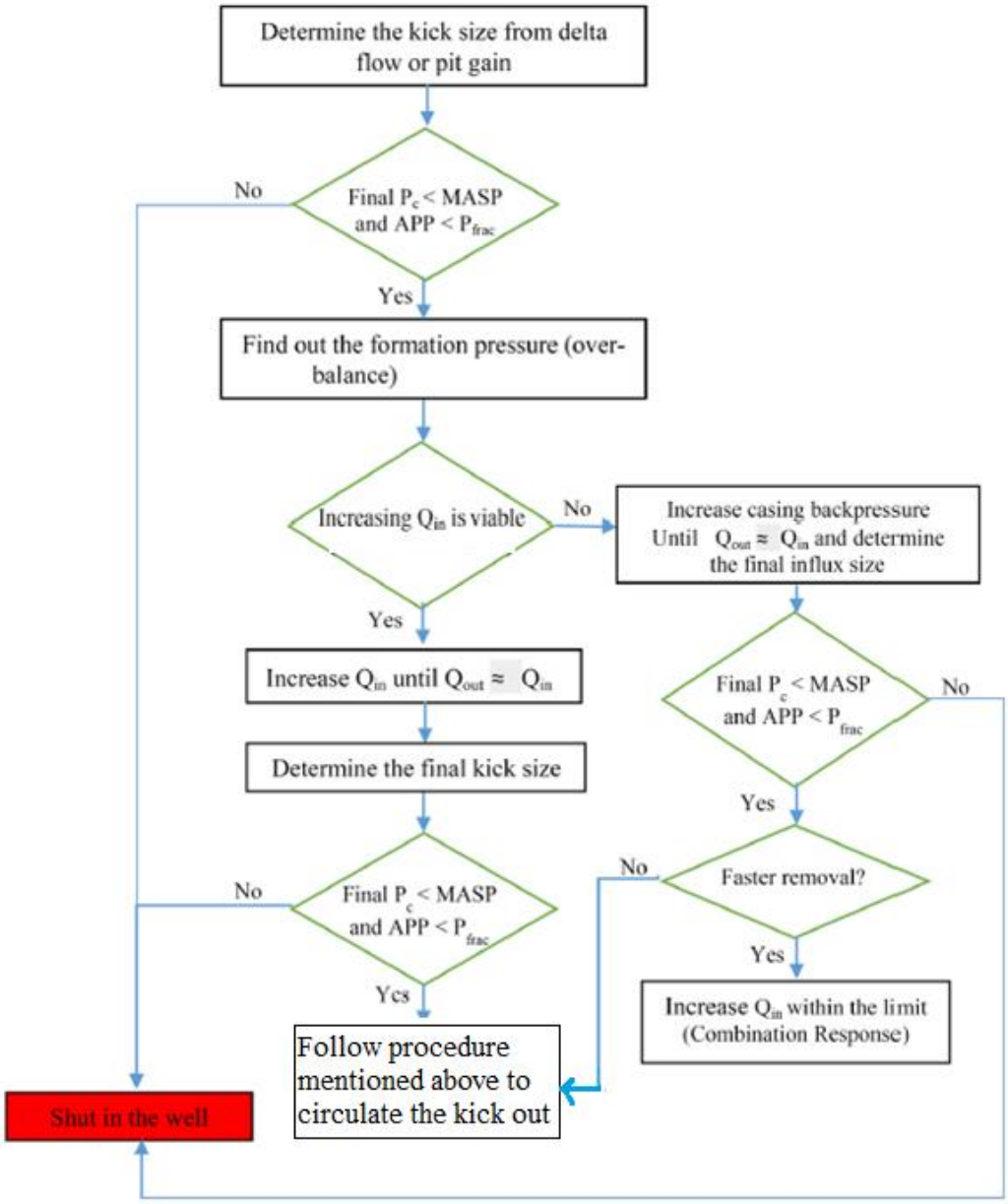

Figure 5.2.1 Algorithm suggested to find the proper response in case of an influx. (Ali Karimi Vajargah, 2014)

Where,

P_c	$Collapse\ pressure$
P_{frac}	$Minimum\ fracture\ pressure$
Q_{in}	$Flowrate - in$
Q_{out}	$Flowrate - out$

The formation pressure is calculated using the following equation,

$$Formation\ overbalance\ pressure = Hydrostatic\ pressure\ in\ drillpipe\ (psi) + influx\ intensity\ calculated\ for\ specific\ influx\ size\ \left(\frac{lb}{gal}\right) \times 0.052 \times TVD\ (ft) \quad \text{Eq. 5.21}$$

Chapter 5.3 Influx control for automated operation

The automated operation used in case study is based on the PI controller (Chapter 6). The BHP is kept constant by defining a set point in the controller design. The reference, or the set point is allowed to be increased, after a certain amount of time. This is used to control small influx to enter into the wellbore. The small amount of influx is then circulated out of the wellbore, as done in the manual operation. Choke valve is the manipulated the variable and is automatically adjusted as influx starts to enter the wellbore.

The initial position of the choke valve is fully open, that is 100 %. The mud pump and the back-pressure pump are maintained at a certain level throughout the whole circulation process. Otherwise, the simulation is run exactly the same as described for the manual operation (see Chapter 7.5 for further analysis). The manual and automatic operation is later (Chapter 7.6) compared in case study.

Chapter 6: PID controller

6.1 PID controller theory

PID (Proportional, Integral, Derivative) controller is one of the most used control algorithms in our industry. It can be used in a wide range of operational conditions and is simple to operate. This control system is generally more effective for continuous processes, where two control tasks are performed and is more suitable for linear systems. First, the PID controller keeps the output at a specified set level, and second, process level from one set-point to another are changed instantly at the appointed time.

A simple control system of a closed loop, consists of an input, an output, a controller and a plant.

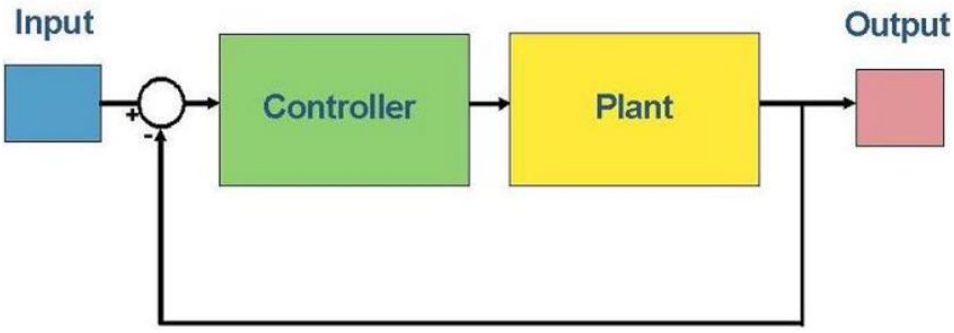

Figure 6.1.1 A simple closed loop control system. (Pai, 2008)

The input to the system, is a desired output and is called a set point. For controller (example PID controller) the input is the error which is the difference between the set point and measured value.

$$e(t) = y_{sp} - y_m \qquad Eq.6.10$$

Where,

t	$time$
y_{sp}	$Set\ point$
y_m	$Measured\ value$

The controllers main task is to reduce the error as much as possible. In this case the controller is the PID controller.

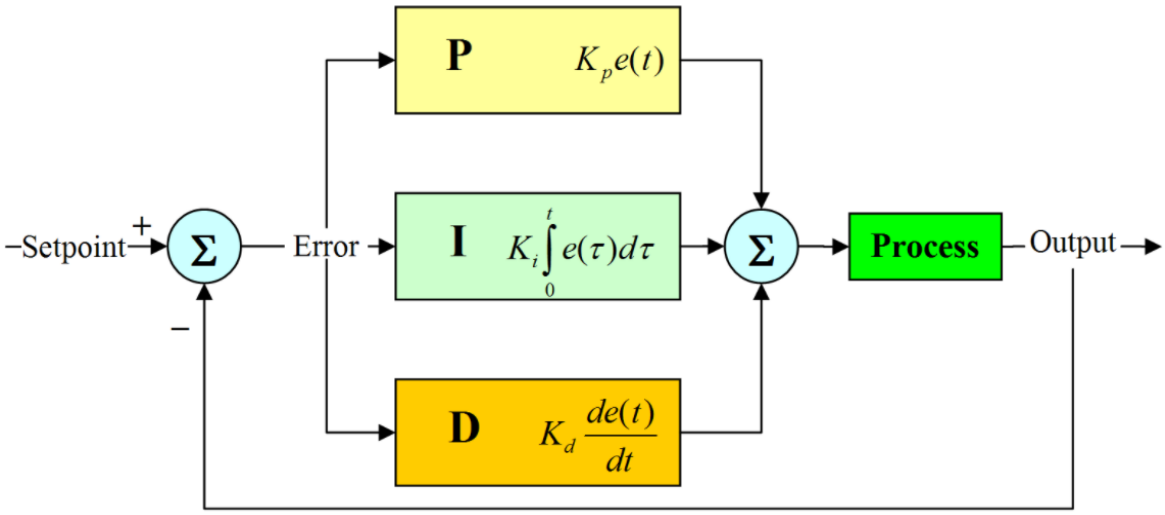

Figure 6.1.2 Block diagram of PID control. (Pai, 2008)

The proportional term (meaning a constant multiple) of the PID controller depends in the difference between the set-point and the process variable, or in other words, it depends on the present error. The controller output is proportional to the error signal and is presented by the following equation:

$$u(t) = u_o + K_p\, e(t) \qquad Eq.6.12$$

Where,

$u(t)$	*Controller output*
K_p	*Proportional gain*
$e(t)$	*Error*
u_o	*Nominal input value*

Hence, larger proportional gain or error creates greater output. If the controller gain is too large, the controller will overshoot the set-point which causes larger oscillations. One of the main disadvantages of the proportional term is when the error becomes very small. This causes the loop output to be insignificant. Which, means that proportional term excludes the error and stabilizes at an incorrect steady state position.

In conclusion, the larger the proportional gain, thus more likely for the loop to become unstable (due to faster response time). In the other hand, a larger value of controller gain gives less steady state error. Due to this instability, a lower K_p value will create an offset that is slightly under the set-point as shown in the Figure 6.1.3.

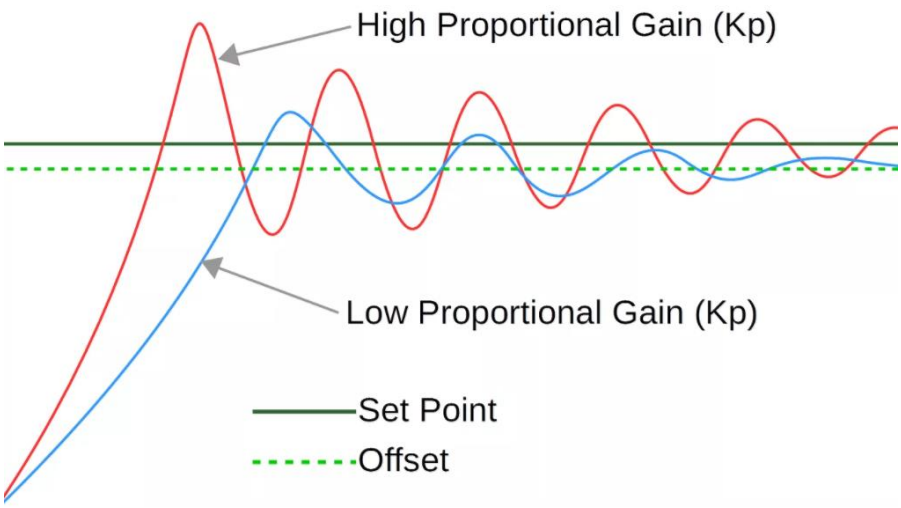

Figure 6.1.3 A hypothetical control system, showing the effect of high and low proportional gain (Kp) (Ant, 2014)

The integral term is used to obtain long term precisions to control loop. It stores all the error from the past. Its main function is to eliminate steady state offset, defined as a term that is proportional to magnitude and extent of the error. It is given by the equation,

$$u(t) = u_o + K_i \int_0^t e(\tau)d\tau \qquad Eq.6.13$$

Where,

K_i	$Integral\ gain\left(\frac{K_p}{T_i}\right)$
τ	$Adjustable\ time\ constant$
T_i	$Integral\ time$

The integral term calculates the average error, which provides a good estimate of accumulated offset over a time period (shown by the integration in Equation 6.3). This accumulated error is multiplied with the integral gain. Accordingly, the controller output will collect previous offset and thus, create the controller output to be more accurate and closer towards the set-point. (Godhavn, 2013)

As aforementioned, the K_i value also requires adjustment. In case of a large value of integral gain, the response will be quicker and create a large overshoot from the set-point.

The disadvantage of integral gain is that it contributes strongly to overshoot of controller output. In case of a short integral time, it works more aggressively, rather than stabilising steadily. The responses are shown in the figure below.

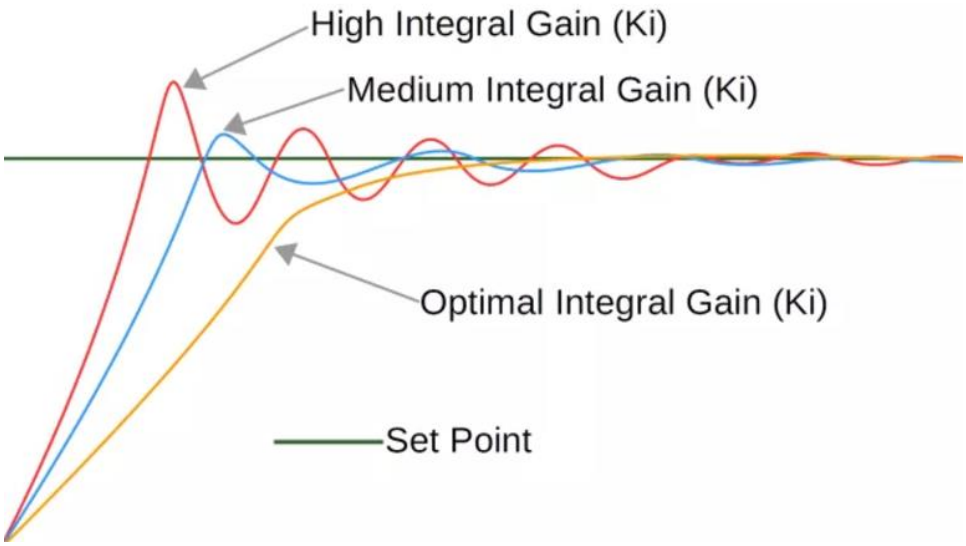

Figure 6.1.4 Response of high versus a tuned Kp value. (Ant, 2014)

The derivative term, K_d is the least used of all terms. For most control systems PI algorithm is sufficient. It is mainly used in specific control systems, where large overshoot is not acceptable. System behaviour, and improvement of settling time is the primary function of the derivative term. In short, it can be used to predict future behaviours.

K_d calculates the rate of change of error. Thus, a substantial change of error creates a large the derivative term. So, it resists the large overshoot created by P and I controller. It is given by the following equation,

$$u(t) = u_o + K_d \frac{d}{dt} e(t) \qquad Eq.6.14$$

Where,

K_d	$Derivative\ gain\ (K_p T_d)$
T_d	$Derivative\ time$

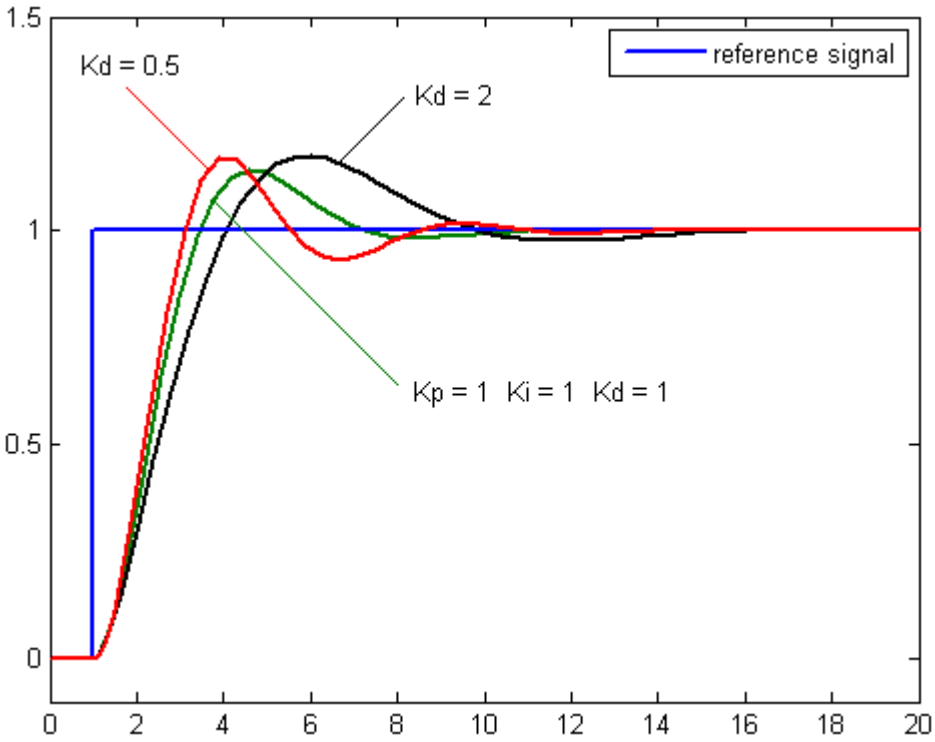

Figure 6.1.5 Shows the effect of the derivative term, Kd. (Araki, 2017)

When all the control functions are added together, PID controller can be estimated by using the following equation.

$$u(t) = u_o + K_p\, e(t) + K_i \int_0^t e(\tau)d\tau + K_d \frac{d}{dt}\, e(t) \qquad Eq.6.15$$

A large value of derivate gain decreases the overshoot; however, it slows down transient response and has a greater chance to become instable. This can happen as an effect of signal noise amplification when difference in error is calculated.

Without proper tuning of gains (Kp, Ki and Kd) controlled process input will become unstable. This means that the output may diverge either with or without oscillations. Normally tuning is performed to systems that have great oscillations, have slow response time, unstable and includes steady state error. Adjustment is therefore crucial to obtain desired control response.

Optimum values of gains depend on the processes and set points, in few cases overshoot is not desired above a certain level. There are several methods to tune a PID loop, where the choice is dependent on the response speed of the system and if the loop can run offline for

tuning. If offline is an option, then step changes in input values, and measurement of output as a function of time, are considered the best methods.

6.2 Tuning of PID controllers

The reason behind tuning of PID controller is to obtain fast response and good stability. Some of the tuning methods are Ziegler-Nichols' method and the good gain method. Both these methods are based on experiments to control the process. The good gain method will be further studied in this chapter.

Obtaining both of these criteria's, fast response and good stability, at the same time for practical systems is not possible. Therefore, it is important to find a good compromise between acceptable stability and adequate response time.

It is difficult to define exactly, the meaning of acceptable stability, however a simple definition as a positive step change of the set point can be used.

A proper definition would be,

"Acceptable stability when the undershoot that follows the first overshoot of the response is small, or barely observable." (Haugen, 2010)

Good gain method is simple and popular method for experiments and simulations. One of the main advantages of this method, is that it does not require control system to be carried in continuous oscillations in the tuning phase. Few simple steps are described to proper use this method for manual operation.

1. The process must be brought to or close to a normal or specified operation point by adjusting the control signal, called u_o.
2. Verify that controller is P controller by setting the proportional gain equal to zero ($T_i = \infty$). Then, increase the value of K_p until the stability is acceptable, for instance a step in set point or in disturbance. One other option is to set $K_p = 1$ and then increase or decrease the value until a slight overshoot is seen with a good damped response.
3. The integral time $T_i = 1.5 * T_{ou}$ (shown in Figure 6.21), T_{ou} is defined to be the time difference, between the first overshoot and the first undershoot, with respect to P controller.

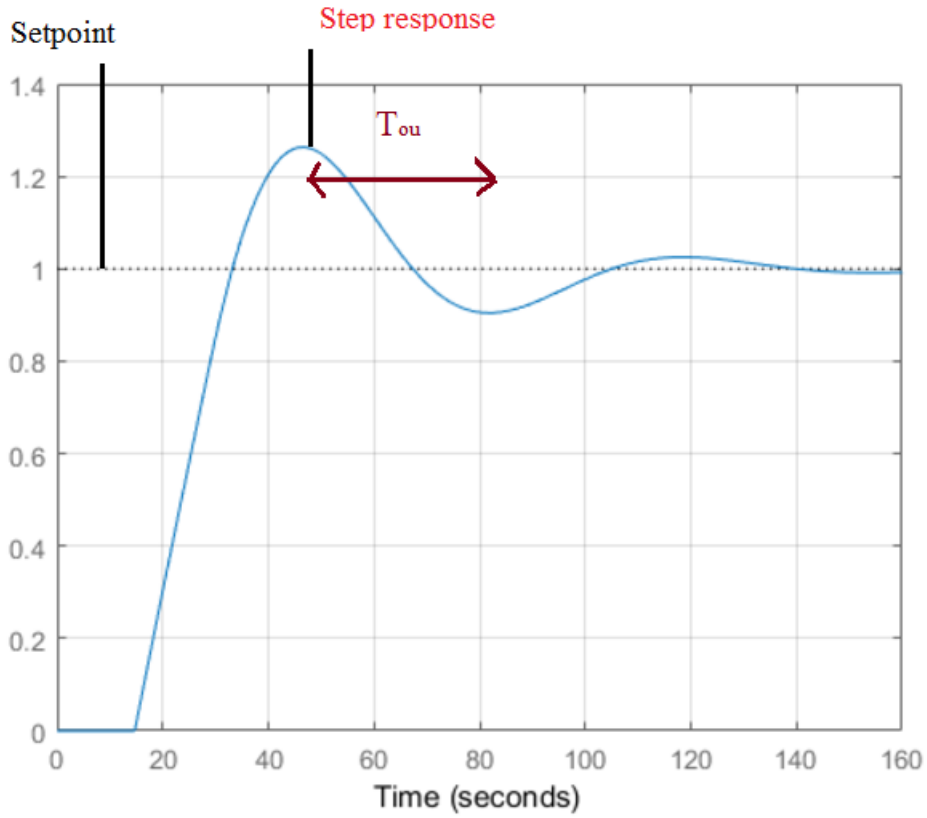

Figure 6.2.1 Observing the time difference between the first overshoot and the undershoot with P controller.

4. Stability of the control system must be controlled, by the application of a set-point step. So, introducing I term will reduce some stability compared to only having a P controller. If the stability gets too poor, then reducing K_p to around 80 % of the original value, may be beneficial.

In this thesis, PI- controller will be used and tuning will be conducted to proportional gain and integral gain terms. The BHP will be the reference value or the set point. The choke opening will be regarded as a variable and it will be manipulated by the control designed to keep BHP constant. (see chapter 7.5 for case study).

Chapter 7: Case study

7.1 Simulation of WBM

The WBM considered for this research paper has the following properties shown, in the configuration. It is given by realistic parameters, used when comparing other scenarios. Different changes of parameters are monitored from the fluid section, such as rheology, density, gel strength and alteration of stresses from PVT (Pressure, Volume Temperature) table. Comparison of pressure responses are made on the base case presented in section 7.11.

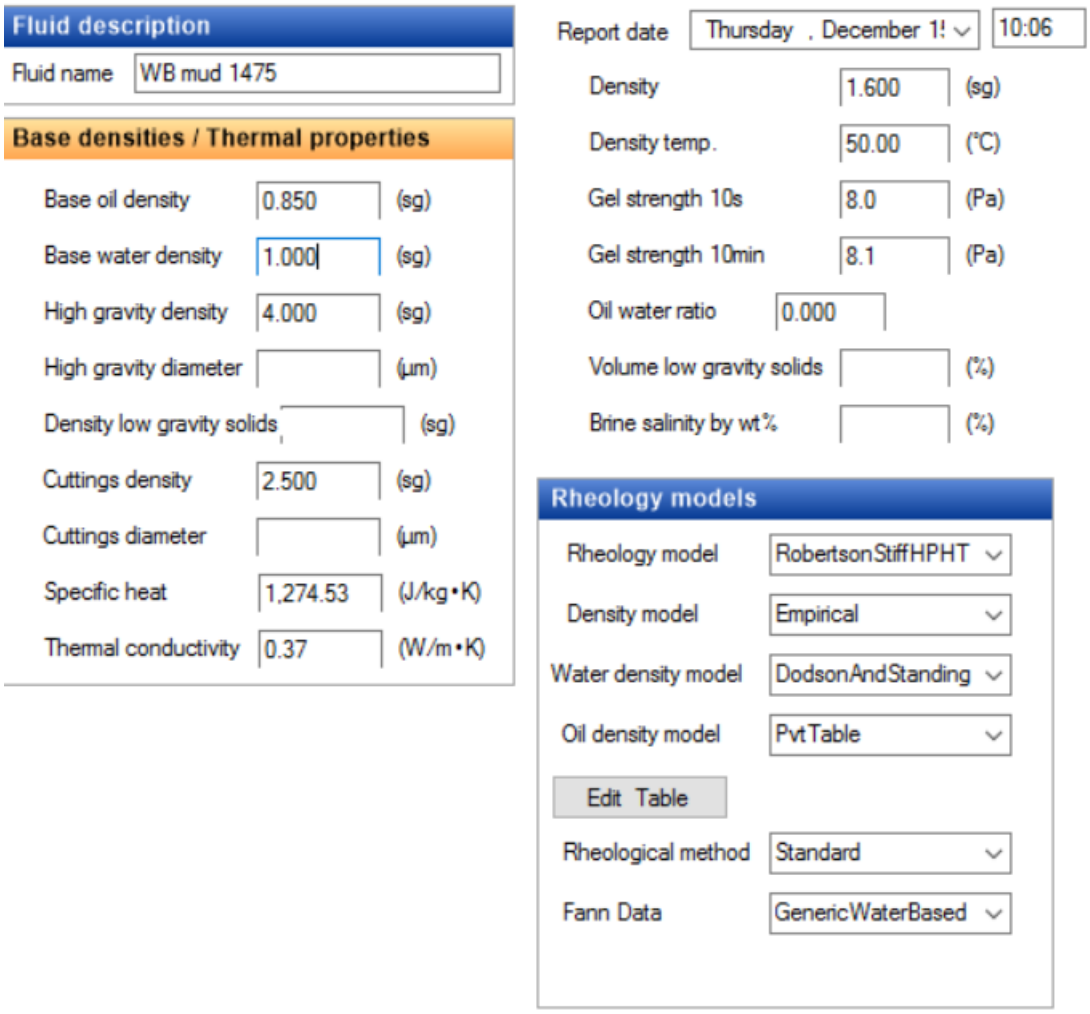

Temp. (°C)	Press. (bar)	Stress at 3 rpm (lb/100ft²)	Stress at 6 rpm (lb/100ft²)	Stress at 30 rpm (lb/100ft²)	Stress at 60 rpm (lb/100ft²)	Stress at 100 rpm (lb/100ft²)	Stress at 200 rpm (lb/100ft²)	Stress at 300 rpm (lb/100ft²)
50.00	1.0	5.0	7.0	17.0	27.0	37.0	59.0	72.0

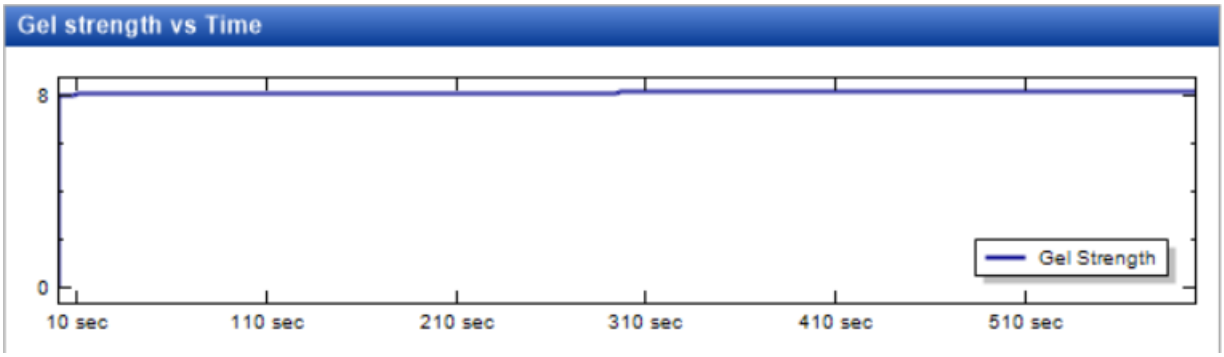

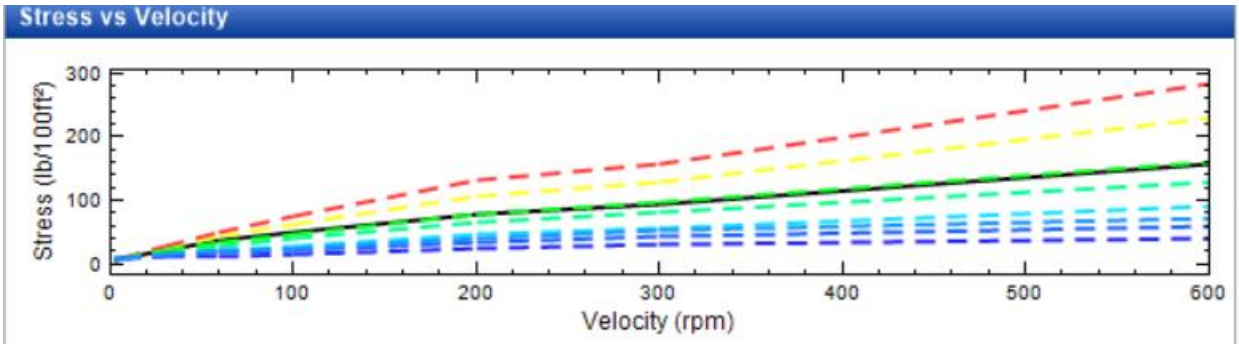

A summary of the simulation plan for WBM is shown. Scenario 1 is taken as a basis when comparing the following 6 scenarios.

Scenario nr.	Mud type	Changing parameter	Value of changed parameter
1	Generic WBM	(shown configuration)	-
2	Generic WBM	Power law HPHT (rheology)	-
3	Generic WBM	Bingham model HPHT (rheology)	-
4	Generic WBM	Density increase	1.800 s.g
5	Generic WBM	Increasing the gel strength for 10s, 10 min	10 Pa (10s) and 15 Pa (10 min)
6	Generic WBM	Bingham model, change the stresses in PVT table with a constant value.	10 ($lb/100ft^2$)

Table 7.1.1 Shows the simulation plan run for 6 different scenarios for WBM and their parameters. The pressure profiles are compared with scenario 1.

7.11 Scenario 1- Base case for WBM

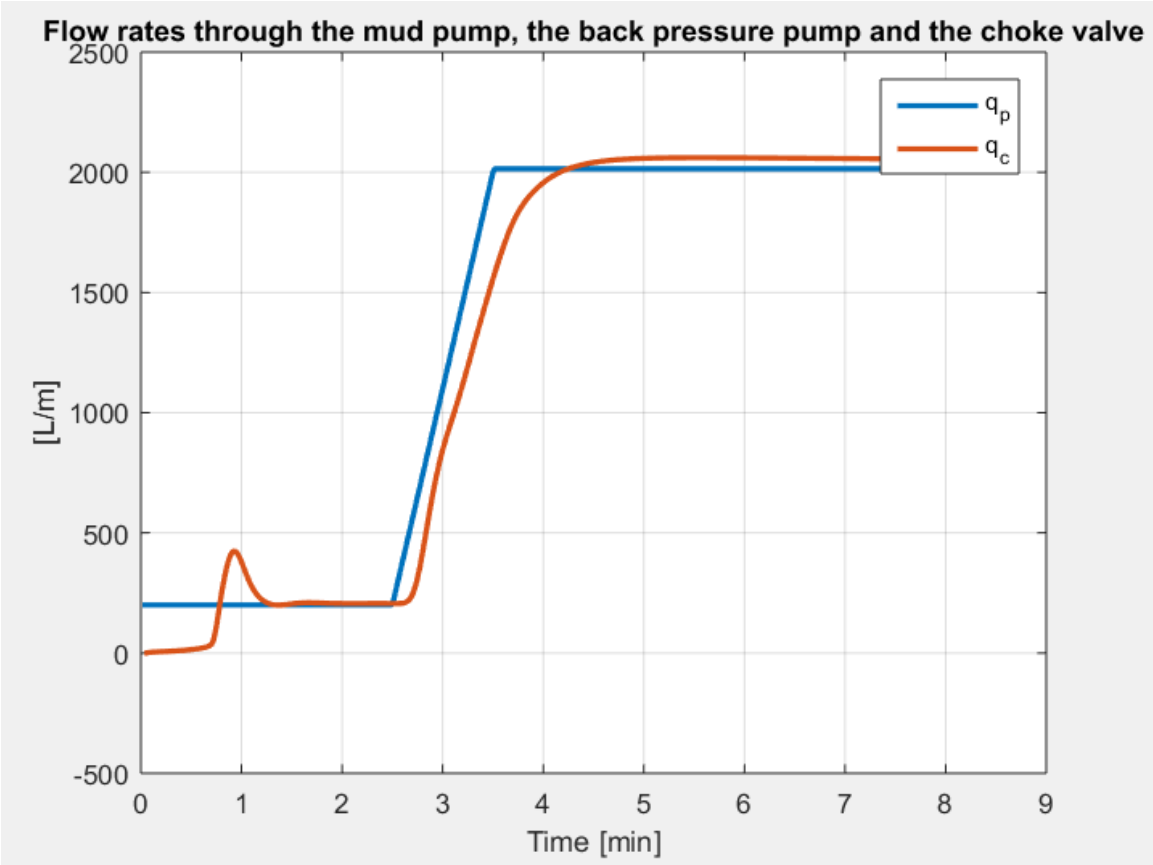

Figure 7.11.1 shows the mud pump flow rate in (shown in blue) and return flow (shown in red) for base case of WBM.

The mud pump flowrate-in, is designed in a certain way to avoid gel breaking, which leads to fracturing of the well. The gel can be broken if the flowrate is increased above a certain value and kept constant for a longer period. This threshold is different for different wells and can be influenced by the type of mud, the downhole pressure and temperature conditions, etc. By starting the pump at 200 lpm as shown in curve, this can be avoided.

Subsequently, by starting the pump at 200 lpm the fill pipe flow rate is also ignored. The fill pipe flow rate is the flowrate that is needed to fill the drill pipe of 30 m (initially empty) on the top of the drill floor, which is done before it enters the well.

As Figure 7.11.1 shows, the flowrate-in is allowed to stabilise itself before it ramped up to the target flowrate, which is 2000 lpm. The return flow shows some oscillation after around 50 seconds, this is mainly after the top connection of the drill pipe is filled with mud. The peak shows that the gel strength is intact and at this point the ECD is very close to fracture pressure gradient. While the peak drops, and stabilises the ECD slowly reduces

towards the target. This behaviour is seen in Figure 7.11.2. During late time (5 minutes) however, the return flow shows some gap to the flowrate-in. This behaviour is mainly due to mismatch of temperature between the mud that is injected and the mud that returns from the annulus. The injected mud is much colder at the surface compared to the one downhole.

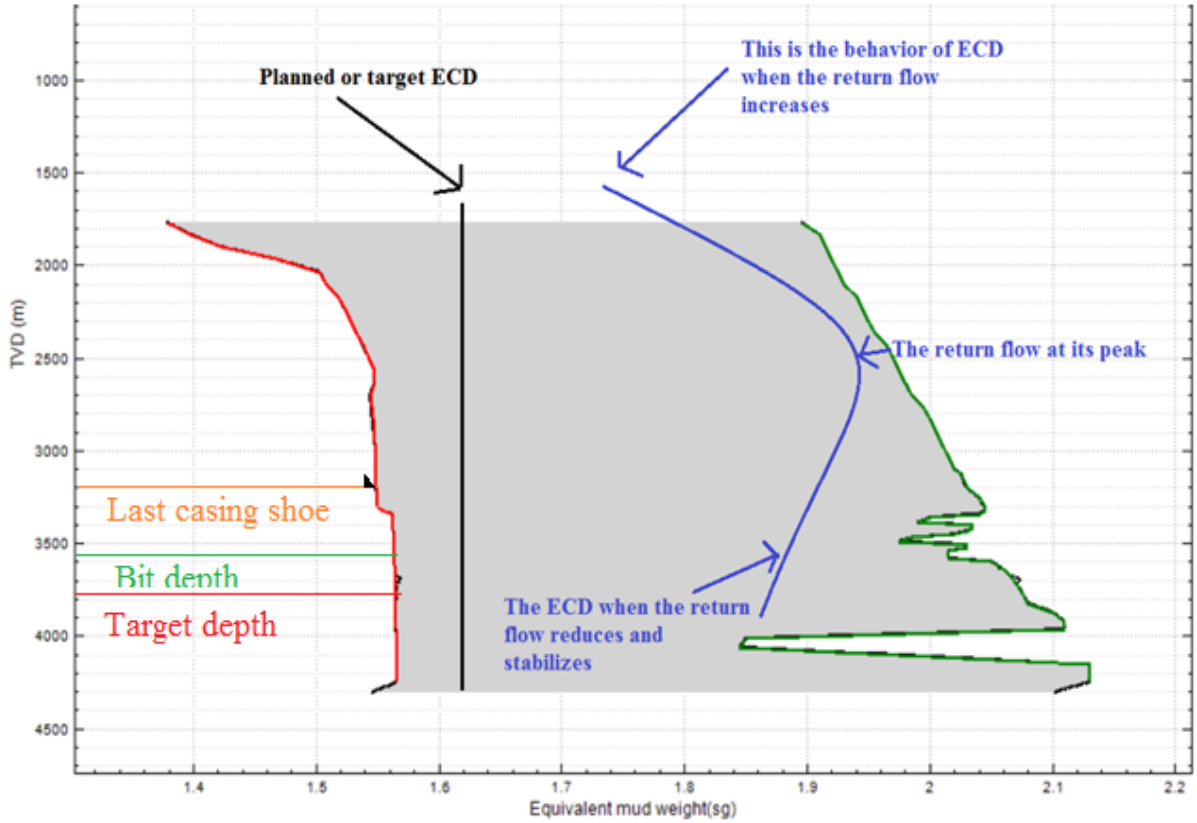

Figure 7.11.2 TVD versus equivalent MW or ECD. Shows the planned ECD and how it behaves as the return flow increases and decreases, respectively.

The target depth of this well will be at 6500 m MD (3571 m TVD). The bit depth will be 50 m MD above the target depth, at 6450 m MD. The last casing shoe is located at 4277 m MD (3201 m TVD). These values are marked on Figure 7.11.2.

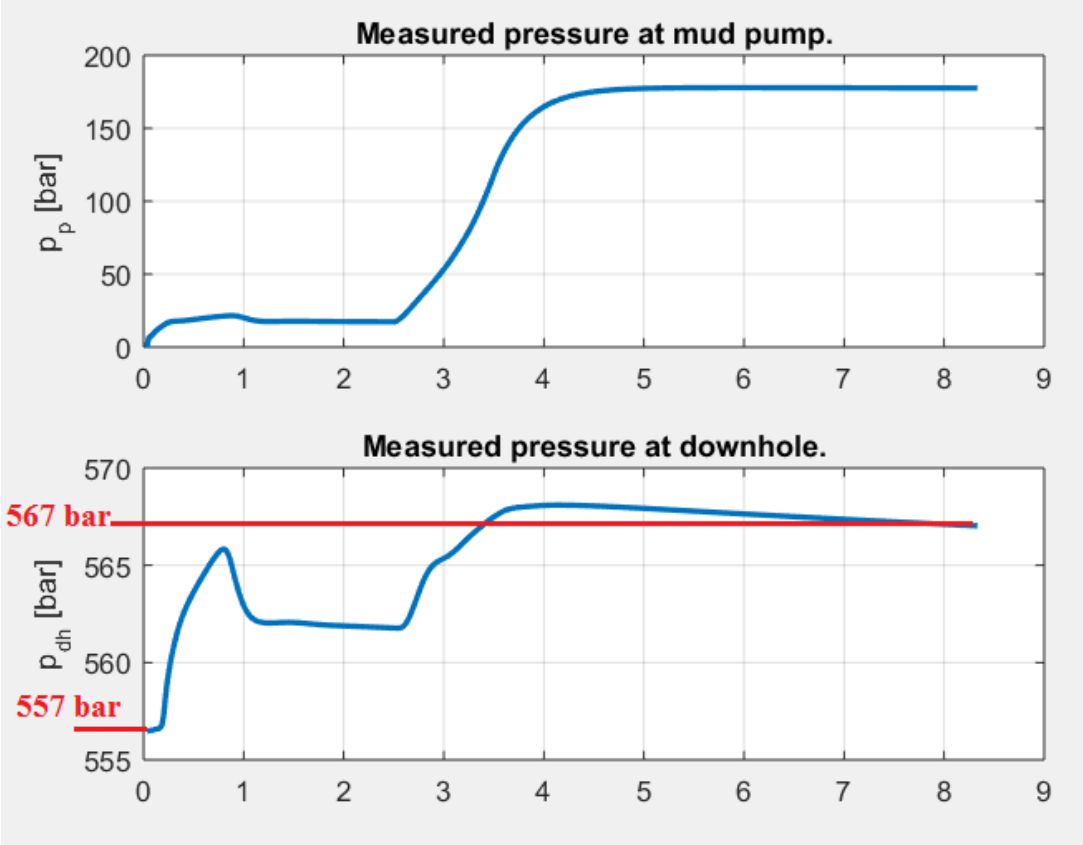

Figure 7.11.3 Shows the measured pressure downhole and the measured pressure at mud pump. The downhole pressure from hydrostatic to maximum pressure are marked.

The Figure 7.11.3 shows the measured pressure downhole and at mud pump. The curve of pump pressure follows the trend of flowrate-in. After around 2,5 minutes the flowrate was ramped up and the pump pressure is also shown to increase at 2,5 mins and stabilise at around 180 bar. The increase in pressure ΔP is equal to 567 – 557 = 10 bar.

Returning to the behaviour of downhole pressure, it starts to build up from the hydrostatic pressure, which is around 557 bar. It reaches its peak when the return flow starts to show. During connection, the increase in downhole pressure is normally around 4 to 7 bars above the normal pressure. The stabilising downhole pressure, after 8 minutes, is around 567 bar.

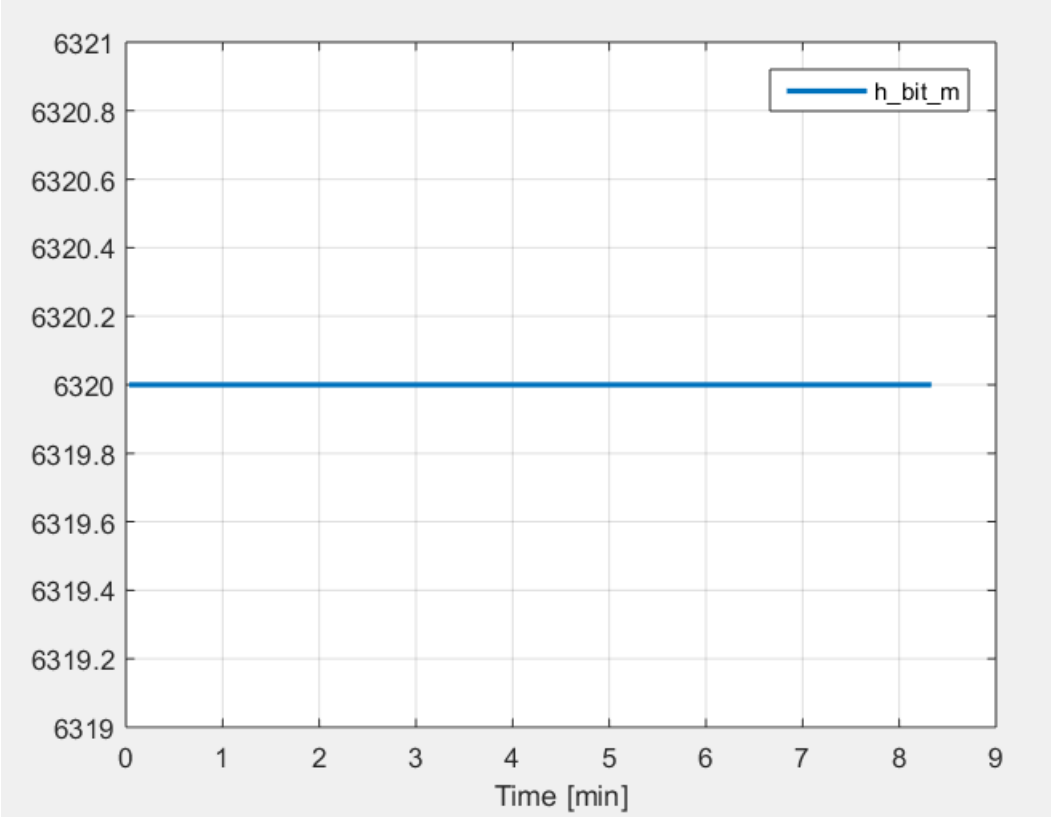

Figure 7.11.4 The bit depth is shown in this curve. This simulation considers constant bit depth at 6320 m.

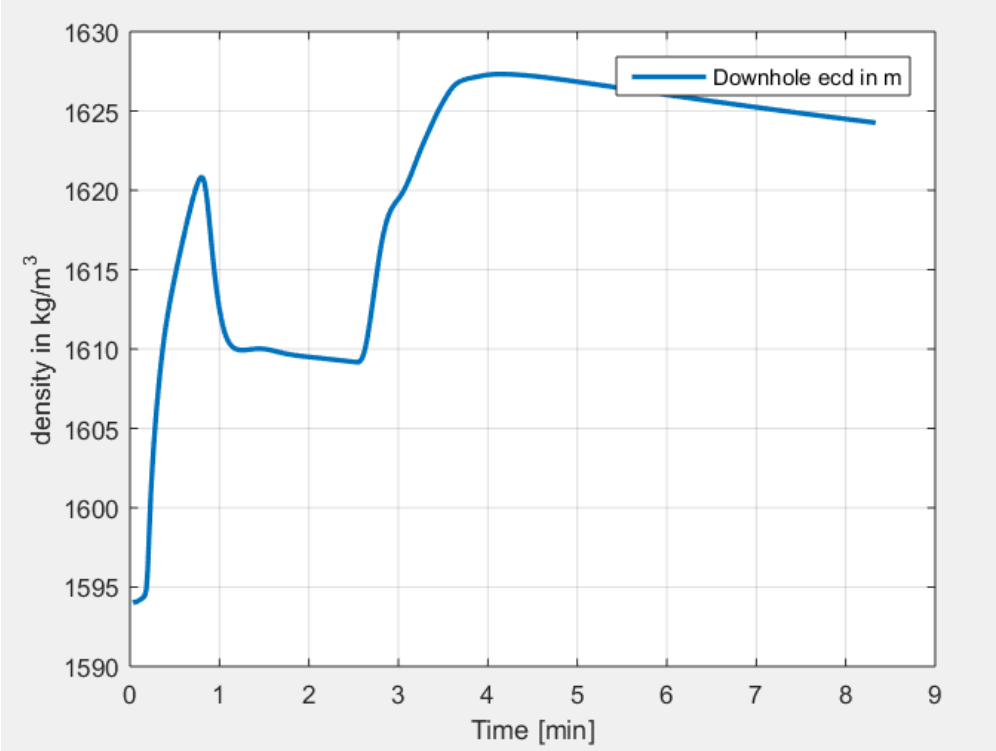

Figure 7.11.5 Shows the density in kg/m^3 versus time or downhole ECD. The mud density was set at 1.60 s.g.

The ECD is found by the equation,

$$ECD = \rho_{mud} + \frac{\Delta P_{annular\ friction} + \Delta P_{cuttings} + \Delta P_{surge\ \&swab} + \Delta P_{rotation} + \Delta P_{acceleration}}{gz} \quad Eq.7.11$$

The ECD shows the total BHP exerted on the formation, that is penetrated. It fluctuates along with the BHP. The gel strength is also responsible for fluctuations around 30 seconds. ECD increases drastically as the return flow is ramped up, as explained in Figure 7.11.2.

7.12 Scenario 2- Power Law

Scenario 2 considers a change in the rheological model from Robertsen and Stiffs HPHT model to Power law HPHT model.

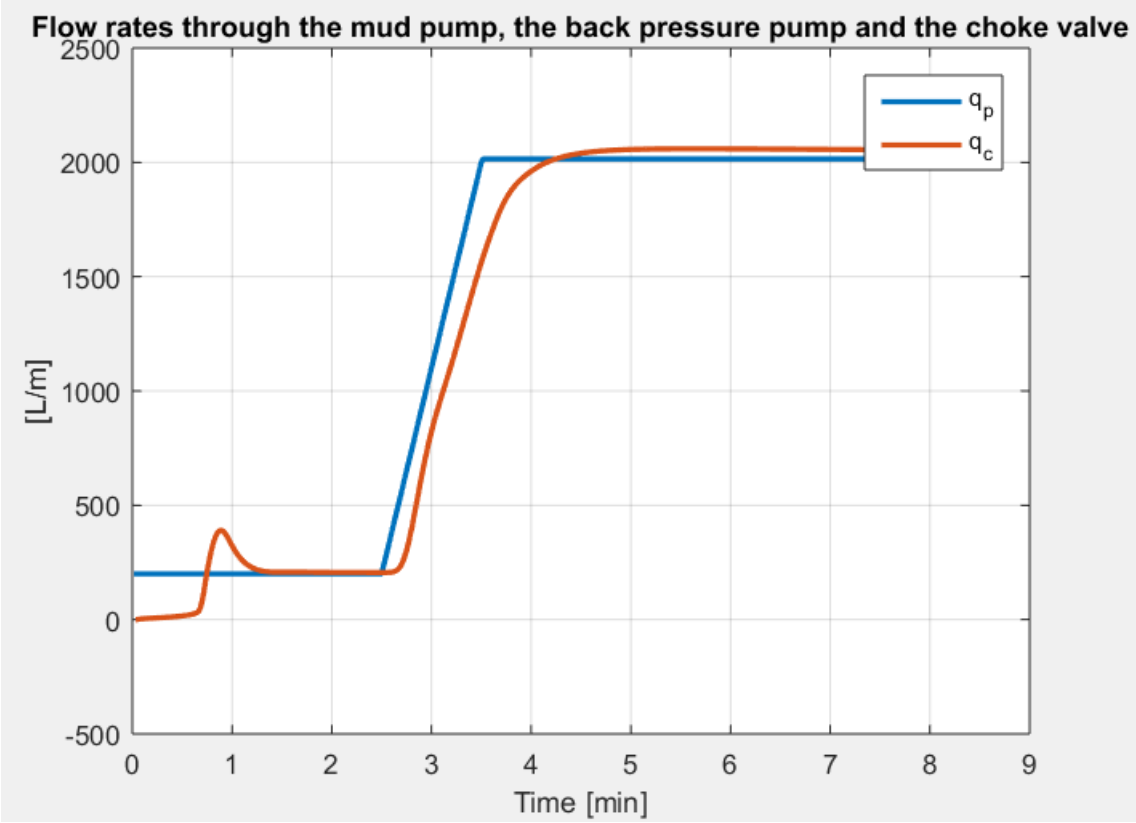

Figure 7.12.1 Shows the mud pump flow rate in (shown in blue) and return flow (shown in red) for PLM.

Figure 7.12.1 shows similar trends as the base case; however, a minor difference is seen early in time (around 50 seconds). The mud pump flowrate-out oscillates less compared to scenario 1, which means that the ECD in this case is further away from reaching the fracture pressure gradient. This is because the PLM provides more information at low shear rate conditions. Since, the parameter n, also known as the flow behaviour index of the PLM (Equation 2.12) is normally given as less than one, as the shear rate goes to zero, the viscosity tries to reach infinity. This condition is true when viscosities act as Newtonian, meaning $n = 1$, at high shear rates for suspensions and polymer solutions, such as in WBM.

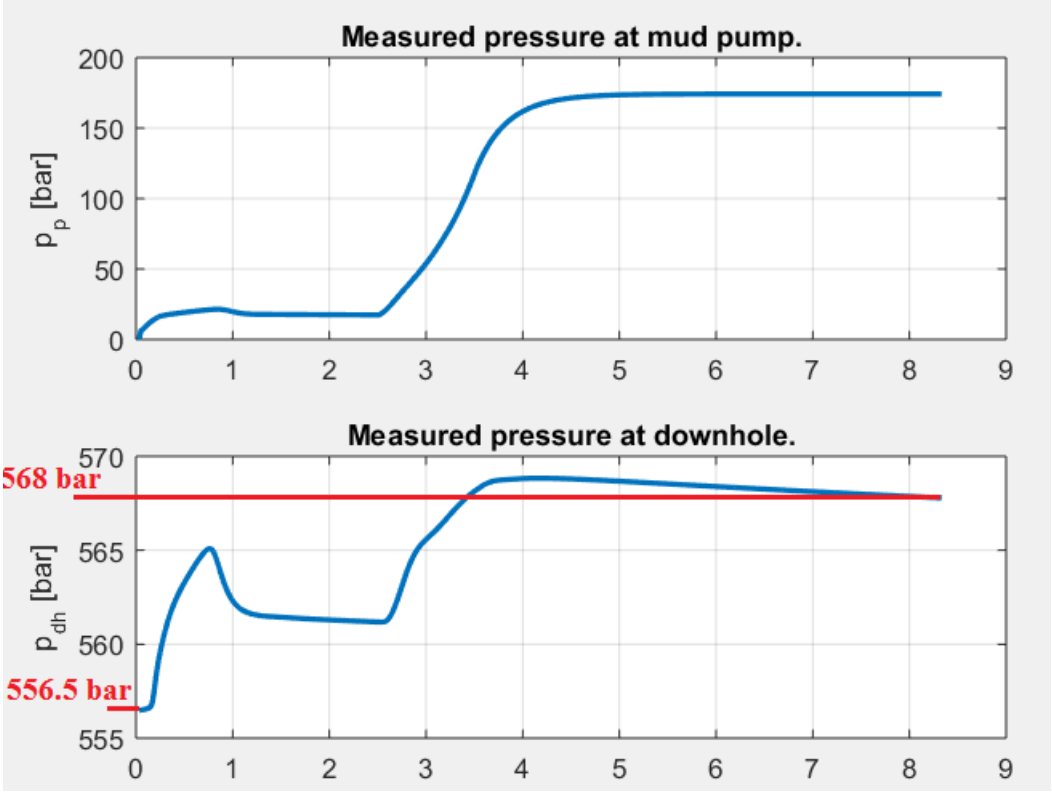

Figure 7.12.2 Shows the measured pressure downhole and the measured pressure at mud pump for PLM.

The mud pump pressure is identical to scenario 1, since the configured flowrate-in is identical. The change of Robertsen and Stiff HPHT model to Power law HPHT has no impact on the mud pump pressure.

The measured pressure downhole however, shows a hydrostatic pressure of 556.6 bar, which is 0.5 bar less than in scenario 1, and the pressure increase after around 500 seconds is, ΔP= 568- 556.5 = 11.5 bar, which is 1.5 bar more than what is seen in previous rheological model.

The bit depth is kept constant and none of the changed parameters will affect its result, therefore it is not mentioned in every scenario.

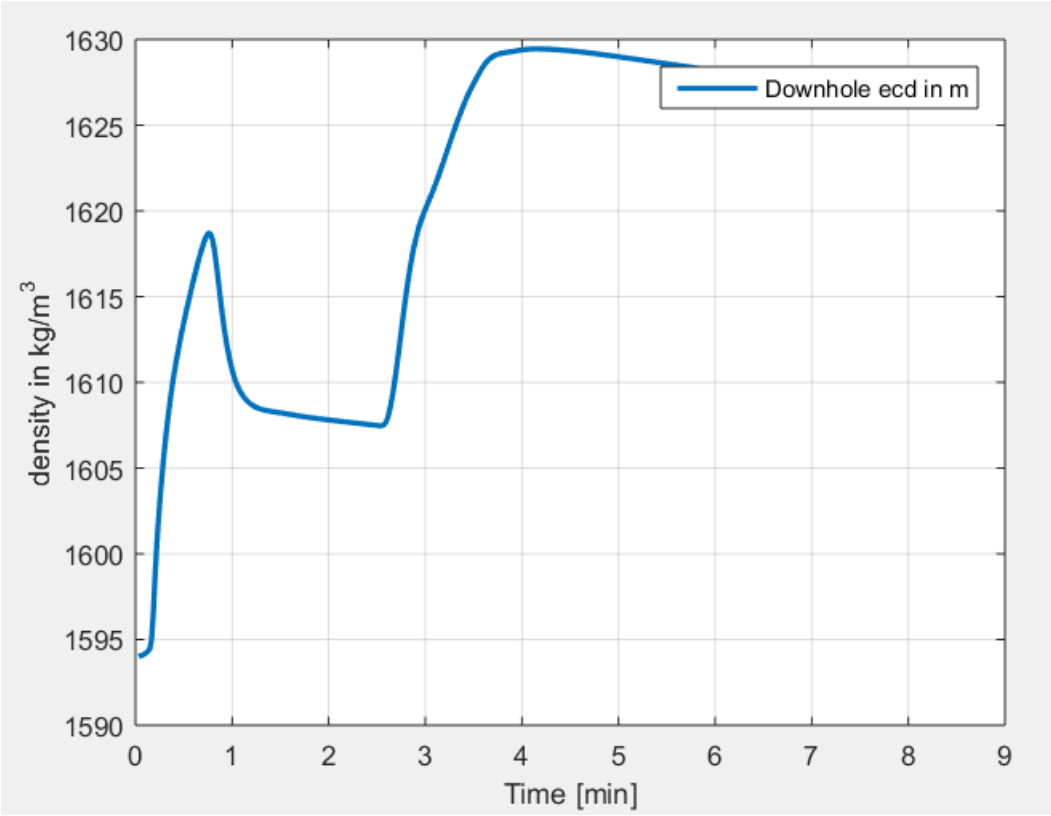

Figure 7.12.3 Shows the density in kg/m^3 versus time or downhole ECD. The mud density was set at 1.60 s.g for PLM.

The initial increase in oscillation in Figure 7.12.3, is mainly due to the gel strength and the filling of empty drill pipe above the drill floor. It is ignored and the late time stabilizing value is more emphasized. The first stability point at around 1 to 2 minutes is closer to the set-point then what was observed in scenario 1. Then the same effect is observed as in Figure 7.11.5, as the flow rate is ramped up to 2000 lpm the ECD becomes more unstable, as the downhole pressure and temperature changes.

7.13 Scenario 3 – Bingham Plastic

Scenario 3 considers another rheological model which is known as the Bingham Plastic HPHT model. This model will be compared to the one of scenario 1, that is, the Robertsen and Stiff HPHT model.

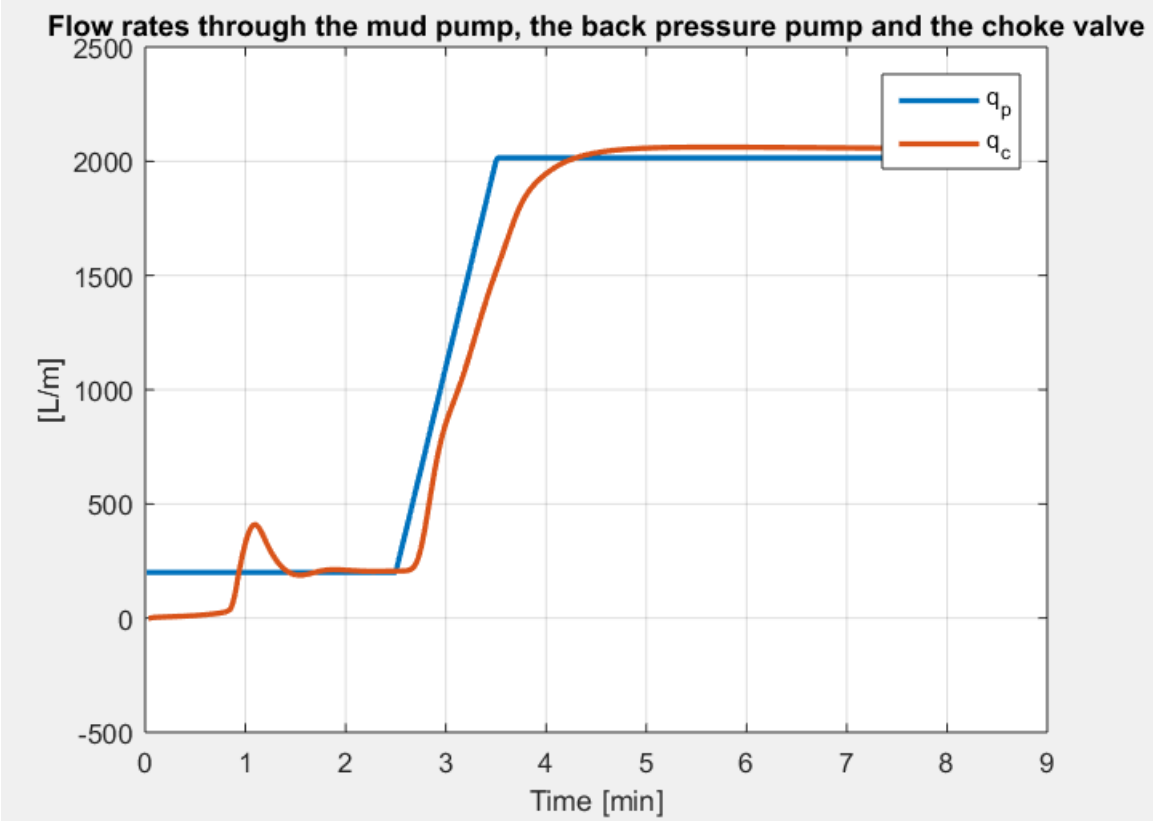

Figure 7.13.1 Shows the mud pump flow rate in (shown in blue) and return flow (shown in red) for BPM.

The trend in Figure 7.13.1 is very similar to scenario 1. One of the main differences is that the return flow, which is seen a few seconds later than in scenario 1, is that the peak of the return flow after 60 seconds is lower. This is because of the gel effect and the difference between the model for calculating the yield stress. The rest of the trend is identical.

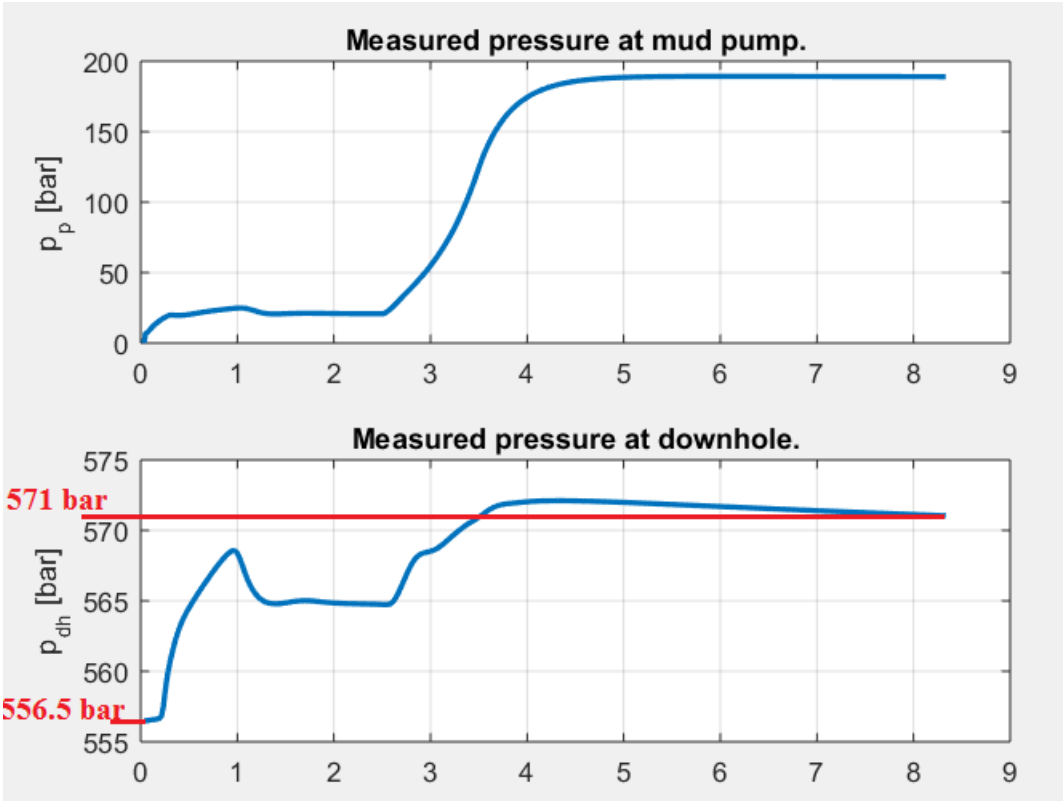

7.13.2 Shows the measured pressure downhole and the measured pressure at mud pump for BPM.

The mud pump pressure initially increases at same rate, but stabilises at a greater pressure, than in scenario 1, due to the BP rheological model.

The measured pressure downhole starts from 556.5 bar, which is about the same as in scenario 1 and hence stabilizes at 571 bar in 500 seconds. The difference in pressure is $\Delta P = 571 - 556.5$ bar = 14.5 bar. The BPM does not represent the behaviour of drilling fluid accurately at low shear rates (in the annulus) or at very high shear rate (at the bit).

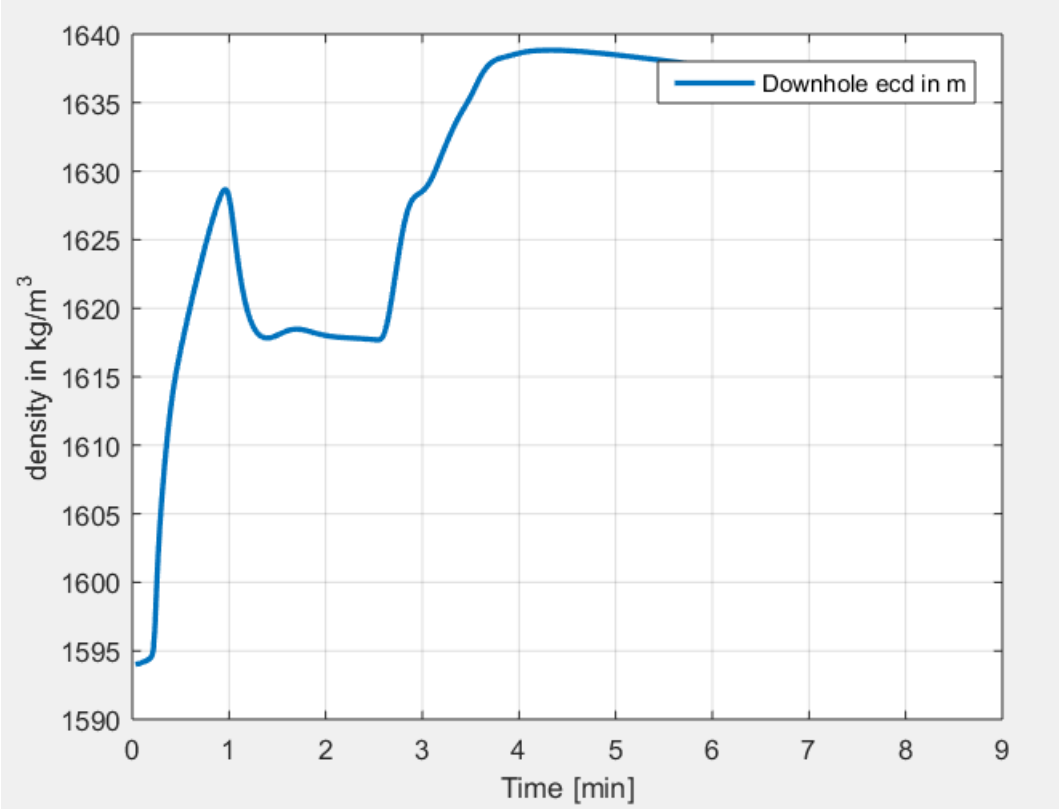

Figure 7.13.3 Shows the density in kg/m^3 versus time or downhole ECD. The mud density was set at 1.60 s.g for BPM

The initial impression of the Figure 7.13.3 is that Bingham model overestimates the downhole ECD. The whole curve is shifted up 10 kg/m^3 compared to other rheological models.

Thus, the conclusion states that the use of Bingham Plastic HPHT model gives more inaccurate ECD.

7.14 Scenario 4 – Increasing density

In this scenario the mud density will be increased to 1.800 s.g and compared to scenario 1 which had a mud density of 1.600 s.g.

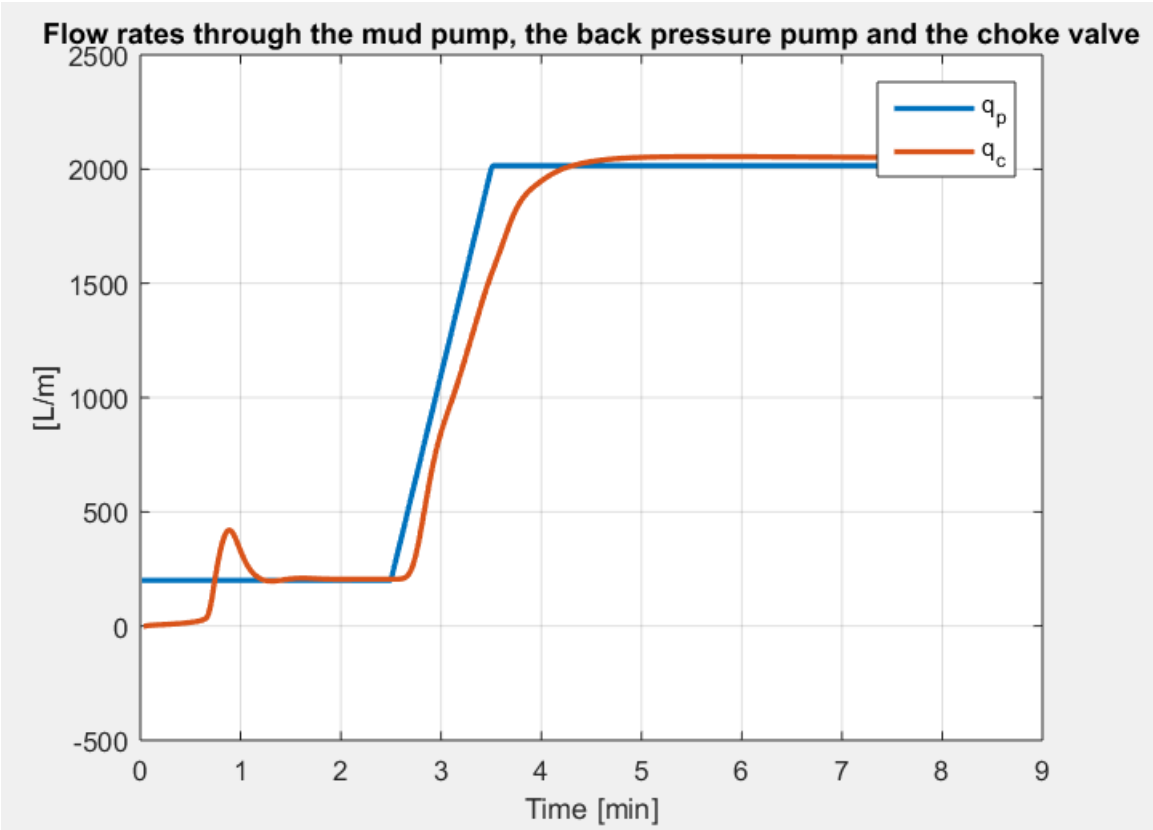

Figure 7.14.1 Shows the mud pump flow rate in (shown in blue) and return flow (shown in red) when density increases to 1.800 s.g.

Since, the change of density has no effect on the return flow, it is identical to scenario 1.

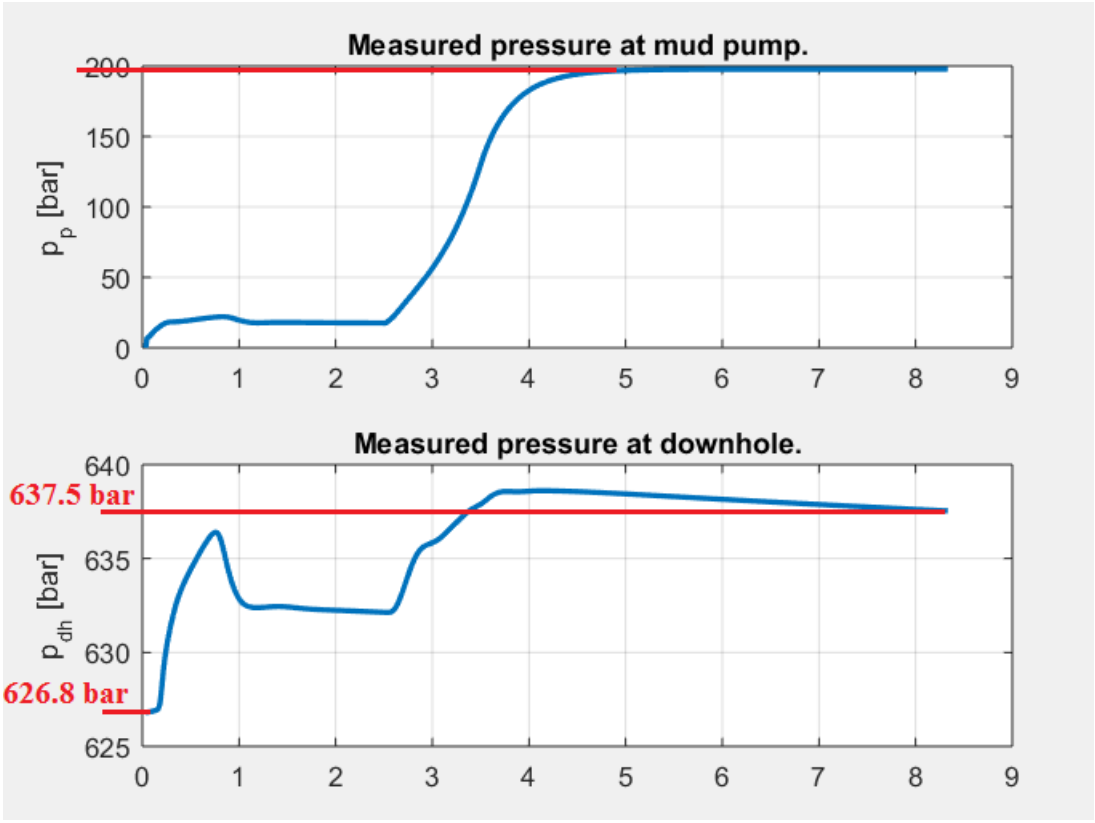

Figure 7.14.2 Shows the measured pressure downhole and the measured pressure at mud pump when density increases to 1.800 s.g.

As the density increases to 1.800 s.g the pump pressure reaches around 200 bar. This behaviour is expected as density is a function of pressure. The increase in pressure alleviates in a difference of around 20 bar, compared to mud density of 1.600 s.g.

The measured pressure downhole starts at 626.8 bar due to the increase of density. The pressure increase to the stabilising point from start is around ΔP=637.5-626.8 bar = 10.7 bar. From what was observed in scenario 1, ΔP was around 10 bar (with some reading error). This value, ΔP is proved to be constant, as expected.

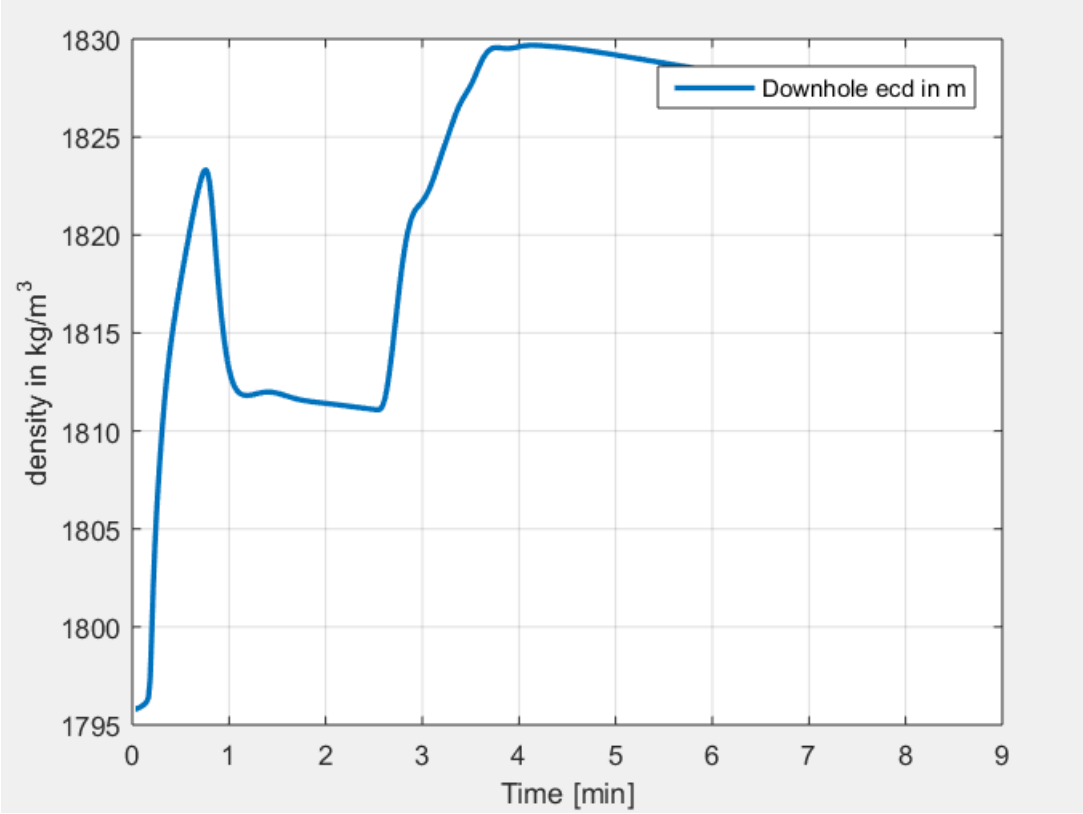

Figure 7.14.3 Shows the density in kg/m^3 versus time or downhole ECD. The mud density was set at 1.80 s.g.

ECD has increased due to the increase of density, which is expected. The ECD is fluctuating even more when it increases and steadies further away from the desired density of 1.800 s.g. Overall difference from the desired density to stabilising point is around 26.5 kg/m^3, whereas in scenario 1 this value was around 24 kg/m^3 Thus, the ECD is more unstable when the density increases.

7.15 Scenario 5 – Increasing the gel strength

Scenario 5 considers increase in gel strength of 10 seconds to 10 Pa and of 10 minutes to 15 Pa, the pressure plots are compared to the base case in scenario 1.

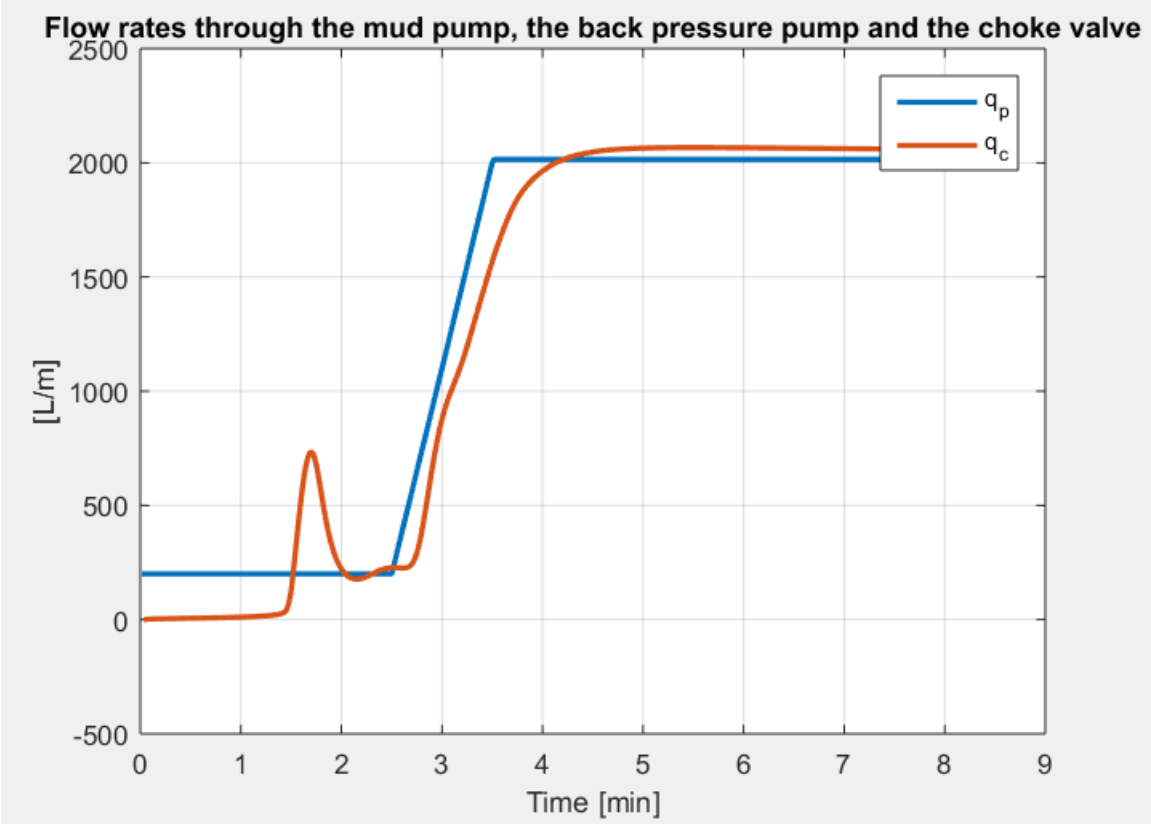

Figure 7.15.1 Shows the mud pump flow rate in (shown in blue) and return flow (shown in red) when gel strength is increased.

By increasing the gel strength, the drilling fluid will have greater ability to suspend drill solids and weighing material such as barite when circulation breaks. Comparing this to Figure 7.11.1, the higher suspension of solids results in greater return flow around 1.5 minutes. The return flow is also seen later than in scenario 1. During the late time (after 5 minutes), the return flow shows no difference from base case.

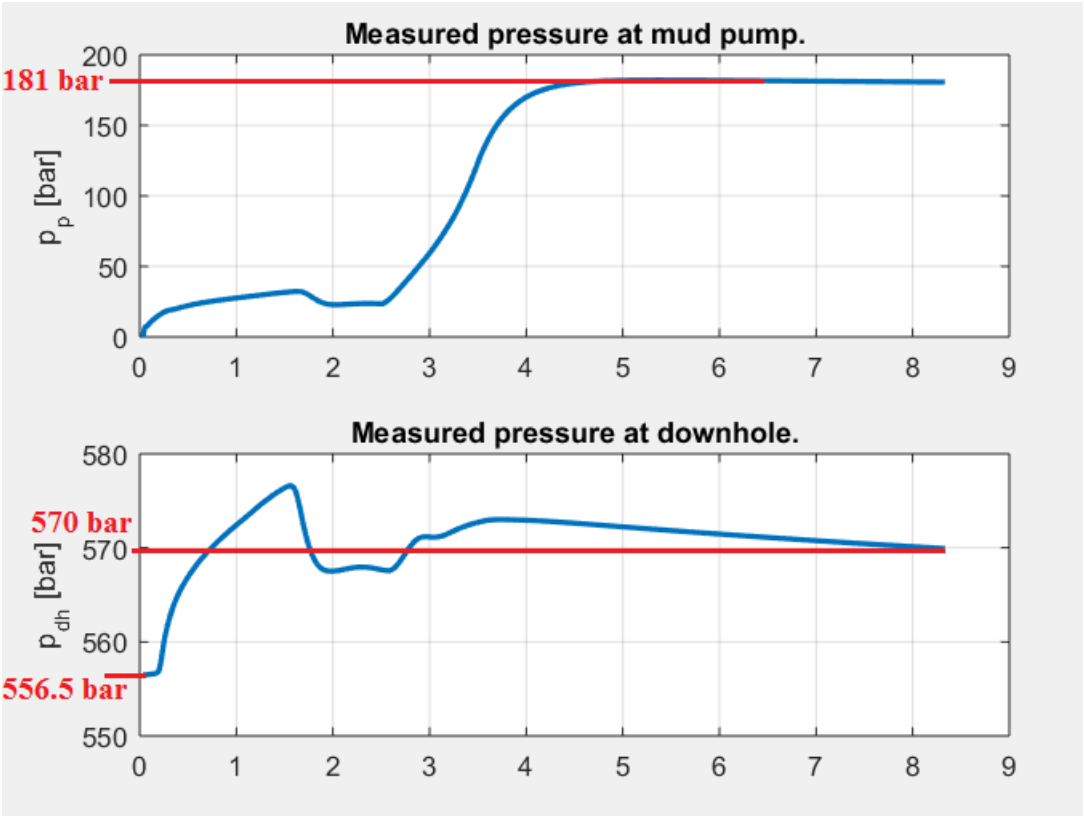

Figure 7.15.2 Shows the measured pressure downhole and the measured pressure at mud pump when gel strength increases.

As the gel strength of the mud is increased, the mud pump pressure has increased by a small pressure around 1-2 bars, in order to break circulation.

The measured pressure downhole also takes longer to build up while the drill string is filled. ΔP is 570-556.5 bar= 13.5 bars. Consequently, it increased compared to the lower gel strength with a pressure of 3.5 bars from scenario 1.

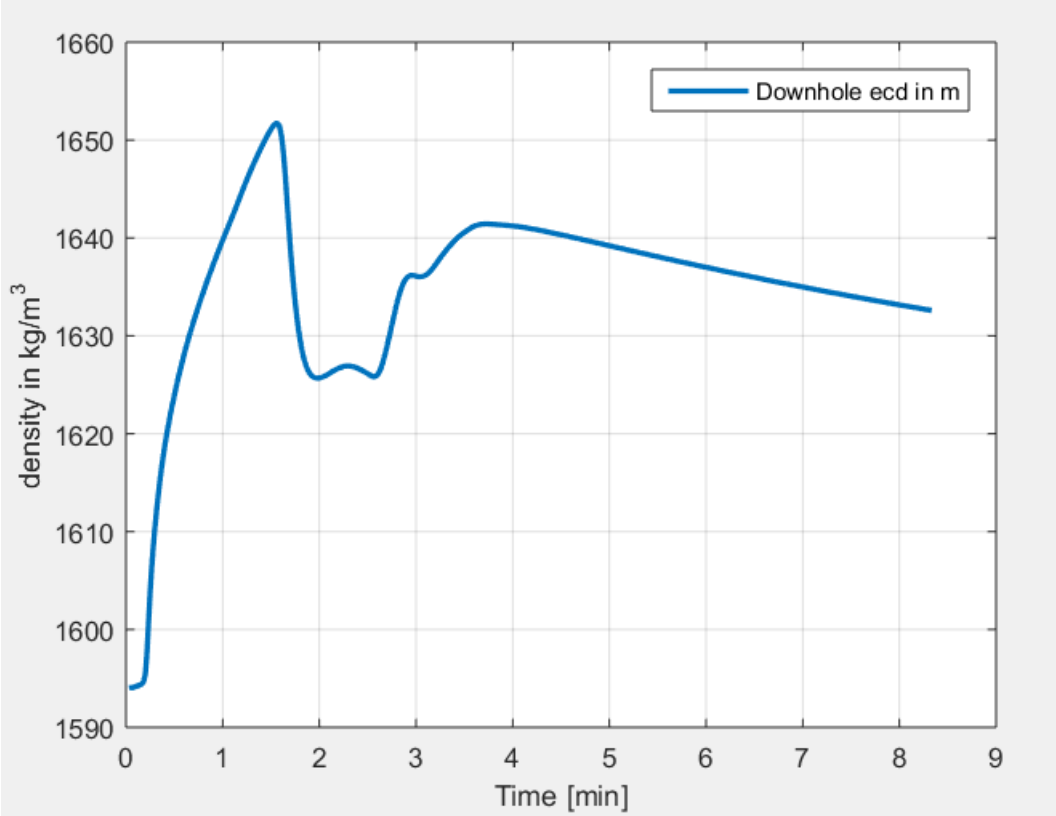

Figure 7.15.3 Shows the density in kg/m^3 versus time or downhole ECD. The mud density was set at 1.60 s.g. The effect of increased gel strength was studied in this figure.

At first glance, the whole trend of ECD is very unlike any other scenarios compared earlier. ECD fluctuates more at early time due to its dependency upon the gel strength, which in return affects the viscosity and hence the density of the drilling fluid. The stabilising ECD around 500 seconds is at 1632.5 kg/m^3. In scenario 1 the stabilising value was around 23 kg/m^3 which gives a difference of around 9.5 kg/m^3. As seen from the curve, higher gel strength fluctuates ECD even further from expected value, considering fluctuations created by downhole pressure and temperature.

7.16 Scenario 6- Alteration of stresses in PVT-table

This scenario considers changing the stresses given in PVT table in the configuration. A constant with a magnitude of 10 lb/100ft^2 will be added to stress at all rpms (rotation per minute). The rheological model of Bingham Plastic HPHT will be studied and compared to scenario 3, where the Bingham model was applied.

	Temp. (°C)	Press. (bar)	Stress at 3 rpm (lb/100ft²)	Stress at 6 rpm (lb/100ft²)	Stress at 30 rpm (lb/100ft²)	Stress at 60 rpm (lb/100ft²)	Stress at 100 rpm (lb/100ft²)	Stress at 200 rpm (lb/100ft²)	Stress at 300 rpm (lb/100ft²)	Stress at 600 rpm (lb/100ft²)
▸	50.00	1.0	15.0	17.0	27.0	37.0	47.0	69.0	82.0	131.0

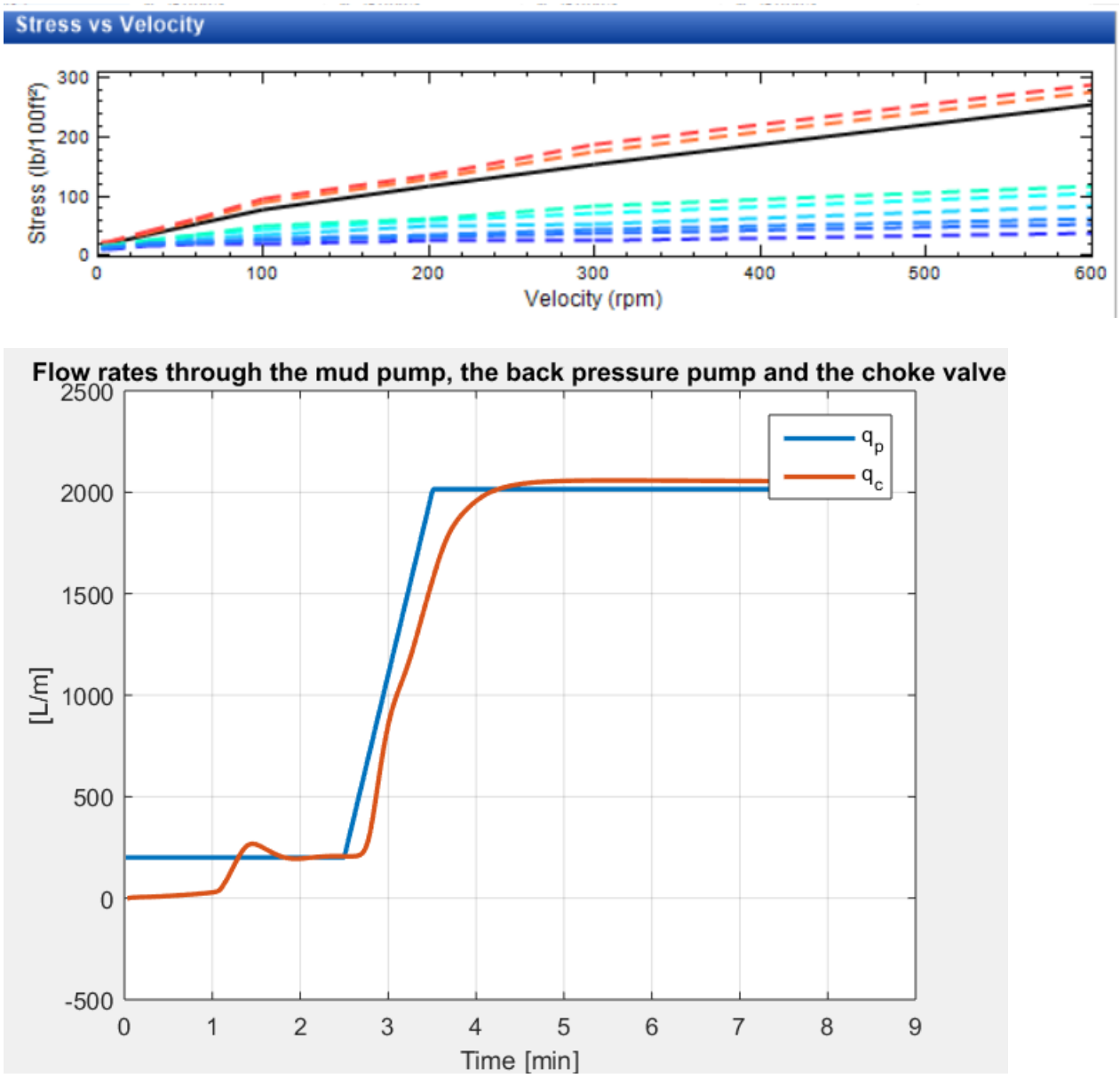

Figure 7.16.1 Shows the mud pump flow rate in (shown in blue) and return flow (shown in red) when stresses in the PVT table are increased.

Compared to Figure 7.13.1 the return flow fluctuates less, this is mainly because by adding a constant value to shear stress at lower rpms the curve of shear stress versus shear rate shifts upwards with 10lb/100ft^2. Since, the Bingham plastic HPHT model includes a constant of YP, τ_0, the model is better fit at low shear rates. The return flow fluctuates therefore much less, while the late time data shows no differences.

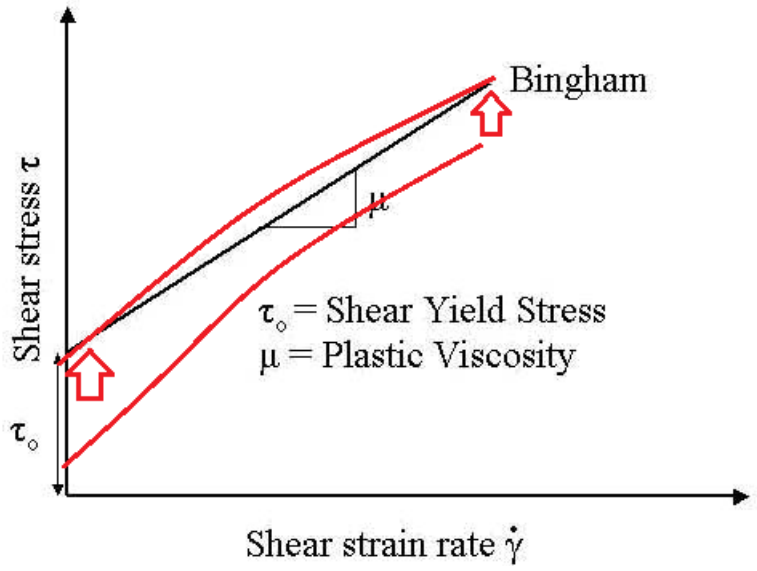

Figure 7.16.2 Bingham Plastic HPHT model showing a better fit when the shear rate is increased with a constant.

This effect is seen on the Figure 7.16.2. The red curve shows measured values an example of WBM to illustrate why Bingham Plastic HPHT model is a better match, when the shear rate is increased with a constant value.

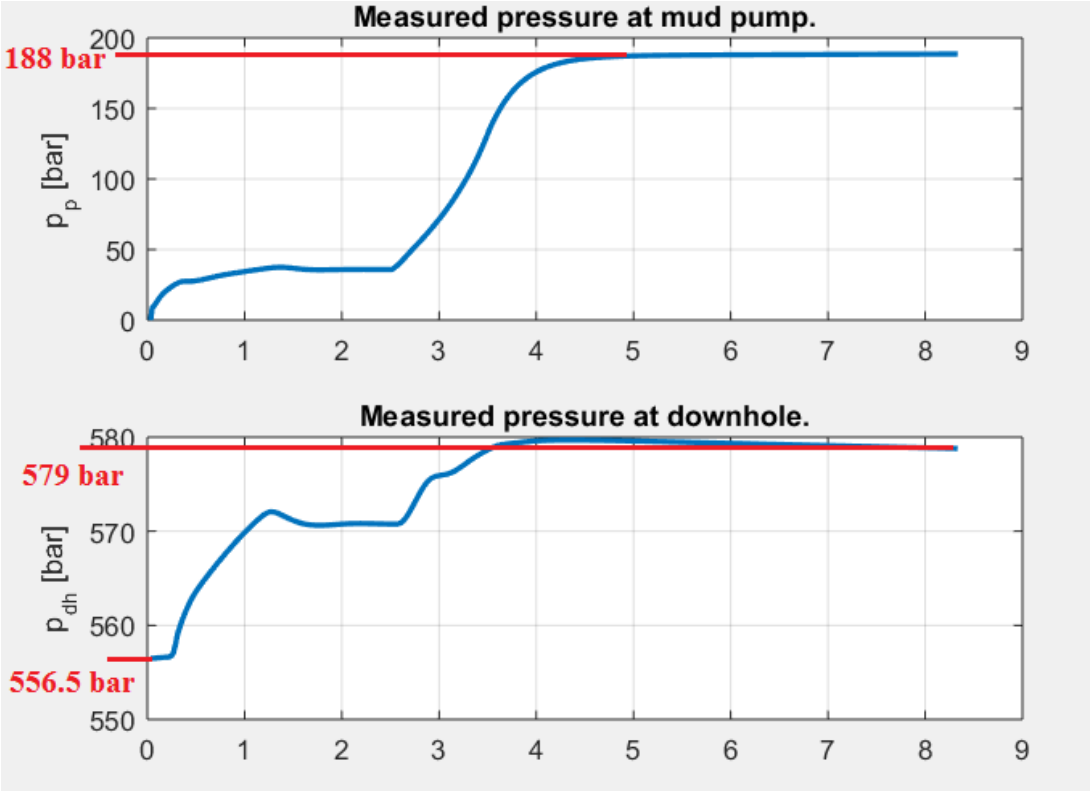

Figure 7.16.3 Shows the measured pressure downhole and the measured pressure at mud pump when stresses in the PVT table are increased with a constant.

The measured pump pressure compared to scenario 3, has not altered. This is because the pump pressure shows no change, when the shear stress changes.

The measured pressure downhole starts with hydrostatic pressure of 556.5 bar similar to Figure 7.13.2. However, after ramping the flowrate to the target the downhole pressure steadies at a higher pressured downhole. The increase in pressure is around ΔP= 579 - 556.5 = 22.5 bar. The fluid moves when shear rate is > 0 when shear stress is greater than the YP. In this case, the YP of Bingham plastic HPHT model increases, which causes a sudden pressure to change, when the fluid starts to move or slows down abruptly. Once the fluid moves from being static, higher BHP is observed due to change of a greater YP.

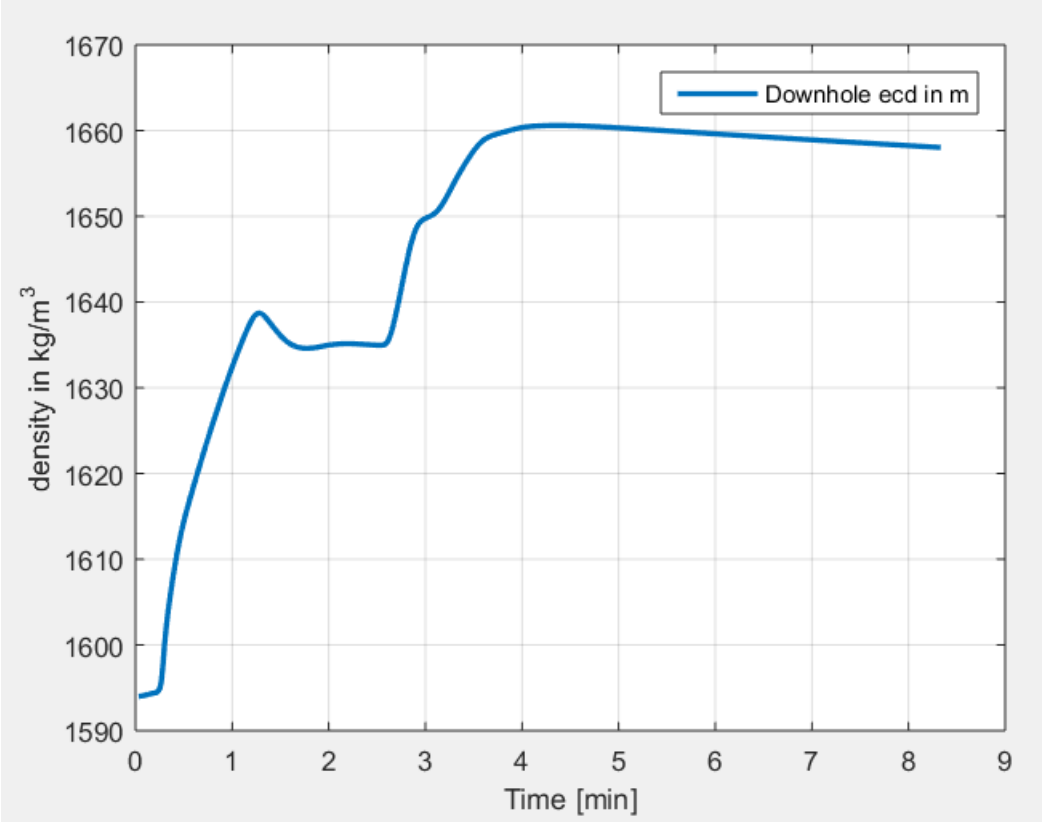

Figure 7.16.4.Shows the density in kg/m^3 versus time or downhole ECD. The mud density was set at 1.60 s.g. The effect of increased stresses in PVT table were studied.

An even greater oscillation and difference in density is seen compared to Figure 7.13.3. The increase in shear stress makes greater fluctuations of density because of the BPM of linear shear stress versus shear rate relationship. By, adding a constant value to PVT table, the error does not change, in fact since the stresses are increasing, ECD is also predicted to fluctuate more compared to scenario 3.

7.2 Simulation of OBM

A realistic OBM is configured in this section and has properties as shown below. While running OBM, the configuration of mud pump flow rate-in was similar to the design presented in WBM. The main difference between WBM and OBM considered in this section is the OWR, the base densities and thermal properties and the PVT table. The mud pumps flowrate-out is affected heavily by alternation of the OWR and the gel strength.

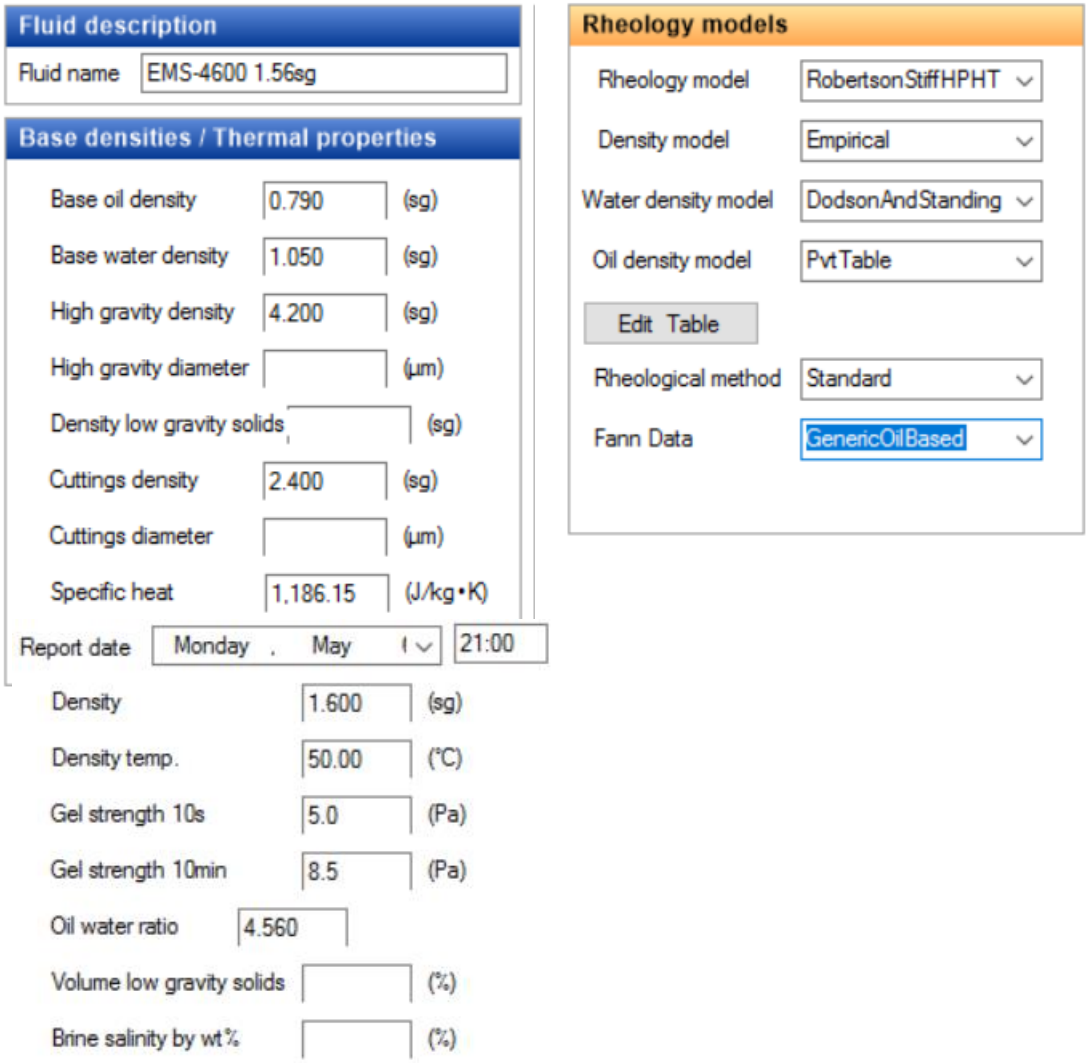

Temp. (°C)	Press. (bar)	Stress at 3 rpm (lb/100ft²)	Stress at 6 rpm (lb/100ft²)	Stress at 30 rpm (lb/100ft²)	Stress at 60 rpm (lb/100ft²)	Stress at 100 rpm (lb/100ft²)	Stress at 200 rpm (lb/100ft²)	Stress at 300 rpm (lb/100ft²)	Stress at 600 rpm (lb/100ft²)
50.00	1.0	9.0	11.0	16.0	22.0	29.0	43.0	58.0	95.0

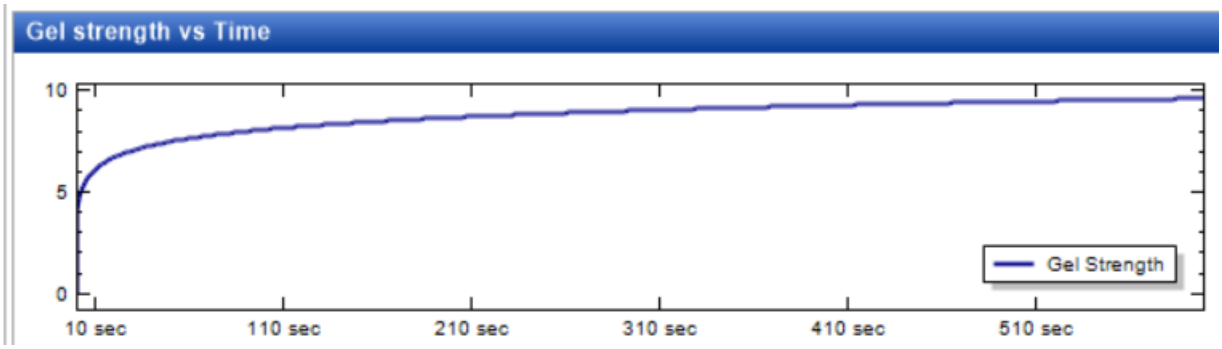

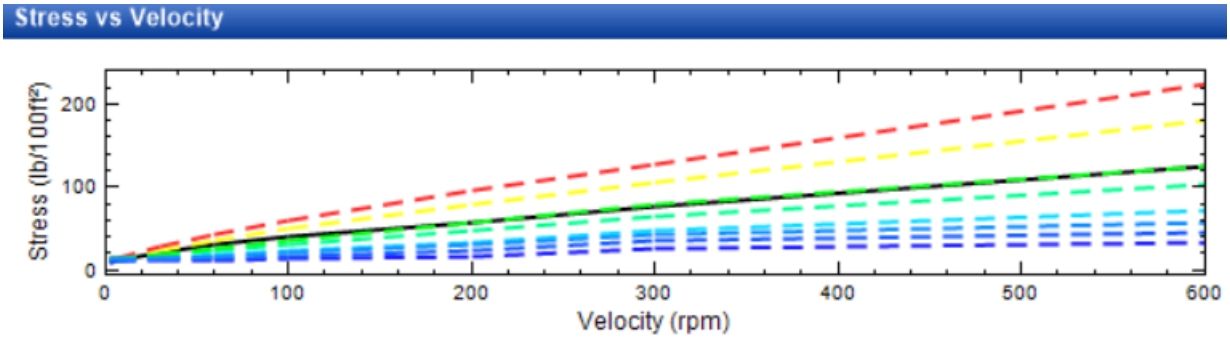

A summary of the simulation plan for OBM is shown. Scenario 7 is taken as a basis when comparing scenarios 8-12.

Scenario nr.	Mud type	Changing parameter	Value of changed parameter
7	Generic OBM	(shown configuration) Realistic OBM	-
8	Generic OBM	Power law HPHT (rheology)	-
9	Generic OBM	Bingham model HPHT (rheology)	-
10	Generic OBM	Density increase	1.800 s.g
11	Generic OBM	Increasing the gel strength for 10s, 10 min	10 Pa (10s) and 15.5 Pa (10 min)
12	Generic OBM	Lowering the OWR	1.0 OWR

Table 7.2.1 Shows the simulation plan run for 6 different scenarios for OBM and the changing parameter. The pressure profiles are compared with scenario 7.

7.21 Scenario 7- Base case for OBM

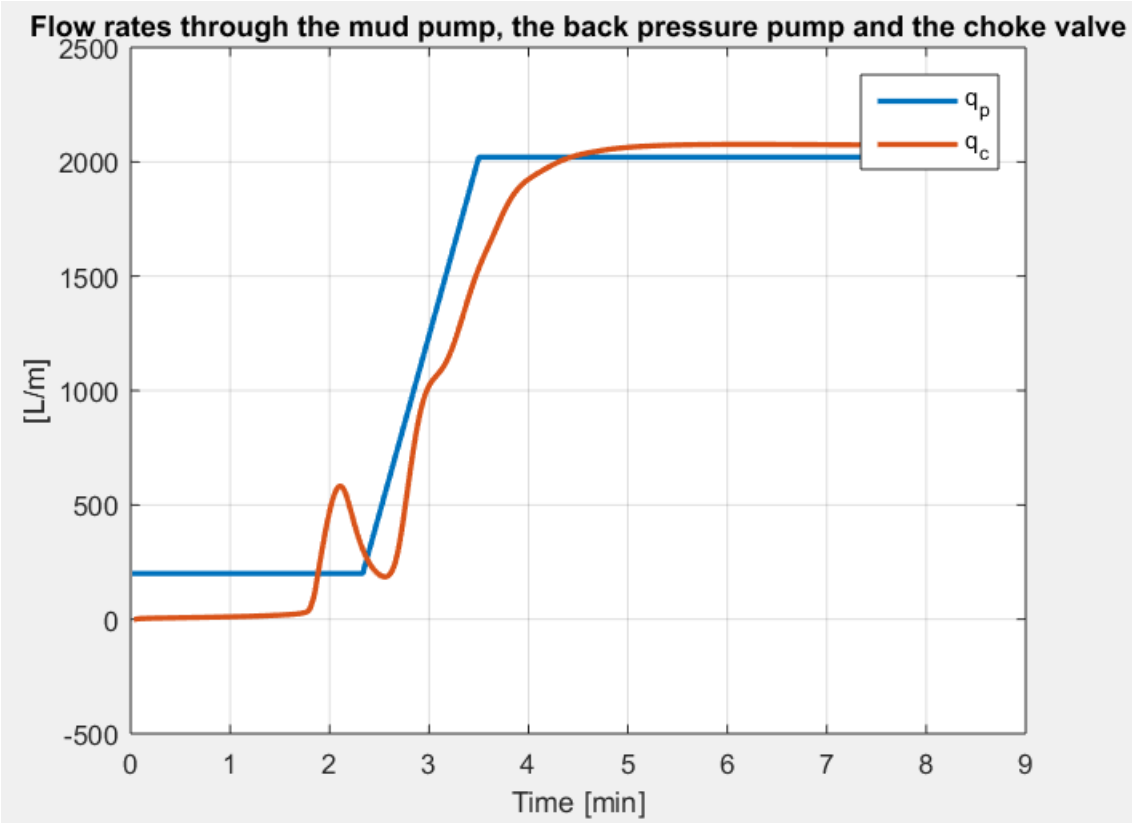

Figure 7.21.1 shows the mud pump flow rate in (shown in blue) and return flow (shown in red) for base case of OBM.

Shows the mud pump flow rate in (shown in blue) and mud pump flowrate out (shown in red). Again, as in WBM, the fill pipe flow rate is ignored and the pump is started at 200 l/min. This flowrate is continued till a return flow is seen. Then the pump ramps up to the target flow rate of 2000 l/min. The return flow arrives late, around 2 minutes. This effect of slow return flow is due to the high OWR. Since, WBM and OBM have different gel effect the return flow is seen later.

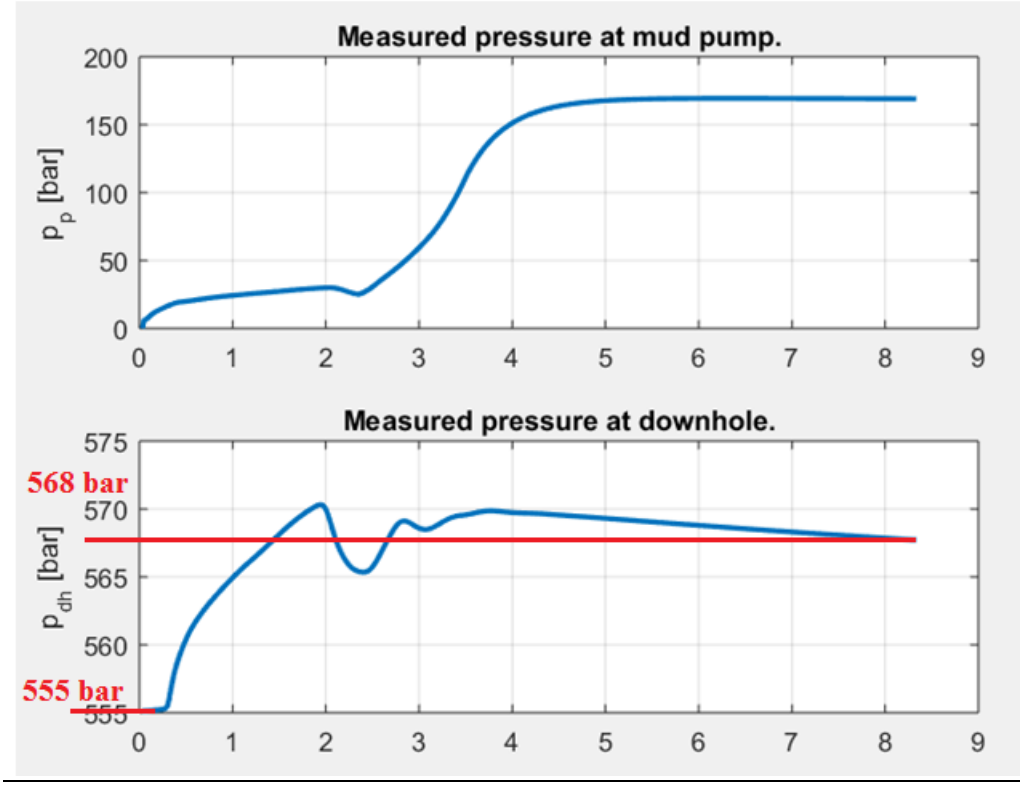

Figure 7.21.2 Shows the measured pressure downhole and the measured pressure at mud pump. The downhole pressure from hydrostatic to maximum pressure are marked.

Measured pump pressure takes some time before it stabilises at 168.5 bar, which is a reflection upon keeping the flowrate at 200 l/min before ramping it up to 2000l/min. The pump pressure is similar to previous analysed WBM.

The measured pressure downhole starts at hydrostatic pressure around 555 bar and stabilises around 568 bar. The increase in pressure is around $\Delta P = 568 - 555 = 13$ bar. The difference in WBM was 10 bar, also an effect of OWR.

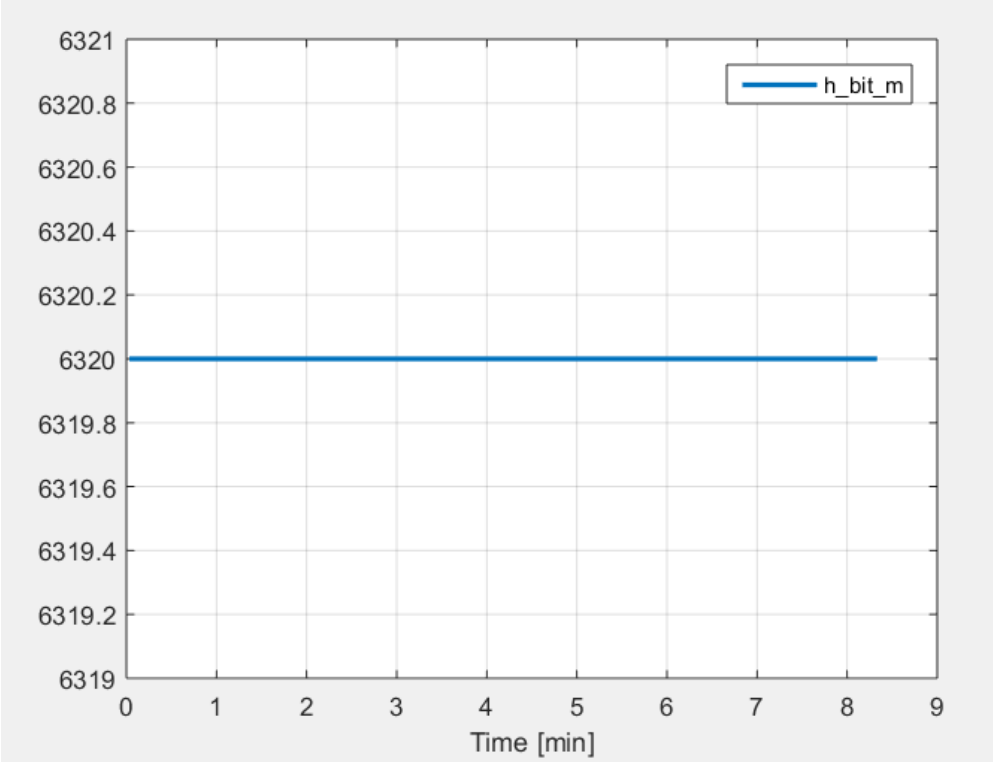

Figure 7.21.3 The bit depth is shown in this curve. This simulation considers constant bit depth at 6320m. As mentioned before the bit depth is not changed and therefore is not included in analysis ahead.

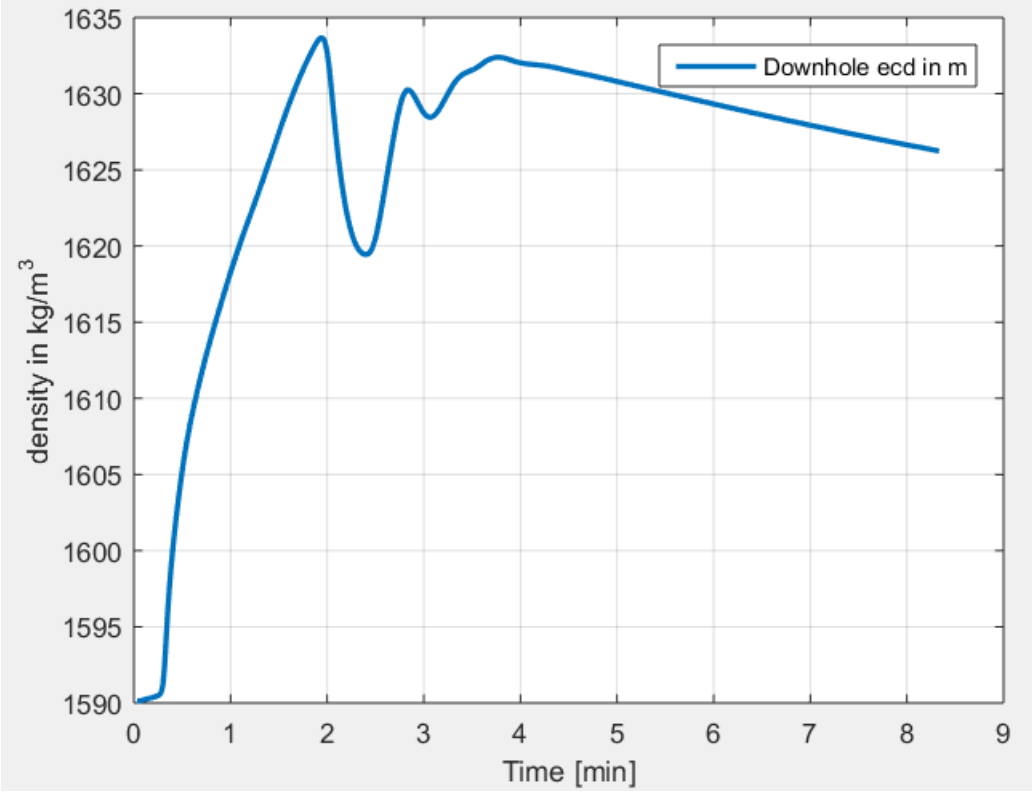

Figure 7.21.4 Shows the density in kg/m^3 versus time or downhole ECD set at 1.60 s.g.

The desired mud density was given to be at 1600 kg/m^3 or 1.6 s.g. The response shows oscillations and takes some time before it stabilises towards the target density. At around 8 minutes the density is shown to be 26 kg/m^3, this is somewhat similar to what we have observed in WBM.

7.22 Scenario 8- Power law

Scenario 8 considers a change in the rheological model from Robertsen and Stiffs HPHT model to Power law HPHT model.

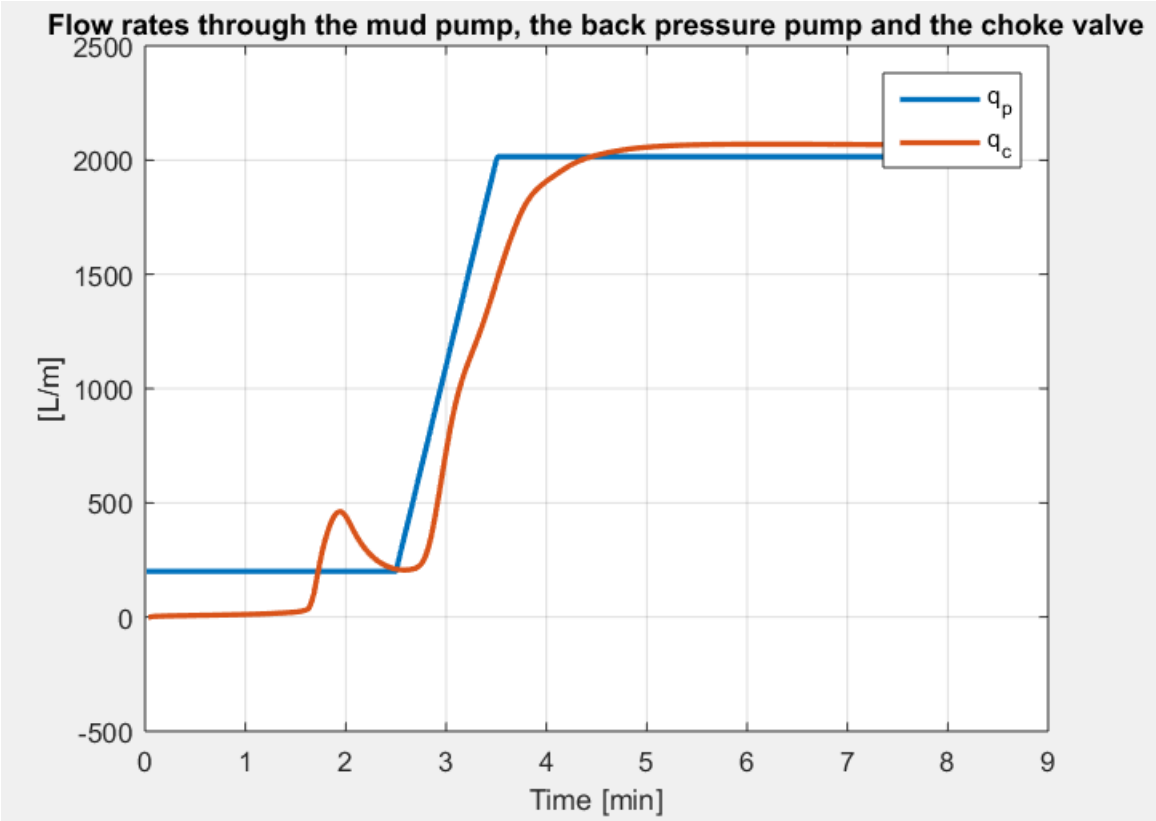

Figure 7.22.1 Shows the mud pump flow rate in (shown in blue) and return flow (shown in red) for PLM.

By changing the rheological model to power law HPHT, the return flow is seen few seconds earlier. The main difference is the oscillation at 2 mins, which decreases with a small amount for the same reason as discussed in WBM. The PLM works well for OBM, because it shows shear thinning behaviour and have some value for shear stress when the shear rate is zero. As explained earlier in WBM, ECD is further away from reaching the fracture pressure gradient. This is because the PLM provides more information at low shear rate conditions.

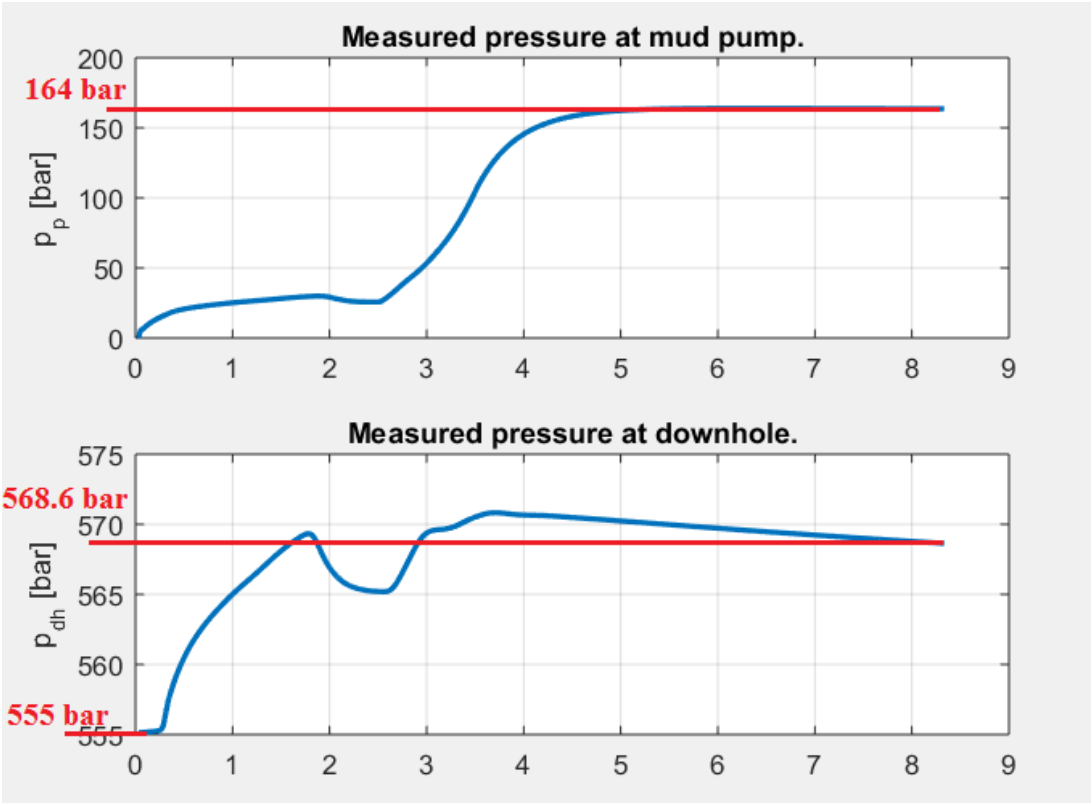

Figure 7.22.2 Shows the measured pressure downhole and the measured pressure at mud pump for PLM.

The mud pump pressure is identical to scenario 7, because the configured flowrate-in is identical. The change of Robertsen and Stiff HPHT model to Power law HPHT has no impact on the mud pump pressure.

The measured pressure downhole, builds up at same hydrostatic pressure of around 555 bar and stabilizes around 568.6 bar. ΔP = 568.6-555= 13.6 bar. Compared to scenario 7 the difference in the downhole pressure is around 0.6 bar.

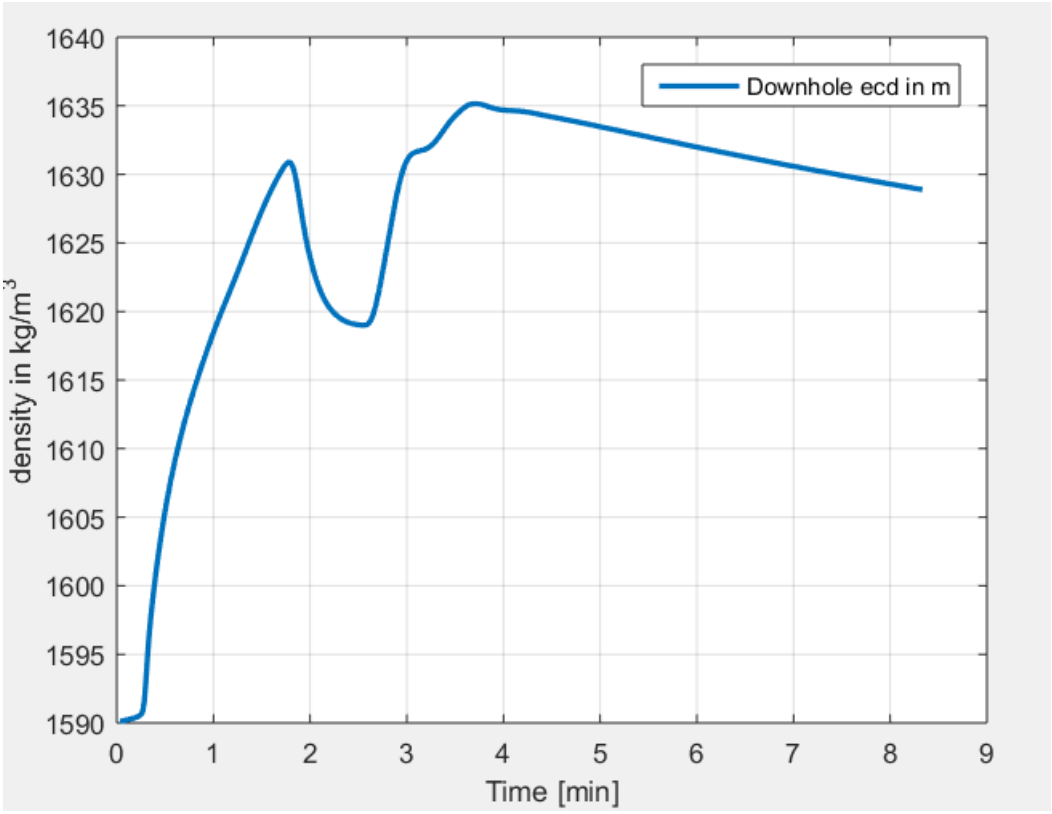

Figure 7.22.3 Shows the density in kg/m^3 versus time or downhole ECD. The mud density was set at 1.60 s.g for PLM.

Changing the rheological model to Power law HPHT, the ECD gives a greater offset to desired density, the reason might be due to the delay of return flow. The PLM does not consist of YP and fluids that flow using this model generally do not have shear stress when the shear rate is zero. This does not match drilling fluids and therefore shows higher ECD than expected. PLM as mentioned earlier lacks to predict drilling fluid behaviour at lower shear rates.

7.23 Scenario 9- Bingham Plastic

This scenario considers another rheological model known as Bingham plastic HPHT model. It is said to be less accurate for drilling mud than the other two seen in scenario 7 and 8.

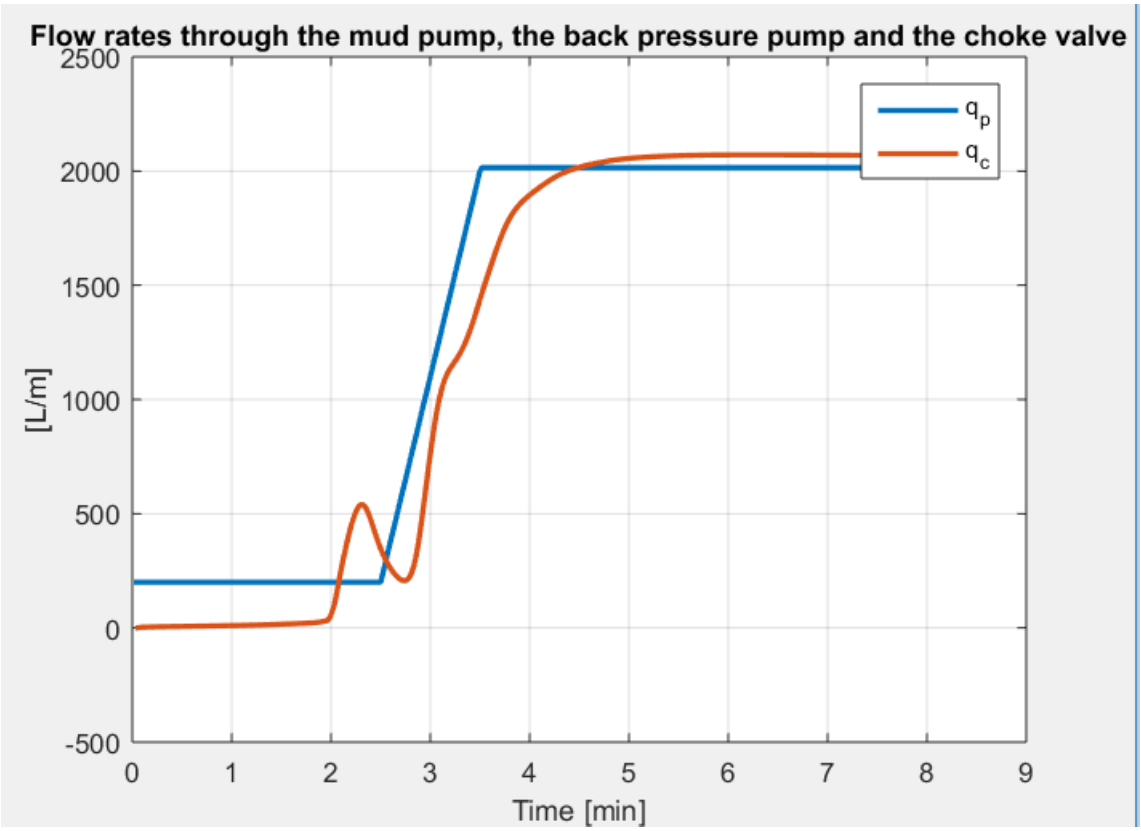

Figure 7.23.1 Shows the mud pump flow rate in (shown in blue) and return flow (shown in red) for BPM.

The response of the return flow is a little slower when Bingham plastic HPHT model is applied, still it is a good fit to the flow in and the overshoot reduces with a small amount.

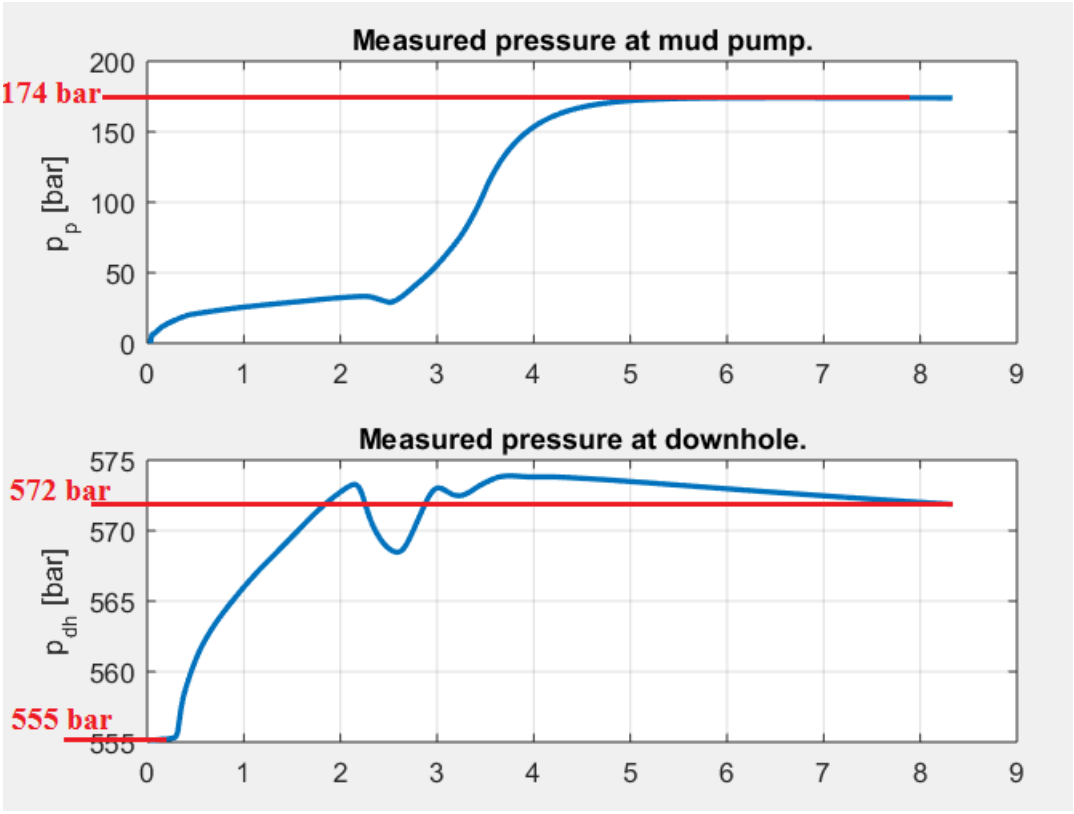

Figure 7.23.2 Shows the measured pressure downhole and the measured pressure at mud pump for BPM.

Measured pump pressure is very similar to scenario 7 and stabilises at a slightly higher pressure (around 1 to 2 bar) compared to Robertsen and Stiff model, due to the rheological model.

The downhole pressure starts at the same hydrostatic pressure compared to scenario 7 at 555 bar and stabilises at 572 bar, using Bingham model. $\Delta P = 572 - 555 = 17$ bar. Scenario 7 showed an increase of 13 bars, which gives an increase of 5 bars by comparison. A slight increase in this pressure indicates that the MW used is increased, and the ECD is also expected to increase.

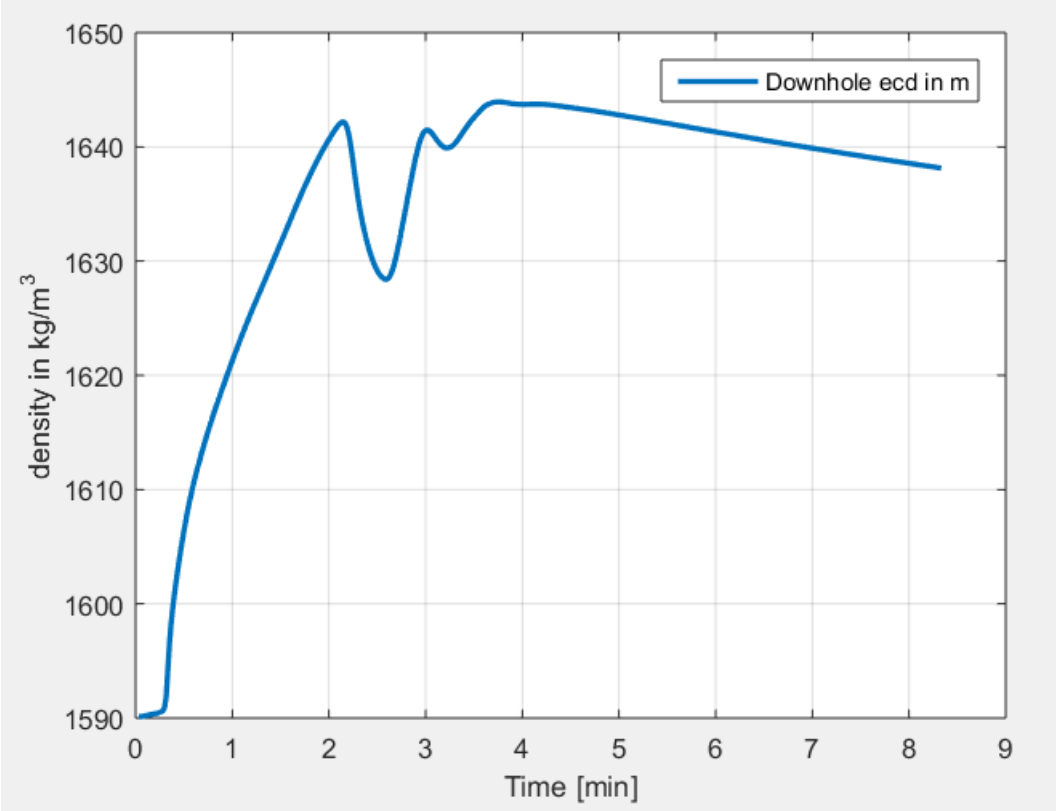

7.23.3 Shows the density in kg/m^3 versus time or downhole ECD. The mud density was set at 1.60 s.g for BPM.

As aforementioned the ECD is expected to rise as a result of increased downhole pressure, this is shown to be true. It also shows evidence that the Robertsen Stiff HPHT model, shows more accurate ECD, compared to Bingham plastic HPHT model.

7.24 Scenario 10 – Increasing density

Scenario 10 considers increase of mud density to 1.800 s.g as previously done in WBM.

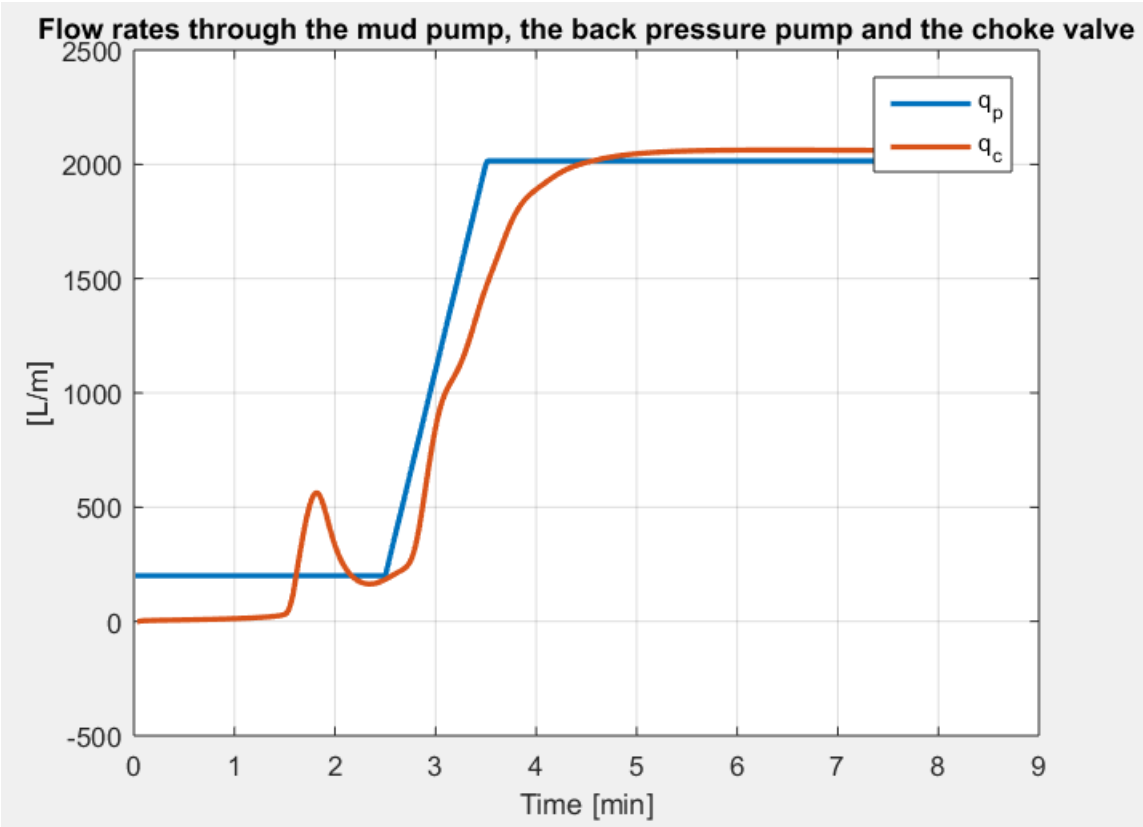

7.24.1 Shows the mud pump flow rate in (shown in blue) and return flow (shown in red) when density increases to 1.800 s.g.

The return flow comes earlier by increment of the density. This might be an effect due to the OWR and the difference in gel model.

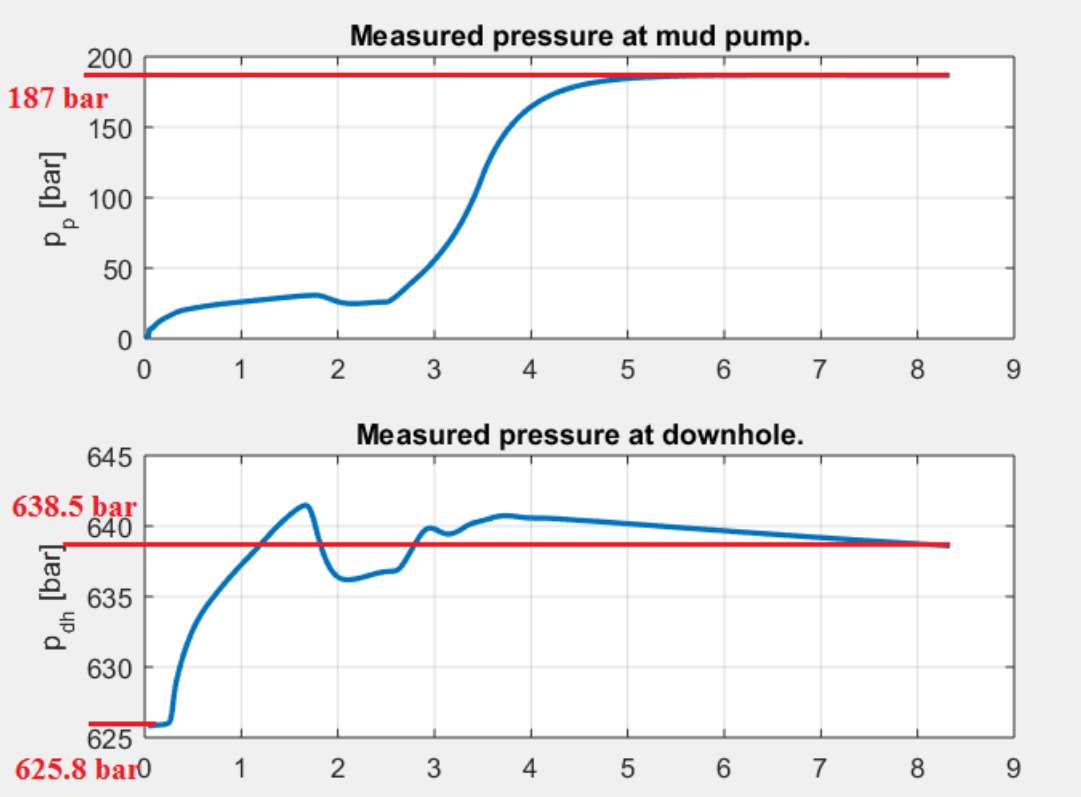

Figure 7.24.2 Shows the measured pressure downhole and the measured pressure at mud pump, when density increases to 1.800 s.g.

As the density increases to 1.800 s.g the pump pressure reaches around 187 bar. This behaviour is expected as density is a function of pressure. The increase in pressure stabilises around in a difference of 18.5 bar compared to mud density of 1.600 s.g.

The hydrostatic pressure seen in downhole pressure increases to 625.8 bar as a result of density increase, this is expected as MW is a function of downhole pressure. The increase in pressure to the stabilising downhole pressure is around 638.5 bar, which gives ΔP = 638 – 625.8 bar = 12.2 bar. From what was observed in scenario 7, ΔP was around 13 bar (with some reading error). ΔP is proved to be constant, as expected.

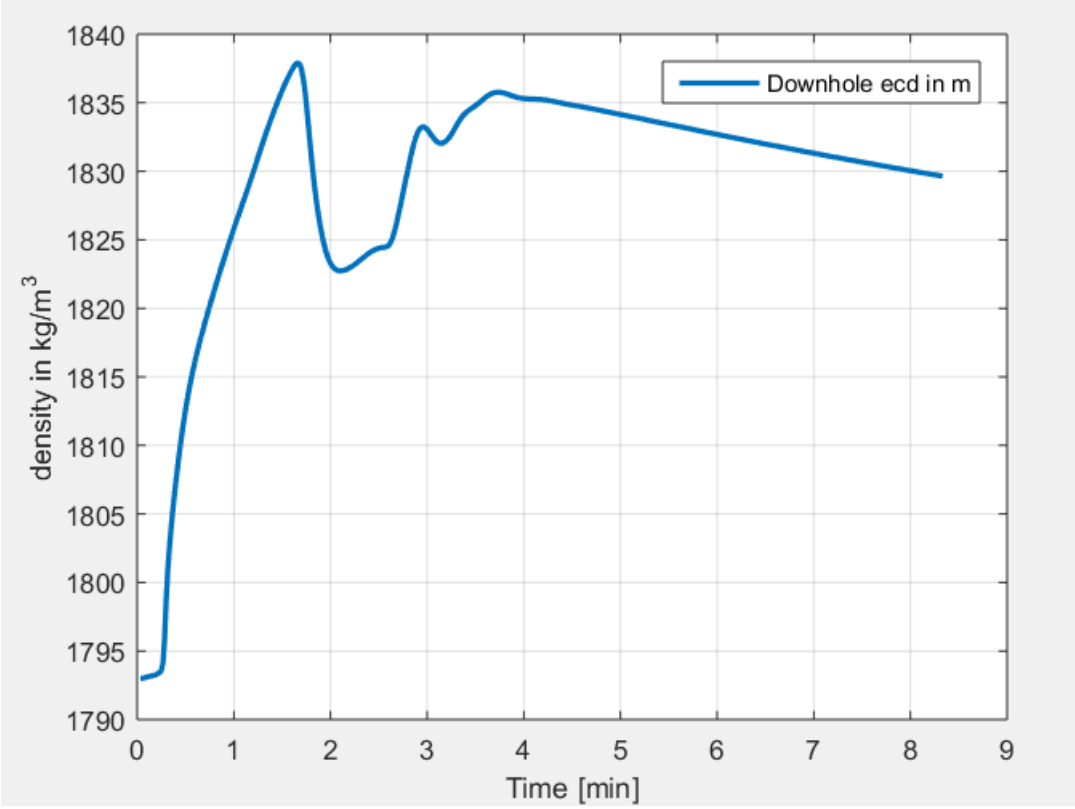

Figure 7.24.3 Shows the density in kg/m^3 versus time or downhole ECD. The mud density was set at 1.80 s.g.

The ECD is increasing as expected and stabilising further away from the desired density of 1.800 s.g. Overall difference from the desired density to stabilising point is around 30 kg/m^{3,} whereas in scenario 7 this value was around 26 kg/m^3. Thus, the ECD is more unstable when the density increases.

7.25 Scenario 11- Increasing the gel strength

This scenario considers the increase of gel strength, 10 seconds to 10 Pa, and 10 minutes to 15.5 Pa. The recorded pressure responses are seen below.

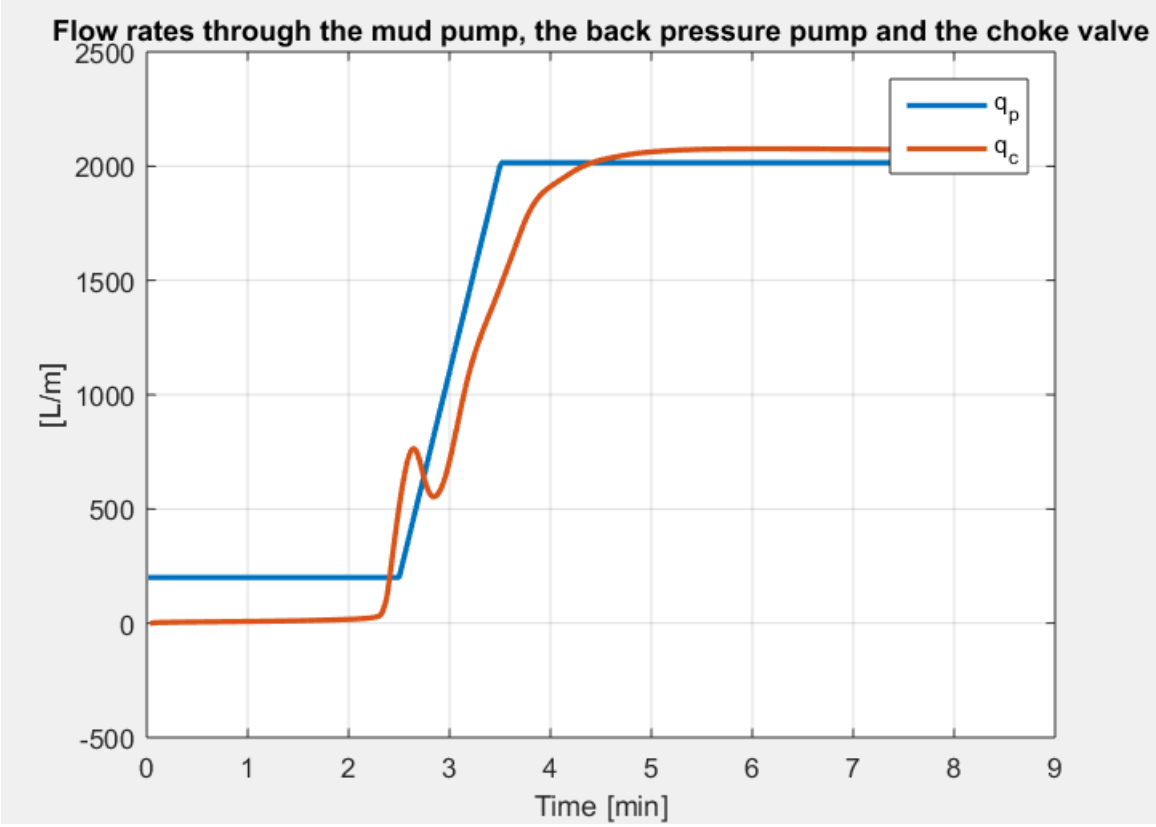

Figure 7.25.1 Shows the mud pump flow rate in (shown in blue) and return flow (shown in red) when gel strength is increased.

When increasing the gel strength, the return flow is much slower compared to scenario 7. Higher gel strength means that the solids are suspended for a greater amount of time and therefore, the return flow takes longer to show. It heavily affected by the increase in gel strength.

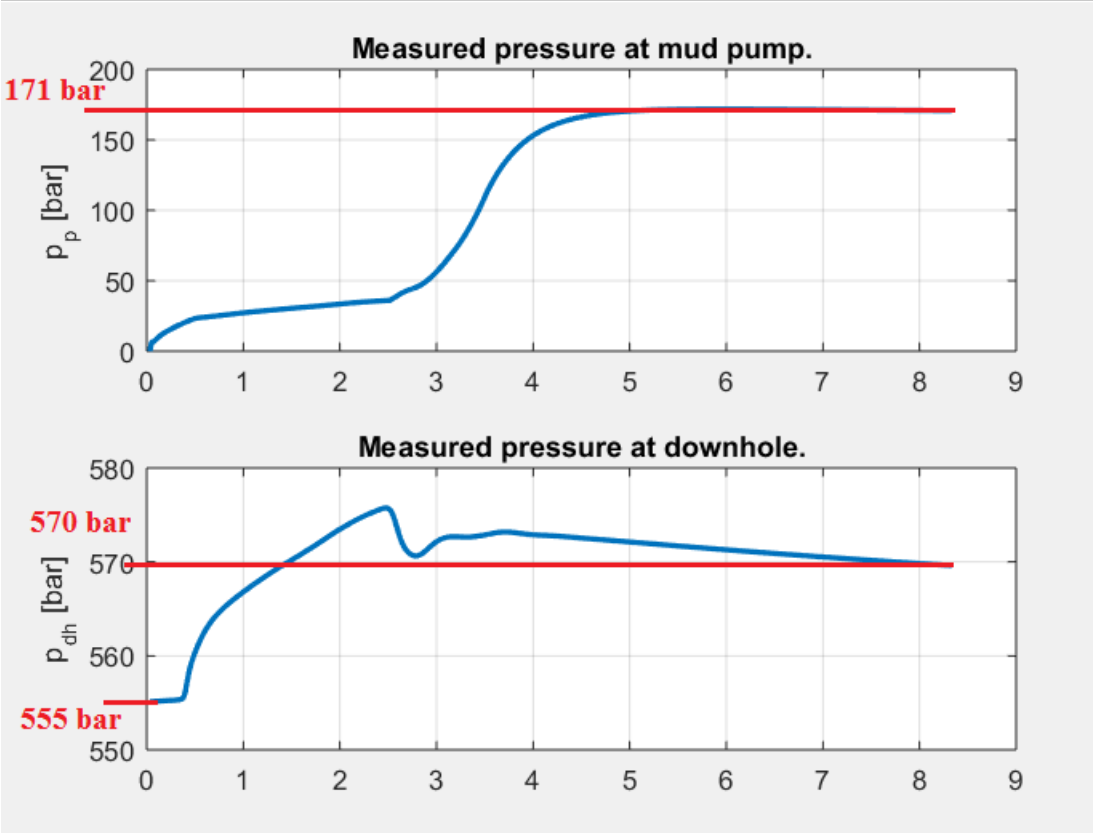

Figure 7.25.2 Shows the measured pressure downhole and the measured pressure at mud pump when gel strength increases.

As the gel strength of the mud is increased the mud pump pressure has increased by a small pressure around 2.5 bars, to break circulation after mud has been static.

The measured pressure downhole also takes longer to build up while the drill string is filled and ΔP is 570 - 555 bar = 15 bars. Thus, means that it was increased compared to the lower gel strength with a pressure of 2 bars from scenario 7.

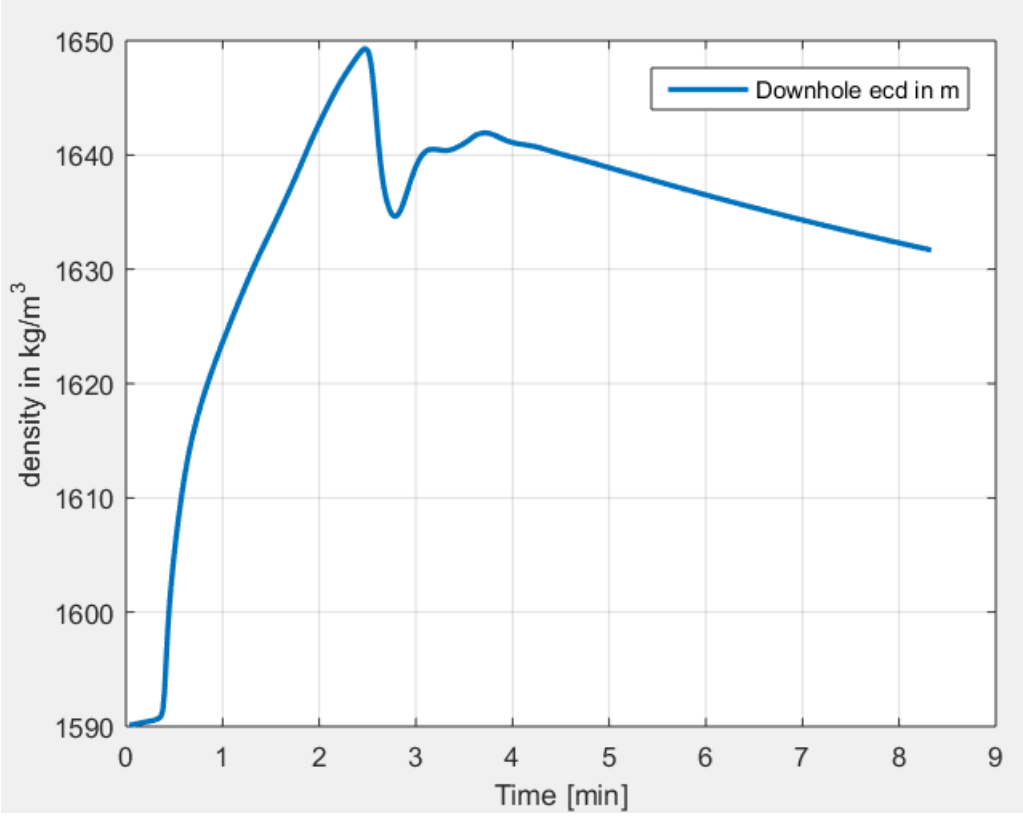

Figure 7.25.3 Shows the density in kg/m^3 versus time or downhole ECD. The mud density was set at 1.60 s.g. The effect of increased gel strength was studied in this figure.

When the gel strength is increased the ECD is more inaccurate and has a greater fluctuation. This is due to the effect of the gel strength and the pressure and temperature conditions downhole.

7.26 Scenario 12 – Decreasing OWR

This scenario considers a parameter that has not been changed in WBM, namely the OWR. The value of OWR is decreased to one, which means the ratio of water and oil are equal. The pressure responses are seen below.

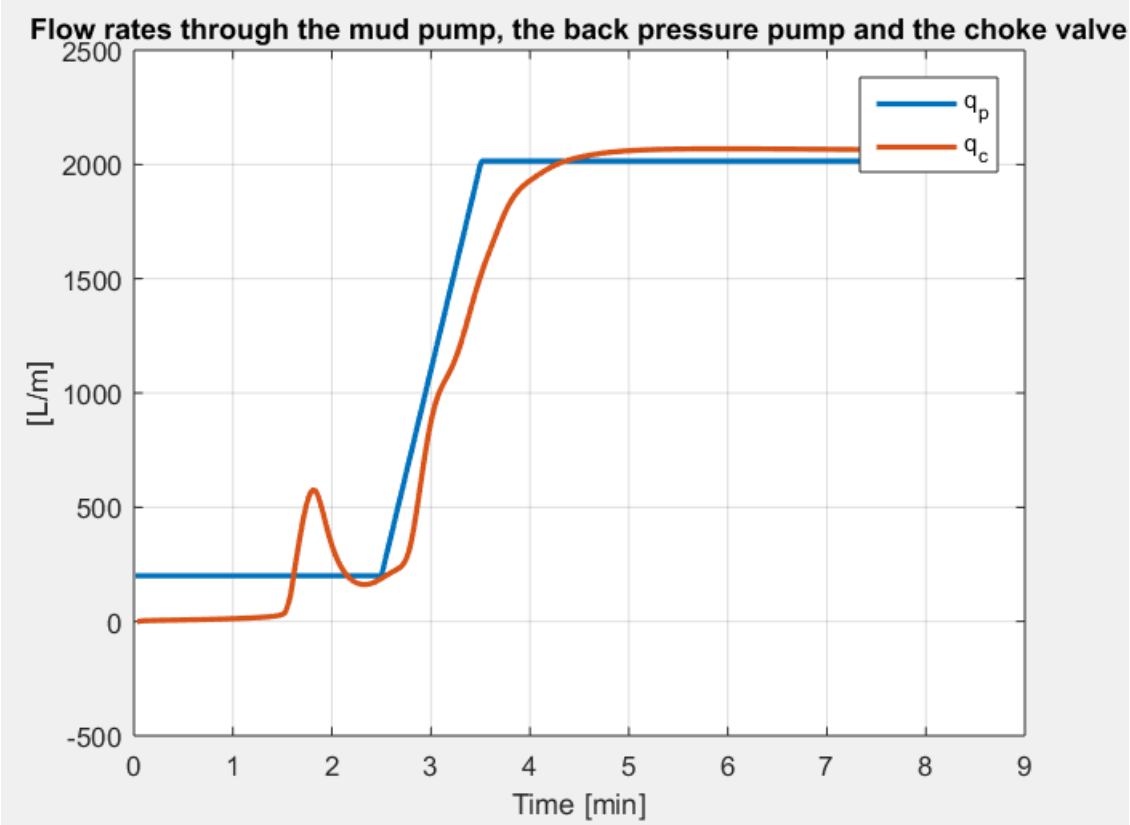

Figure 7.26.1 shows the mud pump flow rate in (shown in blue) and return flow (shown in red) for when the OWR is reduced.

The main observation is the early arrival of return flow, when the volume amount of total mud consists equally of oil and water. Thus, by lowering the OWR, the return flow comes earlier.

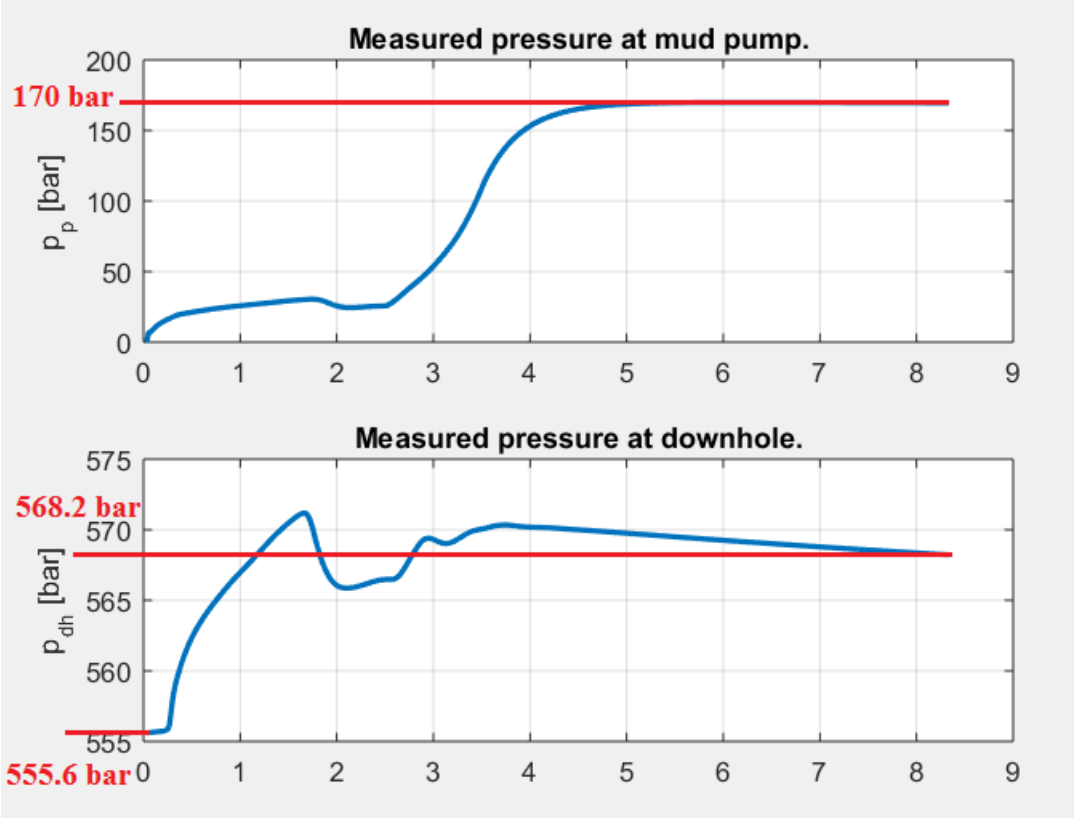

Figure 7.26.2 Shows the measured pressure downhole and the measured pressure at mud pump. The downhole pressure from hydrostatic to maximum pressure are marked, when OWR is reduced.

Pump pressure show slight increase in pump pressure around 1.5 bar, when the OWR is reduced.

The downhole pressure starts to increase after a hydrostatic pressure of 555.6 bar up to 568.2 bar, a difference of, $\Delta P = 568.2 - 555 = 13.2$ bars. Similar to scenario 7, the final increase in pressure is not affected by lowering the OWR.

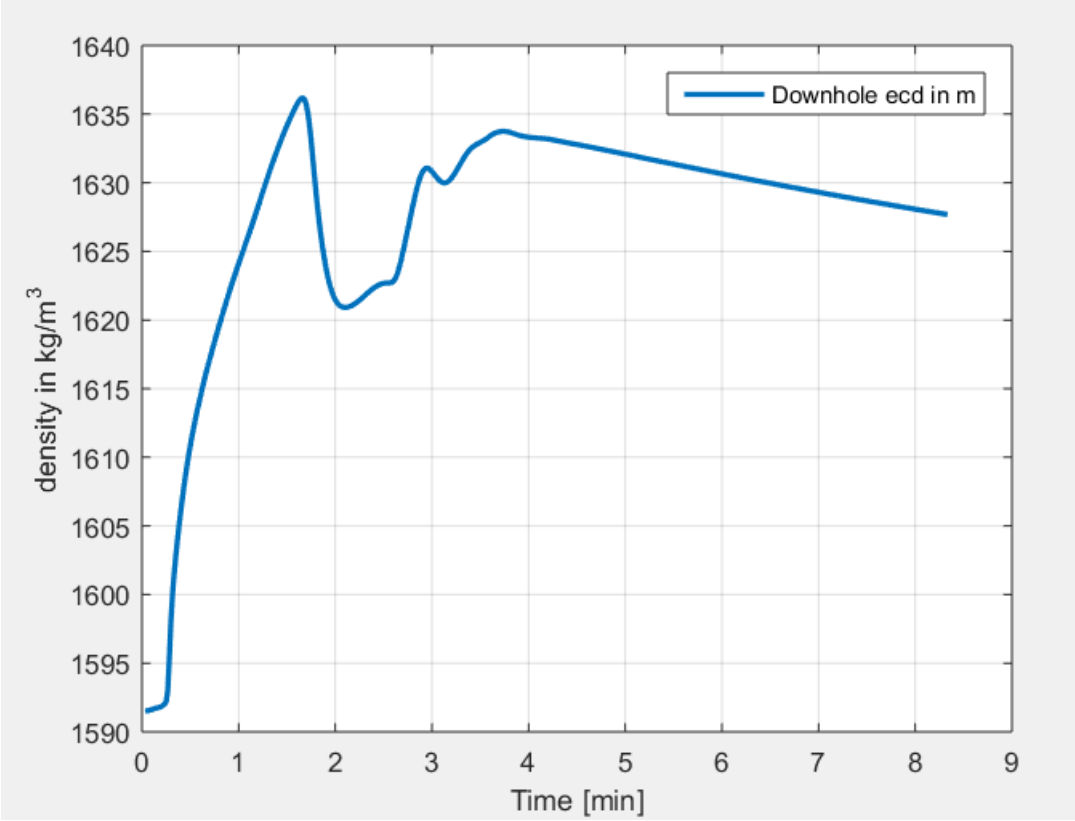

Figure 7.26.3 Shows the density in kg/m^3 versus time or downhole ECD set at 1.60 s.g when the OWR is reduced.

By lowering the OWR the ECD curve is shifted up by around 3 kg/m^3 compared to the base case.

7.3 Comparison between OBM and WBM

This particular WBM is self-configured, to match the parameters of OBM for comparison. The configuration is shown below for WBM. A configuration which is similar to scenario 7 presented earlier. The main difference between the WBM and OBM comparison is the OWR and the stresses on the PVT table (which cannot be similar, due to their identities). The altered configuration of WBM is shown below:

Fluid description

Fluid name: WB mud 1475

Base densities / Thermal properties

Base oil density	0.790	(sg)
Base water density	1.050	(sg)
High gravity density	4.200	(sg)
High gravity diameter		(µm)
Density low gravity solids		(sg)
Cuttings density	2.400	(sg)
Cuttings diameter		(µm)
Specific heat	1,186.15	(J/kg•K)
Thermal conductivity	0.39	(W/m•K)

Report date: Thursday , December 1! 10:06

Density	1.600	(sg)
Density temp.	50.00	(°C)
Gel strength 10s	5.0	(Pa)
Gel strength 10min	8.5	(Pa)
Oil water ratio	0.000	
Volume low gravity solids		(%)
Brine salinity by wt%		(%)

Rheology models

Rheology model	RobertsonStiffHPHT
Density model	Empirical
Water density model	DodsonAndStanding
Oil density model	PvtTable
Edit Table	
Rheological method	Standard
Fann Data	GenericOilBased

Temp. (°C)	Press. (bar)	Stress at 3 rpm (lb/100ft²)	Stress at 6 rpm (lb/100ft²)	Stress at 30 rpm (lb/100ft²)	Stress at 60 rpm (lb/100ft²)	Stress at 100 rpm (lb/100ft²)	Stress at 200 rpm (lb/100ft²)	Stress at 300 rpm (lb/100ft²)	Stress at 600 rpm (lb/100ft²)
50.00	1.0	5.0	7.0	17.0	27.0	37.0	59.0	72.0	121.0

Gel strength vs Time

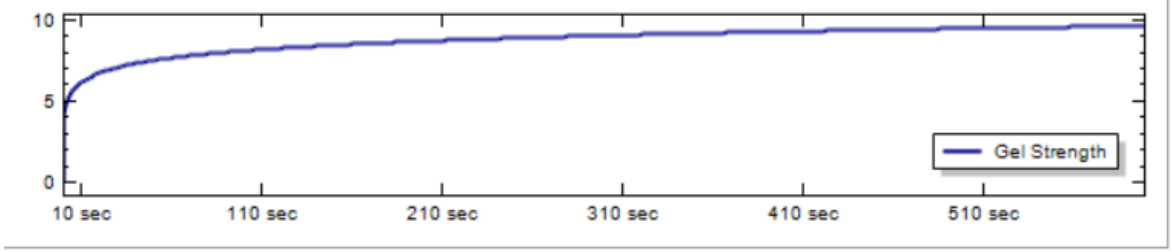

Stress vs Velocity

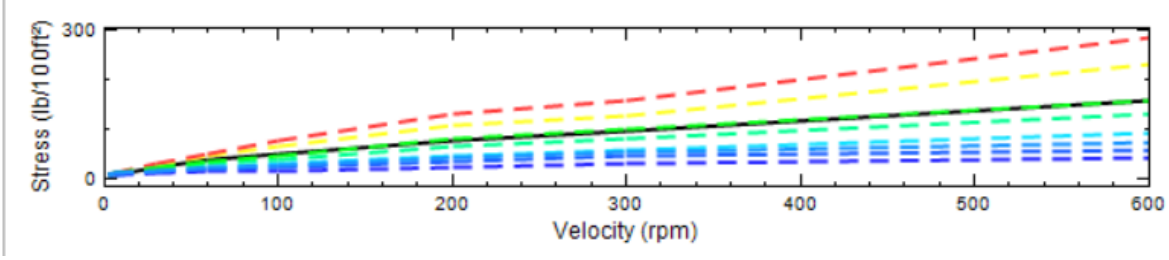

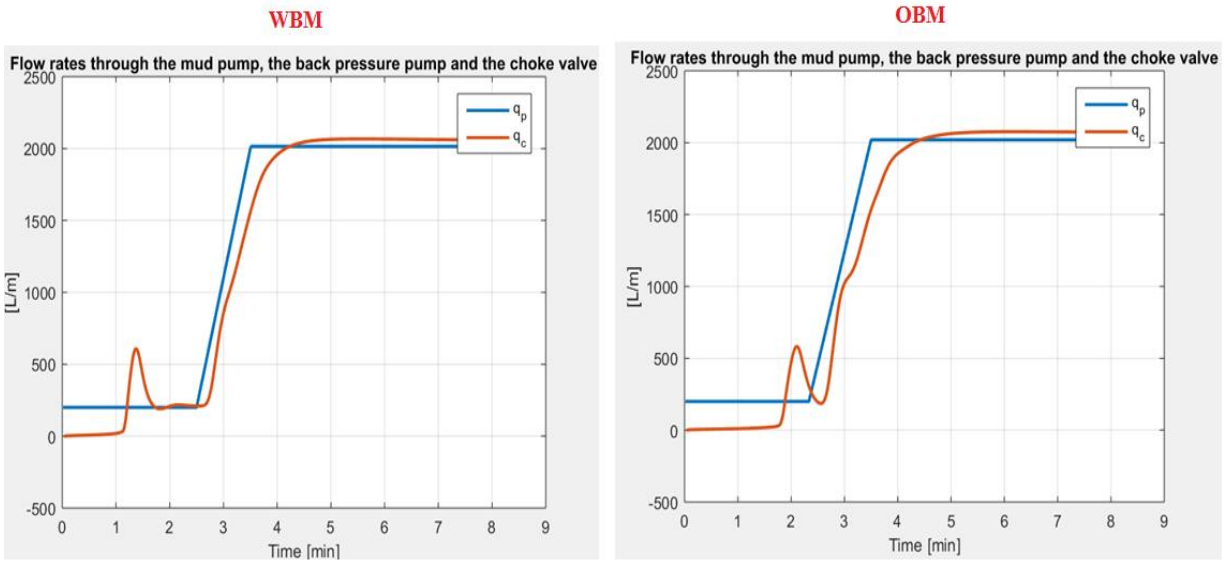

Figure 7.3.1 Comparison of mud pump flow rate in (shown in blue) and return flow (shown in red) for WBM and OBM.

WBM shows return flow earlier than OBM, which is mainly due to OWR, it delays the return flow. The performance after 3 minutes are identical.

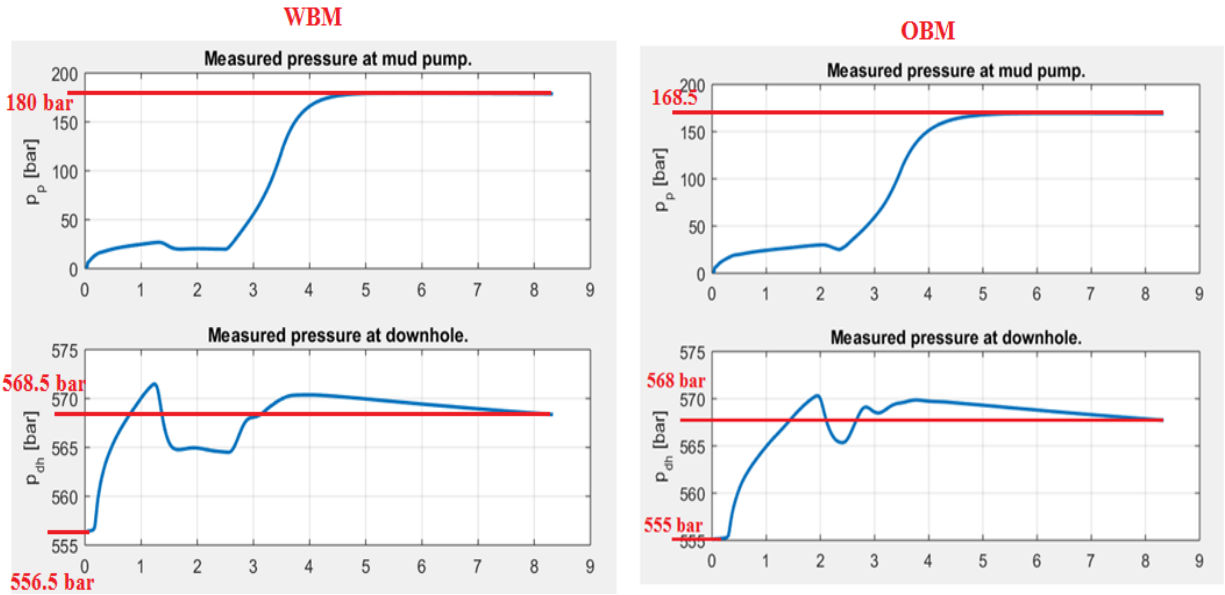

Figure 7.3.2 Comparison of mud pump and downhole pressure of WBM and OBM.

The pump pressure in WBM stabilises at higher pressure than in OBM. A difference of 180-168.5 = 11.5 bar. The downhole pressure of WBM has a greater hydrostatic pressure than of OBM (a difference of 1.5 bar) but their stabilising point after 8 minutes are very similar, 13 bar for OBM and 12 bar for WBM.

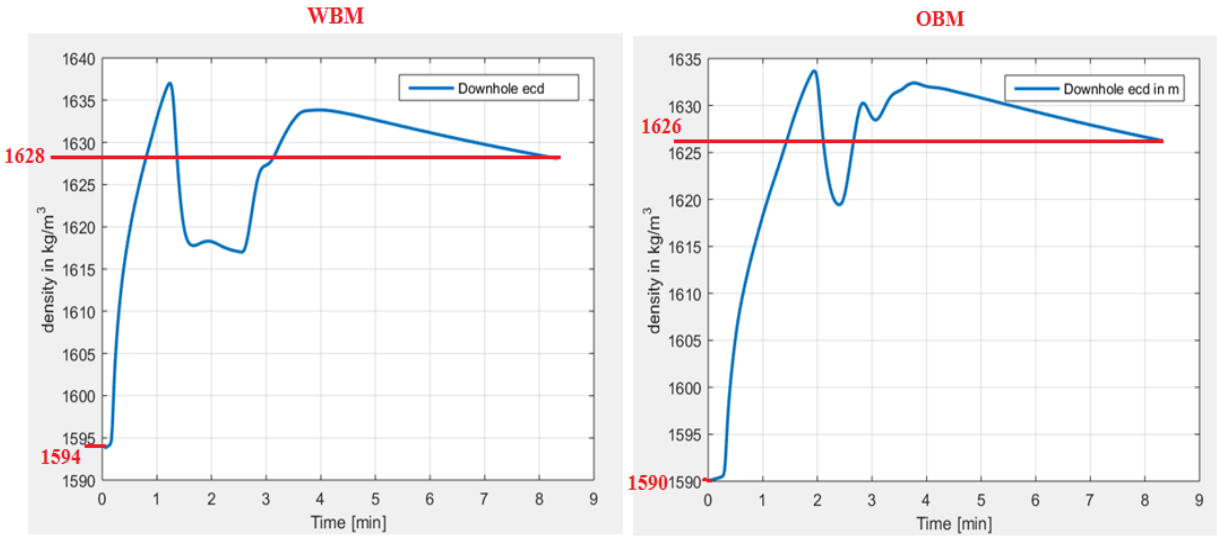

Figure 7.3.3 Comparison of ECD set at 1600 kg/m^3 between WBM and OBM.

The WBM starts with ECD at 1594 kg/m^3, while OBM starts at 1590 kg/m^3. WBM is shown to fluctuate more than OBM and the stabilising density difference of 2 kg/m^3, which is a very minor. The total fluctuation of OBM is higher due to OWR and the changes and the stresses obtained from the PVT table.

Both WBM and OBM have their own advantages and disadvantages, for a well with normal geothermal profile, WBM may be sufficient as it is cheaper than OBM and more environmentally friendly. Considering HPHT wells, OBM is a better choice.

The main concern operating with drilling fluid (WBM) in HPHT condition is the destruction of mud in such conditions. The mud chosen must therefore, be balanced for proper mud properties to avoid kick, formation damage, gas surge and other problems. Previously, both WBM and OBM have been used for HPHT wells, OBM is however more widely used for such conditions. The main reason for using OBM is because of the oil that can withstand excessive high temperatures in the well. Compared to WBM, generally, it would break down and lose mud. Other advantage of OBM, is lubrication of downhole equipment, drilling at greater ROP and better hole gauge. There are also disadvantages linked to OBM, which is mainly its high cost, difficulty to detect kick due to high gas solubility, costly if circulation is lost, environmental concerns of cuttings, damages to surface rubber equipment and concerns with fire hazards.

Due to the environmental concerns and the high cost of OBM, WBM has been increasing in use, even in such high temperature and pressure conditions. WBM has been treated with

additives such as carbon nanotubes in order to be less prone to fluid loss and to improve the rheological stability at high temperatures.

7.4 Kick scenario with OBM for manual operation for HPHT well

Architecture

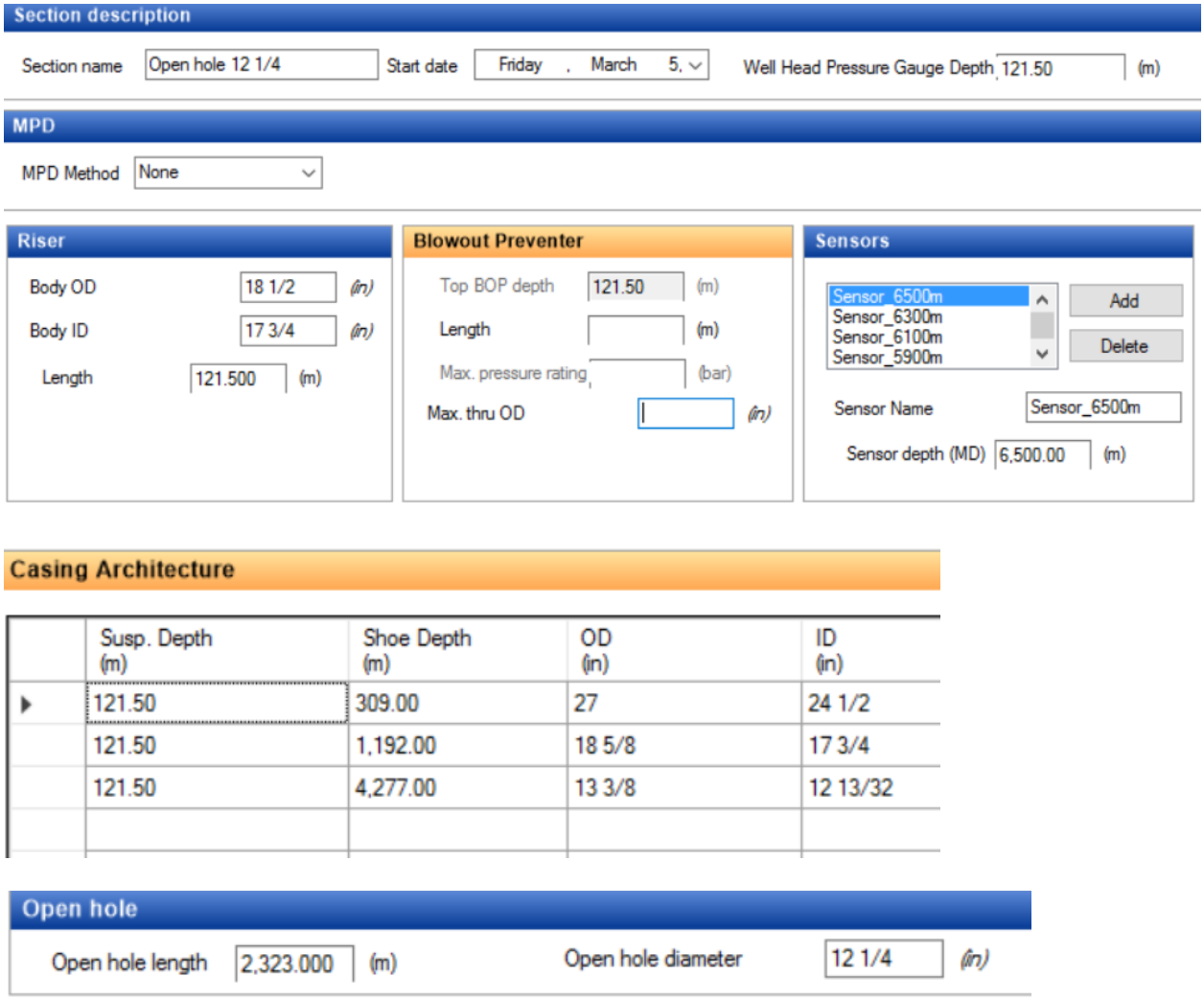

	Susp. Depth (m)	Shoe Depth (m)	OD (in)	ID (in)
▶	121.50	309.00	27	24 1/2
	121.50	1,192.00	18 5/8	17 3/4
	121.50	4,277.00	13 3/8	12 13/32

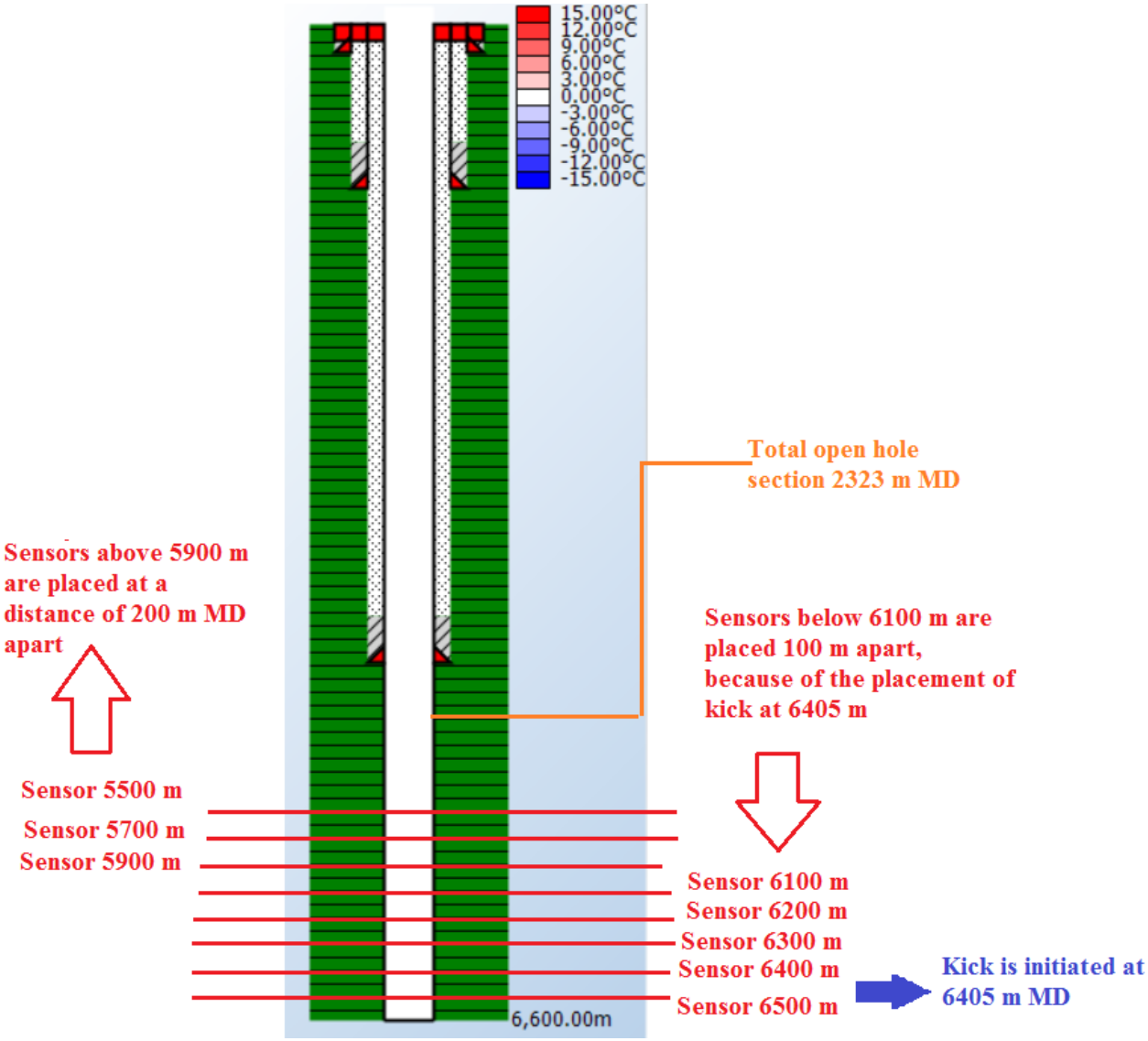

Kick is introduced at 6405 m MD, using the configuration tool. The open hole section includes sensors every 200 m to measure the pressure response at different depths. Extra sensors are placed at 6400 m and 6200 m MD to measure the influx mass rate. The designed well is long and horisontal.

Drill string

Drill-string/BHA description

	Type	Serial number	#	Length (m)	OD (in)	ID (in)	Lin. Weight (kg/m)	Cum. Length (m)	Cum. Mass (kg)
▶	Bit		1	0.290	12 1/4	2 13/16	344.8	0.290	100.00
	Float-sub		1	10.000	8 1/4	2 13/16	200.0	10.290	2,100.00
	MWD		1	15.000	8 1/4	2 13/16	200.0	25.290	5,100.00
	HWDP		1	174.000	6 5/8	3 3/4	123.0	199.290	26,502.00
	Drill-pipe		1	3,990.000	5 1/2	4 25/32	50.0	4,189.290	226,002.00
	Drill-pipe		1	4,000.000	6 5/8	5 31/32	44.7	8,189.290	404,802.00

Drill-string/BHA overview

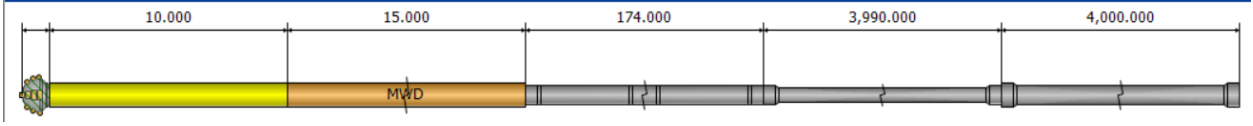

Element details: Bit

Manufacturer		
Model		
Type	Unknown	
Diameter	12 1/4	*(in)*
Length	0.290	(m)
Mass	100.00	(kg)
Gauge length	0.000	(m)
Pass thru diameter		*(in)*
Connection OD	6 3/4	*(in)*
Connection ID	2 13/16	*(in)*
Connection length		(m)
Make-up torque		(m.kN)

	Nozzle diameter (in/32)
▶	17
	17
	17

Fluid

The fluid that is used is OBM, due to its properties in HPHT wells. The same OBM was previously also used in comparison between WBM and OBM. The density of the fluid is kept at 1.605 s.g which is 15°C when it is pumped into the well.

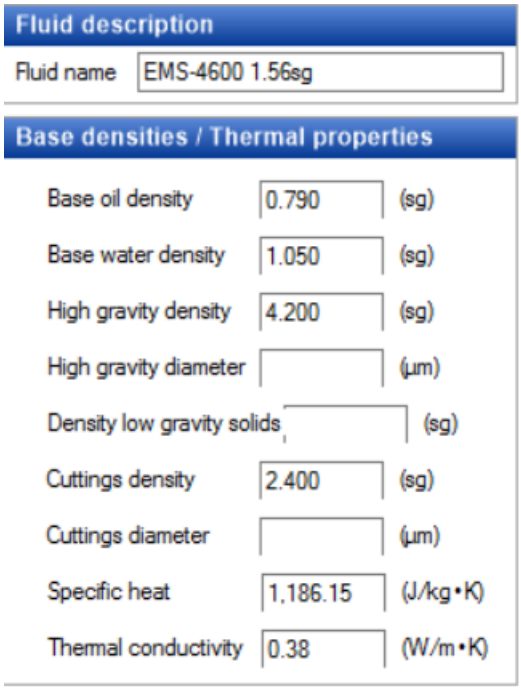

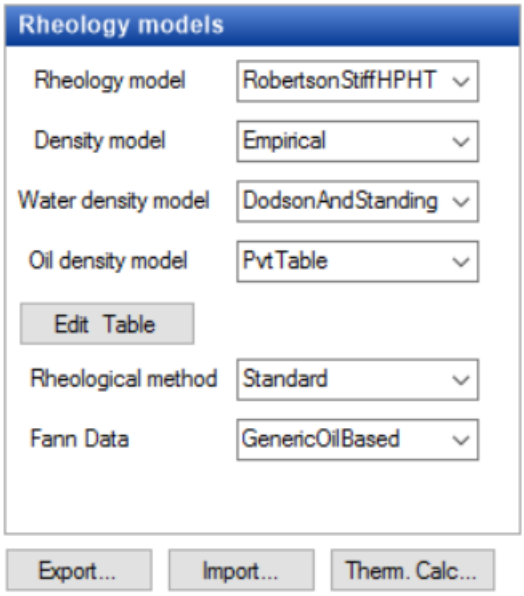

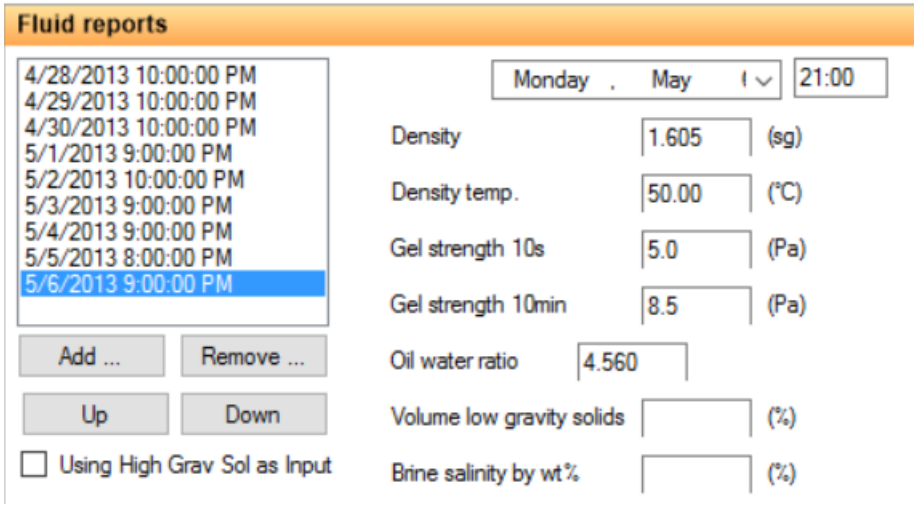

Temp. (°C)	Press. (bar)	Stress at 3 rpm (lb/100ft²)	Stress at 6 rpm (lb/100ft²)	Stress at 30 rpm (lb/100ft²)	Stress at 60 rpm (lb/100ft²)	Stress at 100 rpm (lb/100ft²)	Stress at 200 rpm (lb/100ft²)	Stress at 300 rpm (lb/100ft²)	Stress at 600 rpm (lb/100ft²)	Legend
20.00	600.0	12.6	13.9	26.8	40.9	58.4	95.6	125.9	223.9	
80.00	1.0	9.1	11.1	13.6	17.7	22.7	33.3	45.7	71.5	
80.00	300.0	11.2	12.9	17.1	23.0	30.5	47.0	64.6	101.6	
80.00	600.0	12.8	14.0	19.2	26.6	36.1	57.5	78.8	125.3	
160.00	1.0	9.3	11.8	11.8	11.8	12.4	17.0	24.8	32.6	

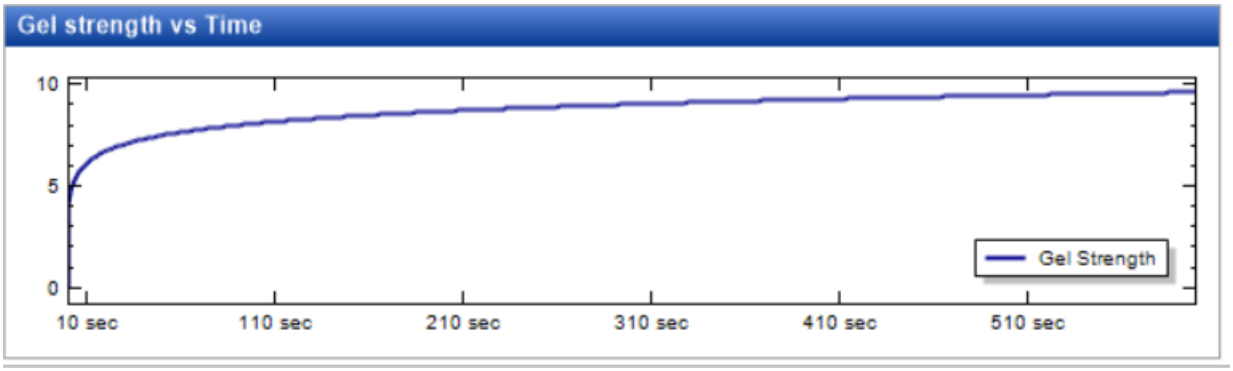
Gel strength vs Time
10
5
0
10 sec
110 sec
210 sec
310 sec
410 sec
510 sec
Gel Strength

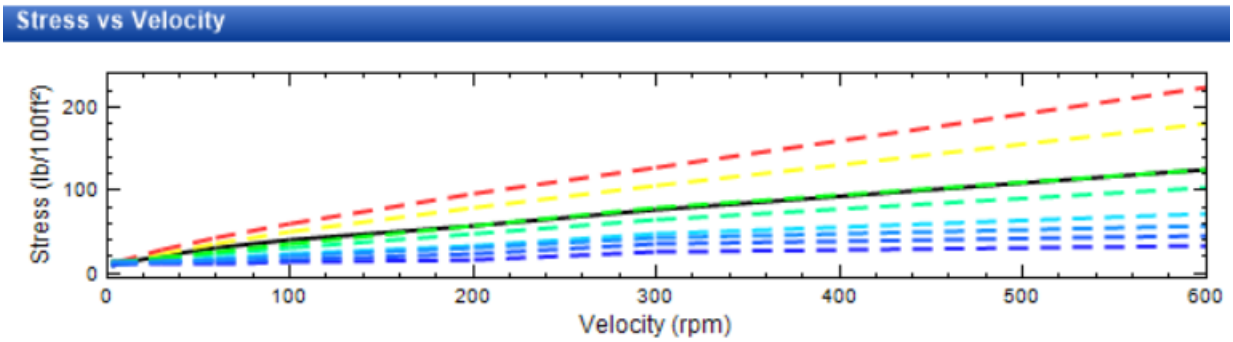
Stress vs Velocity
Stress (lb/100ft²)
200
100
0
0
100
200
300
400
500
600
Velocity (rpm)

Trajectory

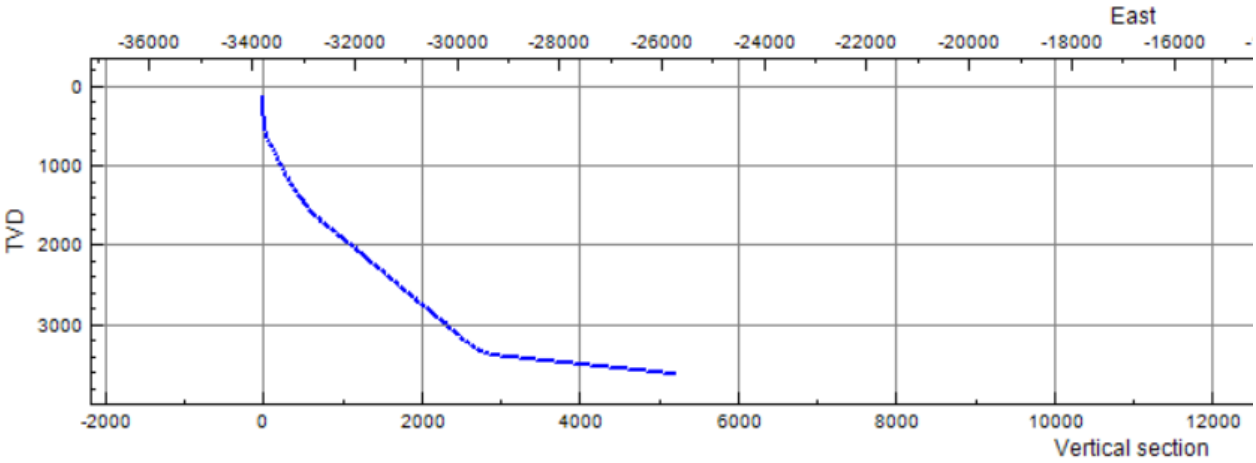
East
-36000
-34000
-32000
-30000
-28000
-26000
-24000
-22000
-20000
-18000
-16000
TVD
0
1000
2000
3000
-2000
0
2000
4000
6000
8000
10000
12000
Vertical section

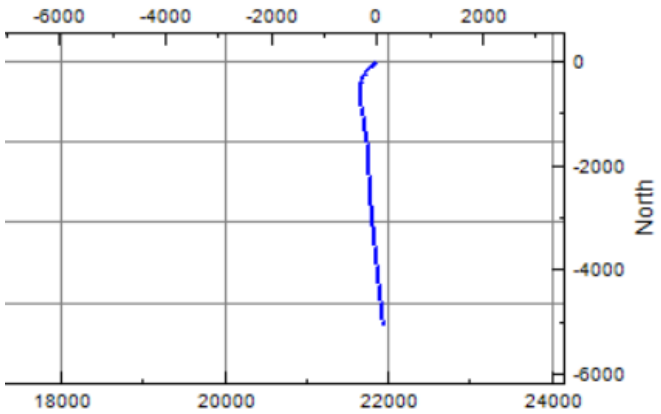
-6000
-4000
-2000
0
2000
0
-2000
-4000
-6000
North
18000
20000
22000
24000

Geothermal

Geo-thermal properties

Default geo-thermal profile | Thermal cond. calculator

	TVD (m)	Type	Formation Name	Lithology Type	Geothermal gradient (°C/100m)	Specific heat (J/kg•K)	Thermal conductivity (W/m•K)	Density (sg)
▶	0.00	Air		Air	0.0	1,005.00	0.02	0.001
	56.00	Water		Water	-2.0	4,180.00	0.58	1.050
	80.00	Water		Water	0.0	4,180.00	0.58	1.050
	121.50	Solid		Unknown	4.8	900.00	2.00	2.500
	1,200.00	Solid		Unknown	3.0	900.00	2.00	2.500
	3,000.00	Solid		Unknown	3.6	900.00	2.00	2.500
	4,200.00	Solid		Unknown	3.6	900.00	2.00	2.500

Geopressure

The kick is introduced at 3562 m TVD, where the pore pressure is increased to 1.638 s.g.

Main geo-pressures

◉ Absolute ○ Relative | Export... | Import...

	TVD (m)	Pore (sg)	Collapse (sg)	Min. stress (sg)	Frac. (sg)
	3,488.50	1.564	1.564		1.975
	3,506.75	1.564	1.564		2.030
	3,525.00	1.564	1.564		2.030
	3,560.00	1.564	1.564		2.015
▶	3,562.00	1.638	1.638		2.015
	3,567.50	1.564	1.564		2.015
	3,599.00	1.564	1.564		2.050
	3,617.50	1.564	1.564		2.055
	3,626.00	1.565	1.565		2.055
	3,636.00	1.565	1.565		2.060

Up | Down | Insert | Remove

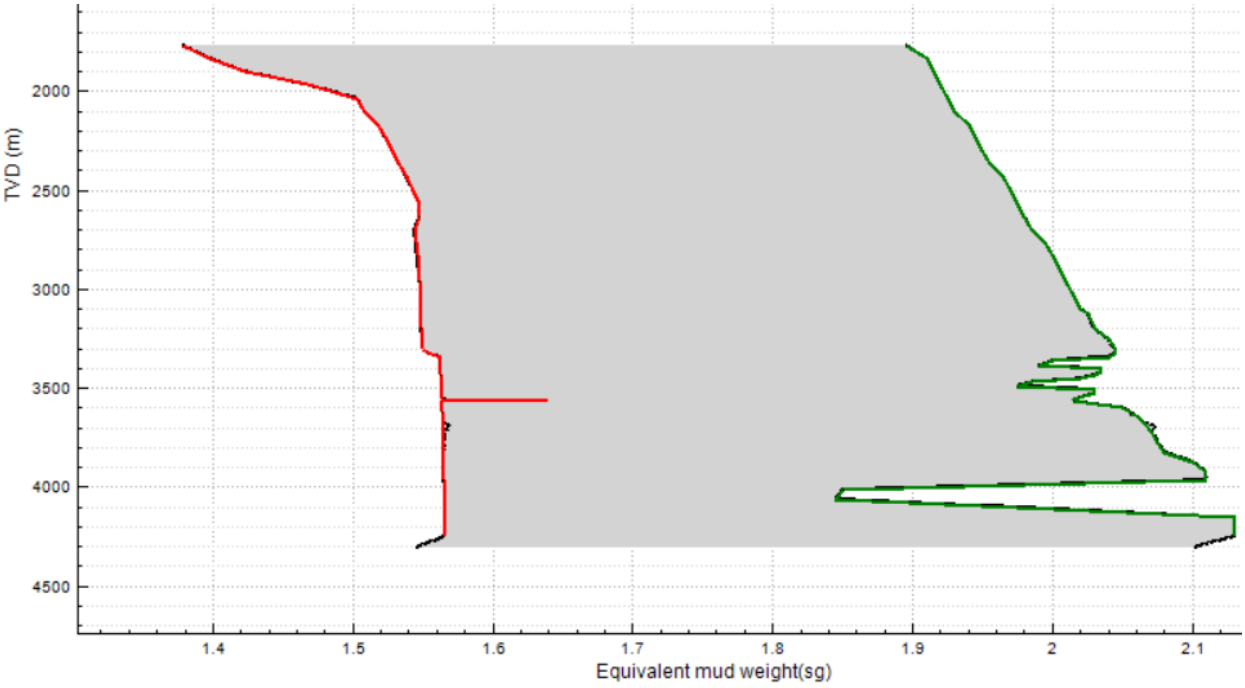

Extrapolation depth 210.00 (m)

	MD (m)	TVD (m)	Min pressure (sg)	Max pressure (sg)
▶	6,385.00	3,560.09	1.567	2.015
	6,390.00	3,560.60	1.586	2.015
	6,395.00	3,561.11	1.605	2.015
	6,400.00	3,561.62	1.624	2.015
	6,405.00	3,562.13	1.636	2.015
	6,410.00	3,562.64	1.629	2.015
	6,415.00	3,563.15	1.622	2.015
	6,420.00	3,563.67	1.616	2.015
	6,425.00	3,564.18	1.609	2.015
	6,430.00	3,564.69	1.602	2.015
	6,435.00	3,565.20	1.595	2.015
	6,440.00	3,565.71	1.588	2.015
	6,445.00	3,566.22	1.581	2.015
	6,450.00	3,566.73	1.574	2.015
	6,455.00	3,567.24	1.567	2.015

Start of extrapolation of pore pressure

The maximum increase in pore pressure due to temperature effects

The total MD that was needed is 65 m MD

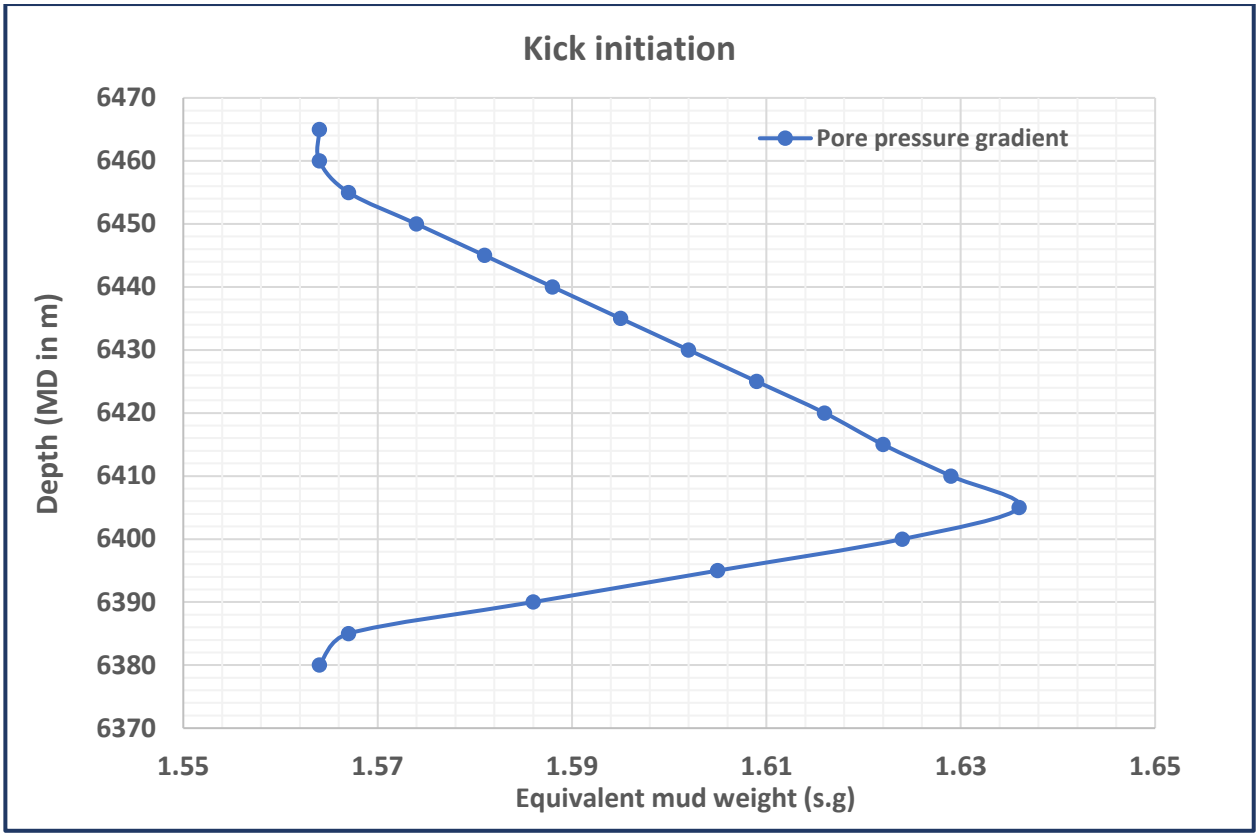

Figure 7.4.1 Shows the kick intensity by the pore pressure gradient versus depth in MD.

Log traces

The target depth and Bit depth have been changed with 50 m MD in difference.

Top of string position trace	0.00	(m)	Choke Opening		(%)
Bit depth trace	6,450.00	(m)	Pressure Before Choke		(bar)
TD trace	6,500.00	(m)	Choke Pump Flow rate in		(l/min)
Flow rate in trace	0	(l/min)	Riser Pump Flow rate in	1,900	(l/min)
Density in trace	1.605	(sg)	Parasite Pump Flow out		(l/min)
Average ROP trace	0.0	(m/h)	Choke Pump Density in	1.605	(sg)
String Velocity	0.0000	(m/s)	Riser Pump Density in	1.605	(sg)
Surface RPM trace	0	(rpm)	Choke Pump Temp. in		(°C)
Surface torque trace	0.0	(m.kN)	Riser Pump Temp. in	15.00	(°C)
Fluid temperature in trace	15.00	(°C)	Choke Line Choke Opening		(%)
Air temperature trace	10.00	(°C)	Kill Line Choke Opening		(%)
Active Volume		(m³)	Annulus Refill Density in	1.605	(sg)
Trip Tank Volume		(m³)	Annulus Refill Temp. in	15.00	(°C)

Rig

The Rig includes another choke pump which is the back-pressure pump, used together with the choke opening to control the kick and stabilise the BHP.

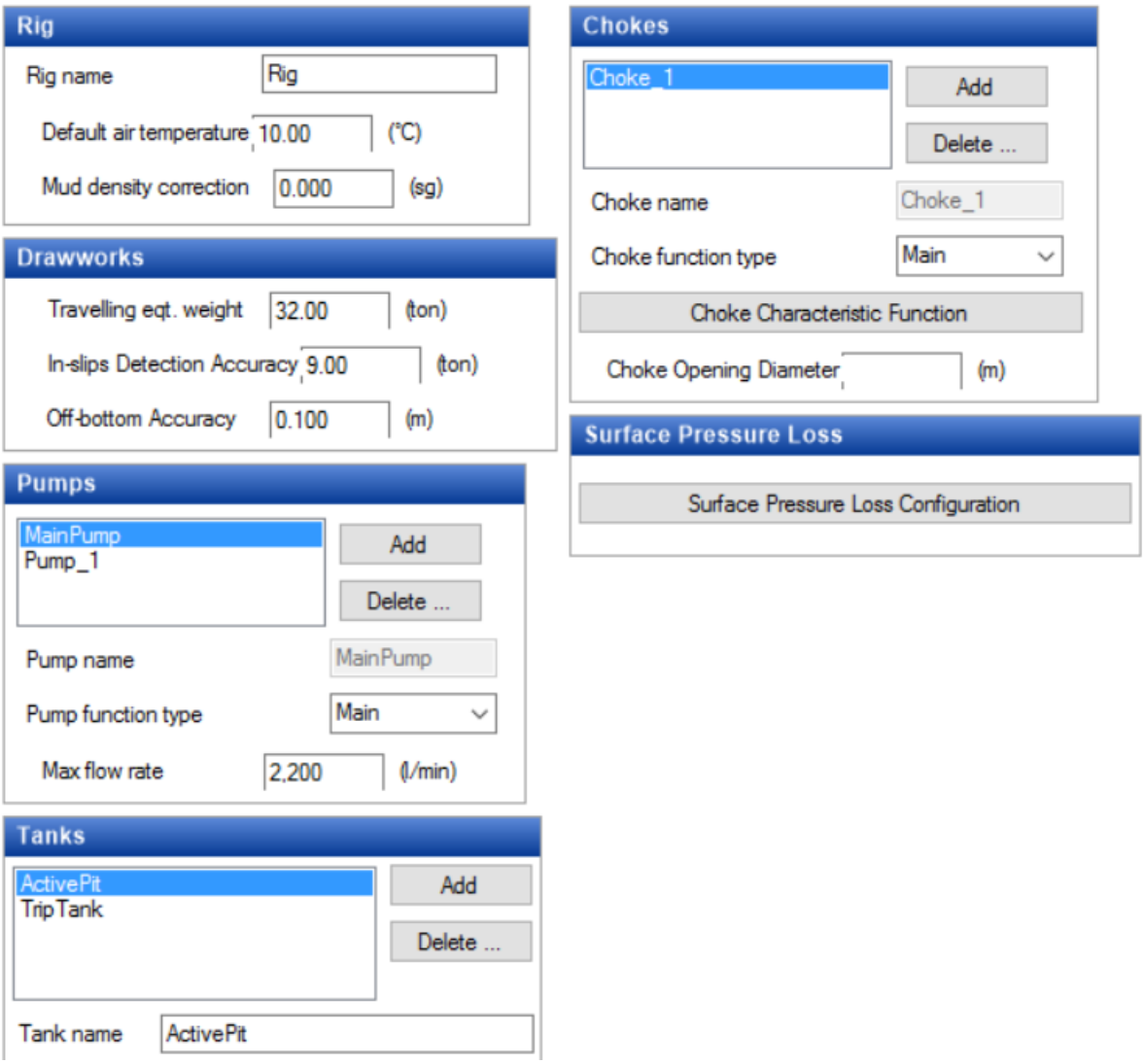

The initial gel breaking at early stage is seen around 30 seconds, that is, when the return flow shows some fluctuations in the very beginning of the simulation. The main focus in this section is to initiate a small kick and to be able to circulate the kick out properly using the back-pressure pump and the reduction of the choke opening. The time count is started from 30 seconds.

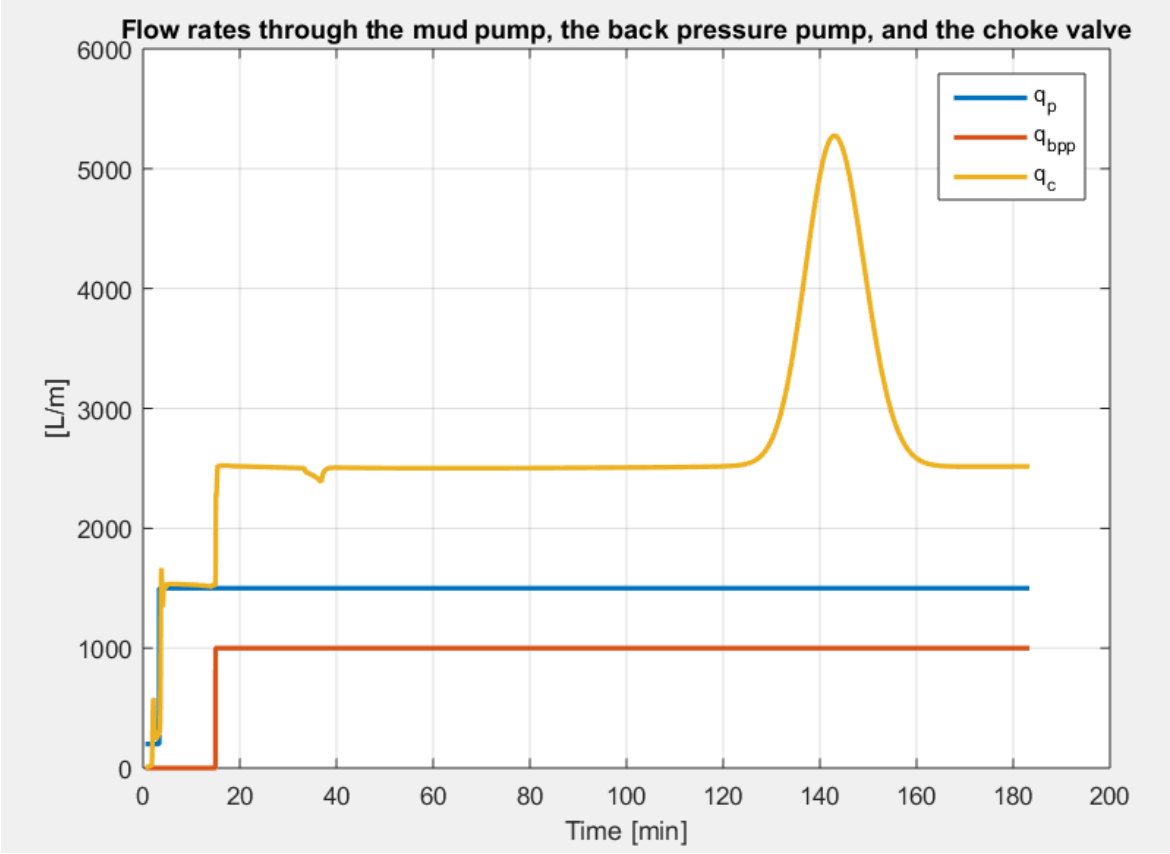

Figure 7.4.2 Shows the mud pump flowrate-in (blue), the back-pressure pump (red) and the return flow (yellow) versus time for the whole circulation period.

Kick is initiated at around 145 sections into the simulation and is stopped around 550 seconds. Total fraction of time for influx to be allowed into the well was 500-145 = 355 seconds. The mud pump is ramped up from 200 lpm to 1500 lpm at around 200 seconds. The back-pressure pump is initiated to 1000 lpm at 900 seconds to control further influx. As seen on the Figure 7.4.2 the pump pressure and the back-pressure pump is kept constant after around 20 minutes, until the kick is circulated out, at 150 minutes. The choke opening is reduced to control the influx.

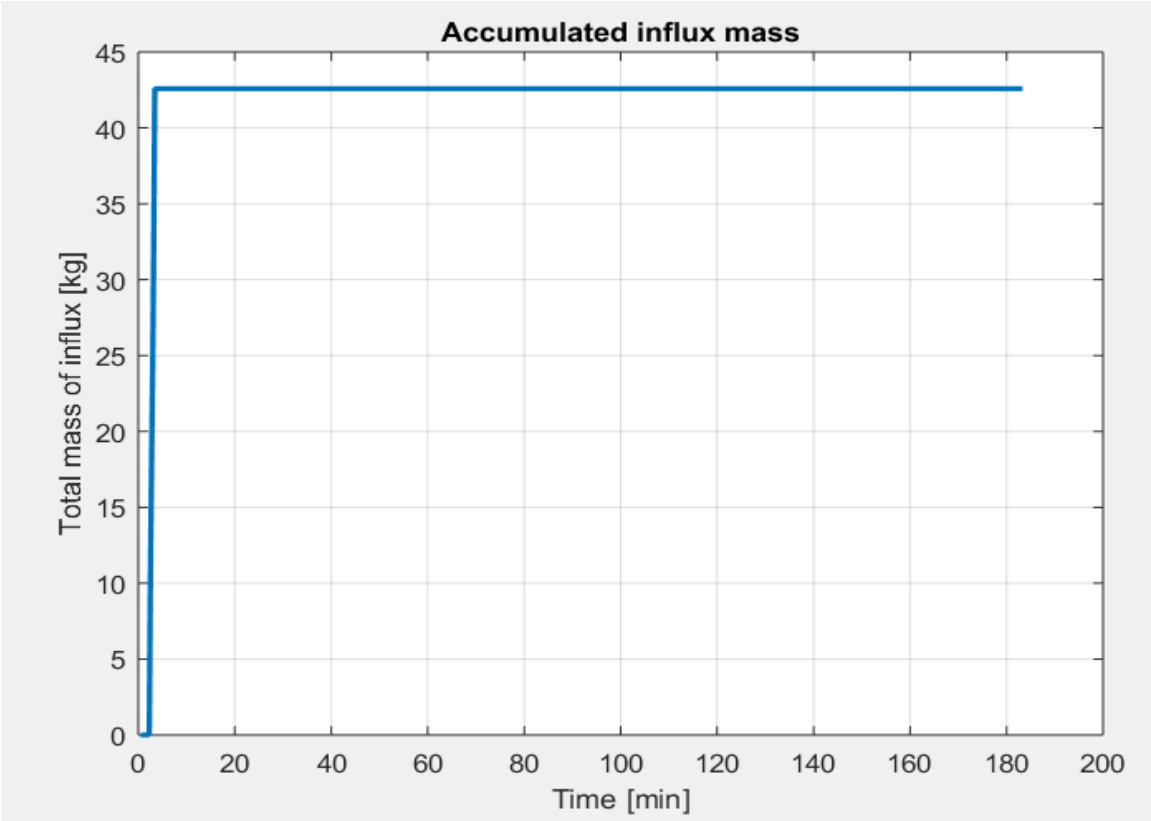

Figure 7.4.3 Shows the total mass of influx in kg versus time. The total influx circulated out was 43 kg initiated after 145 seconds.

43 kg of influx is generated in this simulation and circulated out.

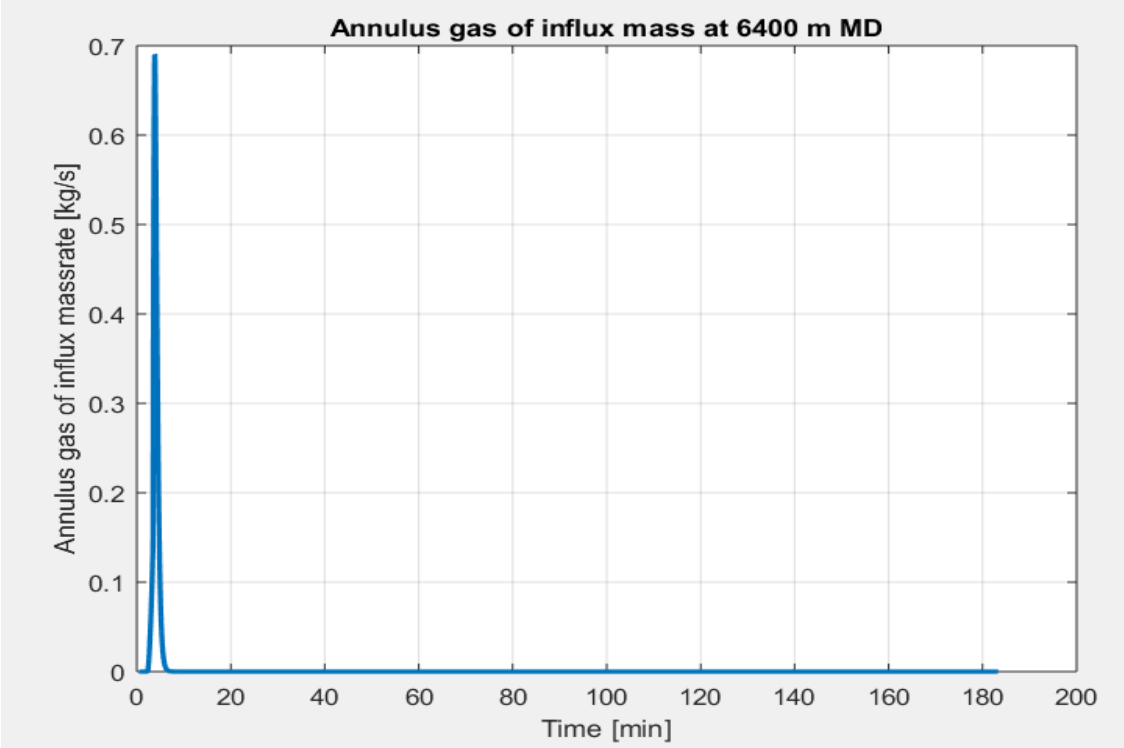

Figure 7.4.4 Shows the sensor measurement of influx mass at 6400 m MD versus time, for the whole circulation period for manual operation.

The annulus gas of influx mass rate recorded from the sensor at 6400 m MD, closest to where the kick was initiated. During the whole circulation period of around 180 minutes the kick it is controlled and circulated so that another kick does not start. No further influx is seen from the sensor at 6400 m MD, which means that kick was only allowed once in the borehole.

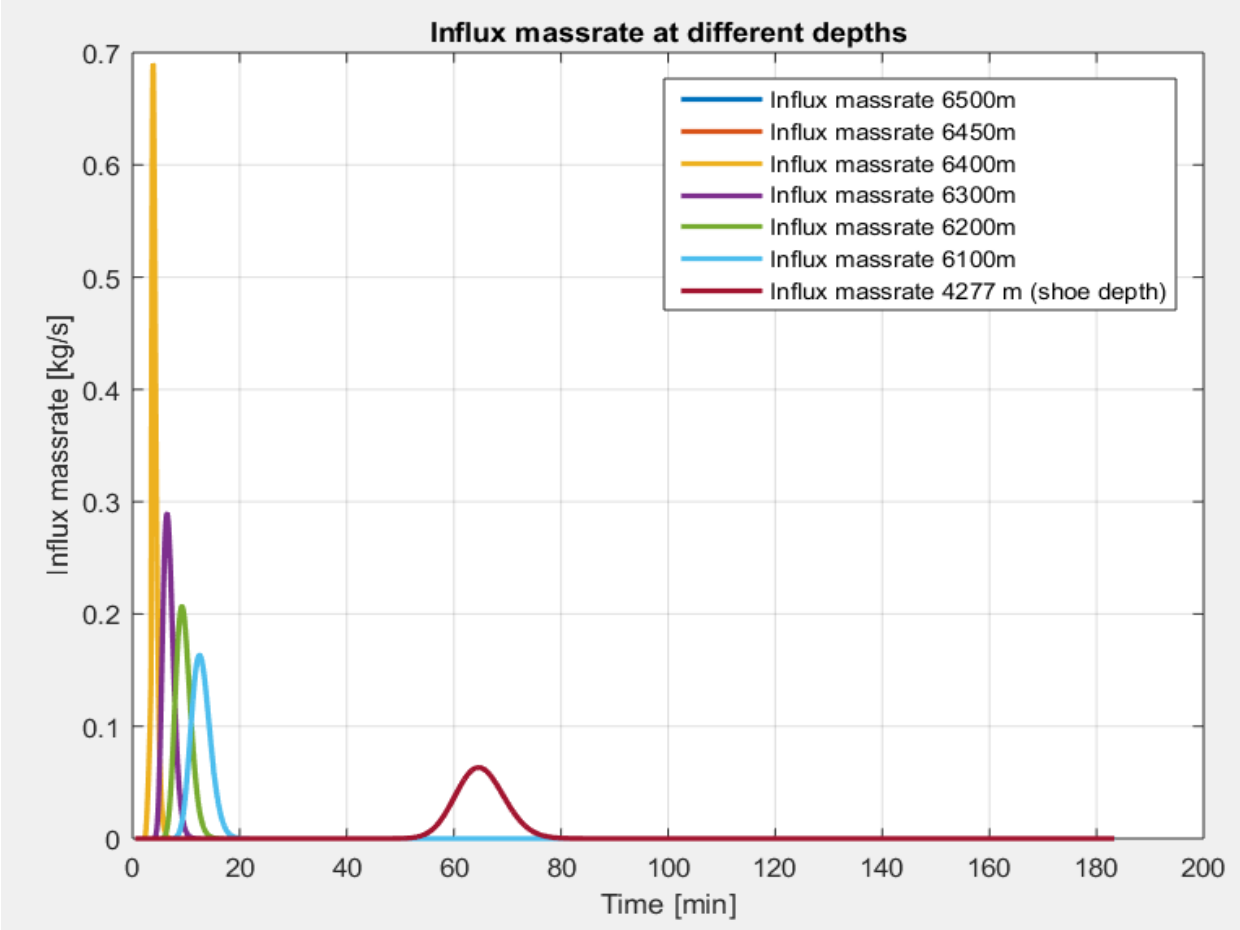

Figure 7.4.5 Shows the influx mass rate at different depths (MD), from different sensors placed in the open hole section.

From the Figure 7.4.5, the influx is only seen in the beginning from 0 to 20 mins, and is controlled through the whole circulation period of 180 minutes. The influx reaches the last casing shoe at around 63 minutes.

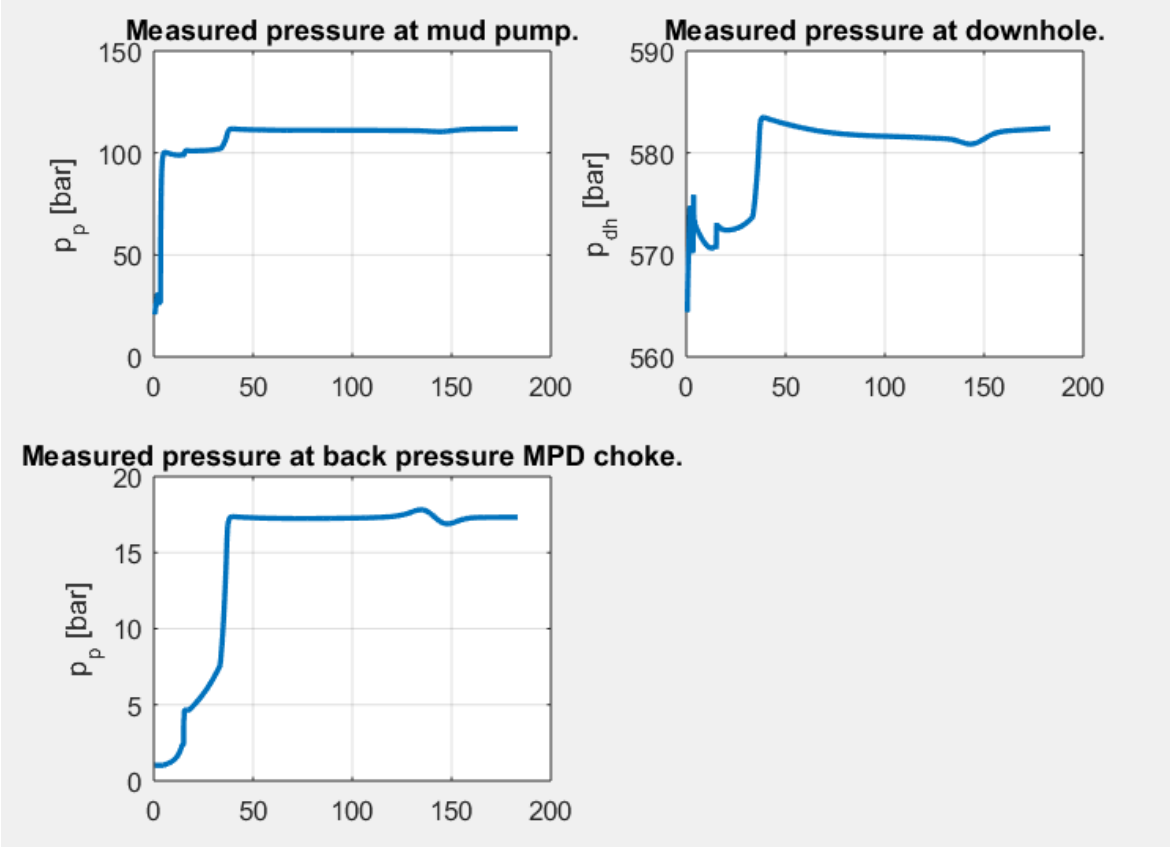

Figure 7.4.6 Shows the pump pressure, the downhole pressure and the back-pressure pump.

The pump pressure increases and stabilises around 110 bar. The measured pressure downhole also stabilizes due to the back-pressure pump at around 582 bar. The measured pressure at choke increases and stabilizes to 17 bar. The pressure responses will in section 7.5 be compared to manual operation.

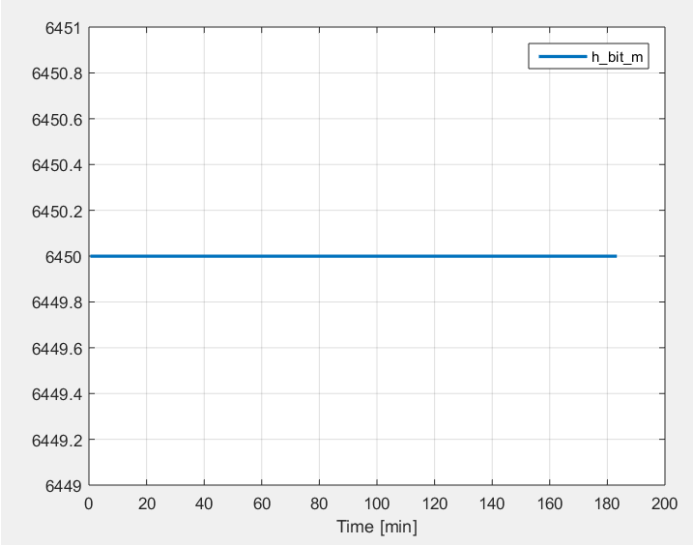

Figure 7.4.7 Shows the bit depth versus time.

The Bit depth is kept constant at 6450 m MD throughout the whole circulation period.

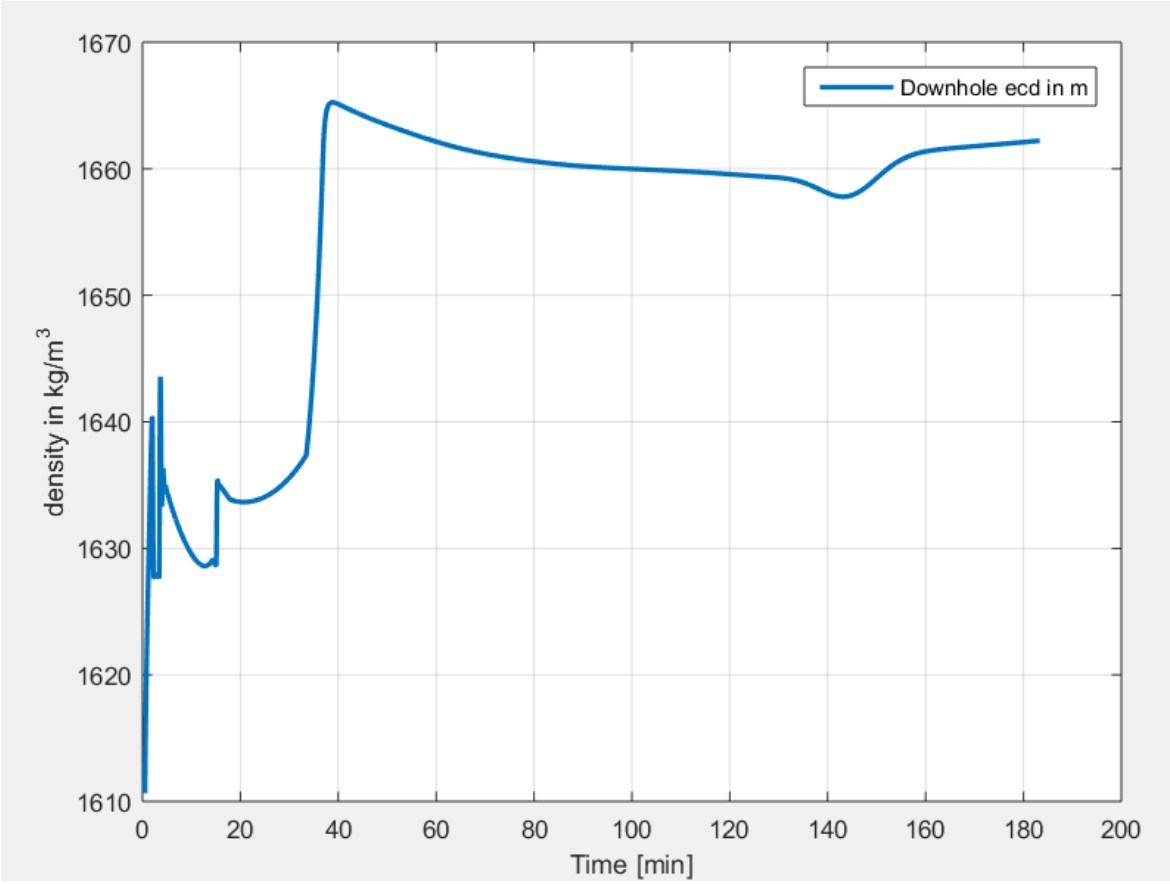

Figure 7.4.8 Shows the downhole ECD change with time.

The downhole ECD is fluctuating according to the choke opening. To around 18 min the choke opening decreases and therefore, the ECD decreases trying to stabilise. The choke is hence kept constant and ECD increases further. The main goal is to avoid lowering the ECD under 1.63 s.g so that another kick does not initiate while circulating. The final ECD stabilizes around 1.66 s.g and the circulation is successfully complete.

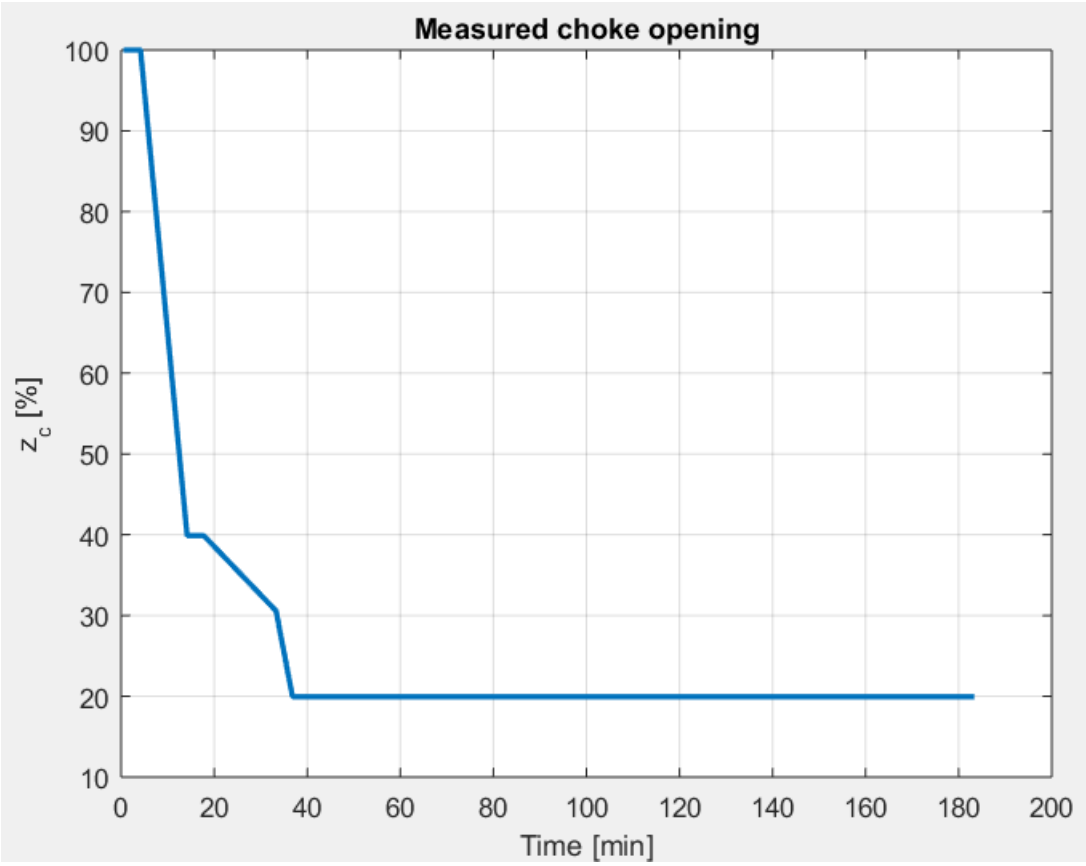

Figure 7.4.9 Shows the choke opening change with time. The opening is planned manually.

The choke is initially 100% open. It reduces to 40 % within 16 minutes and is kept constant for about a couple of minutes before it is again lowered to stabilize at 30 % at around 18 minutes. The final reduction starts at 33 minutes and reduces the choke opening to 20%. The choke opening after around 40 minutes is kept at 20 %, and the kick is circulated out using this opening.

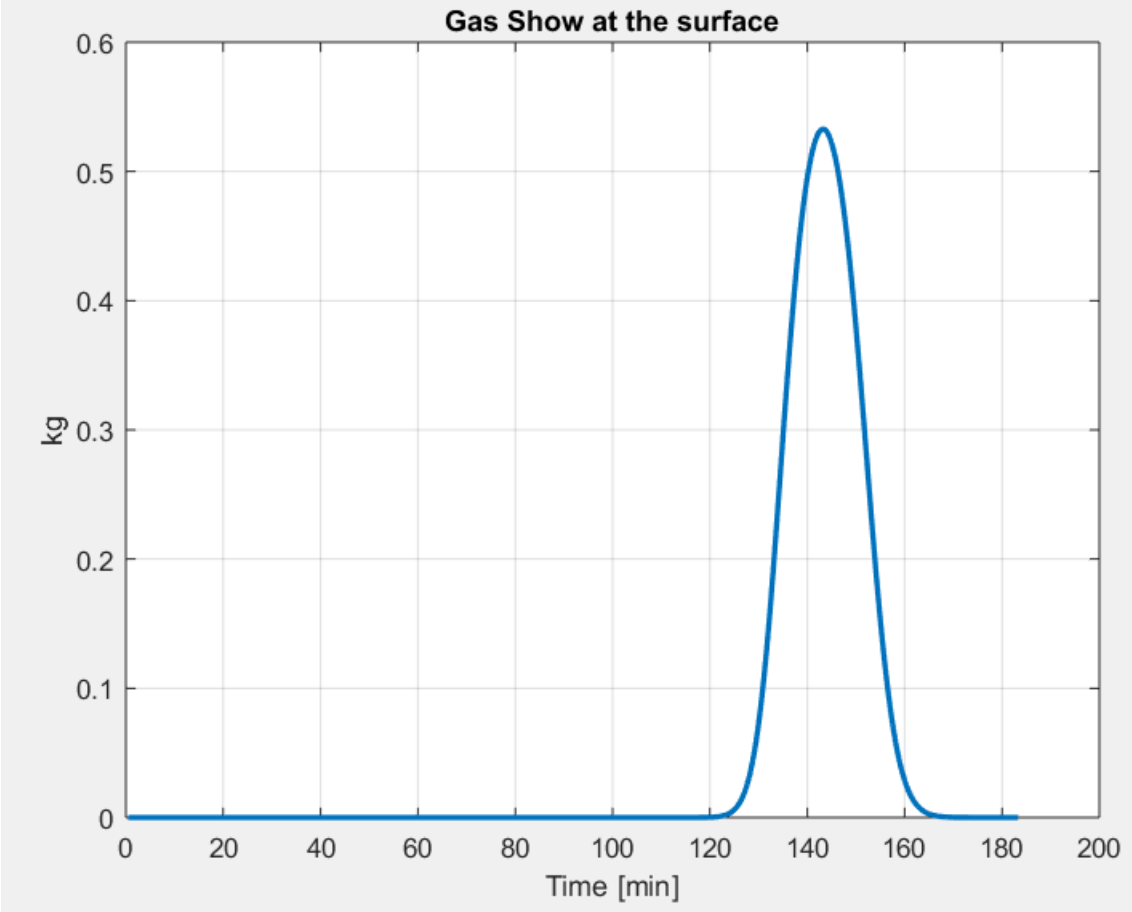

Figure 7.4.10 Shows the gas show to surface versus time.

The Figure shows and confirms that the influx has been circulated out safely at around 150 minutes. The gas show then decreases to zero after around 165 minutes.

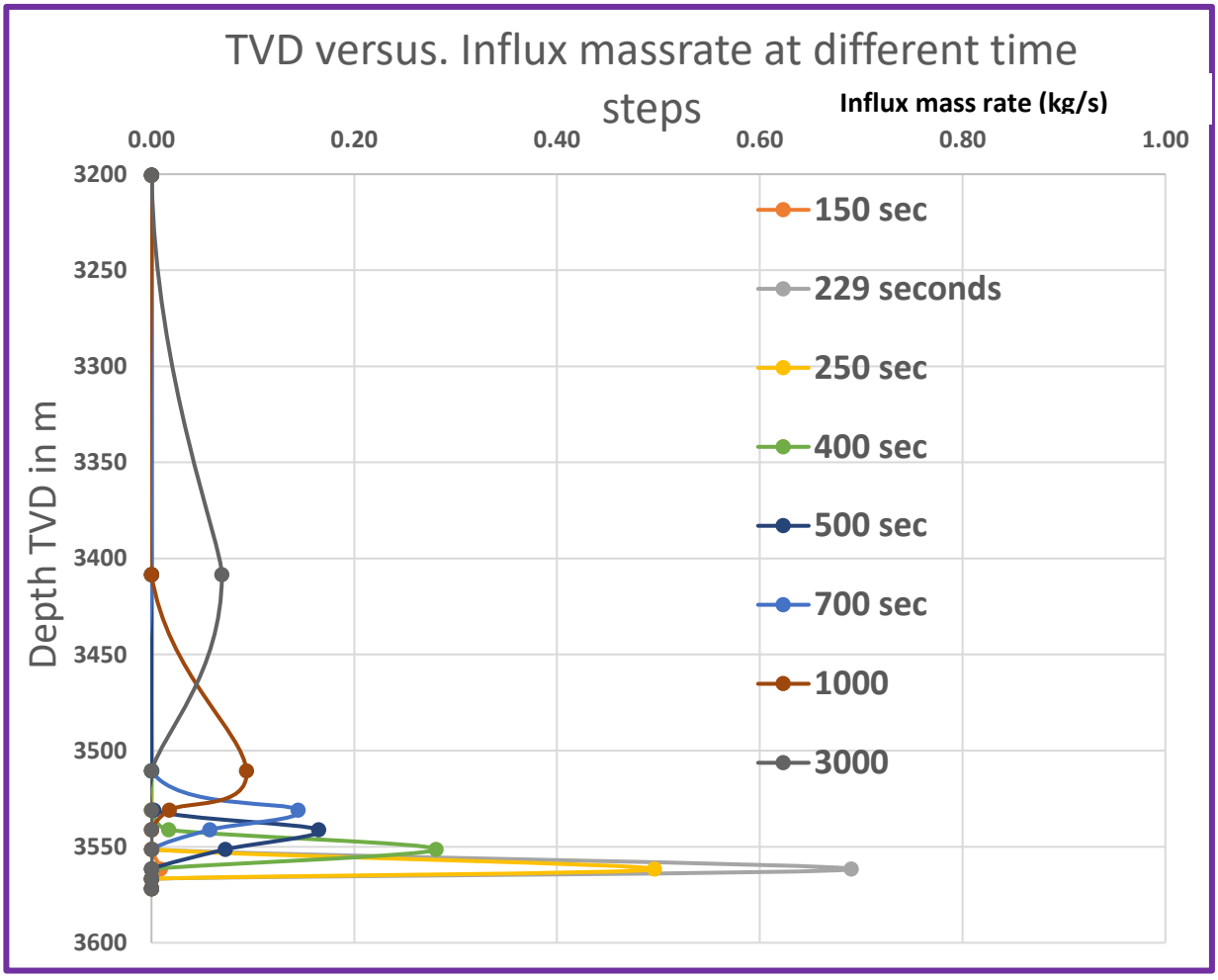

Figure 7.4.11 Shows the movement of influx through time.

The Figure shows the development of influx through time, from its initiation till it gets closer to the surface.

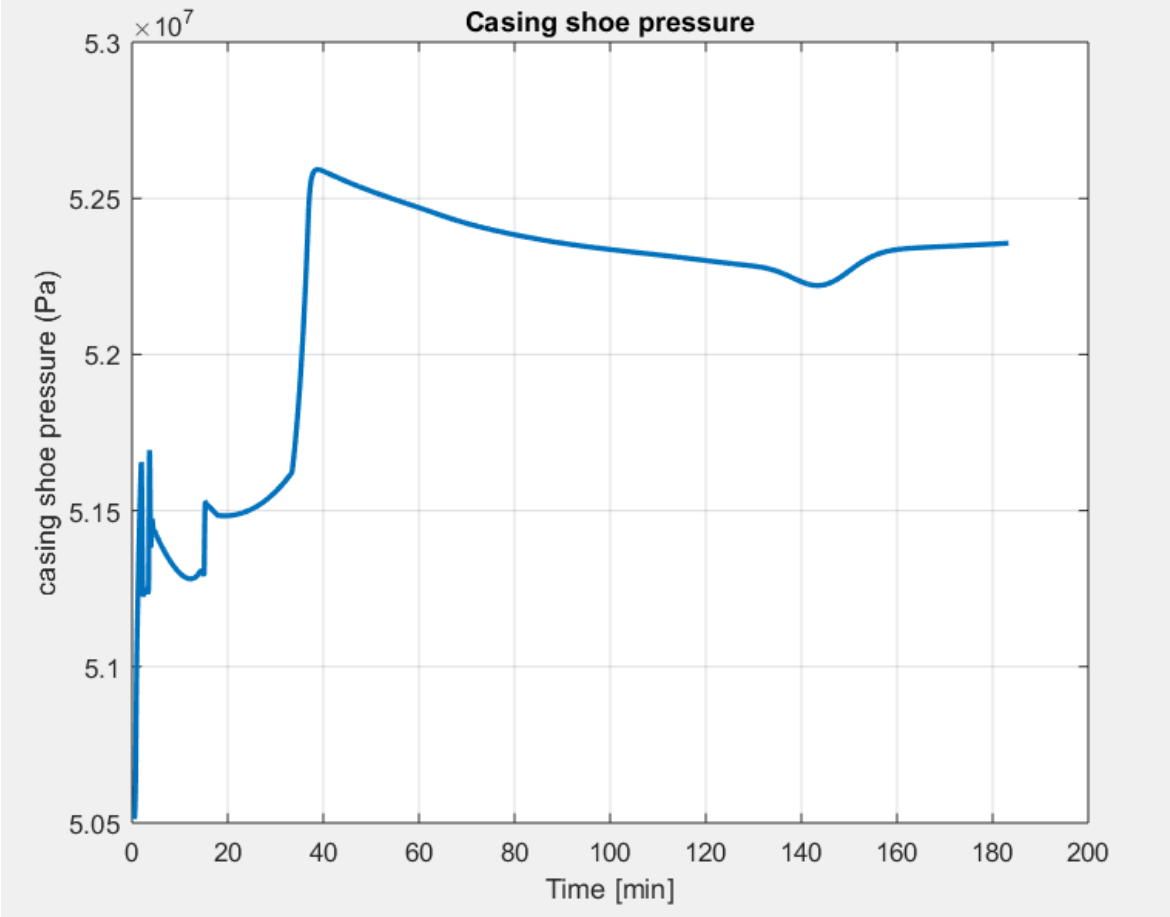

7.4.12 Shows the casing shoe pressure at 4277 m MD development through time.

The casing shoe pressure for the influx at 43 kg is seen. This shoe pressure will change according to the choke opening.

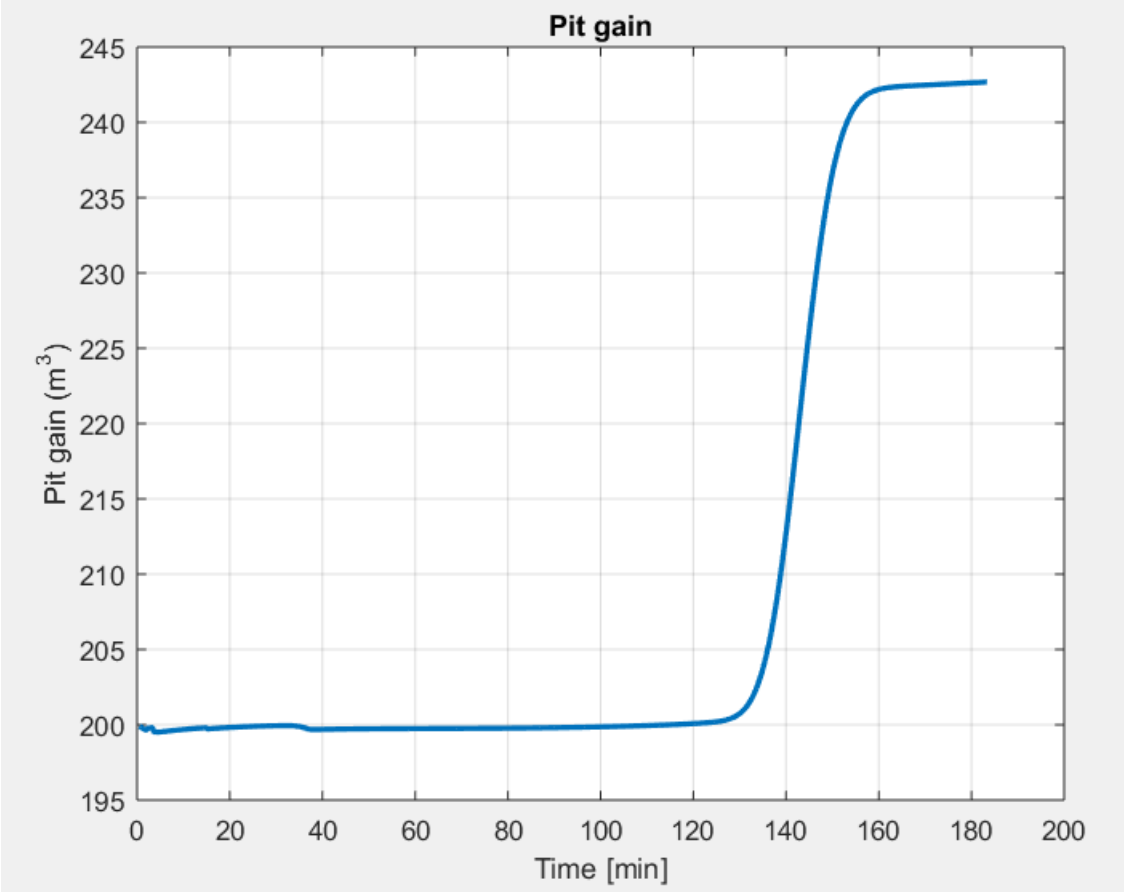

Figure 7.4.13 Shows the pit gain development through time for the whole circulation period.

The maximum influx can be shown when the maximum casing shoe pressure versus influx is drawn. This can be achieved in several ways,

1. Let more gas into the well and general more values for influx and note the maximum casing shoe pressure.
2. Change the choke opening, mud pump or the back-pressure pump
3. Change the time when choke/pumps are added.

By using one of these methods a curve of casing shoe pressure versus influx size (in kg) can be constructed as seen in Figure 7.4.14.

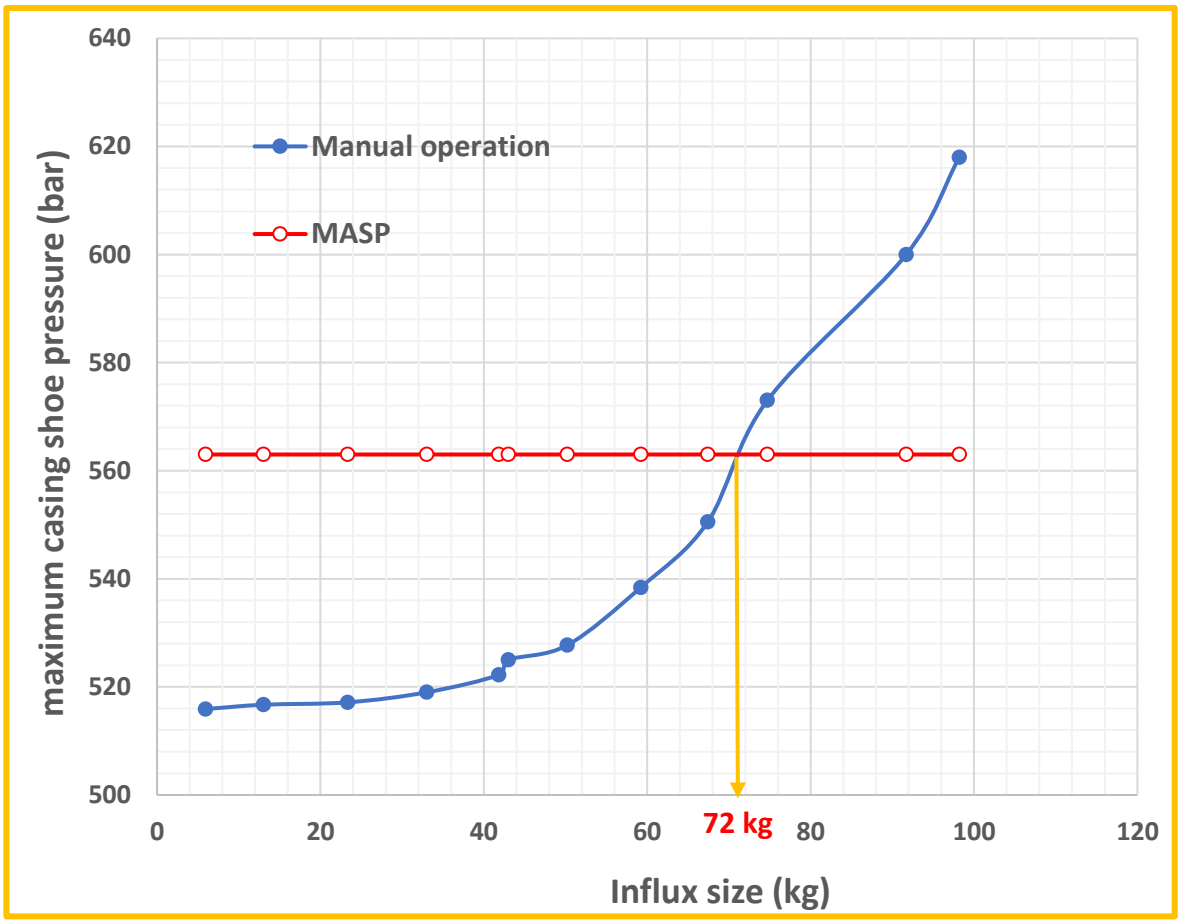

Figure 7.4.14 Shows the maximum casing shoe pressure versus influx size for manual operation.

MASP was shown earlier Chapter 3.3, calculated to be equal to 563 bars. The maximum influx size that can be circulated out of the wellbore without exceeding the MASP is around 72 kg for manual operation. The casing shoe was located in the deviated section, and the highest BHP was less than the fracture pressure therefore, according to the Figure 7.4.14, 72 kg is the limit of the influx size can be safety removed from the well.

7.5 Kick simulation with automated operation for HPHT well

A similar approach will be conducted for the automated operation. The controller is designed with the basis of PI controller from Chapter 6. The controlled variable will be the choke opening. The mud pump and back pressure pump will be set the same as for manual operation, so that they can be compared later in Chapter 7.6. The BHP will be the set-point will be at 580 bar with an allowance of fluctuations of +/- 100 bars.

The kick size will be similar to manual operation. The simulated results of automated operation are shown below.

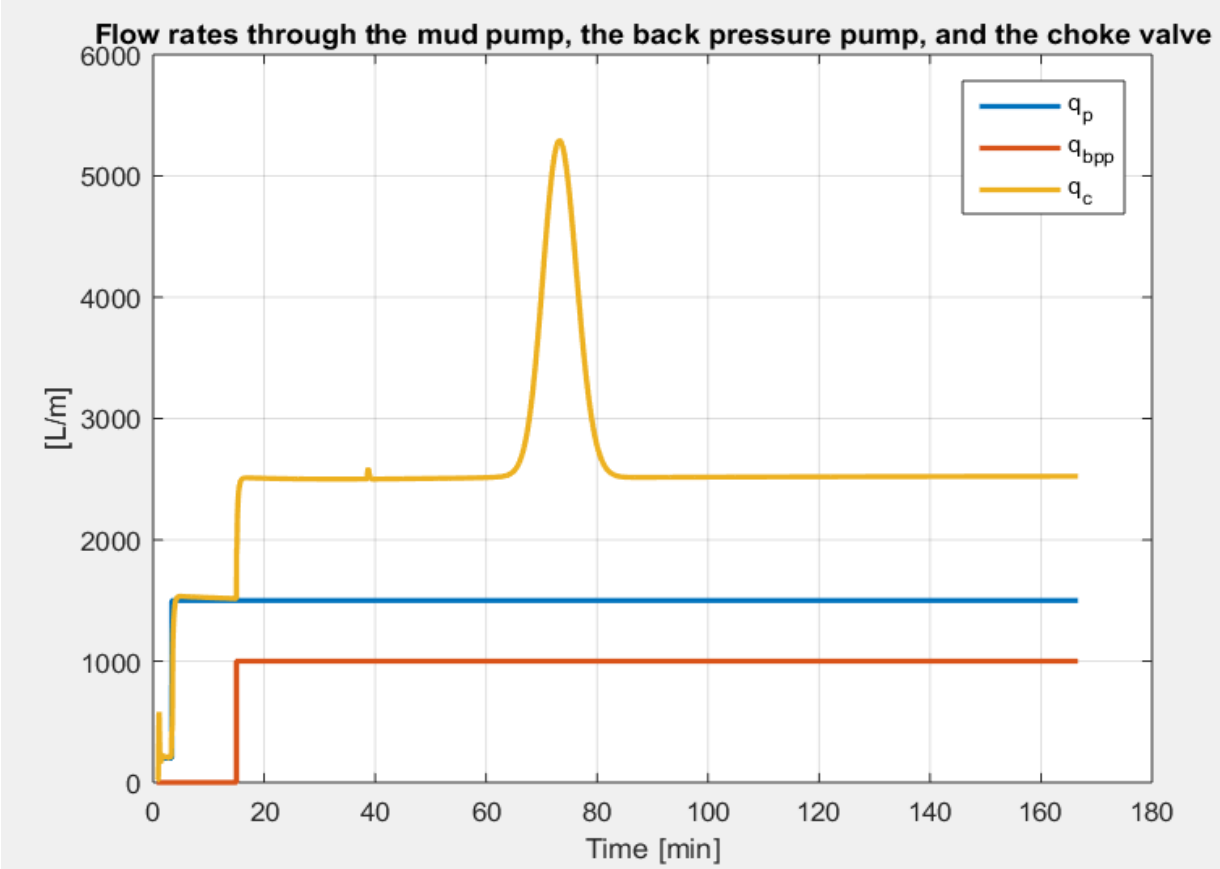

Figure 7.5.1 Shows the Shows the mud pump flowrate-in (blue), the back-pressure pump (red) and the return flow (yellow) versus time for the whole circulation period for automated operation.

The influx for automated operation starts from 194 seconds. The gel breaking takes place within 30 seconds. The kick is then circulated out. The main difference between the manual and automated operation, is that even if the influx enters the well a few seconds later, the circulation is quicker with PI controller. The influx is circulated out at around 85 minutes, as for the manual operation it was circulated around 150 minutes considering the same influx size.

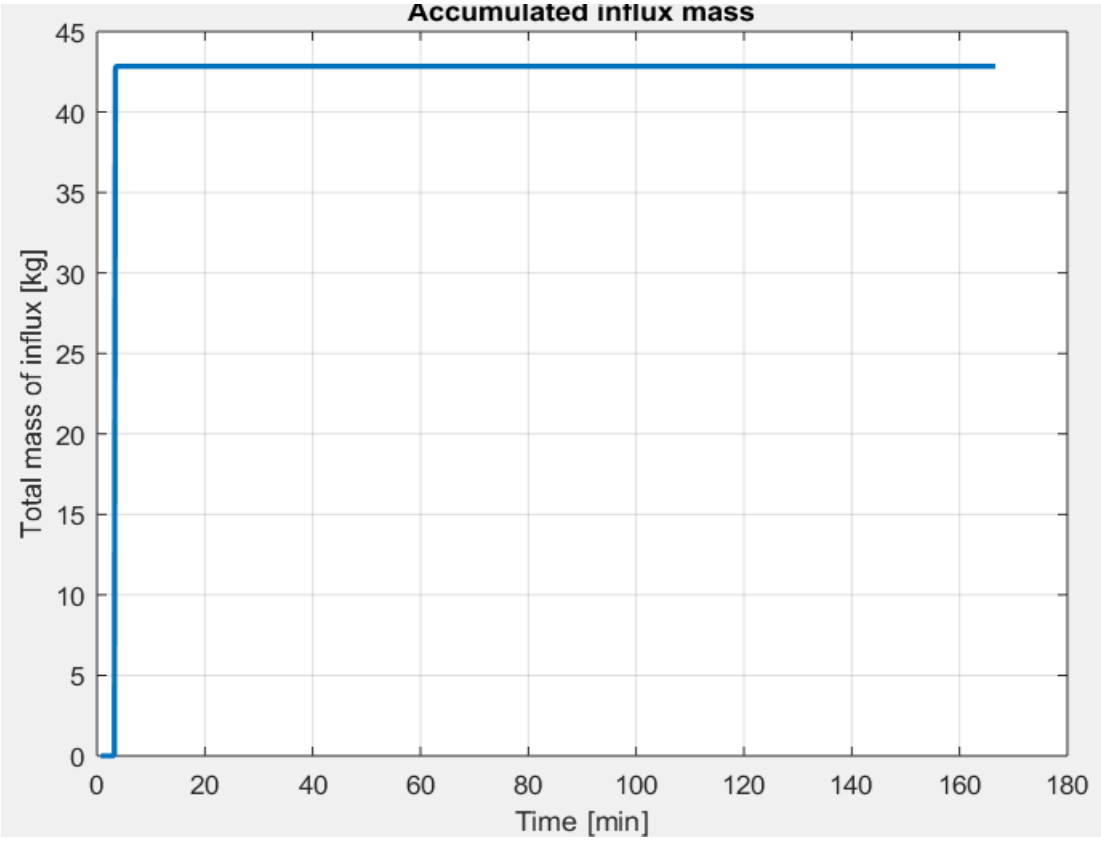

Figure 7.5.2 Shows the total mass of influx in kg versus time. The total influx circulated out was 43 kg initiated for automated operation.

The accumulated influx mass as mentioned above starts at 192 seconds, but the intensity is equal and this curve matches the one for manual operation.

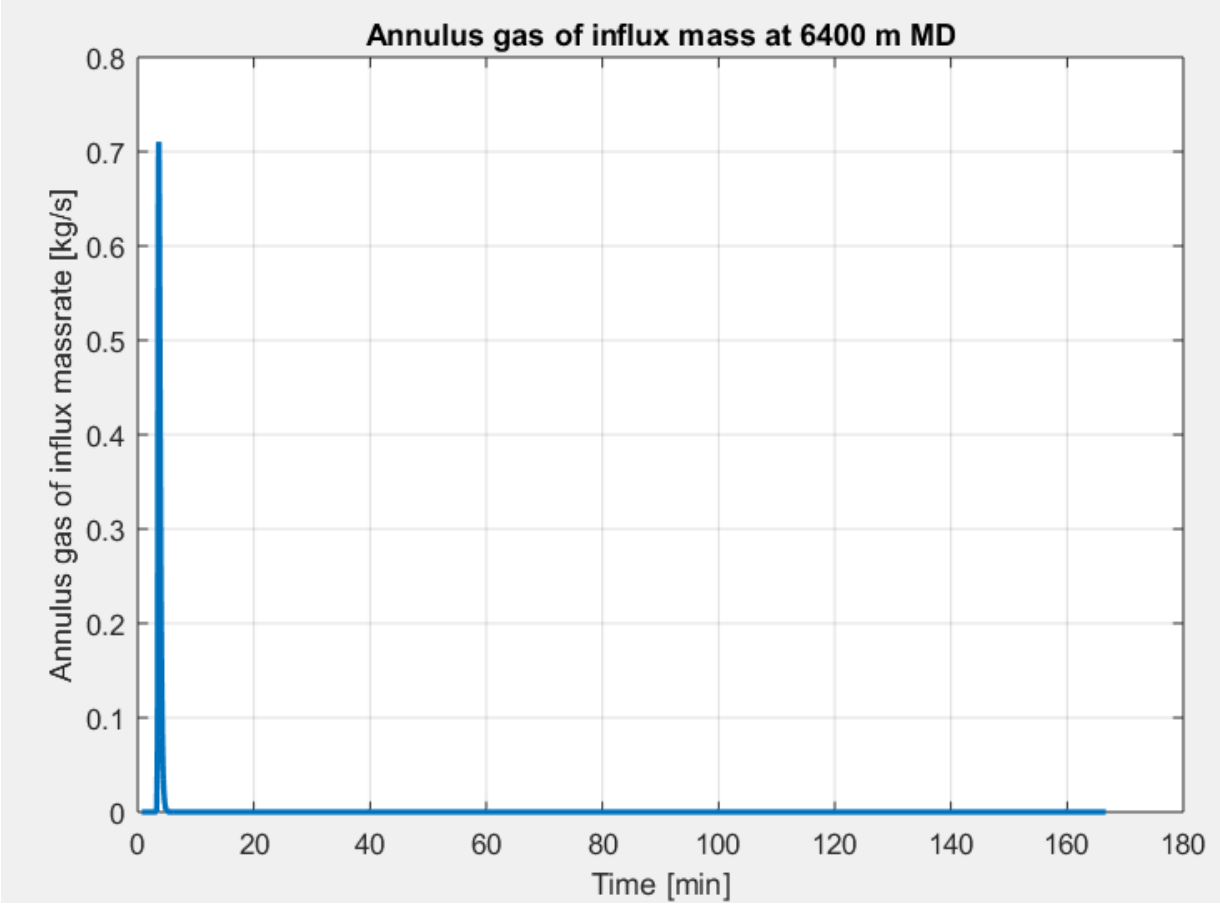

Figure 7.5.3 Shows the sensor measurement of influx mass at 6400 m MD versus time, for the whole circulation period for automated operation.

The intensity shown for the sensor closet to the influx peaks at slightly more than 0.7 kg/s. Even if the sensor experiences influx later than for manual operation, the gradient of increase is quicker, meaning that the sensor measures influx entering 6400 m MD faster.

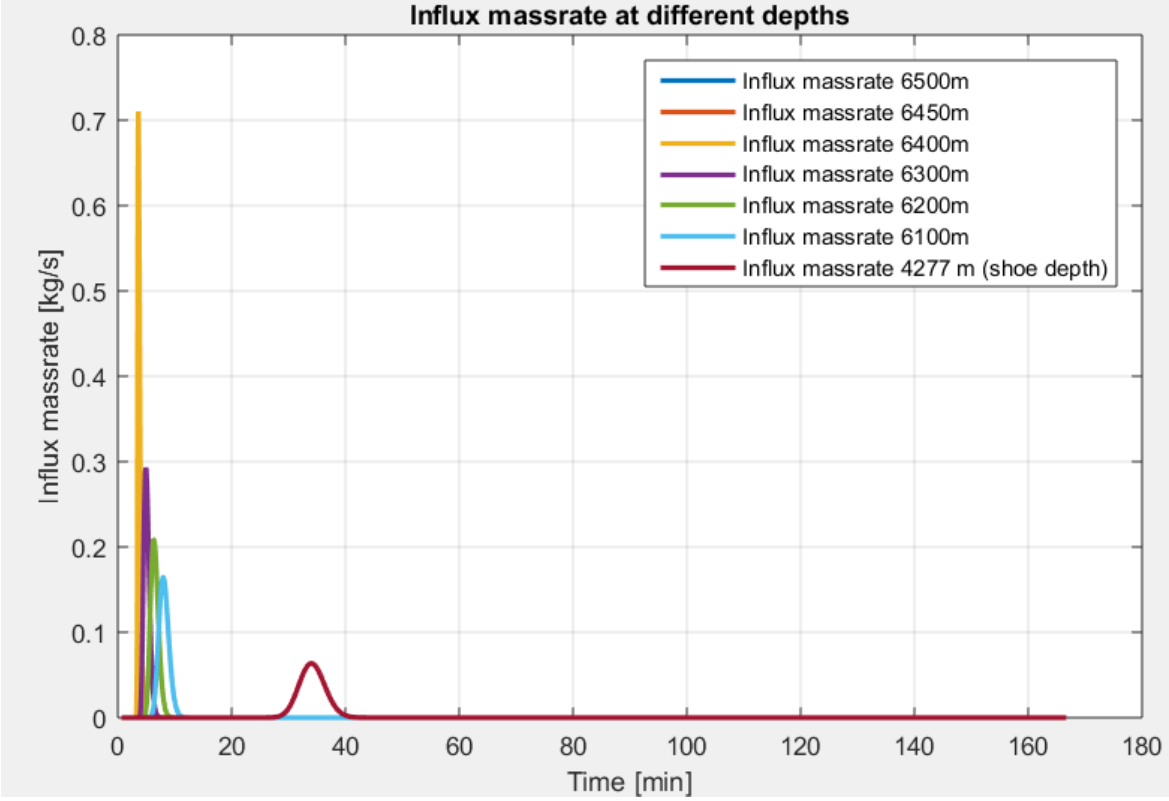

Figure 7.5.4 Shows the influx mass rate at different depths (MD), from different sensors placed in the open hole section for automated operation.

The influx is entering the wellbore quicker than with the manual operation and therefore due to the quick reduction of choke opening of the controller the influx mass rate at the last shoe is shown to be quicker than for manual operation. The intensity at the shoe for automated operation is slightly less than 0.1 kg/s which is the same as for the manual operation. The influx enters quicker at the shoe and consequently, passes above the shoe more rapidly.

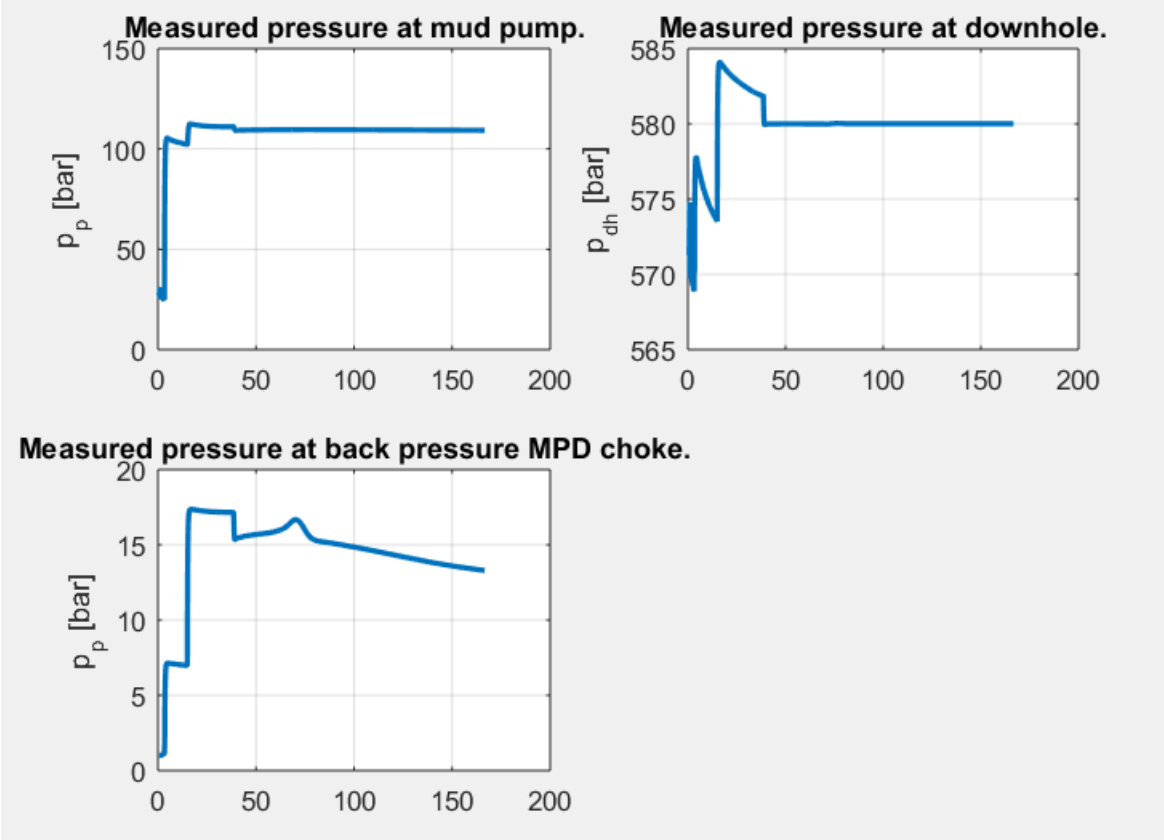

Figure 7.5.5 Shows the pump pressure, the downhole pressure and the back-pressure pump for automated operation

The mud pump pressure shows a few slight changes from 0 to 50 min compared to the manual operation, otherwise both of them stabilize at the same pressure. The downhole pressure fluctuates less in automated operation from 0 to 50 min and is shown to be more stable from 50 min till the circulation is complete. In manual operation, the downhole pressure at late time was fluctuating between 100 to 150 min before stabilizing. The measured pressure at back pressure MPD choke, shows more stability after 50 minutes for the manual operation compared to the automated operation. Figure 7.5.5 shows that it is stabilizing with a decreasing gradient at around 13 bar.

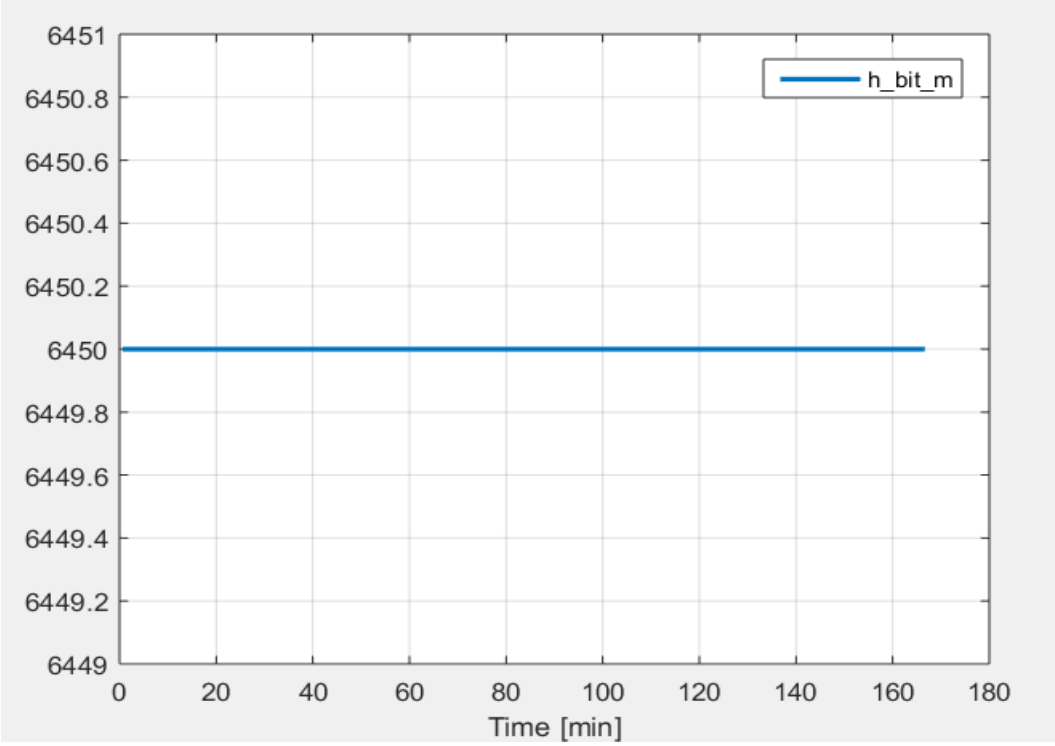

Figure 7.5.6 Shows the bit depth versus time for automated operation.

The bit depth as mentioned for manual operation does not change with time.

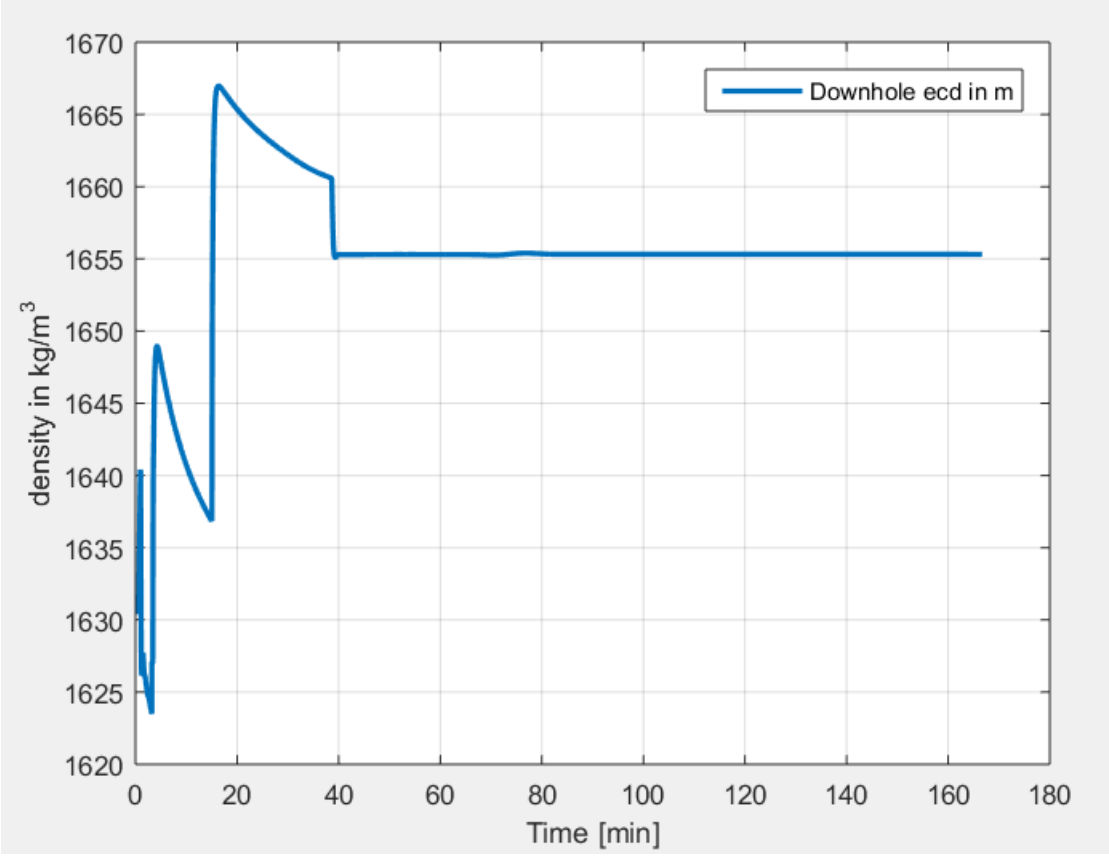

Figure 7.5.7 Shows the ECD change versus time for automated operation.

The downhole ECD is fluctuating according to the choke opening. To around 15 min the choke opening decreases and therefore, the ECD decreases trying to stabilise, the choke is hence kept constant and ECD increases further. The main goal is to avoid lowering the ECD under 1.63 s.g so that another kick does not initiate while circulating. The final ECD stabilises around 1.655 s.g and the circulation is successfully complete. Comparing to the manual operation, where the ECD is more stable after 80 minutes at a density of 1.66 s.g. The automated operation shows more sudden and abrupt changes in the density, while for the manual operation a slower change is observed. In reality the change of ECD is slow.

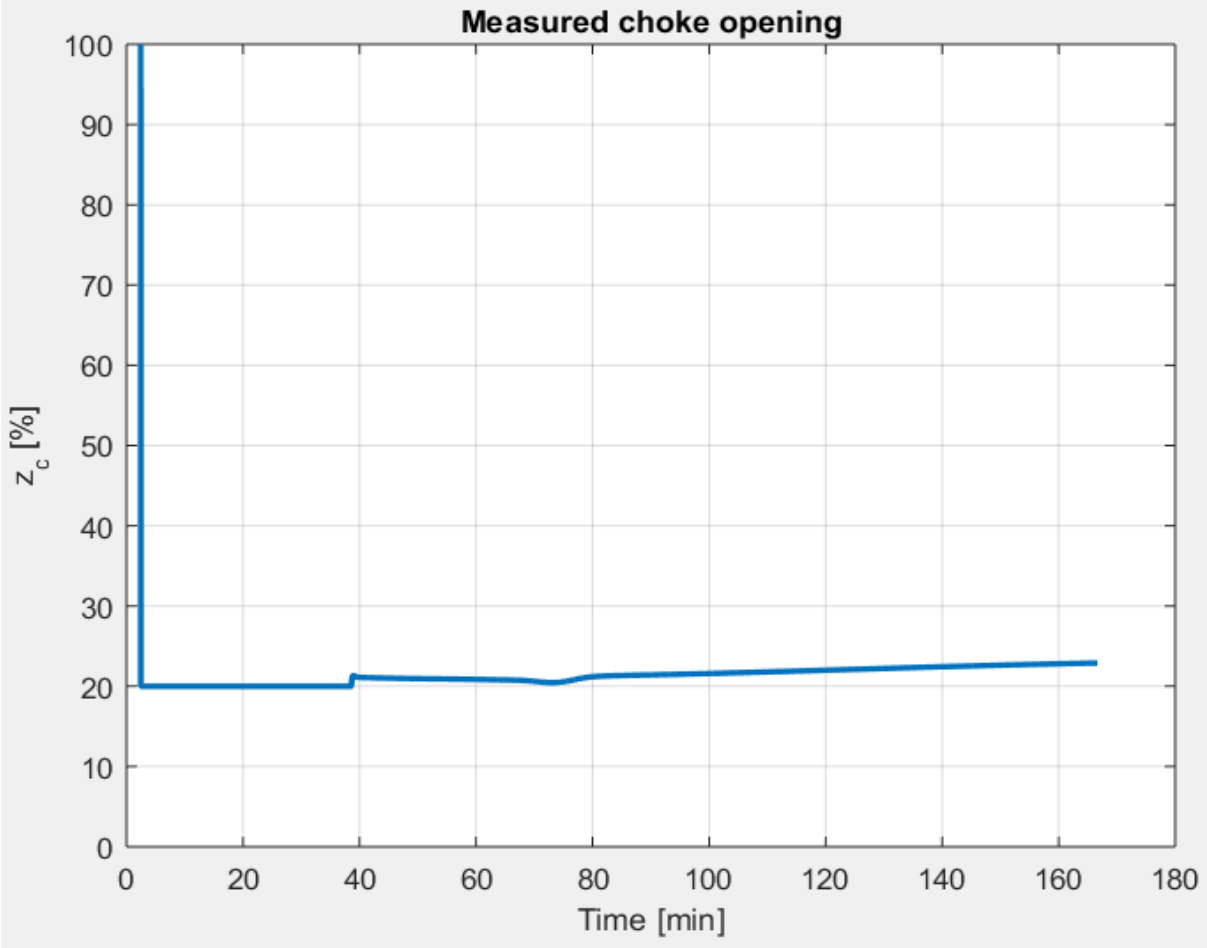

Figure 7.5.8 Shows the choke opening change with time for automated operation. The opening is controlled by the PI- controller.

The choke is initially 100% open. It reduces to 20 % at 3.5 minutes. The controller closes the choke suddenly due to large influx entering quickly into the wellbore. After the stabilising point is met, the choke is adjusted to slightly above 20% after 40 minutes. The choke opening during circulation is 21 %. Such rapid changes in choke opening is not realistic.

For the manual operation the kick was circulated at 20% opening.

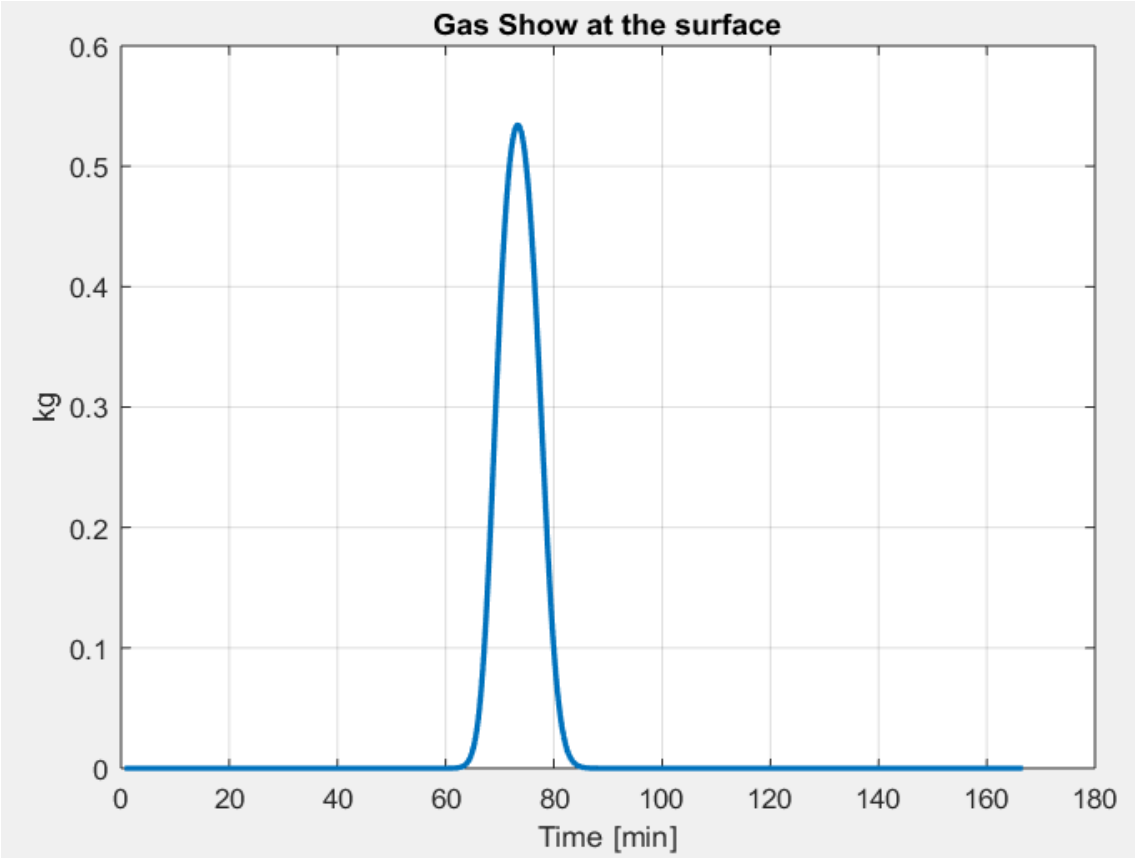

Figure 7.5.9 Gas show at the surface can be seen for automated operation.

The gas show at the surface, as mentioned earlier, confirms that the kick was circulated out. This occurs from around 62 to 82 minutes, earlier than for manual operation. The main reason behind this is because of quick and sudden change of choke opening. For manual operation, the gas at surface was seen from 122 to 162 minutes.

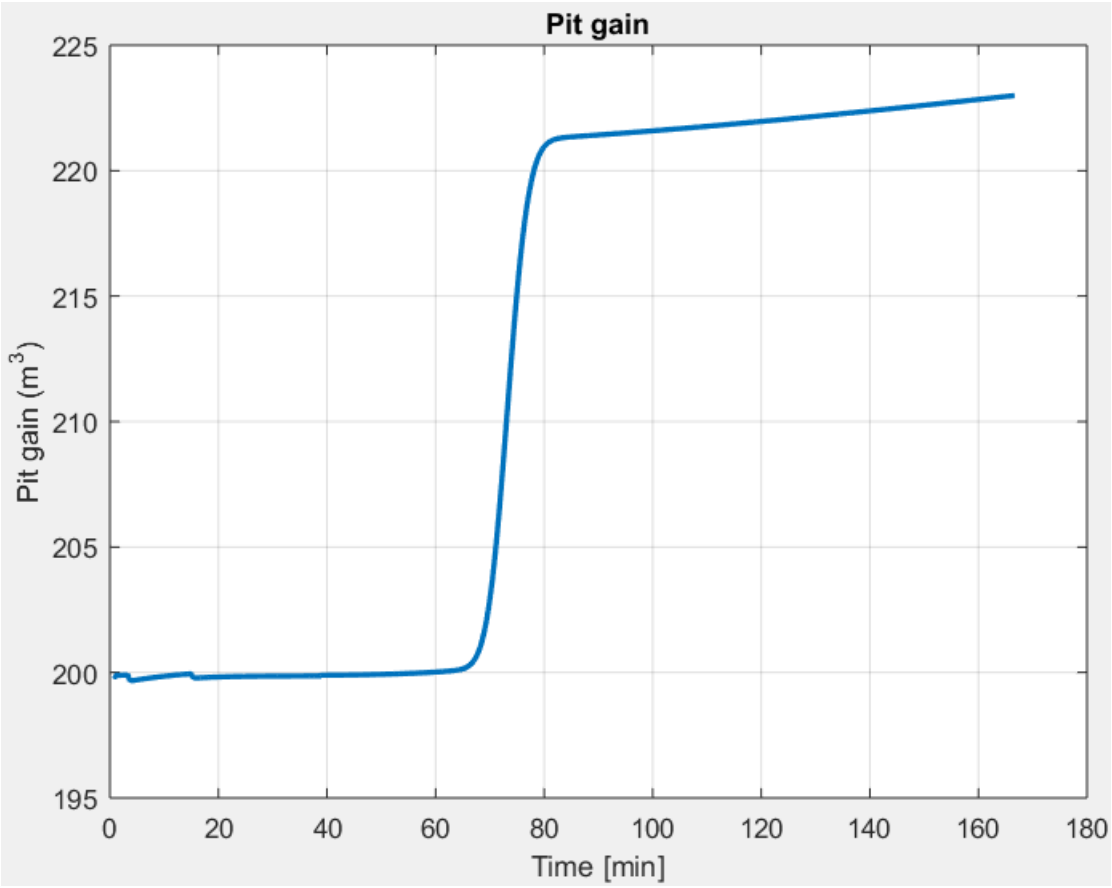

Figure 7.5.10 Shows the pit gain versus time for automated operation.

Since, the gas show and the circulation is completed earlier than for manual operation, the increase in pit gain curve is also earlier, as expected.

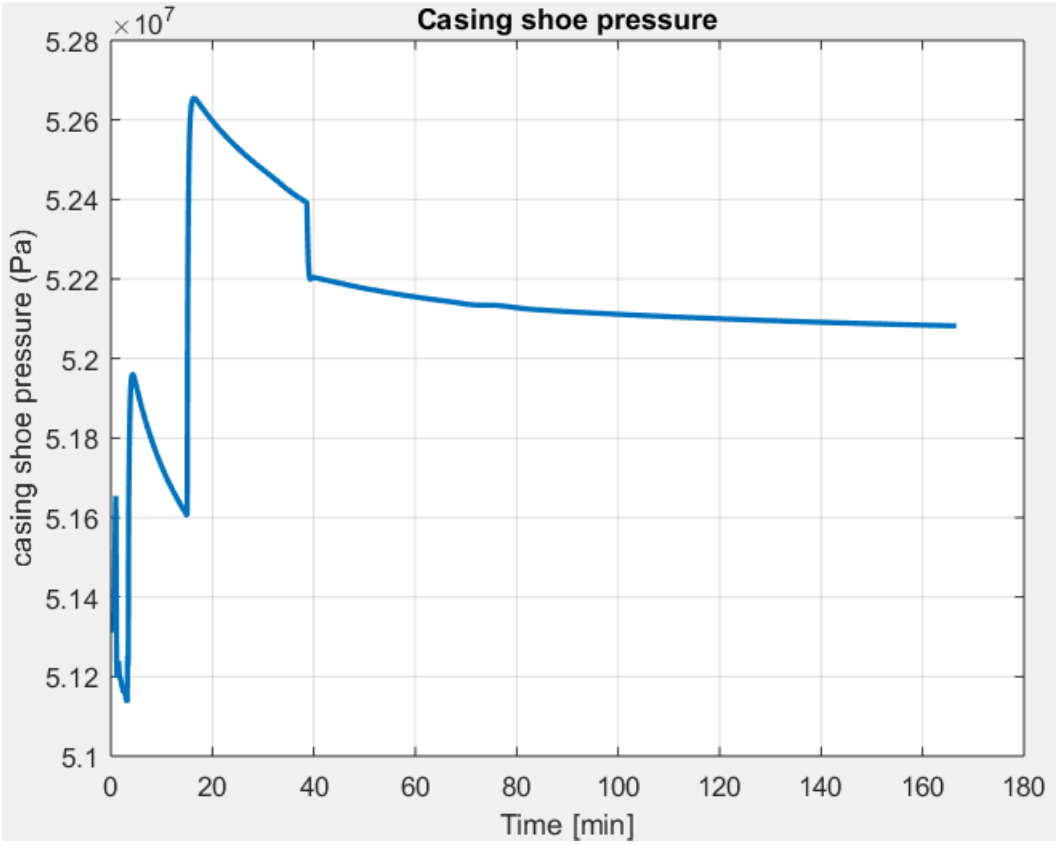

Figure 7.5.11 Shows the casing shoe pressure change with time for automated operation.

The change casing shoe pressure is seen from changes in the choke opening. The stability of casing shoe pressure is seen from 40 min to a pressure of 521 bar. For manual operation the stability was only observed after 80 min to a pressure of 523 bar.

The influx detection time was for the automated operation at 192 seconds, and the total time after influx stops was at 205 seconds. Thus,

$$\Delta t = 205 - 192 = 13 \text{ seconds}$$

Since, the total time difference < the time difference for manual operation.

As a result, the Figure 7.4.14 will shift to the right proving that the automated operation is able to handle and circulate a greater influx size. This effect is illustrated in Figure 7.5.12.

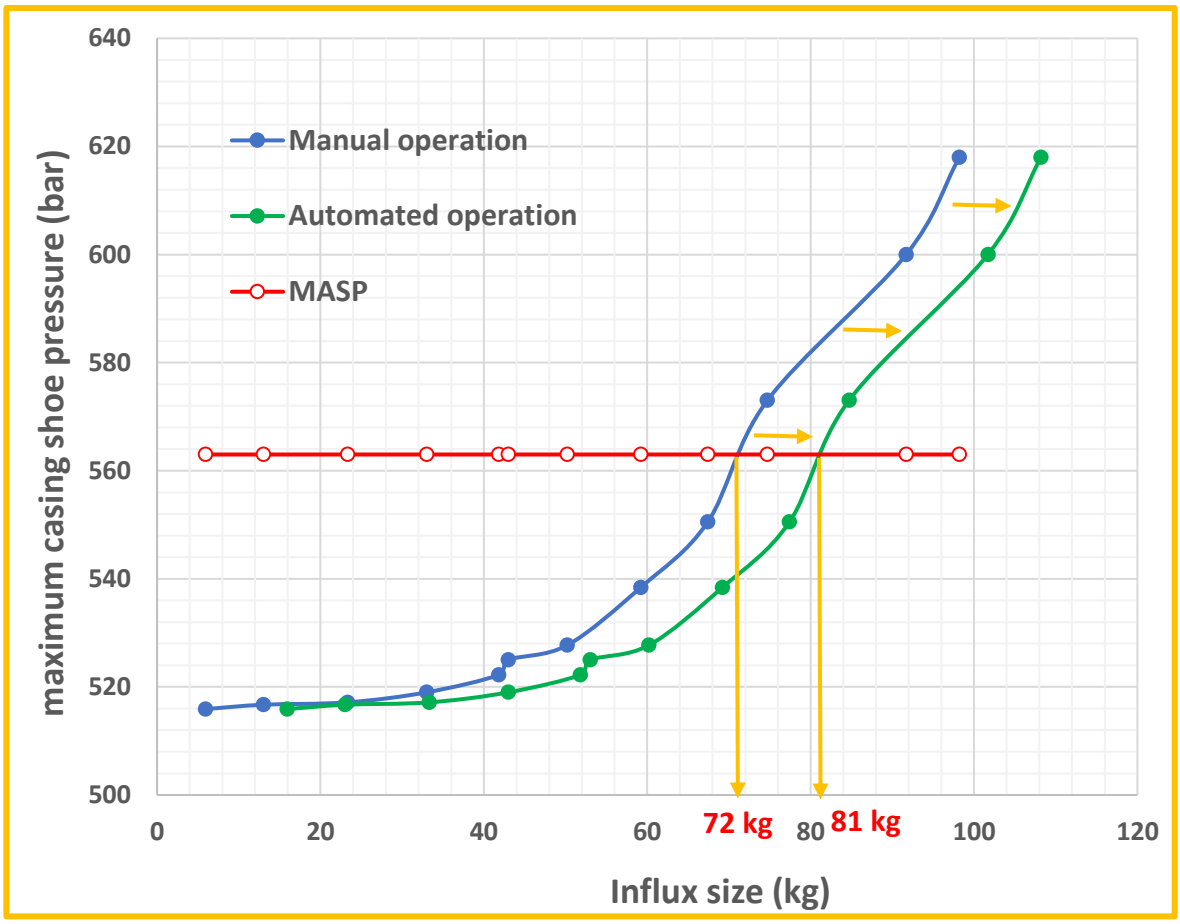

Figure 7.5.12 Maximum casing shoe pressure versus influx size for manual and automated operation.

As, a conclusion the manual operation has more gradual changes and the circulation takes much longer to perform, as the choke is planned to close at a certain speed to a certain level. However, in automated operations, a small amount of influx changes the choke opening rapidly. The difference between the detection time and the total time is greater for manual operation, meaning that kick tolerance for manual operation is lower than for automated operation. From Figure 7.5.12 the automated operation shows greater advantage compared to manual operation.

There are two main advantages from automated operation.

1. Shorter circulation time of influx
2. Able to handle greater influx time

7.6 Kick simulation with automatic operation for comparison of WBM and OBM for a conventional well.

The case study done in Chapter 7.4 and 7.5 is considered for a HPHT well, where the maximum downhole temperature is 189 °C. Comparison of OBM and WBM is not possible because of the HPHT conditions of the well. Therefore, another study is conducted where, the geothermal properties is manipulated to be lower, around 80°C, at the target depth. The geo-pressure properties have also been altered, since the density is a function of pressure and temperature. As the temperature is reduced kick initiation was not possible with the maximum pore pressure of 1.638 sg. A value of 1.655 s.g has been used to compare OBM and WBM.

TVD (m)	Type	Formation Name	Lithology Type
0.00	Air		Air
56.00	Water		Water
80.00	Water		Water
121.50	Solid		Unknown
1,200.00	Solid		Unknown
3,000.00	Solid		Unknown
4,200.00	Solid		Unknown

Geothermal gradient (°C/100m)	Specific heat (J/kg•K)	Thermal conductivity (W/m•K)	Density (sg)
0.0	1,005.00	0.02	0.001
-2.0	4,180.00	0.58	1.050
0.0	4,180.00	0.58	1.050
2.0	900.00	2.00	2.500
2.0	900.00	2.00	2.500
2.0	900.00	2.00	2.500
2.0	900.00	2.00	2.500

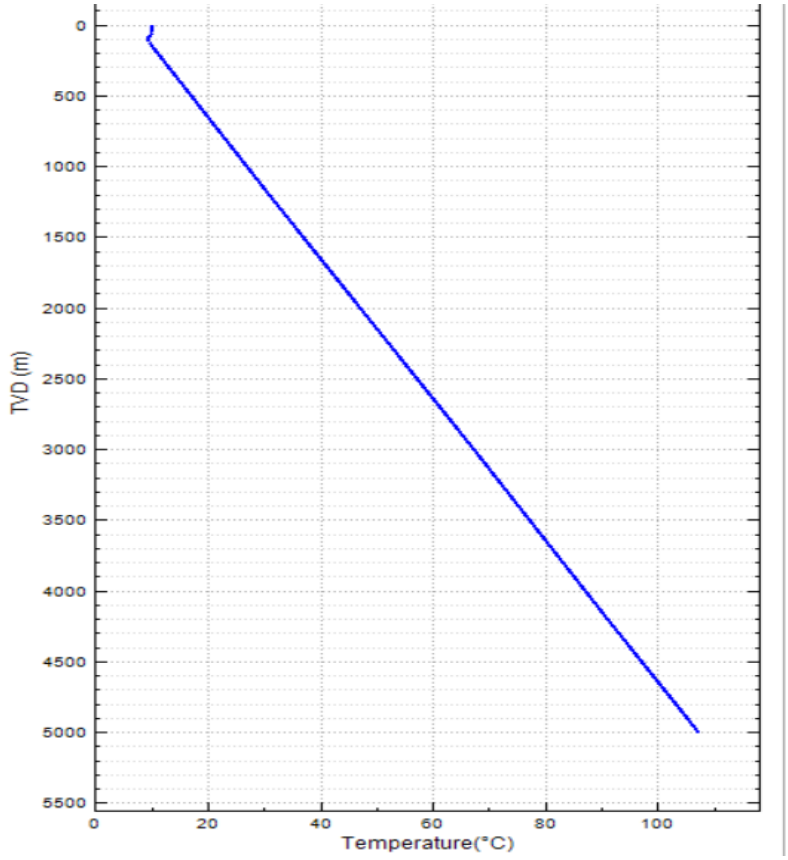

A comparison between the OBM and WBM is shown for the first 3000 seconds. Later, the full circulation is also shown.

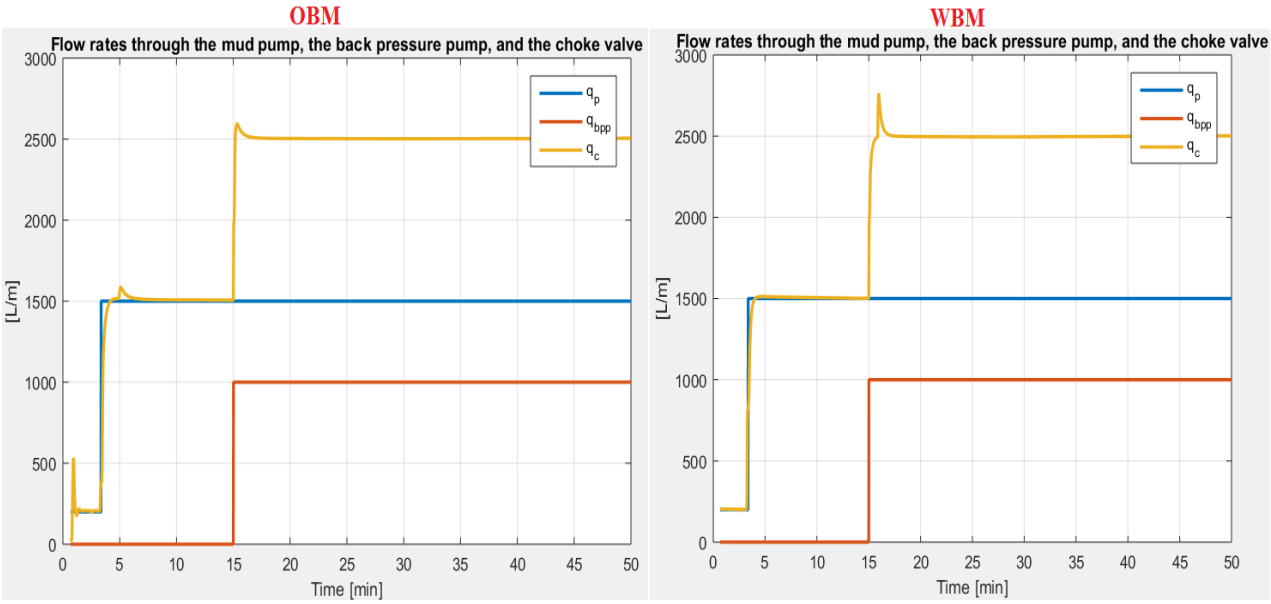

Figure 7.6.1 Comparison of mud pump flowrate-in and return flow for OBM and WBM to 3000 seconds.

At around 3 minutes the return flow increases due to gel breaking, this is not observed for WBM. As the mud pump rate is increased the return flow increases slightly, due to the

change in choke opening (as a result of involvement of back-pressure pump). Since, the choke opening is kept constant at this position (around 4 to 5 minutes), for WBM, shows no change in return flow. After the back-pump pressure is initiated to 1000 lpm at 15 minutes, the return flow is again increasing for both cases. The choke opening is also increasing, but the increase is greater for WBM and therefore the return flow peaks higher. Figure 7.6.2 shows the whole circulation period of 10 000 seconds (167 minutes).

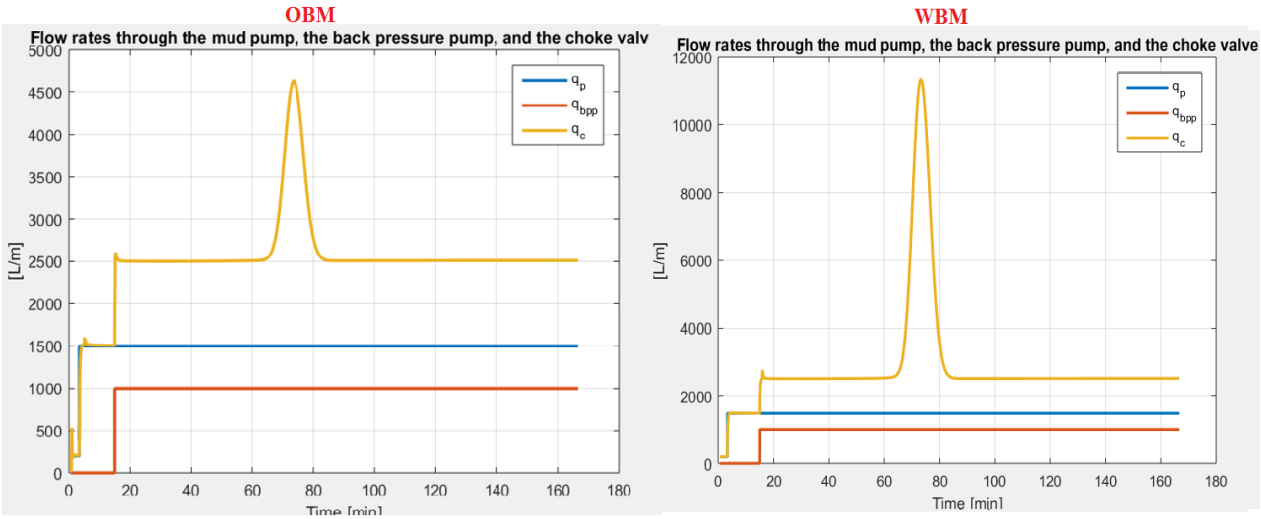

Figure 7.6.2 Shows the mud pump flowrate-in and return flow for OBM and WBM for whole circulation period.

The back-pressure pump is increased after 15 minutes because, it is used to control the downhole pressure and the ECD. Due to consistency for the work presented above, the same configuration of back-pressure pump was applied.

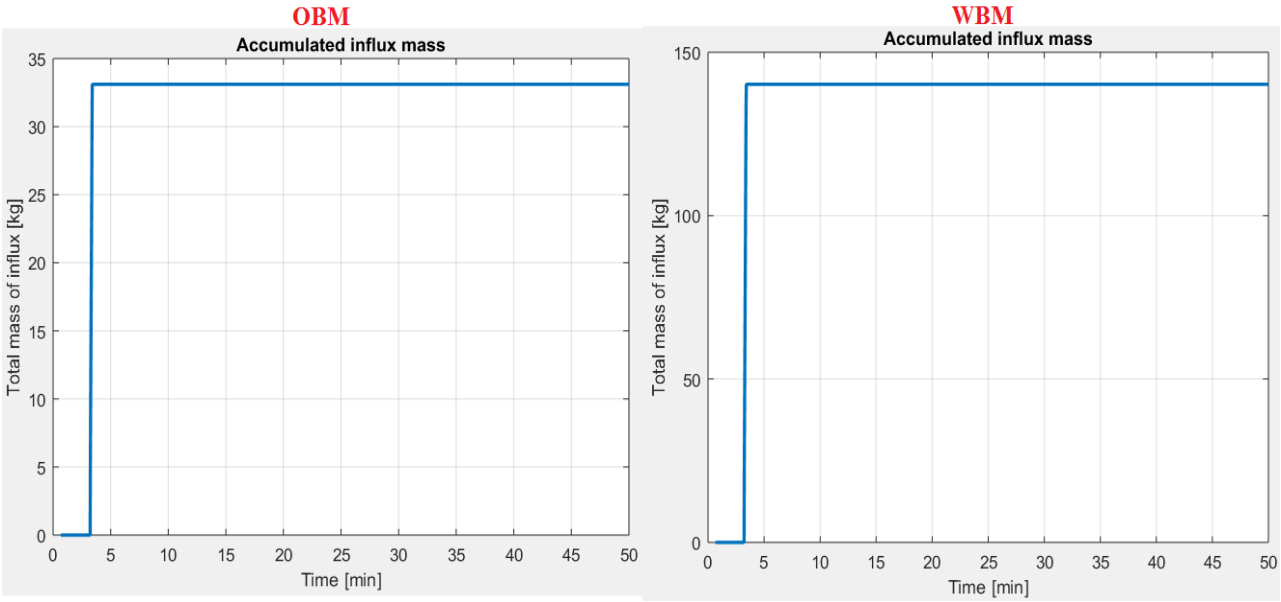

Figure 7.6.3 Comparison of accumulated influx mass for same configuration for OBM and WBM, to 3000 seconds.

The accumulated influx clearly shows 33 kg for OBM and 140 kg for WBM, meaning that, for the same conditions more influx is seen, as kick tends to hide in OBM. The kick initiation time for both cases are same. Figure 7.6.4 shows the full circulation period.

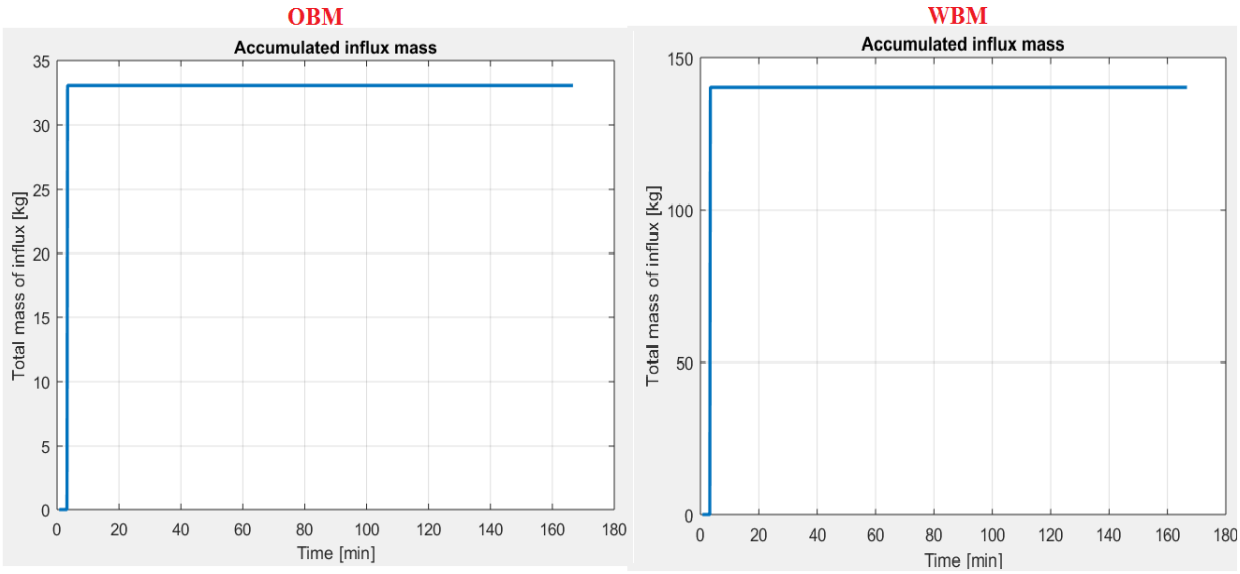

Figure 7.6.4 Comparison of the accumulated influx mass for OBM and WBM for the circulation period.

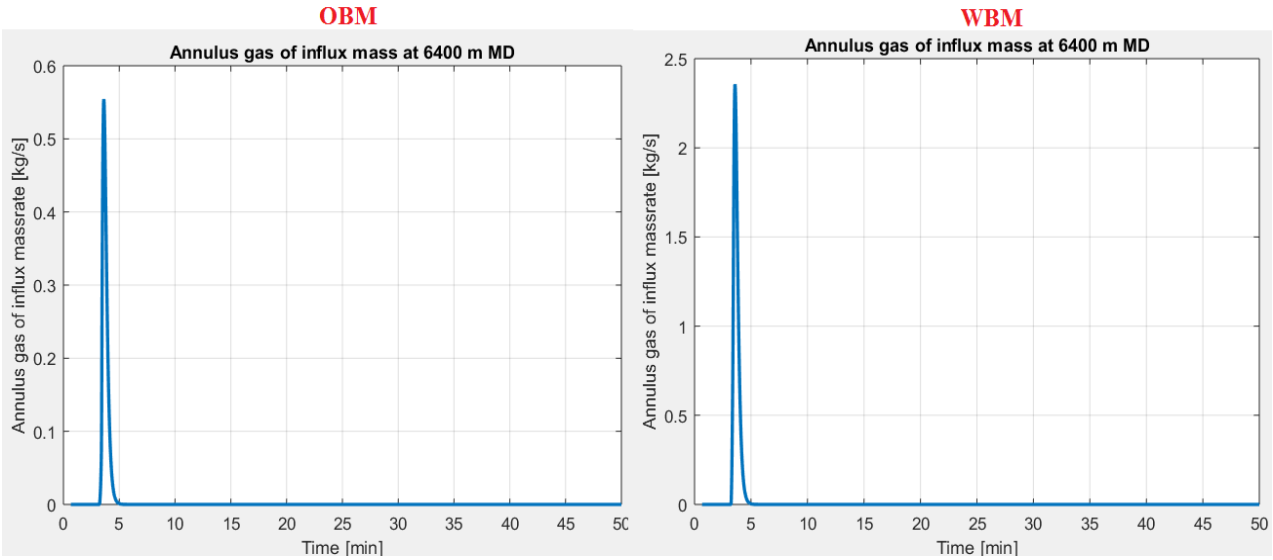

Figure 7.6.5 Comparison of mass influx at 6400 m MD (sensor closet to influx) for OBM and WBM, to 3000 seconds.

The influx mass rate seen at the sensor at 6400 m MD shows is much greater magnitude for WBM. This influx when added to the accumulate influx, becomes a large kick of 140 kg. The total circulation period is seen is the next figure, where the sensor shows that no more influx has entered the wellbore after the initial influx.

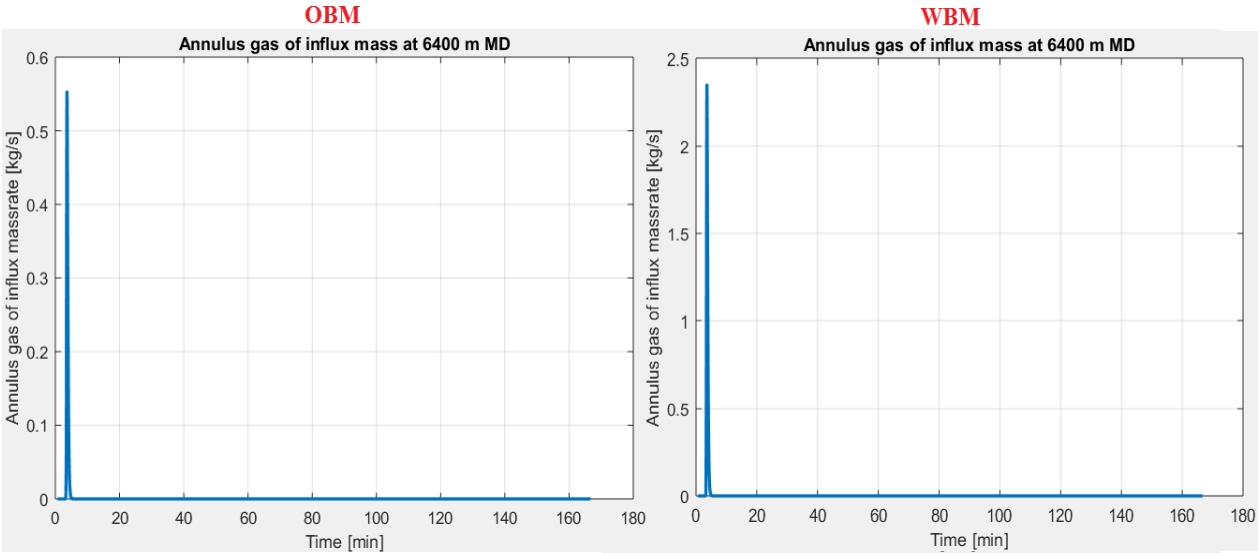

Figure 7.6.6 Shows the annulus mass rate measured at sensor placed in 6400 m MD for OBM and WBM for the whole circulation period.

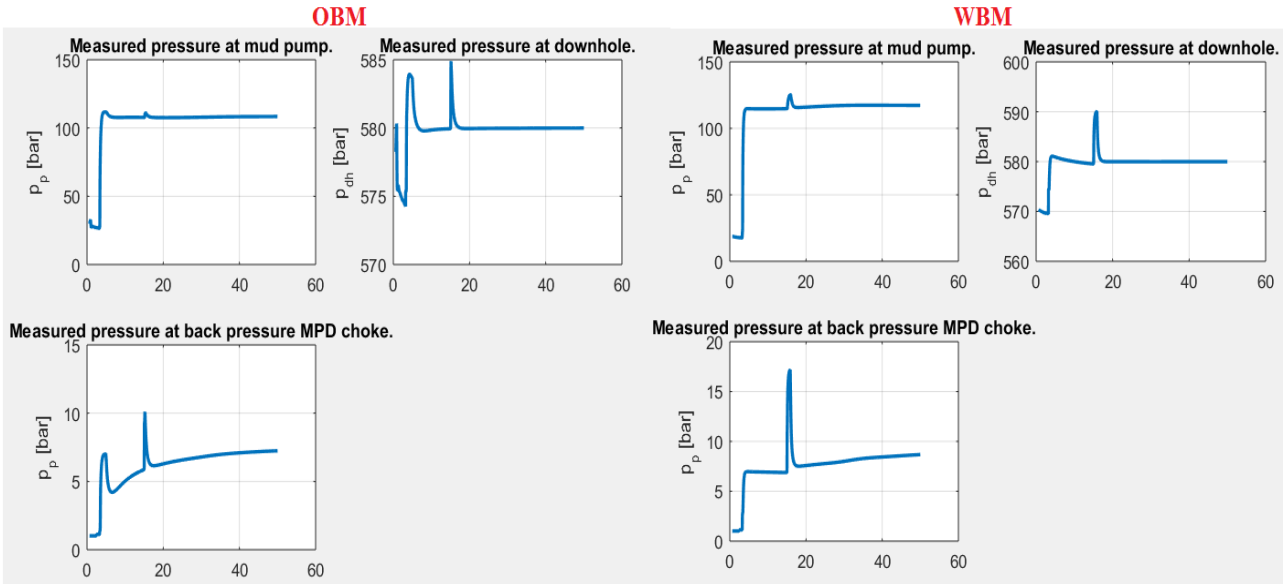

Figure 7.6.7 Shows the mud pump pressure, downhole pressure and the back pressure MPD choke, for OBM and WBM to 3000 seconds.

The pump pressure stabilises at lower pressure for OBM compared to WBM. The choke opening at 18 minutes makes a jump on the downhole pressure curves for both WBM and OBM. Since, the choke opening shows greater difference for WBM, the downhole pressure also jumps to a maximum of 590 bars. The measured back-pressure MPD choke, oscillates more in WBM at 18 minutes and stabilises also at a slightly greater pressure then OBM. The pressures for the whole circulation period is seen in Figure 7.6.8.

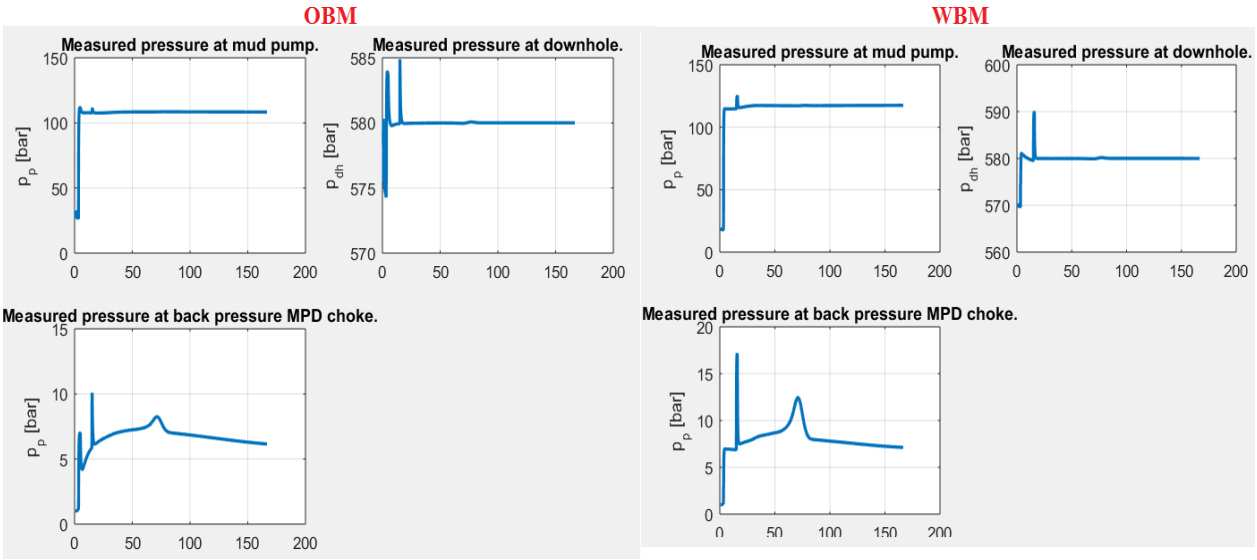

Figure 7.6.8 Comparison of mud pump pressure, downhole pressure, back pressure MPD choke of OBM and WBM for whole circulation period.

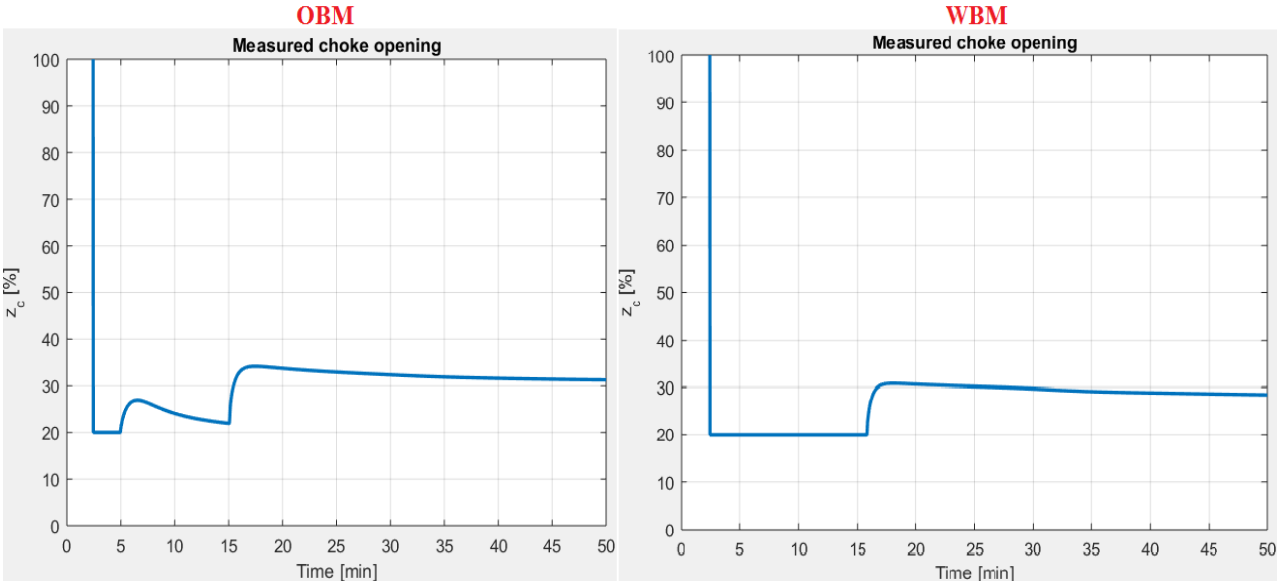

Figure 7.6.9 Shows the measured choke opening with time for OBM and WBM for 3000 seconds.

The choke opening is controlled by the PI-controller and its changes can be seen for OBM and WBM. Since, the kick size is different and less for OBM, it shows more frequent changes, whereas for the WBM, the choke opening of 20 % is kept for a longer period of time. The figure shows only simulation up to 3000 seconds. The increase in choke opening is due to the sudden increase of back-pressure pump (causes all the peaks on casing shoe pressure and ECD).

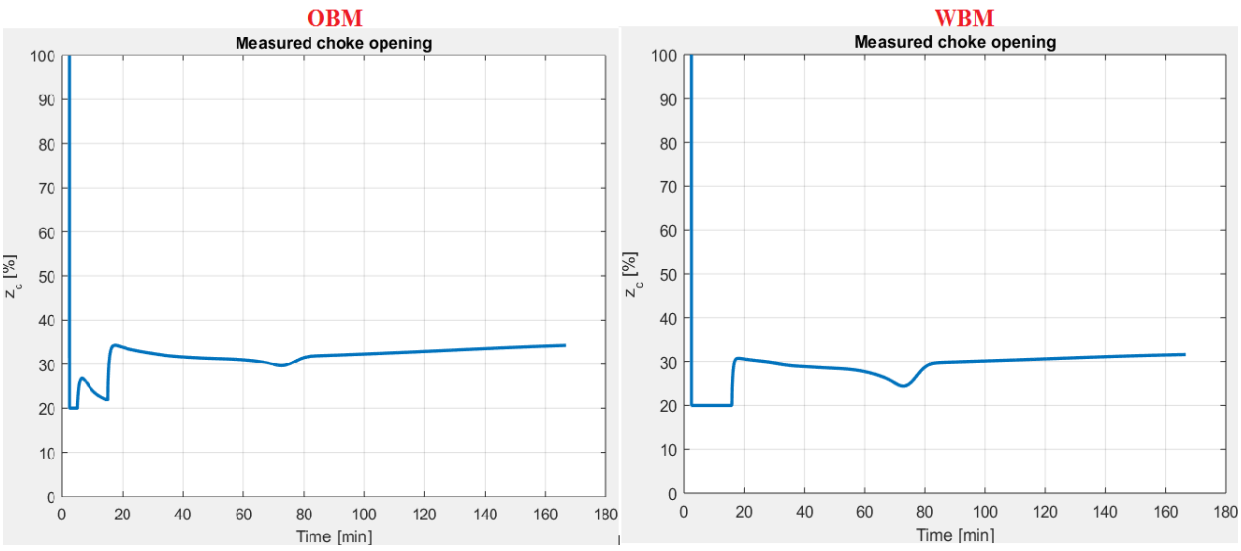

Figure 7.6.10 Shows the measured choke opening for OBM and WBM for whole circulation period.

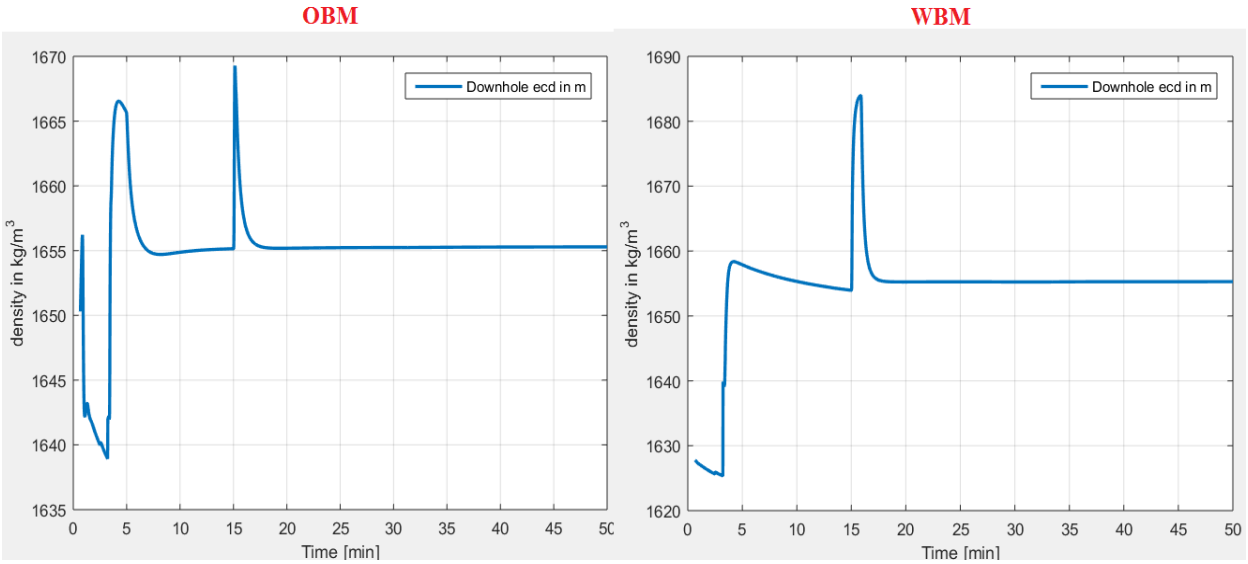

Figure 7.6.11 Comparison of downhole ECD change with time for OBM and WBM to 3000 seconds.

The ECD change shows two peaks for OBM, because of the two changes of choke opening, while the WBM only shows one peak. Both of ECD curves stabilise around 20 minutes, both at 1.655 sg.

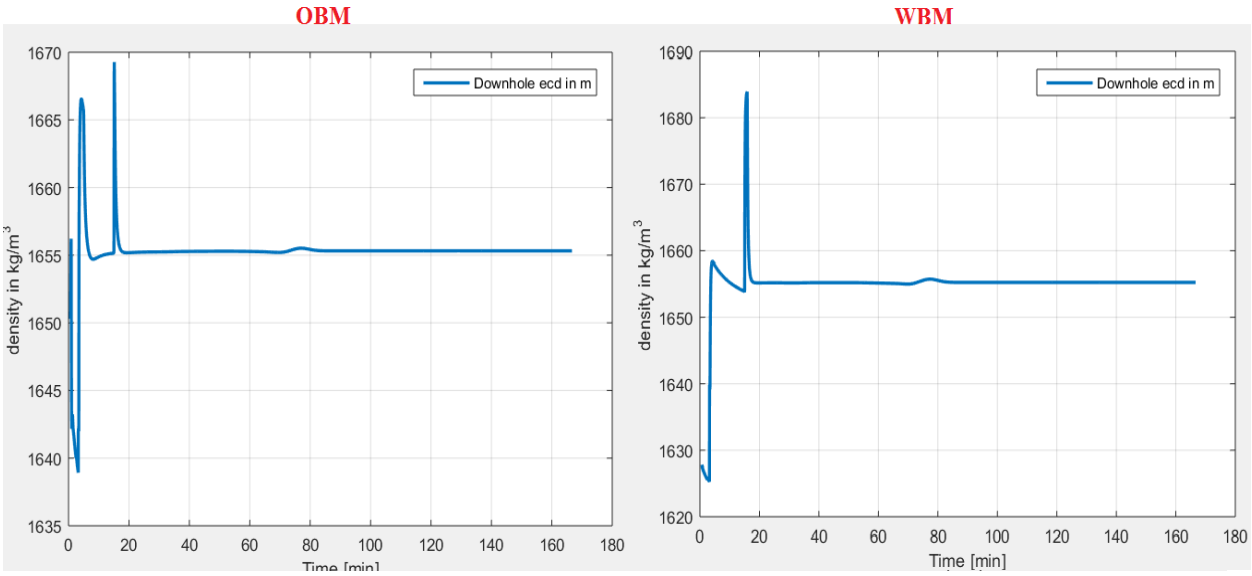

Figure 7.6.12 Comparison of OBM and WBM of downhole ECD for whole circulation period.

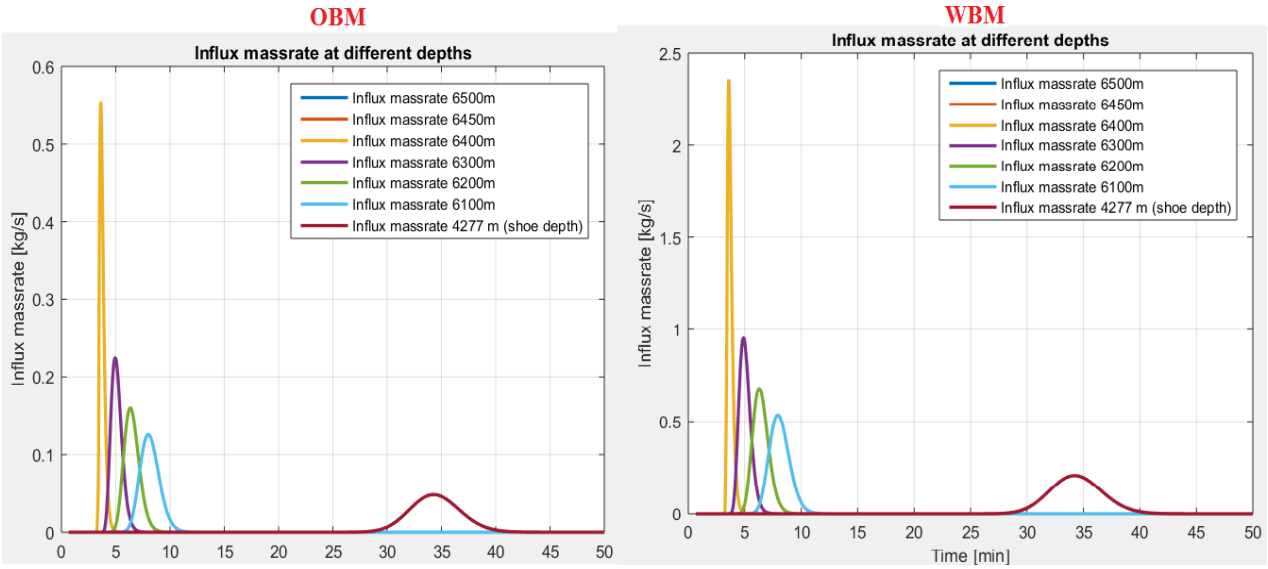

Figure 7.6.13 Influx mass rate at different depths measured by different sensors for OBM and WBM for 3000 seconds.

The main difference between the two curves is that, the mass rate is higher for WBM for the same properties. WBM shows an influx of 140 kg, while the OBM only shows 33 kg. The influx reaches the shoe, for both cases, at approximately the same time.

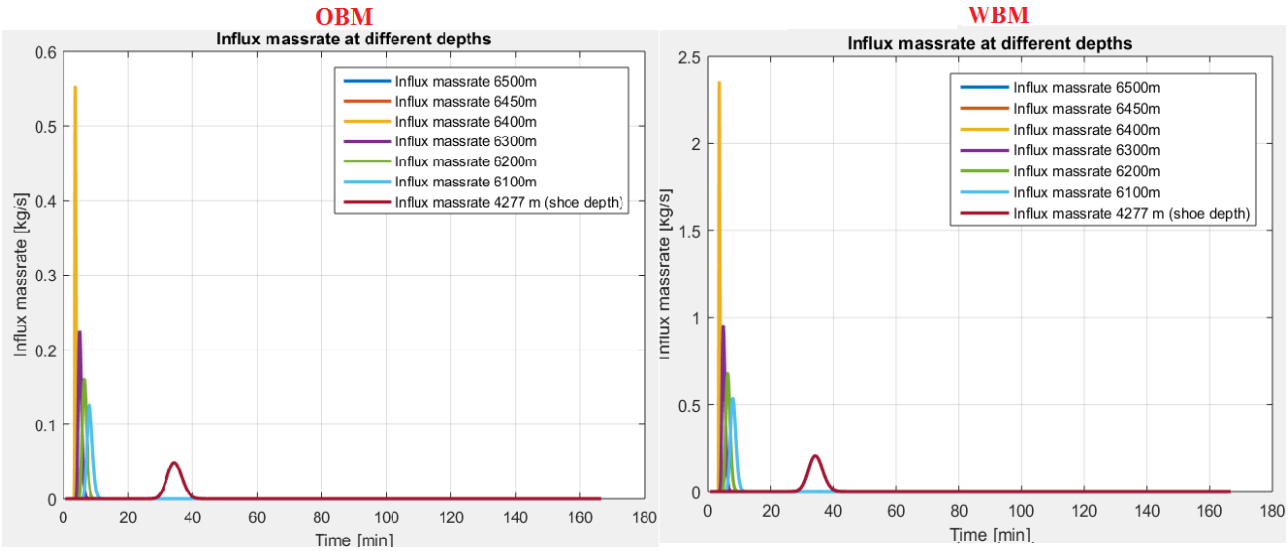

Figure 7.6.14 Influx mass-rate at different depths measured by different sensors for OBM and WBM for whole circulation period.

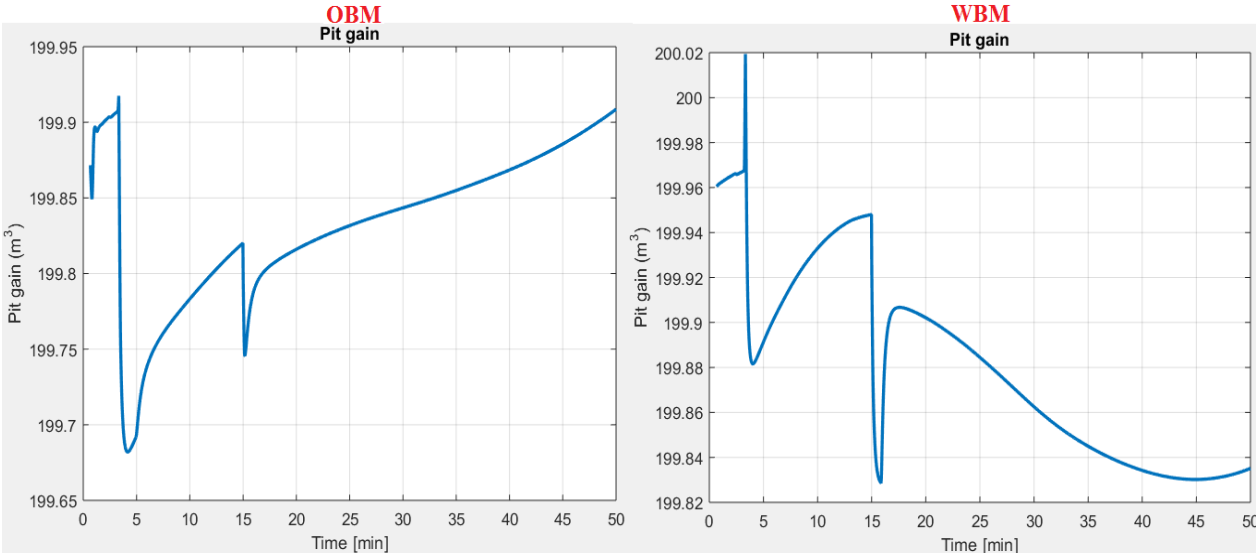

Figure 7.6.15 Shows the pit gain change with time for the first 3000 seconds.

The pit gain behaviour shows changes according to response of return flow in Figure 7.6.2. The y-axis scale is shown in Figure 7.6.15 has very small difference in scale, the actual fluctuation is more in OBM (range in y-axis 0.4 m^3) than shown in WBM (range in y-axis 0.2 m^3).

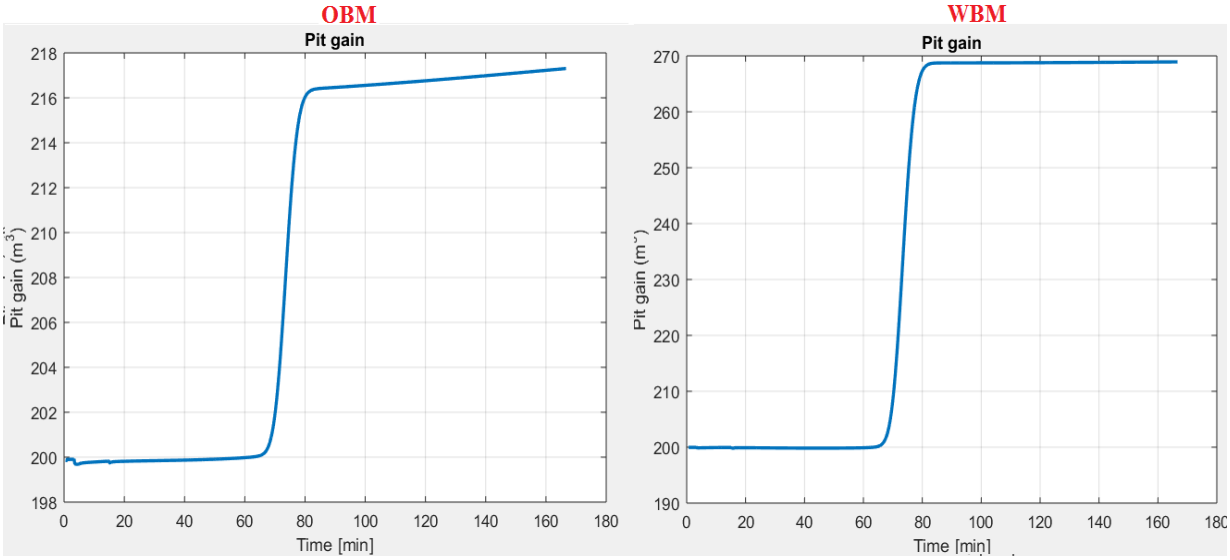

Figure 7.6.16 Shows the pit gain change with time for OBM and WBM for the whole circulation period.

A clear picture of pit gain is seen in Figure 7.6.16. As expected the greater influx of WBM creates a greater increase in the pit gain after around 70 minutes.

Difference can be seen in the gas show between OBM and WBM, only the Figure for whole circulation period is shown.

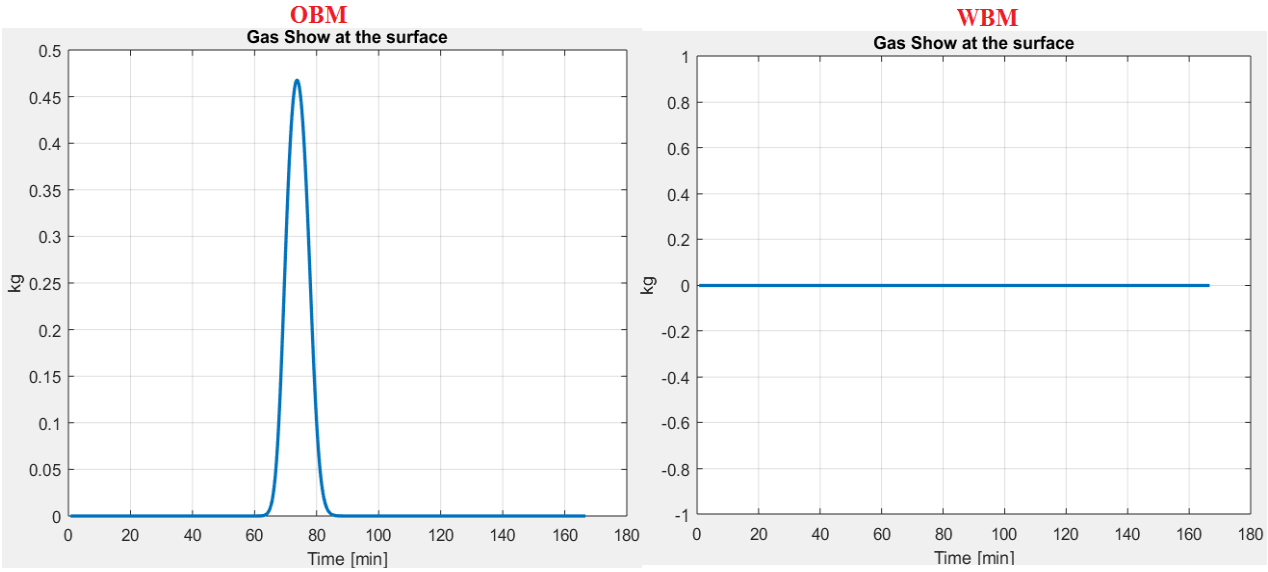

Figure 7.6.17 Represents gas show at surface for their respected influx size for OBM and WBM for the whole circulation period.

The clear difference is seen between the OBM and WBM, the kick is circulated out for OBM while for WBM, no response is seen. This may have two reasons, either the influx is too large to be circulated for WBM or the simulation shows some numerical error. Further investigation of the WBM was taken place, by placing few more sensors below the surface to observe if the influx reaches close (800 m MD, 400 m MD and 100 m MD) to the surface. The result is seen in the Figure 7.6.18.

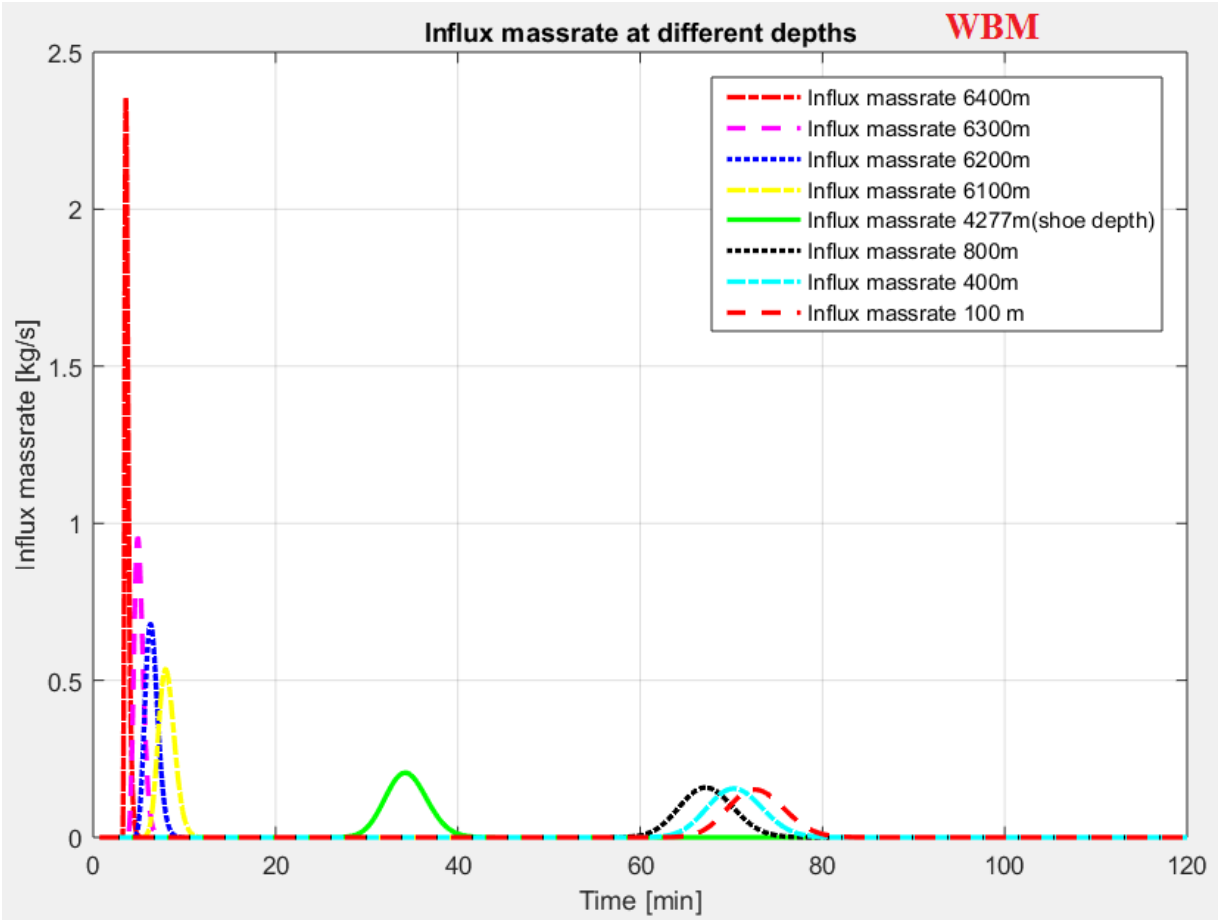

Figure 7.6.18 Further investigation of influx just below the surface, by using sensors.

From the sensor 100 m below the surface, the gas influx is seen (red dash line). By considering the Figure 7.6.12 the ECD for WBM shows a small change just before 80 minutes. Both of these Figures confirm that, the Figure 7.6.17 is incorrect. All these factors with evidence show that, there exists some numerical error for WBM and the gas show is not seen.

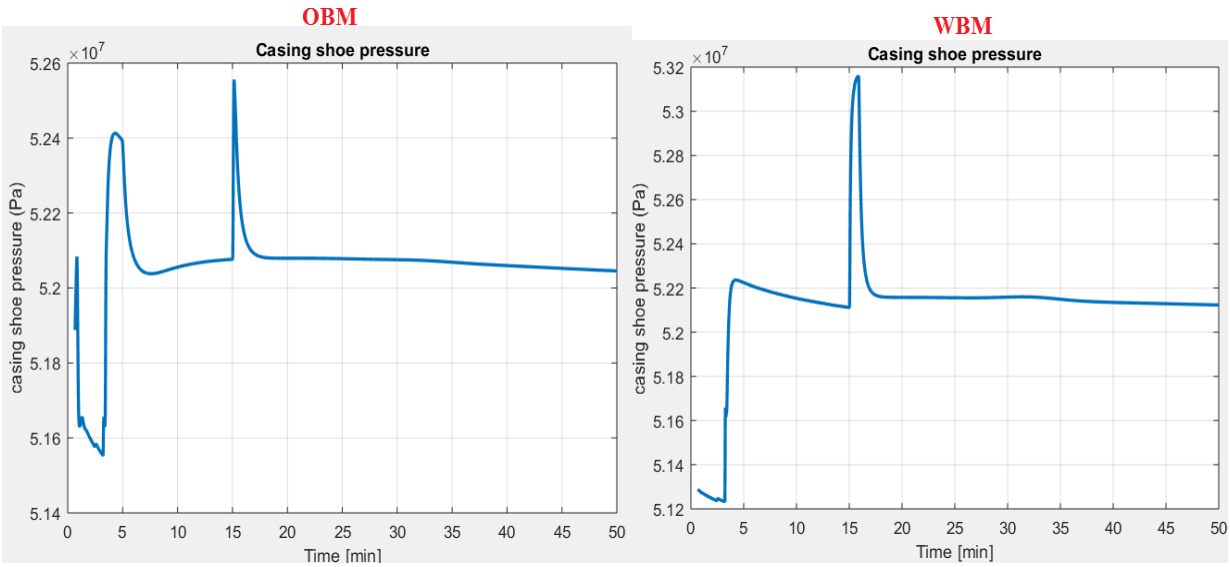

Figure 7.6.19 Shows the casing show pressure for OBM and WBM for time period of 3000 seconds.

The casing shoe pressure increases or shows peaks as the choke opening is changed. The choke opening changes twice in OBM at 4 and 15 minutes and therefore two peaks are seen there. The casing shoe pressure for both curve stabilise at around 521 bar. The peak is due to the sudden increase in back-pressure pump.

The casing shoe pressure for full circulation period is seen in Figure 7.6.20.

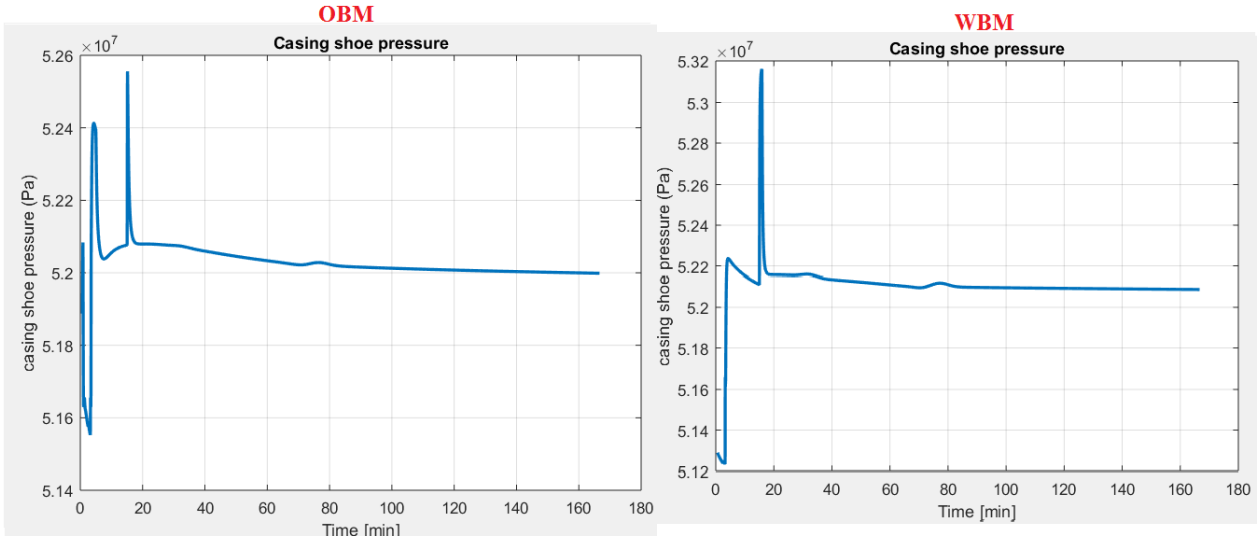

Figure 7.6.20 The casing shoe pressure of OBM and WBM for the whole circulation period.

Chapter 8: Result and conclusion

Simulation study performed in section 7.1 and 7.2, proves that RS model gives a good match for fluids that describe yield-pseudo plastics such as in drilling fluids and cement slurries. BPM shows that the return flow is slower compared to RS model, while the PLM shows slightly less oscillations than RS model, verifying that PLM provides more information at low shear rate conditions due to high shear rates for suspensions and polymer solutions, such as in WBM.

Downhole pressure stability point after 8 minutes of simulation is shown to be lower for RS model, than for PLM and BPM. As a result of that, the stability point of ECD after 8 minutes is lower for RS model compared to other rheological models.

Simulation studies shows us that by increasing the density, the downhole pressure and the ECD both increases, as expected, while the return flow shows no effect. Furthermore, increasing the gel strength, increases the oscillation of return flow with a higher mud pump pressure and downhole pressure. Moreover, by increasing the stresses of PVT table by a constant value, the return flow shows damped oscillations and the downhole pressure also shows some increment.

When comparing OBM and WBM, WBM shows return flow earlier, which is mainly due to OWR. Subsequently, the pump pressure in WBM stabilises at higher pressure than in OBM. The hydrostatic pressure shown in the downhole pressure curve of WBM shows evens out at a higher value than of OBM. All of these effects are due to difference in OWR and stresses on the PVT table.

Results from the kick scenario between the manual operation and automated operation shows that circulation time is half in automated operation. This verifies that the automated operation can handle a greater influx time, and circulate the same influx size quicker. Moreover, the choke opening required much longer time to plan, so that further influx was not seen in the well, for the manual operation. Simulation time was much shorter for manual operation than for automated operation, by including PI controller.

For a comparison between the two fluid types used in simulator, WBM and OBM; the OBM is shown to hide the influx to a large extent, due to the oil content in the mud. As, expected the influx was much smaller than for WBM. However, circulation took just as much time to perform. Overall, WBM shows its advantage in cost and is more

environmental friendly, while OBM is more preferable solution for HPHT conditions or long wells.

Further work recommendations

All of the scenarios and case study performed were done for long horizontal wells, a study of vertical wells and the performance of fluids in such wells would be an interesting future work. Furthermore, a comparison between automated operation versus manual operation would be interesting for vertical well.

For the automated control system PI- controller was used, an additional work may test other controller methods, that can handle two variables, choke opening and the back-pressure pump. The performance may become much better, as both of the variables are manipulated by the controller and smoother transitions is more feasible.

Further improvement can take place by providing a slow and steady ramping up of back pressure pump presented in Chapter 7.6. The sudden peaks and sudden increase in choke pressure pump after initiating back pressure pump will become much smoother. Thus, the choke opening, casing shoe pressure and pump pressure may show gradual change and more stability.

In *Wemod* there are several possibilities, for example by adding a reservoir section and inserting composition of hydrocarbon gases. MPD operation can be added in the configurator, for example a dual gradient operation and the performance can be compared to conventional drilling.

Finally, another flow model could improve the performance of pressure changes further. By considering a model that is more accurate and well defined than presented by IRIS flow model.

References

Abdus Satter, G. M. (2007). *Practical enhanced reservoir engineering, assisted with simulation software.* Oklahoma: PenWell Corporation.

Affendi, H. S. (2015, October 10). *Petroleum Support*. Retrieved from Petroleumsupport.com: http://petroleumsupport.com/drilling-fluid-test-on-field/

Ali Karimi Vajargah, B. B. (2014). Automated Well control Decision- Making during MPD operations. *SPE-170324-MS*, 4-7.

Ant. (2014, May 4). *Coder-tronics*. Retrieved from http://coder-tronics.com/pid-tutorial-c-code-example-pt1/

Araki, M. (2017, May 24). *Wikepedia* . Retrieved from wikipedia.com: https://en.wikipedia.org/wiki/PID_controller

Avery, P. (2009, March 1). *Machine Design*. Retrieved from machinedesign.com: http://www.machinedesign.com/sensors/introduction-pid-control

Bashforth, M. (2016, January). *Ikon science* . Retrieved from ikonscience.com: https://www.ikonscience.com/solutions/drilling-completions/well-stability

Bendiksen, K. M. (1991). *The Dynamic Two-Fluid Model OLGA, Theory and Application" .* oslo: SPE Prod. Eng.

Cooper, M. R. (2010). Methods and Applications in Reservoir Geophysics. *Society of exploration geophysists*.

Cult, M. (2016, january 1). *Wipertrip Drilling and well engineering resources*. Retrieved from wipertrip.com: http://www.wipertrip.com/well-control/secondary-control/184-well-control-drillers-method.html

Dave Elliot, j. M. (2011). Managed pressure drilling erases the lines . *Oilfield review*, 1-10.

Doster, M. a. (1999). *"Numerical Stability of the Mixture Drift-Flux Equations" .* Chicago: Nucl. Sci. Eng.

Effendi, H. S. (2015, October 12). *Petroleum support* . Retrieved from Petroleum support.com: http://petroleumsupport.com/types-of-drilling-fluid-on-oil-and-gas-well/

Færgestad, I. M. (2016). Rheology. *The defining series*, 1-2.

Galindo-Rosales, F. J. (2017, february 15). *Wikepedia* . Retrieved from https://en.wikipedia.org/wiki/Dilatant

Glossary, O. (2017 , Febrary). *Schlumberger* . Retrieved from http://www.glossary.oilfield.slb.com/Terms/m/managed_pressure_drilling.aspx

Godhavn, G. N.-M. (2013). *Automated Drilling Operations.* Stavanger : University of Stavanger, Norwegian University of Science and Technology.

Gravdal, J. E. (2011). Transient pressure behavior in long & deep HPHT wells during pipe connections and well control incidents using conventional and new drilling techniques. *University of Stavanger, IRIS,*, 14-30.

H.H.Fan, H. Q. (2014). A GENERALIZED HYDRAULIC CALCULATION MODEL. *China University of Petroleum*, 1-9.

Haugen, F. (2010). *Basic dynamics and control.* Skien, Norway: TechTeach.

Helge Hodne, A. S. (2014). *Drilling and well fluids technology, Stavanger.* Stavanger: University of stavanger .

Helio Santos, P. S. (2012). *Transitional kick tolerance.* Texas, USA: SPE.

J.E. Gravdal, R. L. (2010). *Wired drill pipe telemetry enables real time evaluation of kick during MPD.* Australia, Queensland: SPE.

Jhonny Frøyen, O. S. (2000). Discretization, implementation and testing of semi implicit method . *IRIS* , all.

Jing Zhou, J. E. (2016). *Automated kick control procedures for an influx in MPD operations by utilizing PWD.* Stavanger: University of Agder, IRIS, Statoil ASA, NOWVA.

Johnny Frøyen, O. S. (2000). Model equations and solution techniques for multi phase flow in pipe networks. . *IRIS* .

Jr, W. M. (1989). Reservoir- Fluid Property Correlations. *SPE 18571*, 1-10.

K, K. F. (2015). *Automated dynamic well control with MPD, case study and simulation analysis.* Madrid: Weatherford, SPE.

Kjell kåre fjelde, J. E. (2014). *A simple transient flow model for MPD and UBD applications* . Stavanger: SPE, University of Stavanger.

Liles, D. a. (1978). *A Semi-Implicit Method for Two-Phase Dynamics.* Texas: J. Computational Physics 26.

Lulu, R. (2016, December 10). *Rheosense*. Retrieved from rheosense.com: http://www.rheosense.com/what-is-viscosity

Mahdianfar, H. (2016). *Pressure Control for Offshore Managed Pressure Drilling (MPD): Analysis, Design, and Experimental Validation.* Trondheim: NTNU.

Mahmood Amani, M. A.-J. (2012). Comparative Study of Using Oil-Based Mud Versus Water-Based Mud in HPHT. *CScanada*, 28-27.

Ochoa, M. V. (2006). *Analysis of drilling fluid rheology and tool joint effect to reduce errors in hydraulics calculations.* Texas: Texas A&M University.

Pai, R. (2008, May 11). *My Weblog*. Retrieved from Weblog: https://radhesh.wordpress.com/2008/05/11/pid-controller-simplified/

R.E Robertsen, H. S. (1976). An imporved mathmatical model for relating shear stress to shear rate in drilling fluids and cement slurries. *Atlantic Richfield Co.*, all.

R.Rommetveit, K. B. (1997). Temperature and Pressure Effects on Drilling fluid Rheology and ECD in Very Deep wells. . *SPE*, all.

Rachain J, S. C. (2010, January 10). *Drilling formulas.com*. Retrieved from Drilling Formulas : http://www.drillingformulas.com/drilling-fluid-properties/

Rachain.J, S. C. (2014, November 15). *Drilling formulas.* Retrieved from http://www.drillingformulas.com/learn-about-maximum-surface-pressure-in-well-control-masp-misicp-and-maasp/

Rana S Roy, C. J. (2009). *Driller's Method versus Wait and Weight Method: One offers distinct well control advantages.* Houston: Drilling contractor .

Rao, A. (2014). Flow and Functional Models for Rheological Properties of Fluid Foods. *Springer*, 2-7.

Reed, P. (1993). A New Model for Laminar, Transitional, and Turbulent Flow of Drilling Muds. *SPE 25456*.

Robin, J. (2017, January 10). *Baroid Industrial drilling products*. Retrieved from baroididp.com: http://www.baroididp.com/idp/resources/technical-assistance/publications/tech-papers/fluid-properties-for-horizontal-applications/horizontal-apps.page?node-id=hm8zxxls

Ryazanov, M. (2017, February 26). *Wikepedia*. Retrieved from https://en.wikipedia.org/wiki/Dilatant#/media/File:Shear_rate_versus._Shear_stress.png,21.05.2011

Swensen, I. (2014). Modeling and Non-linear Control of Gel. *NTNU*, 1-20.

Toralde, D. M. (2011, January 11). *Thewayahead*. Retrieved from spe.org: https://www.spe.org/en/twa/twa-article-detail/?art=645

Trapp, J. a. (1986). *A Nearly-Implicit Hydrodynamic Numerical Scheme for Two- Phase Flows".* Texas: J. Computational Physics 66.

Y.A. Hazov, Y. H. (1993, november 29). *Oil and gas journal*. Retrieved from ogj.com: http://www.ogj.com/articles/print/volume-91/issue-48/in-this-issue/drilling/leak-off-tests-help-determine-well-bore-compressibility.html

Z.Ma, A. V. (2016). Multi-phase Well Control Analysis During Managed Pressured Drilling Operations. *SPE-181672-MS*, 13-18.

Z.Ma, K. V. (2016). Multi phase well control analysis during MPD operations . *society of petroleum engineers*, 14-18.

Appendix 1: Introduction to Wemod

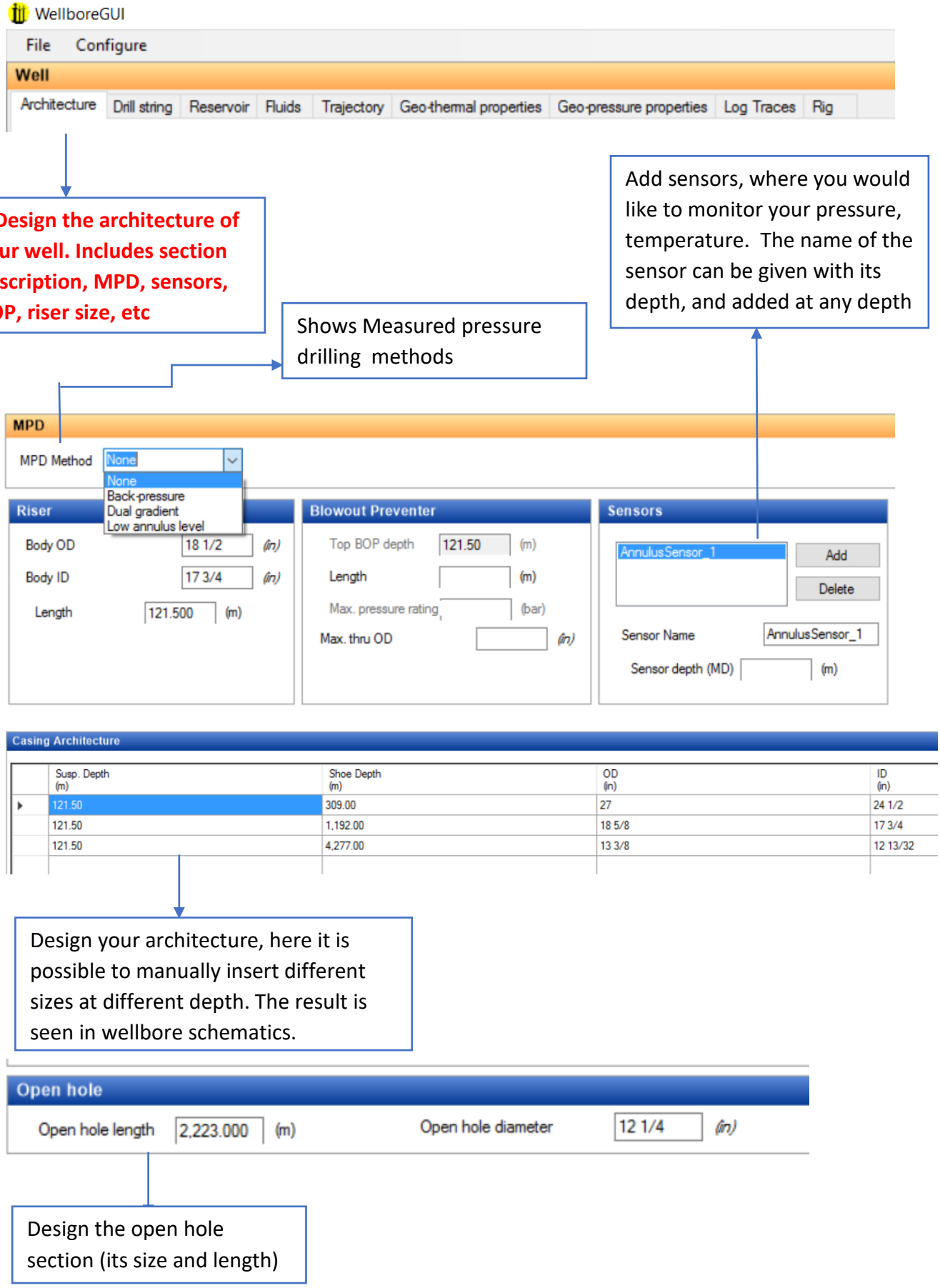

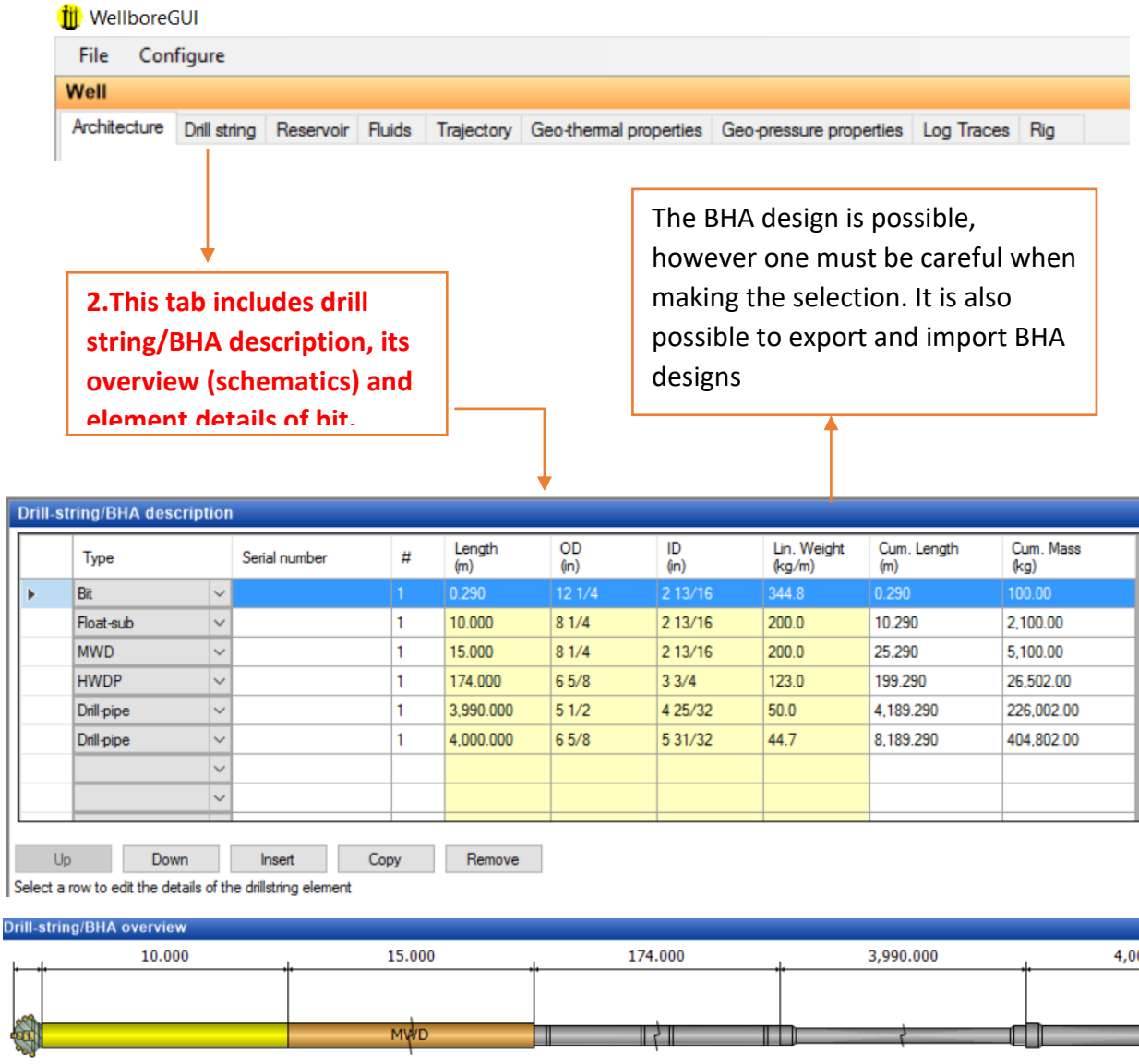
WellboreGUI
File
Configure
Well
Architecture
Drill string
Reservoir
Fluids
Trajectory
Geo-thermal properties
Geo-pressure properties
Log Traces
Rig
2.This tab includes drill string/BHA description, its overview (schematics) and element details of bit.
The BHA design is possible, however one must be careful when making the selection. It is also possible to export and import BHA designs
Drill-string/BHA description
Type
Serial number
#
Length (m)
OD (in)
ID (in)
Lin. Weight (kg/m)
Cum. Length (m)
Cum. Mass (kg)
Bit 1 0.290 12 1/4 2 13/16 344.8 0.290 100.00
Float-sub 1 10.000 8 1/4 2 13/16 200.0 10.290 2,100.00
MWD 1 15.000 8 1/4 2 13/16 200.0 25.290 5,100.00
HWDP 1 174.000 6 5/8 3 3/4 123.0 199.290 26,502.00
Drill-pipe 1 3,990.000 5 1/2 4 25/32 50.0 4,189.290 226,002.00
Drill-pipe 1 4,000.000 6 5/8 5 31/32 44.7 8,189.290 404,802.00
Up
Down
Insert
Copy
Remove
Select a row to edit the details of the drillstring element
Drill-string/BHA overview
10.000
15.000
174.000
3,990.000
4,000.000
MWD

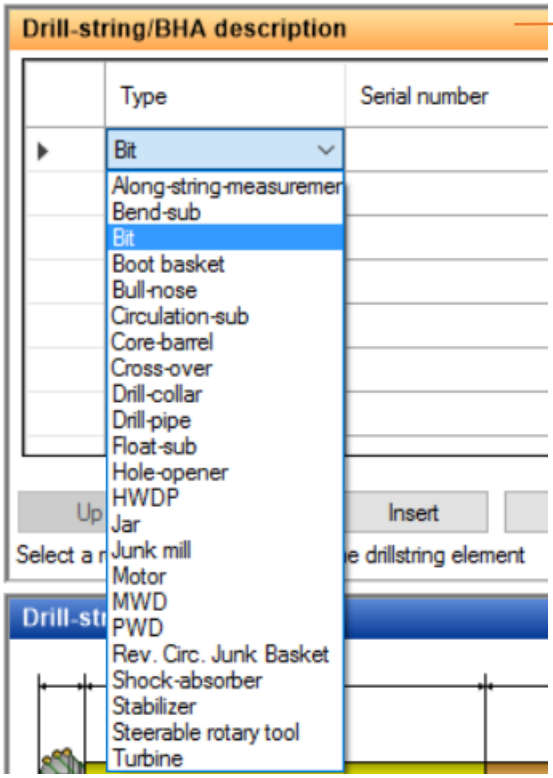

Shows the components that can be added to the BHA/drill string. The order of the components is directly reflected in the same order in the overview of BHA.

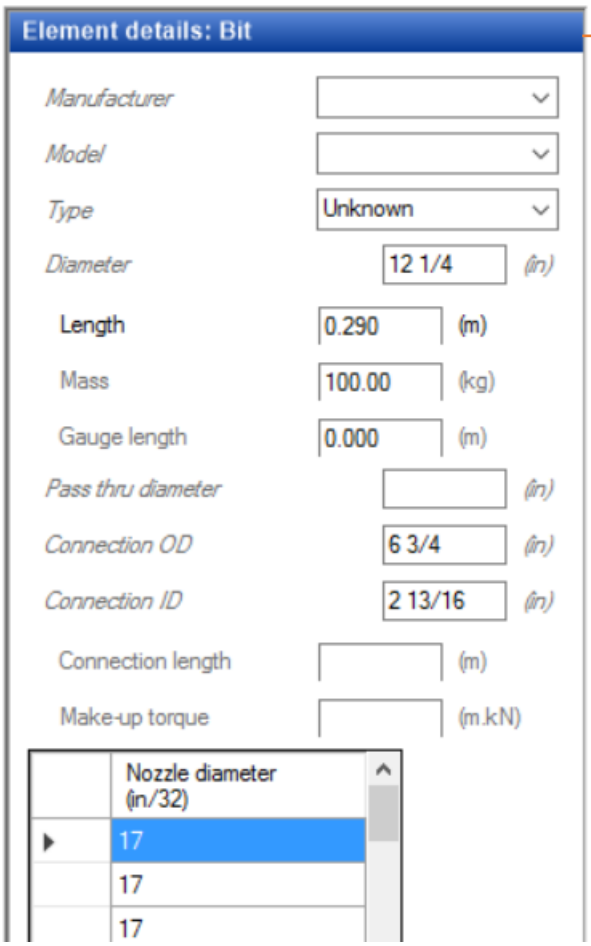

Add further details about the bit and various OD and ID size.

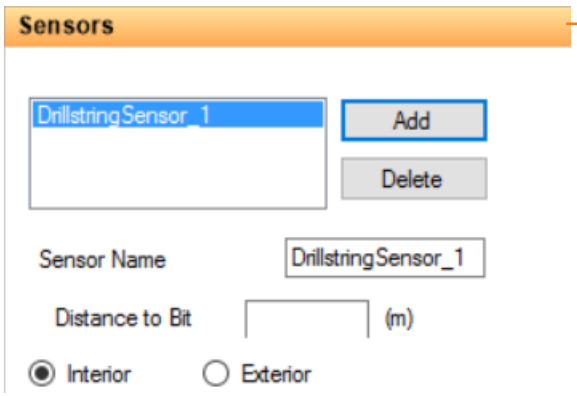

Drill string sensors may also be added in this section.

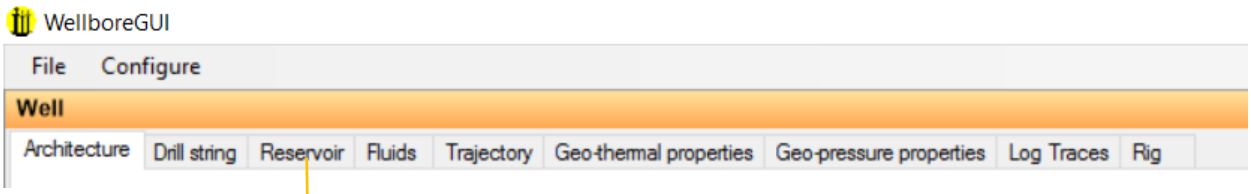

3. The reservoir section can be included. Any fluid influx can be added here, at a certain depth, including the duration (in length) of the influx. An example is given for a kick. Reservoir pressure must be calculated.

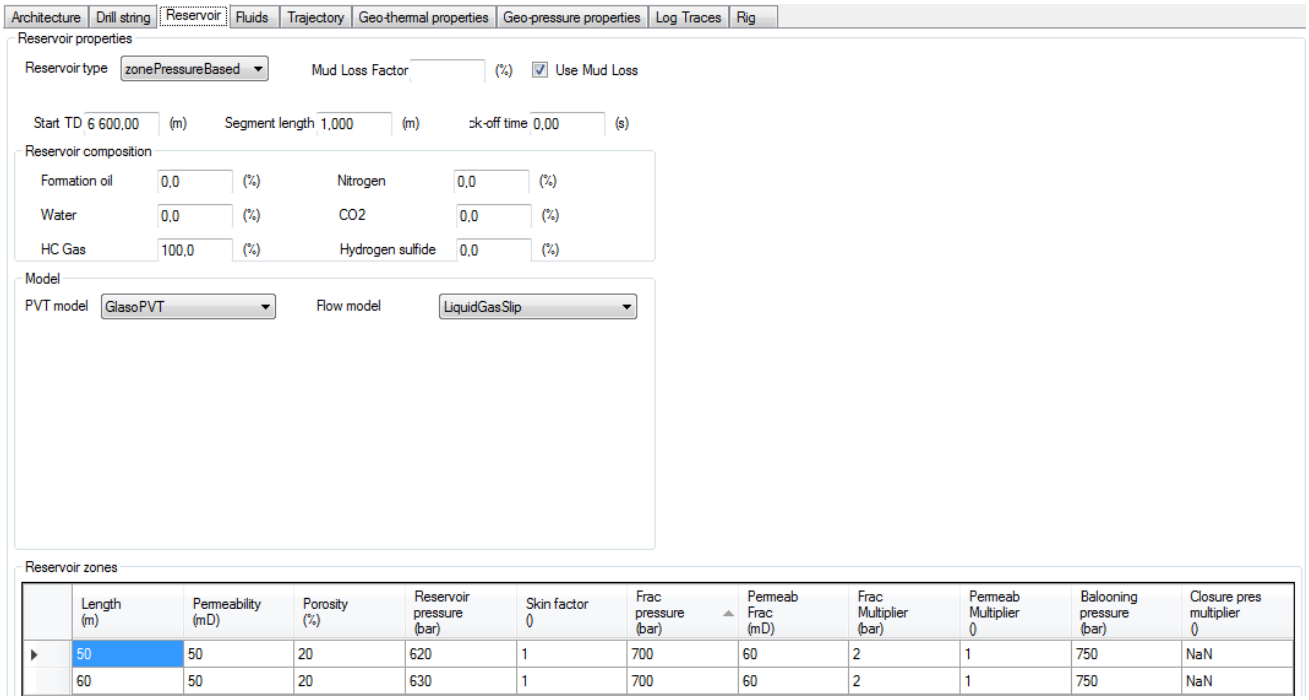

Length (m)	Permeability (mD)	Porosity (%)	Reservoir pressure (bar)	Skin factor ()	Frac pressure (bar)	Permeab Frac (mD)	Frac Multiplier (bar)	Permeab Multiplier ()	Balooning pressure (bar)	Closure pres multiplier ()
50	50	20	620	1	700	60	2	1	750	NaN
60	50	20	630	1	700	60	2	1	750	NaN

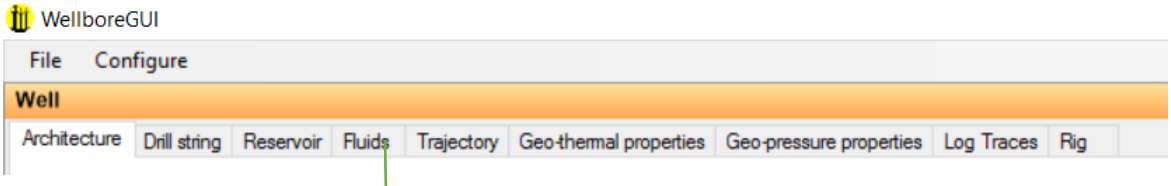

4. This tab includes the fluids selection, MW, PVT table, rheology selection etc.

This section shows the fluid currently selected. Names are given by its density and it is possible to add or remove fluid.

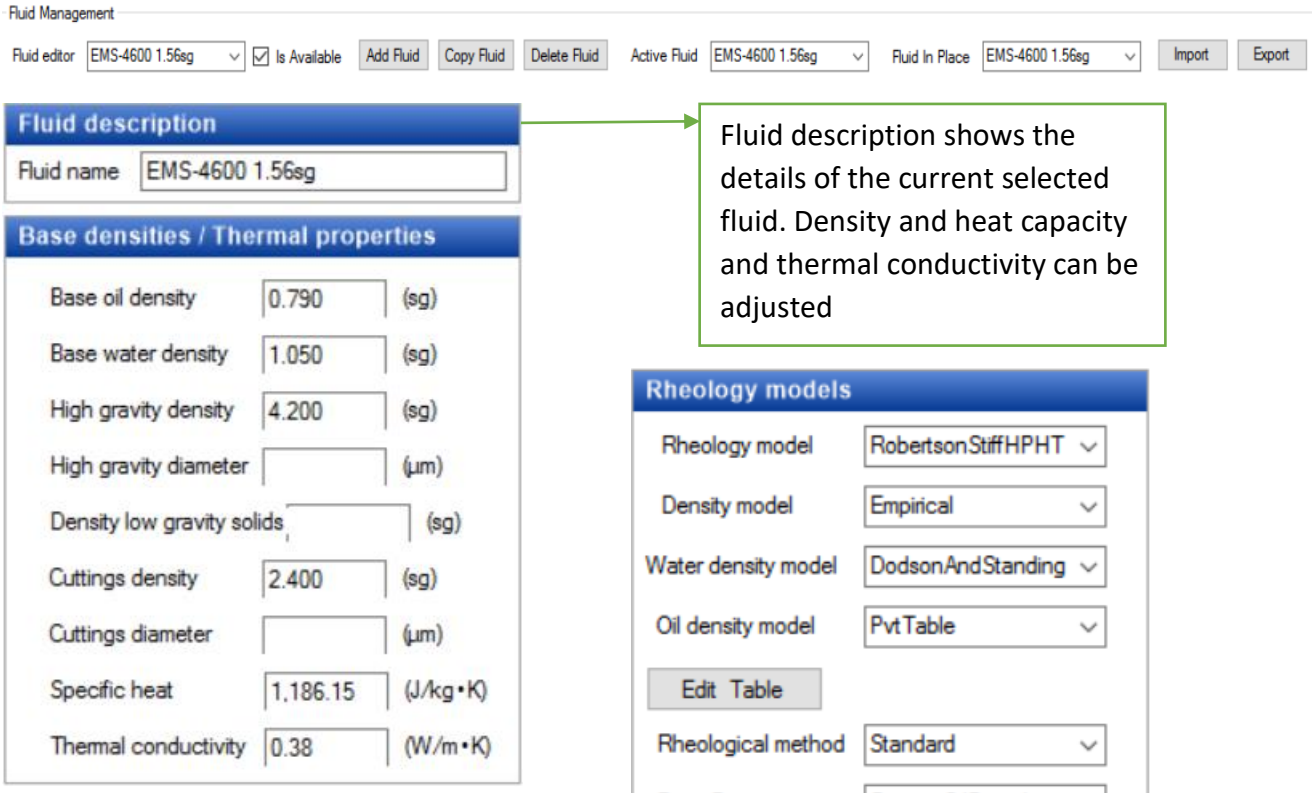

Fluid description shows the details of the current selected fluid. Density and heat capacity and thermal conductivity can be adjusted

This section shows the rheology models used their details is given. Fann data shows which type of fluid to

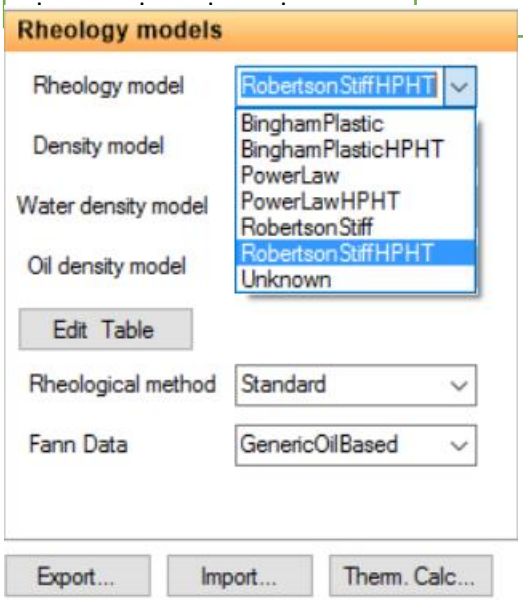

Different rheology models can be chosen in the

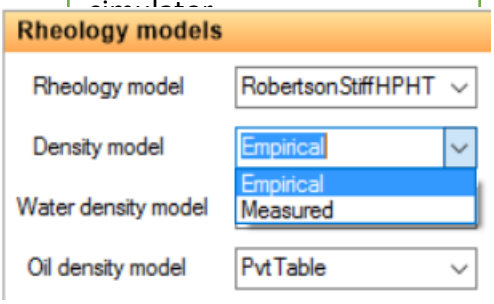

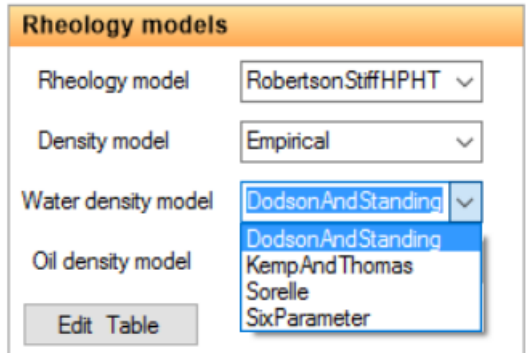

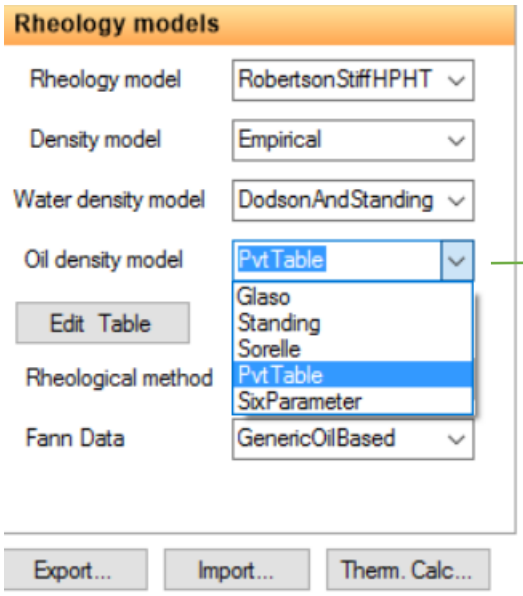

Different oil density model can be chosen. This research, will base on the PVT table.

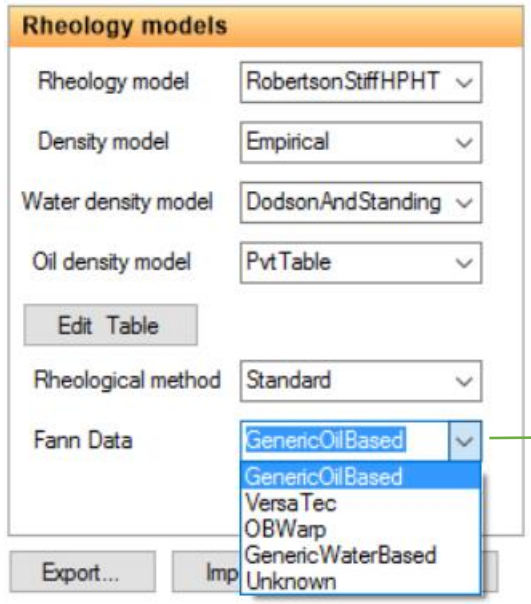

The Fann data determines the type of fluids you have. Basically, if the fluid in question is an oil based or water based fluid. Warp is an OBM that uses oil based Warp concentrate as a weight material. Whereas VersaTec is also an OBM which uses barite as a weight

	Temp. (°C)	Press. (bar)	Stress at 3 rpm (lb/100ft²)	Stress at 6 rpm (lb/100ft²)	Stress at 30 rpm (lb/100ft²)	Stress at 60 rpm (lb/100ft²)	Stress at 100 rpm (lb/100ft²)	Stress at 200 rpm (lb/100ft²)	Stress at 300 rpm (lb/100ft²)	Stress at 600 rpm (lb/100ft²)
▸	50.00	1.0	9.0	11.0	16.0	22.0	29.0	43.0	58.0	95.0

Insert | Remove | Fill R30 and R60 | Copy Rheology | Update rheometer values | Configure extrapolation | Export Rheology... | Import Rheology...

This is the first PVT table, it shows rheology measurements for the fluid in question at atmospheric pressure and 50 deg. Celsius.

The second PVT table is an extrapolation of those measured values over several pressure and temperature combinations where other parameters such as density and OWR are taken into account.

	Temp. (°C)	Press. (bar)	Stress at 3 rpm (lb/100ft²)	Stress at 6 rpm (lb/100ft²)	Stress at 30 rpm (lb/100ft²)	Stress at 60 rpm (lb/100ft²)	Stress at 100 rpm (lb/100ft²)	Stress at 200 rpm (lb/100ft²)	Stress at 300 rpm (lb/100ft²)	Stress at 600 rpm (lb/100ft²)	Legend
▸	20.00	1.0	9.0	10.7	20.8	29.6	39.2	57.3	76.3	123.7	
	20.00	300.0	11.1	11.9	24.5	36.5	50.5	79.1	104.6	181.4	
	20.00	600.0	12.6	12.7	27.2	41.5	59.1	96.6	127.0	224.9	
	80.00	1.0	9.1	10.5	13.8	18.0	23.0	33.8	46.4	72.1	
	80.00	300.0	11.2	11.8	17.4	23.4	30.9	47.5	65.3	102.1	

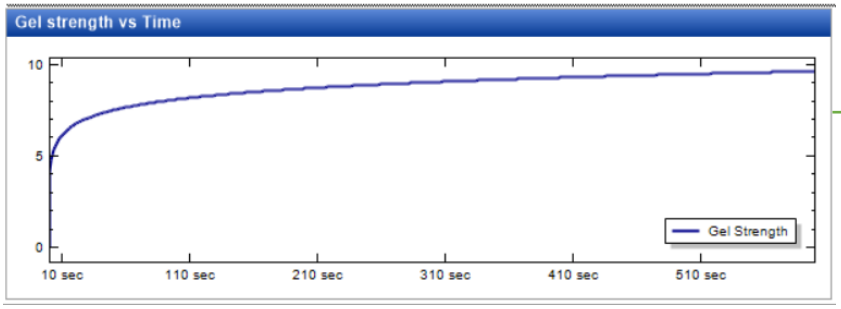

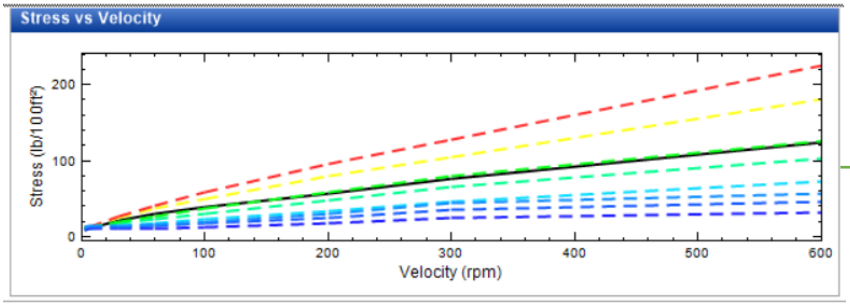

The graphs show the gel strength versus time, and stress versus velocity. This can be manipulated by the use of PVT table and different rheology models.

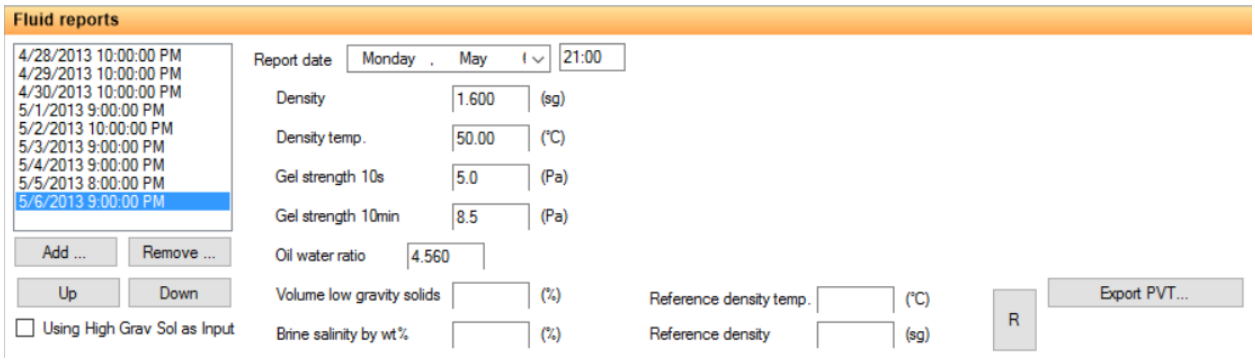

This is the main section where fluid density is adjusted, along with the gel strength and OWR is also manipulated.

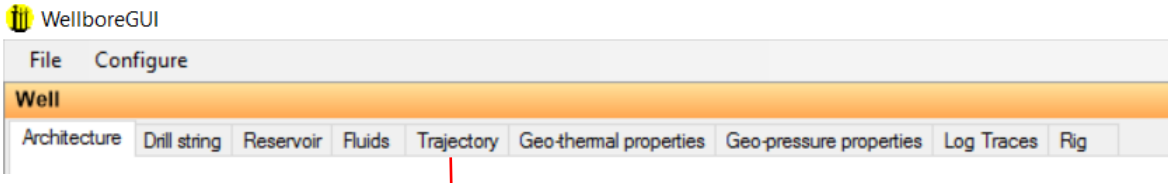

5. This tab includes the trajectory of the well, which includes a table and the schematic of vertical and horizontal projection.

The trajectory table can also be exported, imported and

Trajectory

MD (m)	Incl (°)	Az (°)	TVD (m)	North (m)	East (m)	DLS (°/30m)	BUR (°/30m)	TR (°/30m)
0.00	0.00	230.72	0.00	0.00	0.00			
121.50	0.00	0.00	121.50	0.00	0.00	0.00	0.00	-56.97
129.90	0.49	230.72	129.90	-0.02	-0.03	1.75	1.75	824.00
139.90	0.50	227.28	139.90	-0.08	-0.09	0.09	0.03	-10.32
149.89	0.54	229.20	149.89	-0.14	-0.16	0.13	0.12	5.77
159.87	0.54	230.19	159.87	-0.20	-0.23	0.03	0.00	2.98
169.96	0.54	228.32	169.96	-0.26	-0.30	0.05	0.00	-5.56
179.94	0.53	230.40	179.94	-0.32	-0.38	0.07	-0.03	6.25
189.93	0.48	233.20	189.93	-0.38	-0.44	0.17	-0.15	8.41
199.92	0.50	224.90	199.92	-0.43	-0.51	0.22	0.06	-24.92
209.93	0.52	229.28	209.93	-0.49	-0.57	0.13	0.06	13.13
219.89	0.48	224.50	219.89	-0.55	-0.64	0.17	-0.12	-14.40
229.96	0.46	226.17	229.96	-0.61	-0.70	0.07	-0.06	4.98
239.94	0.49	228.41	239.94	-0.67	-0.76	0.11	0.09	6.73
249.90	0.48	221.09	249.90	-0.73	-0.82	0.19	-0.03	-22.05

Up Down Insert Remove

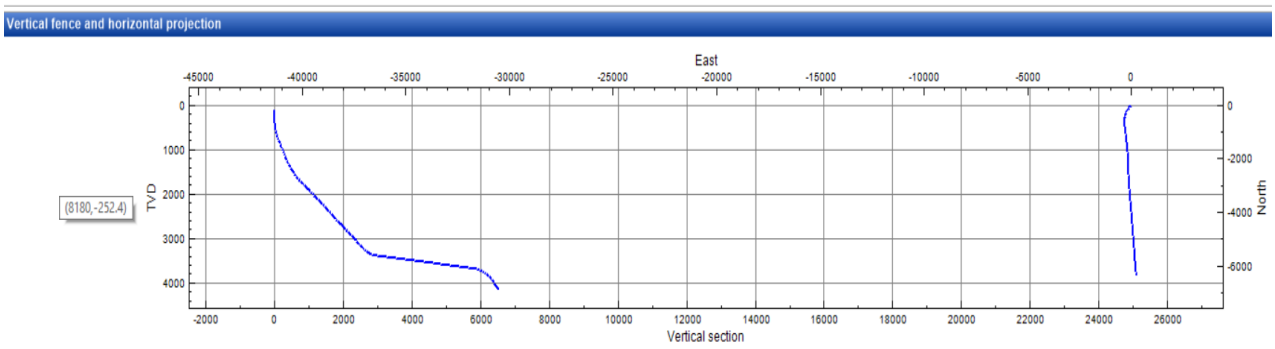

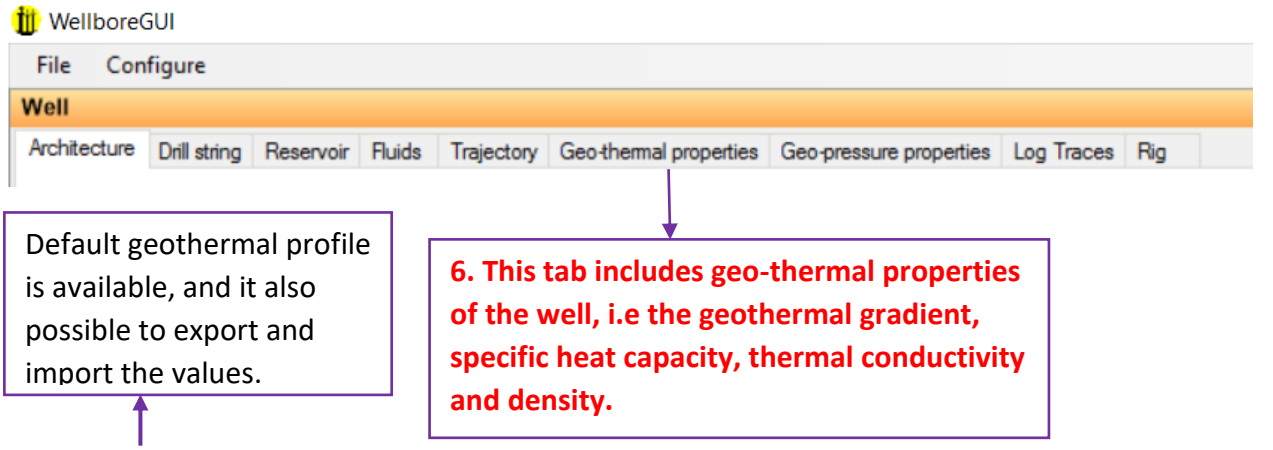

Default geothermal profile is available, and it also possible to export and import the values.

6. This tab includes geo-thermal properties of the well, i.e the geothermal gradient, specific heat capacity, thermal conductivity and density.

Geo-thermal properties

Default geo-thermal profile | Thermal cond. calculator

TVD (m)	Type	Formation Name	Lithology Type	Geothermal gradient (°C/100m)	Specific heat (J/kg•K)	Thermal conductivity (W/m•K)	Density (sg)
0.00	Air		Air	0.0	1,005.00	0.02	0.001
56.00	Water		Water	-2.0	4,180.00	0.58	1.050
80.00	Water		Water	0.0	4,180.00	0.58	1.050
121.50	Solid		Unknown	4.8	900.00	2.00	2.500
1,200.00	Solid		Unknown	3.0	900.00	2.00	2.500
3,000.00	Solid		Unknown	3.6	900.00	2.00	2.500
4,200.00	Solid		Unknown	3.6	900.00	2.00	2.500

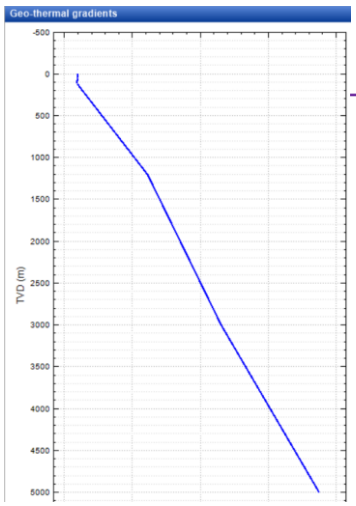

The graph shows the geothermal gradient versus TVD.

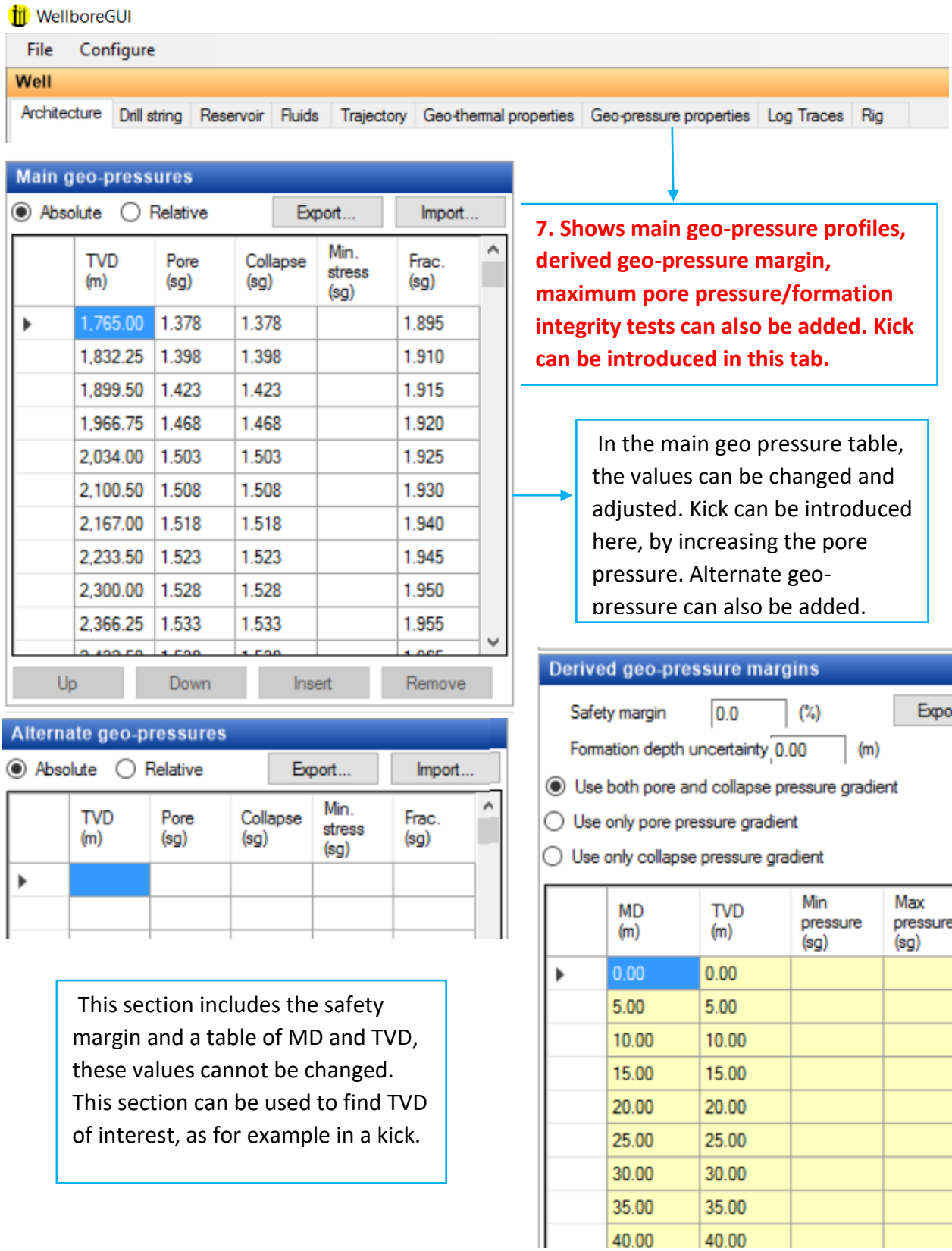

7. Shows main geo-pressure profiles, derived geo-pressure margin, maximum pore pressure/formation integrity tests can also be added. Kick can be introduced in this tab.

In the main geo pressure table, the values can be changed and adjusted. Kick can be introduced here, by increasing the pore pressure. Alternate geo-pressure can also be added.

This section includes the safety margin and a table of MD and TVD, these values cannot be changed. This section can be used to find TVD of interest, as for example in a kick.

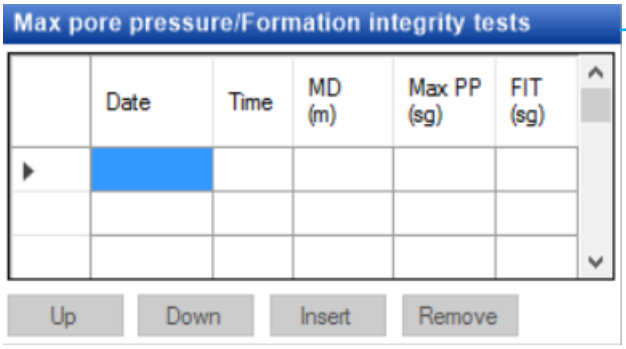

It is possible to add max pore pressure and formation integrity tests, for this thesis I have not used it.

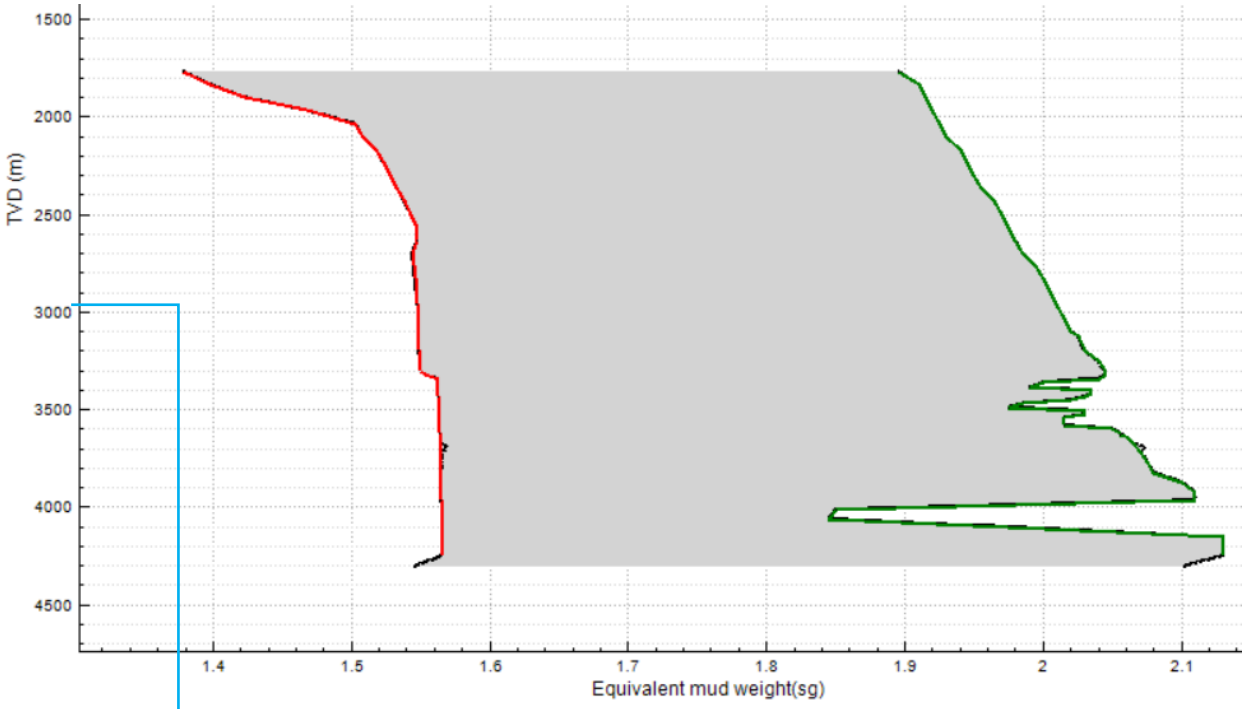

This graph shows the TVD as a function of pore pressure, collapse pressure and fracture pressure gradient (ECD). The chosen mud, weight for this profile was 1.6 sg.

Main geo-pressures

Absolute Relative Export... Import...

	TVD (m)	Pore (sg)	Collapse (sg)	Min. stress (sg)	Frac. (sg)
	3,200.00	1.549	1.549		2.030
	3,252.00	1.550	1.550		2.040
	3,304.00	1.550	1.550		2.045
	3,322.50	1.553	1.553		2.045
	3,341.00	1.563	1.563		2.040
▶	3,359.50	1.65	1.65		2.000
	3,378.00	1.65	1.65		1.995
	3,388.50	1.563	1.563		1.990
	3,400.50	1.563	1.563		2.035
	3,415.00	1.563	1.563		2.035

Up Down Insert Remove

An example, where kick is introduced, by increase the pore and the collapse pressure gradient. This increase can be seen in the pore/frac gradient curve.

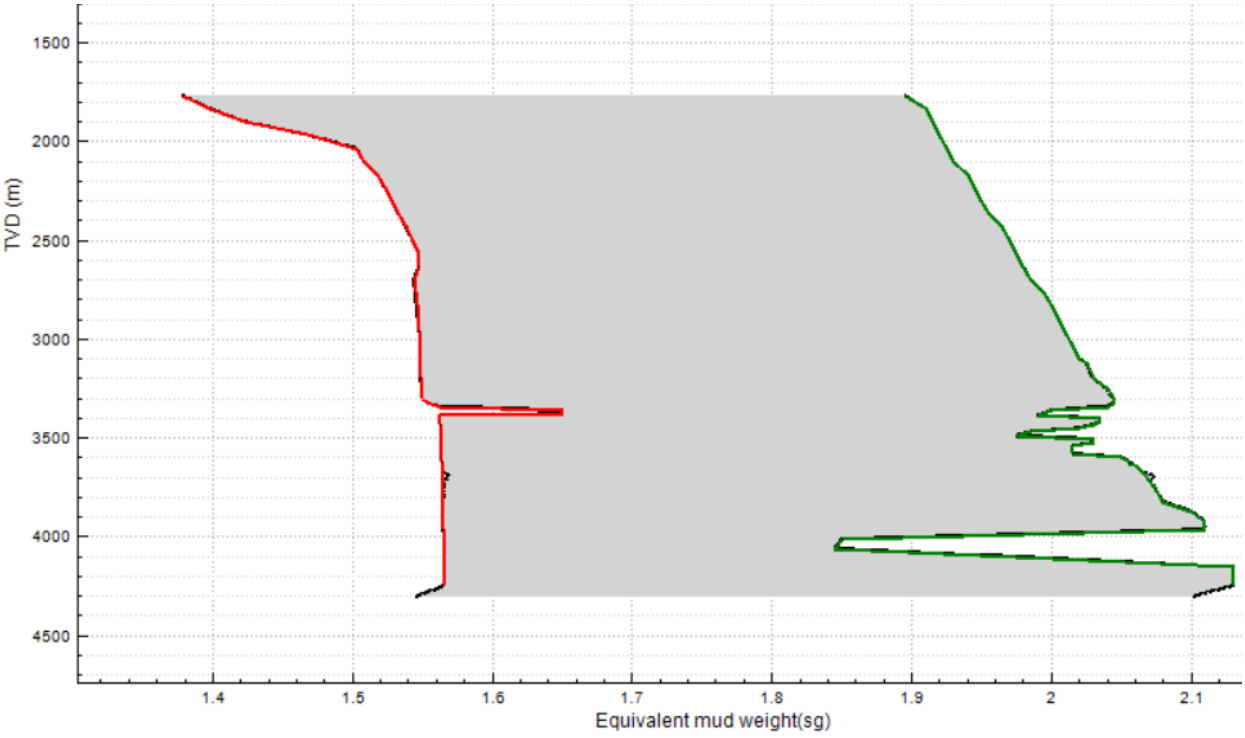

Extrapolation depth 210.00 (m)

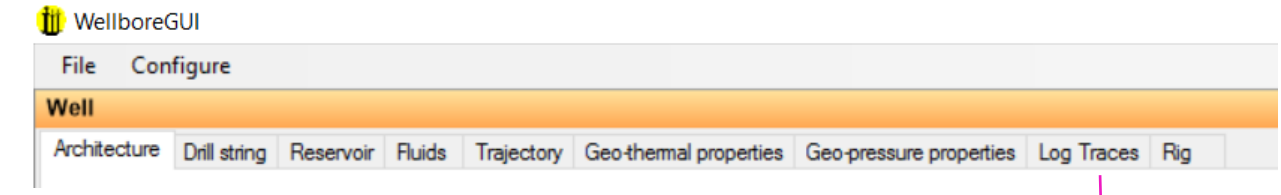

8. This tab shows the log traces, and the information given in the rest of the tabs must match to obtain correct results.

The mud density and any other information that was previously set on the rest of the other tabs must match any information asked in this section. This is crucial to obtain correct xml file.

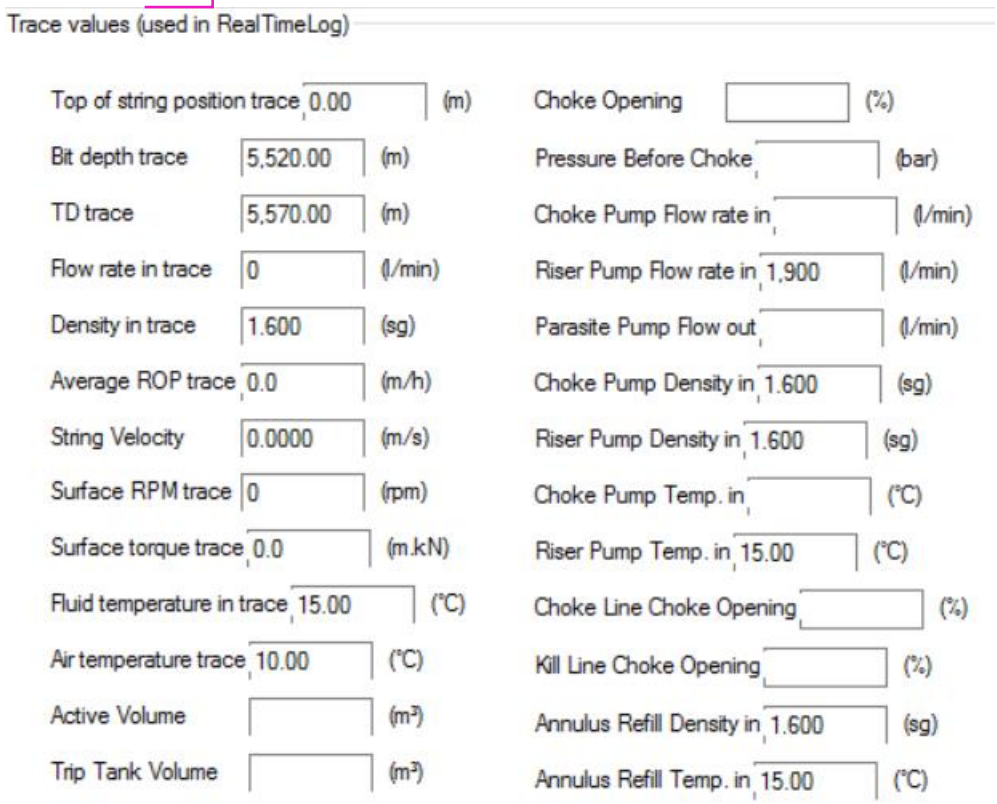

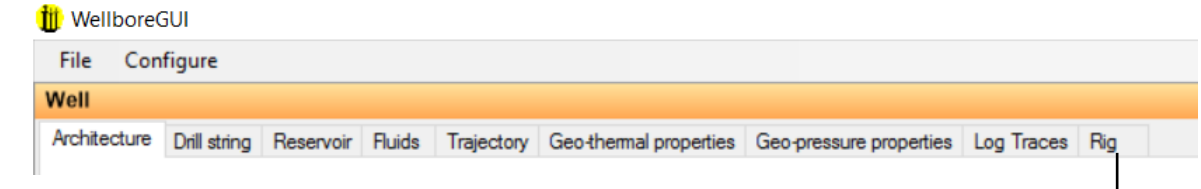

9. Includes, rig, drawworks, pumps, tanks, chokes and surface pressure loss.

Add a rig name, and default temperature. This research paper does not include a mud density correction

Add choke if it main or not, and the opening diameter, the xml file still needs to be adjusted according to the desired choke opening.

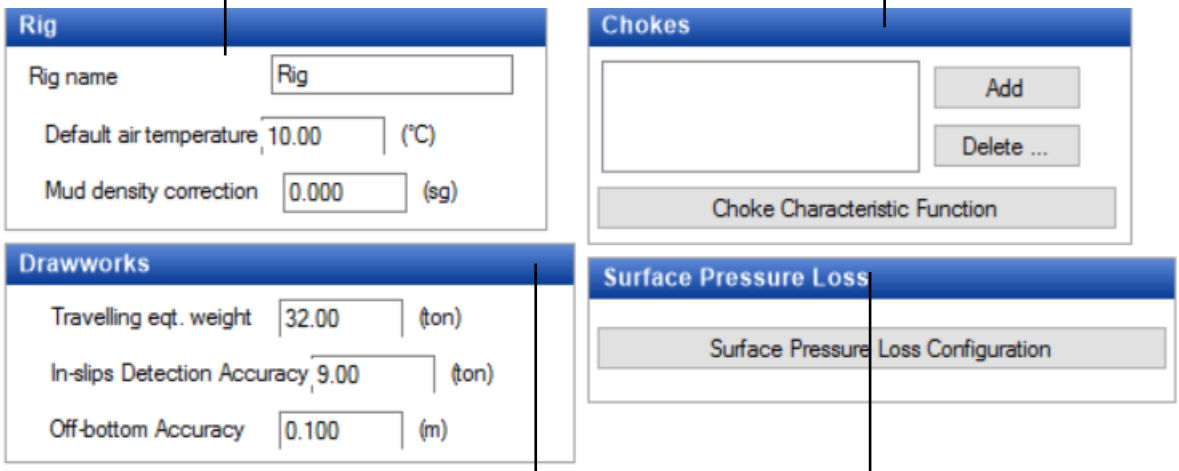

Includes details about the draworks used in the rig.

Surface pressure loss dialog can be imported but this research does not consider this.

Pumps can be added in this section, (main and back pressure pump)

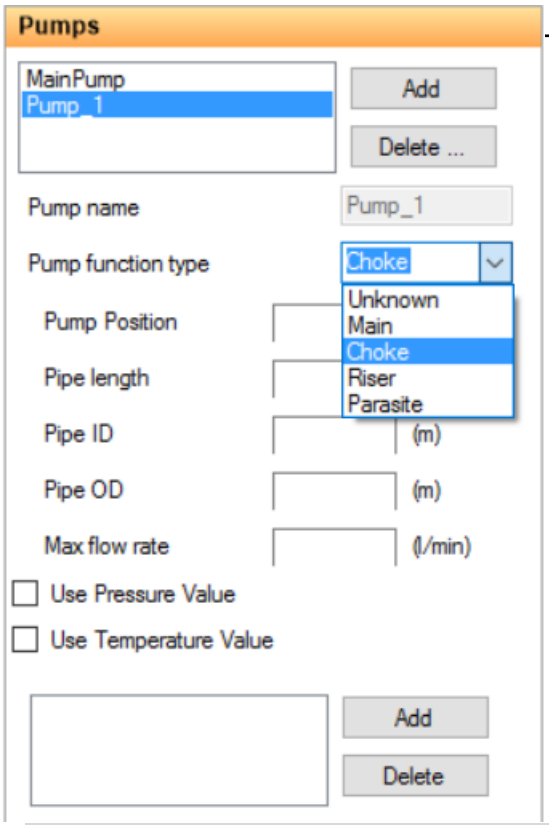

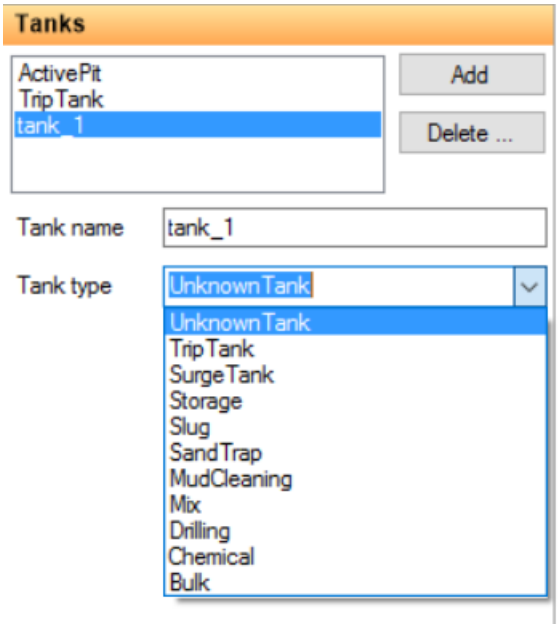

Tanks may be added, with a several options for the tank type.